Earth, wind, and fire: The impact of burning on potential dust emissions from partially vegetated dunes in the southwest Kalahari

Rosemary Alice Huck
St. John's College

Supervisors:
Professor Giles F.S. Wiggs
Professor David S.G. Thomas

A thesis submitted for the degree of
Doctor of Philosophy
at the University of Oxford
Trinity Term 2025

Abstract

Sand dunes are not typically considered to be a significant contributor to atmospheric dust loading due to coarse grain sizes and a lack of observed emission events. In vegetated dune systems, dust emission is rarer due to plant cover preventing the wind from reaching the surface. However, disturbed vegetated dunes have the potential to emit dust through the release of resident fine grains. Fire represents one such significant disturbance factor, forcing rapid shifts in the ecosystem state resulting in an increased propensity for aeolian erosion. Accordingly, this thesis investigates potential dust emissions after de-vegetation of dunes through burning in the southwest Kalahari Desert.

First, satellite imagery is used to assess the spatiotemporal extent of burning in the dune field for 2000-2023. Fires were common in the region and occurred most frequently during or just after La Niña extreme events which provide moisture for biomass build up. However, fire is limited by anthropogenic modulation of the fire regime. Different land uses have significant differences in fire occurrence and size, with more, but smaller, burns occurring on privately owned land with larger, but less frequent, burns occurring within the National Park. National Park burns also had longer durations.

Post-fire vegetation recovery was also tracked from space and found to be swift after burning, with cover returning to unburned levels within two years of being burned, limiting the period where bare ground is available for wind erosion. This finding was confirmed by ground surveys which identified that in a wet year, vegetation can recover within 10 months of burning. However, burned plots are more vulnerable to further disturbance, i.e. through drought, than unburned plots.

Field studies assessed the grain size distribution of the dunes and found a proportion of dust-sized material (<62.5 μm). Portable wind tunnel experiments found that this material can be mobilised in the form of dust, but the burned sites had a higher erosion threshold than the unburned sites. Surfaces were further disturbed by removing the top 2 cm of sediment, and fluxes of dust from these mechanically disturbed surfaces could exceed 77 times those of both the unburned and burned surfaces. This finding indicates the importance of biocrusts, which were found at 95% of the interdune plots, and how their survival limits post-fire dust emissions.

Results presented in this thesis show that currently there is little potential for dust emission in the post-fire de-vegetation period. Yet, this potential might be high under different environmental conditions such as droughts or high grazing intensities, where reduced biocrust cover unlocks the resident fine sediment. But post-fire conditions have quick vegetation recovery and the protective effect of biocrusts surviving fire limits the availability of fine sediment for wind erosion.

Acknowledgements

First, I would like to thank my supervisors, Prof. Giles Wiggs and Prof. David Thomas. I am incredibly grateful for your unwavering support, wisdom, and guidance throughout the last four years. You have pushed me to become a better scientist whilst making the experience both fun and memorable – especially whilst in the field! I have learnt and continue to learn so much from you both, thanks for putting up with me.

This research would not have been possible without the financial support from the Oxford University Press Clarendon and Rosemary and Ioan James Graduate Scholarship. I am very grateful to all my funders who enabled fieldwork to be conducted as part of this DPhil: St. Johns College, the Royal Geographical Society (with IBG), the International Association of Sedimentologists, the Geological Society of London, Jesus College, and the British Sedimentological Research Group (BSRG). Many thanks go to the BSRG, British Society of Geomorphology, and the International Society of Aeolian Research for funding my attendance to conferences. This thesis greatly benefitted from the wealth of freely available satellite data from the European Space Agency, the National Aeronautics and Space Administration, and the European Organisation for the Exploitation of Meteorological Satellites. I am thankful to Jesus College for allowing me to teach and join the wonderful academic community there and develop my teaching skills.

This research is indebted to the landowners who generously let me conduct research upon their land in the Kalahari. Their kindness, hospitality, and passion for the Kalahari is infective, and I am immensely grateful to them all. Thank you to South African National Parks who allowed me to conduct measurements in the Kgalagadi Transfrontier Park, and to Gobabeb Namib Research Institute for providing a base for aspects of my research.

Thank you to Jo Nield, Matthew Baddock, the late Joanna Bullard, Rob Byrant, Julie Durcan, the late Andrew Thomas, Jenny Richards, Natasha Wallum, Sebastian Engelstaedter, Katrin Wilhelm, Heather Viles, Richard Bailey, and Richard Grenyer who took time to provide some feedback, academic or career advice whether that be conservations in the field, in the corridor, or over lunch. Your advice has been immensely helpful.

This thesis would not have been possible without my support networks. My friends who became or will soon become doctors in SoGE and beyond, thank you for putting up with my constant distractions and providing a fun and supportive community in which we can flourish. Sport has always been a large passion of mine, thank you to OUWPC and the many people who make the hours in the pool, gym, and road enjoyable. Finally, thank you to my family who have picked up every call and been endlessly supportive in my pursuit of becoming a doctor. I am forever in your debt.

Professor Joanna Bullard passed away a few months after examining this thesis. It was an honour and privilege to have been examined by, and to have known, Jo. Her contributions to aeolian research are far-reaching and profound. Jo's research laid the foundations for this thesis, with her early work in dust production from sand dunes being a central theme together with her more recent investigations into biocrusts. More importantly, her influence on the people around her, through her generosity, enthusiasm, and willingness to help, has left a lasting impact on countless lives. Jo showed me great kindness during the time I knew her, offering encouragement and engaging conversations. For this, I will be forever grateful and will continue to look to Jo as a source of inspiration.

Table of Contents

Abbreviations

AI	Aridity Index
ANOVA	Analysis of Variance
AOD	Aerosol Optical Depth
AVHRR	Advanced Very High Resolution Radiometer
B	Burned plot/site
BA	Burned Area
BSC	Biological Soil Crust
BSCI	Biological Soil Crust Index
BSNE	Big Spring Number Eight
Biocrust	Biological soil crust
C	Control plot/site
CCI	Climate Change Initiative
CV	Coefficient of Variation
ECMWF	European Centre for Medium-Range Weather Forecasts
ENSO	El Niño- Southern Oscillation
EPS	Extracellular polymeric substances
ERA5	ECMWF Reanalysis version 5
ESA	European Space Agency
EVI	Enhanced Vegetation Index
GFED	Global Fire Emissions Database
GUM	Global Unconsolidated sediments Map
ID	Interdune
IPCC	Intergovernmental Panel on Climate Change
K-W test	Kruskal-Wallis rank sum test
KTP	Kgalagadi Transfrontier Park
LAI	Leaf area index
LOI	Loss-on-ignition
M	Mechanical disturbance
MODIS	Moderate Resolution Imaging Spectroradiometer
MODIS BA	Moderate Resolution Imaging Spectroradiometer burned area product
MSG-SEVIRI	Meteosat Second Generation-Spinning Enhanced Visible and Infrared Imager
n	Sample size
NASA	National Aeronautics and Space Administration
NDVI	Normalised Difference Vegetation Index
NIR	Near Infrared
NOAA	National Oceanic and Atmospheric Administration
NOAA CPC	National Oceanic and Atmospheric Administration Climate Prediction Center

NP	National Park
Ob	Objective
PI-SWERL	Portable In-Situ Wind ERosion Laboratory
PPF	Primarily Private Farmland
RGB	Red Green Blue
ROI	Region Of Interest
RPM	Revolutions Per Minute
RSQ	Research Question
S3	Sentinel-3
SASSCAL	Southern African Science Service Centre for Climate Change and Adaptive Land Management
SATVI	Soil-Adjusted Total Vegetation Index
SATVI-TVFC	Soil-Adjusted Total Vegetation Index-Total Vegetation Fractional Cover
SAVI	Soil Adjusted Vegetation Index
SD	Standard Deviation
SSA	Sub-Saharan Africa
SW	Southwest
SWIR	Short Wave Infrared
TOMS	Total Ozone Mapping Spectrometer
TSF	Time Since Fire
UNEP	United Nations Environment Programme
USDA	United States Department of Agriculture
VIIRS	Visible Infrared Imaging Radiometer Suite

Glossary of Terms

Parameter	Description	Units
E_i	PM10 emission flux at PI-SWERL step level *i*	mg m^{-2} s^{-1}
u_{*eff}	Wind shear velocity exerted by the PI-SWERL to the effective area	m s^{-1}
A_{eff}	The effective area of the PI-SWERL	m^2
C	Measured PM10 concentration	mg m^{-3}
C_1	Unitless constant in PI-SWERL calculation	-
C_2	Unitless constant in PI-SWERL calculation	-
d	zero-plane displacement	m
F	Airflow rate	L s^{-1}
FireCCI311	ESA global fire product using Sentinel-3 and VIIRS data from 2019-2022	-
FireCCI51	ESA global fire product using MODIS data from 2001-2020	-
FireCCILT11	ESA global fire product using AVHRR data from 1982-2018	-
GFED5	Global Fire Emissions Database 5 using mainly MODIS data from 1997-2020	-
i	PI-SWERL step level	-
L	SATVI soil adjustment factor	-
MCD64A1	Terra and Aqua combined Version 6 Burned Area data product	-
MOD09GA	Surface spectral reflectance of Terra	-
PM_{10}	Particulate matter with an aerodynamic diameter of 10 micrometres or less	mg m^{-3}
$PM_{62.5}$	Particulate matter with an aerodynamic diameter of 62.5 micrometres or less	mg m^{-3}
t	Duration of step *i*	s
u_*	Wind shear velocity	m s^{-1}
u_{*T}	Threshold wind shear velocity for PM_{10} Emission	m s^{-1}
Z_0	Aerodynamic roughness length	m
α	PI-SWERL roughness value	-

List of Figures

List of Tables

Chapter 1 - Introduction and Aims

Burned dune crests in South Africa with shrubs and grasses in foreground.

1.1 Research setting

Mineral dust is the most abundant aerosol by dry mass in the atmosphere and modulates many key systems on Earth (Adebiyi et al., 2023; Kok et al., 2023). Presently, scientific understanding has a low confidence in predicting future changes in dust emissions and impacts (Szopa et al., 2021). One reason for this uncertainty stems from a lack of reliable mapping of source areas (Okin et al., 2011). Current methods of dust detection largely rely upon space-based remote sensing platforms which struggle to detect small spatial scale, quasi-permanent, or transient sources of dust, such as dust from mines, farms, and fire scars (Eckardt et al., 2020; Ginoux et al., 2012; Okin et al., 2011; Wagenbrenner et al., 2017). These sources of dust have been modelled to be significant contributors to the global dust budget but are rarely captured by satellites (Okin et al., 2011; Wagenbrenner et al., 2017; Wagner and Schepanski, 2025).

Sand dunes are not typically considered to be a significant contributor to atmospheric dust loading (Prospero et al., 2002) due to coarse grain sizes (< 5% silt and clay), which require higher thresholds for aeolian entrainment (Kok et al., 2012). However, recent research has shown that dunes when experiencing aeolian processes have the potential to emit dust due to aeolian abrasion (Crouvi et al., 2012; Cui et al., 2019; Sweeney et al., 2022).

In their typically stabilised state, vegetated dune systems are often excluded from investigations of dust emissions as biomass cover, depending on its extent and nature,

commonly prevents sand movement. The body of plants increase surface roughness and provide physical sheltering, but also trap allochthonous dust particles and allow a finer fraction of sediment to build up at the surface (Gonzales et al., 2018; Suter-Burri et al., 2013; Yan et al., 2011). Disturbance events remove vegetative cover and increase the efficiency of aeolian processes (Wiggs et al., 1995, 1994). Accordingly, large dust emission events have been reported from recently disturbed and activated vegetated dune systems (Bullard et al., 2008; McGowan and Clark, 2008; Yu and Ginoux, 2022).

Fire represents one such significant disturbance factor, forcing rapid shifts in the ecosystem state (e.g., from vegetated to bare) resulting in an increased propensity for aeolian erosion (Mayaud et al., 2017a; Miller et al., 2012; Wasson and Nanninga, 1986; Wiggs et al., 1994). Therefore, it is often assumed that the disturbance and activation of vegetated sand dunes, whether triggered by fire events or caused by the climate-induced aridification of drylands, may increase the prominence of dunes as a significant source of global dust in the future (Bhattachan et al., 2012; Pye, 1989; Sweeney et al., 2023). Further, both the desiccation of drylands (Park et al., 2018) and wildfires (Sullivan et al., 2022) are predicted to increase with anthropogenic induced climate change, further necessitating the need to quantify if dunes can emit dust.

Currently subtropical southern Africa is warming at over twice the global rate of temperature increase, with precipitation rates also being predicted to decrease into the future (Attwood et al., 2024; Dunning et al., 2018; Engelbrecht et al., 2015; Ranasinghe

et al., 2023; Thomas et al., 2005). The predicted heating and drying out of the region raises the debate as to whether it will become a source of dust (Bhattachan et al., 2012; Webb et al., 2020). Yet, while dust emissions from vegetated dune systems have been investigated in other regions, such as the Simpson Desert in Australia (Bullard et al., 2008; McGowan and Clark, 2008; Strong et al., 2010), research remains limited in the geomorphologically and ecologically similar southwest Kalahari dune field. The southwest Kalahari is the driest part of the largest sand sea on Earth and is vulnerable to large scale vegetation dry back from drought, leading to an increased dune activation risk (Thomas et al., 2005) and subsequent dust emission potential (Bhattachan et al., 2012). Dust emissions from the southwest Kalahari can have global implications, particularly dust which is blown into the nutrient poor south Atlantic Ocean (Dansie et al., 2022) or Madagascar Sea (Gittings et al., 2024) which impact marine nutrient and carbon cycles.

Accordingly, this research investigates whether burning is a significant disturbance event that leads to dust emission in the southwest Kalahari dune system. This research advances knowledge on this topic through quantifying the spatiotemporal extent of fire disturbance, quantifying changes in vegetation cover of dunes and other surface properties and measures subsequent changes in emissivity in the southwest Kalahari. Satellite remote sensing data and high-resolution field-based data are used to investigate the occurrence (both frequency and extent) of burning on sand dunes,

determine how fire impacts erosivity and erodibility controls, and to quantify potential dust emissions from the partially vegetated Kalahari linear dune system.

1.2 Research Aim, Questions, and Objectives

The research presented in this thesis aims to improve understanding of the changes in dust emission processes on the southwest Kalahari linear dunes after burning events to address the **overarching aim which is to investigate if the Kalahari dunes emit dust after disturbance by burning.** This thesis adopts a hybrid approach, using both remotely sensed data to understand the spatiotemporal scale of fire in the region, and ground-based measurements to quantify changes in surface properties and dust emissions at burned sites. The overarching aim will be met with three research questions (RSQ) which are divided into sub-objectives.

Research Question 1. What is the pattern, frequency, and timing of fire in the Kalahari dune landscape?

To establish the significance of post-fire dust emissions from the southwest Kalahari dune system, first the spatiotemporal dynamics of burning in the region needs to be inventoried. The first part of the thesis seeks to investigate the spatial and temporal scale of fire using satellite imagery over a 24-year period (2000-2023) and determines

seasonal and annual trends in fire occurrence. This provides the ecological context for investigations into the potential scale of dust emissions in the following chapters.

Research Objectives:

- *Ob 1.1:* Ascertain annual and seasonal trends in both the spatial and temporal distribution of fires on the southwest Kalahari linear dunes from 2000-2023.
- *Ob 1.2:* Establish controls on burning in the southwest Kalahari by investigating land use and global climate cycles.
- *Ob 1.*3: Quantify the duration of the impact of fire on vegetation.

Research Question 2. Does fire affect dust emission potential?

Whilst RSQ1 investigates the amount and frequency of post-fire bare surfaces vulnerable to wind erosion, RSQ 2 investigates if fire affects the emission threshold and flux from dune surfaces. A small portable wind-tunnel (PI-SWERL) is utilised to measure potential dust emissions from control (unburned), burned, and mechanically disturbed surfaces and surface sediment texture is examined to identify fine (dust-sized) particles and any statistical significance between burned and unburned plots. These data are then used to assess if burned surfaces are capable of emitting dust and if fire influences dust emission.

Research Objectives:

- *Ob 2.1:* Establish potential dust flux from burned and control plots.
- *Ob 2.2:* Measure the erosivity threshold on burned and control plots.
- *Ob 2.3:* To determine differences in surface grain size distribution between burned and unburned surfaces.

Research Question 3. What is the impact of fire on dune surface properties?

RSQ 3 focuses on identifying controls on dust emissions through examining in-situ dust emission and surface properties that impact surface erodibility, the longevity of the impact of fire on the surface, and the difference between burned and unburned surfaces. These data help towards resolving the complex interactions between climatological and ecological that influence fire and dust emission in the southwest Kalahari.

Research Objectives:

- *Ob 3.1:* To determine differences in surface properties (surface cover and strength) between burned and unburned surfaces.
- *Ob 3.2:* Establish any immediate post-fire in-situ dust emissions.

1.3 Thesis Structure

This DPhil thesis is presented in the academic paper format; the main body of the thesis consists of three academic papers which have been submitted to peer-reviewed journals (Chapters 5, 6, and 7; Figure 1.1). These chapters are accompanied by an introduction which outlines the research context, aims, and methodology (Chapters 1, 2, and 3), a chapter which enhances the space-based methodology (Chapter 4), and a final discussion and conclusion (Chapters 8 and 9) that summarises the main findings of the thesis and future research directions. Each paper is presented in its journal submission format, albeit some minor formatting changes which are in line with the submission guidelines. A statement of author contribution for each paper is provided in Appendix A.

Following this introductory chapter, a review of dust emission from burned surfaces is then provided in **Chapter 2**, with a focus on partially vegetated dune systems. Subsequently the chapter discusses mineral dust emission, dunes and dust, vegetated dunes, dune disturbance events, and fire. **Chapter 3** details the research approach and methods, starting with the research setting of the southwestern Kalahari dune system. Following this the research methodology is outlined and justified.

To quantify the impact that fire has on the aeolian landscape, first the frequency and extent of fire needs to be mapped. **Chapters 4 and 5** mainly address RSQ1 and focus

on establishing an inventory of fire on the southwest Kalahari linear dunes to achieve this aim. First, methods for burned area detection are discussed and compared in **Chapter 4.** The inventory is established in **Chapter 5** using the Moderate Resolution Imaging Spectroradiometer (MODIS) burned area product (Giglio et al., 2018) which also discusses drivers of fire and records the persistence of the disturbance on the landscape.

Chapters 6 and 7 use ground-based methods to establish the effect fire has on surface properties. A portable wind tunnel is used in **Chapter 6** to answer RSQ 2 and to examine if fire changes the potential dust emission flux from the dune surfaces. **Chapter 7** assesses RSQ 3 and uses in-situ dust measurements and ground cover surveys to elude controls on dust emissions post-fire, as well as explore the duration of bare surface and the temporal window for dust emission opportunity.

The final chapters summarise the main findings of this research and discusses the implications of the findings in the boarder research context. The objectives of the thesis are discussed, and future avenues for research are recommended

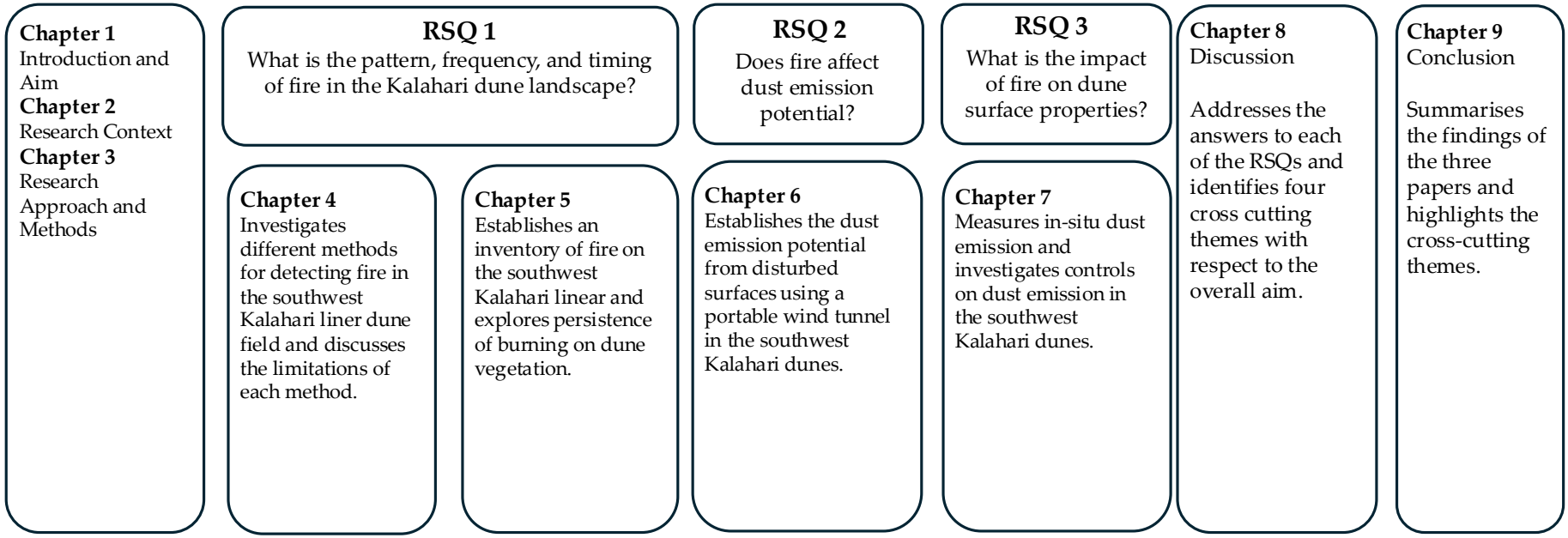

Figure 1.1. Structure of the thesis

Chapter 2 - Research Context

A recently burned dune with active crest and slip face.

2.1 Mineral dust

Wind-blown mineral dust is the most abundant atmospheric aerosol, accounting for more than two-thirds of the global dry aerosol mass (Adebiyi et al., 2023; Kok et al., 2017). Dust comprises small, suspended soil-derived particles in the atmosphere which range in size from < 0.1 μm to more than 100 μm in diameter (Adebiyi et al., 2023; Mahowald et al., 2014; Ryder et al., 2019). The cycle of mineral dust consists of the emission of dust into the atmosphere, suspension, and deposition. Further, dust is considered an important factor in the Earth system, due to its abundance and its associated effects at each stage of the cycle on the Earth system including the ability to modulate the Earth's temperature (Schepanski, 2018). Yet, the *IPCC Report on Climate Change 2021: The Physical Science Basis*, highlights that current scientific understanding has low confidence in estimating future changes in dust emissions and their subsequent impacts (Szopa et al., 2021).

The importance of atmospheric mineral dust

The lack of understanding regarding dust and future global change stems from the wide impacts dust has on the Earth system (Kok et al., 2021b). Airborne dust modulates both the Earth's shortwave and longwave radiation budget through intercepting, scattering, reabsorbing, and re-emitting radiation (Di Biagio et al., 2019; Dufresne et al., 2002; Kok et al., 2023; Schepanski, 2018; Yoshioka et al., 2007). When suspended in the atmosphere, dust also impacts atmospheric chemistry (Gaston, 2020;

Klingmüller et al., 2019; Usher et al., 2003), cloud properties, and precipitation (Adebiyi et al., 2023; Karydis et al., 2017; Storelvmo, 2017). Once dust has been deposited, it can affect biogeochemical cycles through the provision of important nutrients in both marine (Dansie et al., 2022; Hamilton et al., 2022; Jickells et al., 2005; Li et al., 2021; Mahowald et al., 2009) and terrestrial environments (Dong et al., 2020; Harley et al., 2017; Hladil et al., 2010; von Suchodoletz et al., 2013; Winton et al., 2024). The deposition of dust in the ocean can enhance bio-productivity, thus increasing carbon uptake (Dansie et al., 2022; Jickells et al., 2005). It has been suggested that dust deposition has contributed to historic and future atmospheric carbon dioxide concentration fluctuations (Mahowald et al., 2018, 2010). Deposited dust impacts the cryosphere through affecting surface albedo and rates of ice melt (Dong et al., 2020; Lambert et al., 2013; Naple et al., 2025; Skiles et al., 2018; Winton et al., 2024). Furthermore, dust is know it have adverse effects on visibility (Baddock et al., 2014; Hyslop, 2009; Mahowald et al., 2007) with associated transport (Bojdo et al., 2020; Li et al., 2018), human health (Gill, 2018; Goudie, 2014; Middleton, 2020), and air quality hazards (Ardon-Dryer and Aziz, 2025; Chin et al., 2007; Giannadaki et al., 2014; Hilly et al., 2025; Middleton, 2017).

Additionally, atmospheric desert dust provides up to 95% of iron in the global atmospheric iron cycle and the transport of dust provides micronutrients to nutrient-limited ocean ecosystems (Mahowald et al., 2009). As iron is an essential micronutrient that limits ecosystem functions in many of the world's oceans (Crusius et al., 2011),

much attention has been paid to quantifying potential iron content in the dust (Baddock et al., 2013; Bhattachan et al., 2012; Bullard et al., 2007; Bullard and White, 2005, 2002; Crusius et al., 2017; Dansie et al., 2022, 2017a) and identifying sources of iron (Mahowald et al., 2009).

The impacts of dust on the Earth system are heterogenous in both space and time, as the chemical composition of dust, alongside dust loading, is dependent on the underlying geology of their origin (Journet et al., 2008; Kok et al., 2021b). Therefore, quantifying the first stage of mineral dust cycle, emission, is critical to understanding the Earth system.

Erosivity and erodibility controls on dust emission

The emission of dust into the atmosphere is driven by complex interactions between the erodibility of the surface and the erosivity of the wind (Engelstaedter and Washington, 2007; Parajuli and Zender, 2017; Treminio et al., 2024; Webb and Strong, 2011). Erodibility refers to the susceptibility of soil to detach from the surface and entrained by the wind, whereas erosivity refers to the capacity of the wind to detach and transport loose grains (Webb et al., 2021). Generally, when erosivity exceeds the resistance of the erodibility factors, sediment can be detached, and erosion will occur. Surface characteristics complicate this notion, as many properties (such as slope and vegetation) can affect both erodibility and erosivity (Daudon et al., 2024; Wiggs and Weaver, 2012; Wolfe and Nickling, 1993). These interdependent factors, hamper

calculations of dust flux from surfaces, thus quantifying the role of surface characteristics in enabling or supressing emission has been the aim of many field, laboratory, and numerical modelling studies (e.g., Engelstaedter et al., 2006; Hoffmann et al., 2008; Kim et al., 2000; Tegen et al., 2002).

Dust source regions are defined as areas which have high erosivity (high wind speeds) and high erodibility (lots of loose, fine sediment). Dryland systems fulfil these criteria and are susceptible to wind erosion due to sparse or lack of vegetation cover and dry conditions which expose bare soil to the wind. Yet, within drylands there are varying geomorphologies and not all sources of dust are in dryland locations (e.g., Bullard et al., 2011; Meinander et al., 2022; von Holdt et al., 2019).

Sources

Since the early 2000s satellite technology has enabled sources of dust to be identified with Prospero et al. (2002) producing the first global map of dust sources using the Total Ozone Mapping Spectrometer (TOMS). These data presented by Prospero et al. (2002) have been updated as satellite technology has improved both spatially and temporally over the last few decades (Ginoux et al., 2012; Kok et al., 2023; Middleton, 2020; Washington et al., 2003). But in general, the largest sources of dust identified in the original study have remained the same (Figure 2.1). These prolific sources of dust have been identified as closed topographic depressions where plenty of fine alluvial material is deposited and readily available to be eroded by the wind (Prospero et al.,

2002; Figure 2.1). The largest source of dust in the world is the Bodélé depression in Chad (Washington et al., 2003; Figure 2.1), where Paleo Lake Mega Chad stages led to fine sediment accumulation in the basin, into which today's strong winds are topographically funnelled to the area of deflatable sediments (Warren et al., 2007; Washington and Todd, 2005).

Advances in satellite sensor technology as well as changes in sensor configurations (e.g., the use of both geostationary and polar orbiting sensors) have further enabled sources of dust to be identified revealing patterns in both the seasonality and intermittency of dust emissions (Bryant, 2013; Castellanos et al., 2024; Sowden et al., 2018). For instance, the Meteosat Second Generation Spinning Enhanced Visible and Infrared Imager (MSG-SEVIRI) geostationary satellite provides 15-minute resolution multi-spectral data around 0 and 45.5 degrees longitude. Analysis of MSG-SEVIRI data not only enabled high temporal-resolution information on the development of dust storms in the Sahara dust belt to be examined, but in doing so also revealed some previously unidentified dust sources such as sand dunes (Eckardt et al., 2020; Murray et al., 2016; Schepanski et al., 2007; Vickery et al., 2013).

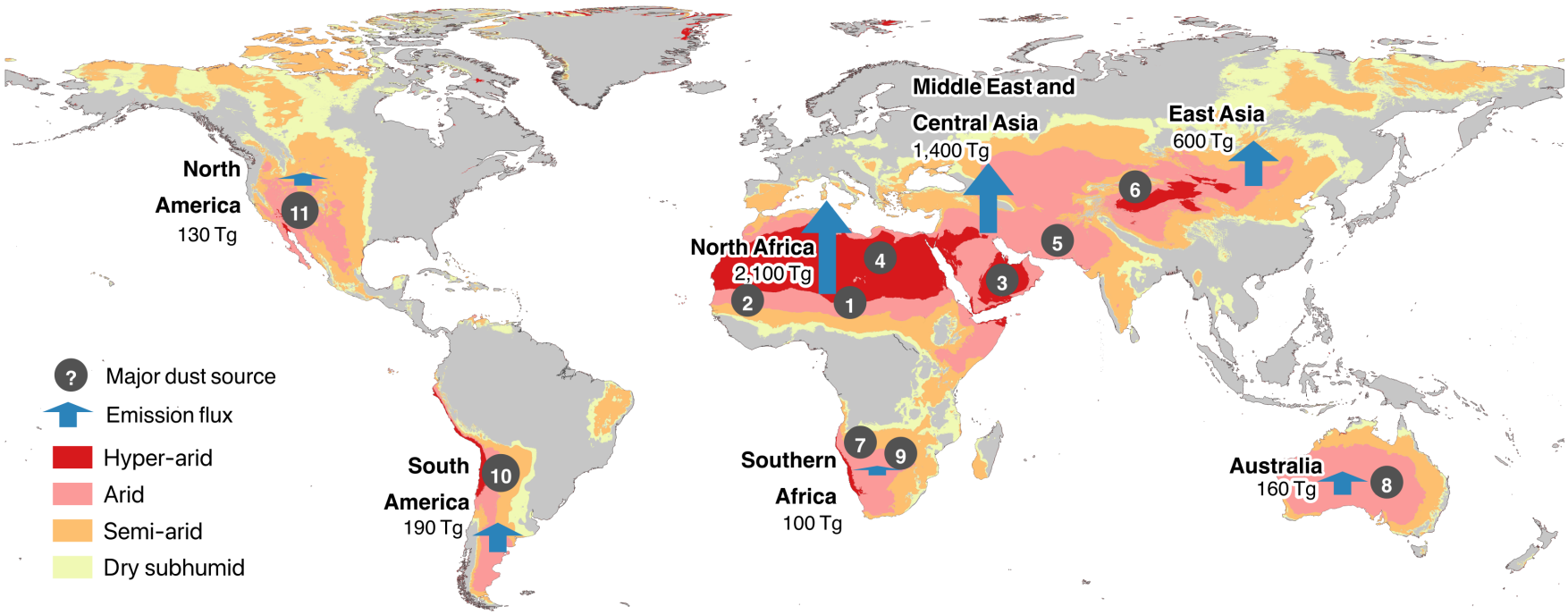

Figure 2.1. Sources of dust in the global dust cycle. The shading represents dryland classification by the aridity index (AI) where hyper-arid regions are in red (AI < 0.05), arid regions are in pink (0.05 < AI < 0.2), semi-arid regions are in orange (0.2 < AI < 0.5), and dry subhumid regions are in yellow (0.5 < AI < 0.65) from Zomer et al. (2022). Emission fluxes (blue arrows) from the main global dust regions are for dust with a geometric (volume-equivalent) diameter of < 50 μm and are based on constraints for 2004-2008 in Kok et al. (2021a). Numbered labels represent locations of major dust sources identified with the Total Ozone Mapping Spectrometer (TOMS) from Washington et al. (2003): **1**: Bodélé Depression; **2:** west Sahara in Mali and Mauritania; **3:** Arabia; **4:** eastern Sahara in Libya; **5:** Makran coast in southwest Asia; **6:** Taklamakan/Tarim Basin; **7:** Etosha Pan; **8:** Lake Eyre Basin; **9:** Makgadikgadi Basin; **10:** Salar de Uyuni; **11:** Great Basin of the United States. Figure is adapted from: Kok et al. (2023) and Wallum (2024) with data sources from Kok et al. (2021a), Zomer et al (2022) and Washington et al. (2003)

Source-specific controls on surface erodibility limit the constraining of fluxes of dust from specific sources in emission models (Bryant, 2013). Many such controls on erodibility are spatially and temporally heterogenous, which models must account for (Kok et al., 2021b). For instance, surface mineralogy can affect the strength of the surface and create areas of erodible and non-erodible material within one geomorphic classification (e.g., an ephemeral lakebed; Reynolds et al., 2007). The surface mineralogy may vary both intra- and interannually as material is deposited and eroded (e.g., due to seasonal flooding; Bryant, 2003). Further factors that affect surface erodibility are vegetation cover, surface crusting (both physical and biological), moisture content, and soil texture (Bryant, 2013; von Holdt et al., 2019; Webb and Strong, 2011). Due to the difficulty in parametrising these conditions, model estimates of dust emission vary vastly (Castellanos et al., 2024; Kok et al., 2021b). For example, dust emission estimates from the global main source areas can vary by up to an order of magnitude between different simulations (Huneeus et al., 2011; Kok et al., 2021a, 2021b; Wu et al., 2020).

The lack of identification of sources of dust has hampered the understanding and modelling of dust emissions (Okin et al., 2011). Investigations into dust emissions have observed that current satellite monitoring struggles to detect small spatial scale, quasi-permanent, or transient sources of dust (Ginoux et al., 2012; Okin et al., 2011; Wagenbrenner et al., 2017). These sources of dust are significant contributors to the global dust budget (Okin et al., 2011; Wagenbrenner et al., 2017). The lack of detection

is due to variabilities in the temporal, spatial, and composition of dust sources (Ginoux et al., 2012; Okin et al., 2011; Urban et al., 2018; Wagenbrenner et al., 2017) and low spatial and temporal resolution imagery (Urban et al., 2018; von Holdt et al., 2019). One such transient dust emission event cause has been identified as vegetation disturbance post-fire (McGowan and Clark, 2008; Wagenbrenner et al., 2017, 2013; Yu and Ginoux, 2022).

Dust after a fire disturbance

Post-fire emissions of dust from burn scars have recently been identified as potential significant contributors to the global dust budget (Hamilton et al., 2022; Meng et al., 2025; Wagenbrenner et al., 2017; Wagner et al., 2018; Yu and Ginoux, 2022). These emissions are hard to quantify as the temporal window for emission can be short due to quick vegetation regrowth (possibly less than 2 months post-burn) and different locations burning each year (Wagenbrenner et al., 2017). Unlike its hydrological counterpart post-fire aeolian soil erosion is relatively under studied, with field investigations spatially limited (mainly in Australia and the USA; Sankey et al., 2012, 2011; Shumack et al., 2017; Strong et al., 2010), a few modelling studies (Wagenbrenner et al., 2017; Wagner et al., 2018; Wagner and Schepanski, 2025), and some more recent remote sensing studies (Yu and Ginoux, 2022).

Yu and Ginoux (2022) produced the first global quantifications of post-fire dust emissions through investigating increases in Dust Optical Depth (DOD) using the

Moderate Resolution Imaging Spectroradiometer (MODIS) Deep Blue Aerosol product. The study revealed increases in DOD over burned aeolian deposits in dryland systems across the globe (Figure 2.2). These sites include fire scars in the partially vegetated dune systems of the Simpson Desert in Australia (also recorded by Bullard et al., 2008 and McGowan and Clark, 2008), Mali and Mauritania, Sudan, the Kalahari Desert in South Africa, and Wyoming, USA (Figure 2.2; Yu and Ginoux, 2022). The post-fire emissions from burned dune systems can be significant sources of dust loading into the atmosphere, for example a dust plume traced to a fire scar in the Simpson Desert covered 85,700 km^2 (McGowan and Clark, 2008).

Figure 2.2. Dust emissions from fire scars on aeolian deposits. In red the MODIS burned area from 2000-2023 (MCD64A1; Giglio et al., 2018) on aeolian deposits from the Global Unconsolidated sediments Map (GUM; Börker et al., 2018) within dryland systems, and dust emission locations identified by Yu and Ginoux (2022) are in orange. Not all burned areas produce dust.

2.2 Sand dunes and dust

Sand dunes are not typically considered to be a significant contributor to atmospheric dust loading (Prospero et al., 2002) due to coarse grain sizes (< 5% silt and clay), which require higher thresholds for aeolian entrainment (Kok et al., 2012). However, many studies pinpointing dust plume origins have placed the sources within both active and vegetated dune fields (Baddock et al., 2011, 2009; Bakker et al., 2019; Bullard et al., 2008; Crouvi et al., 2012; Eckardt et al., 2020; Kandakji et al., 2020; McGowan and Clark, 2008; Vickery et al., 2013). Emissions from dunes have been posited as a potential source for desert loess (Amit et al., 2014; Crouvi et al., 2010, 2008), although this is still debated (Smalley et al., 2019).

Experiments on dust emission from dunes

Wind tunnel laboratory experiments have aimed to understand the dust production process from sand dunes (Baddock et al., 2013; Bullard et al., 2004; Bullard and White, 2005; Sweeney et al., 2023; Swet et al., 2020). The emission of fines from aeolian sand falls into three categories: the suspension of resident fine material already in the sediment, the abrasion of sand grains, and the chipping of clay coatings enveloping the grains (Bullard et al., 2004). Bullard et al. (2004) used sand from the central Australian deserts, a glass 'test-tube' chamber, and air flow to simulate an abrasive environment and found that the removal of grain surface coatings was the main source of fine material generation. Swet et al. (2020) used a wind tunnel to assess fine grain generation from non-coated commercial sand and only found minor emissions

of dust. In a controlled experiment using a portable wind tunnel, Sweeney et al. (2023) used various natural sand surfaces to find that up to 40% of the dust flux came from aeolian abrasion where the presence of coatings or angular grains produced higher concentrations of dust. The same study also concluded that sands with abundant resident fine grains had the largest fluxes of dust which are comparable to the largest dust emitting landforms (such as playas) and found that fluxes of dust increased after 11 minutes of run-time due to aeolian abrasion (Sweeney et al., 2023). Both the creation of fine grains through abrasion and the removal of fine grains by the wind are supply limited. There are no large influx events (i.e., flooding) at a dune field scale and the clay coatings of sand grains also take time to develop. Therefore, sand dunes are supply-limited systems.

In the field, portable wind tunnels have been used to estimate potential dust emissions from dunes (Bacon et al., 2011; Cui et al., 2019; Dickey et al., 2023; King et al., 2011; Sweeney et al., 2022, 2016; Sweeney and Mason, 2013). Sweeney and Mason (2013) matched thresholds of sand movement and dust emission on loess in Nebraska, USA and summarised that the emission of dust is dependent upon the aeolian erosion of sand. Other field studies found that dune surfaces are emissive, but concentrations of dust are lower than other highly emissive sources such as dry washes or playas (King et al., 2011; Sweeney et al., 2016). Some studies highlight the substantial potential for dust emissions from dune fields by highlighting the vast spatial extent of dune fields

(Bhattachan et al., 2012; Bullard et al., 2004; Crouvi et al., 2012; Sweeney et al., 2016). Since dune fields occupy approximately 20% of dryland regions, the total emission flux across large surface area of dune fields is comparable to the concentrated emissions from highly emissive surfaces (Bhattachan et al., 2012). This reasoning is used to classify dune fields as significant potential contributors to global dust emissions historically and in the future (Bhattachan et al., 2012; Bullard et al., 2004; Crouvi et al., 2012).

Dust from vegetated dunes

Pye (1989) hypothesised that vegetated dunes are sinks of dust; the vegetation traps allochthonous dust and some fine grains can be produced by pedogenesis. Pye (1989) further proposed that active dunes are sources of dust, hence if a vegetated dune becomes de-vegetated, it may transition from a dust sink to a dust source (Figure 2.3.; Pye, 1989). The emission of dust from activated dunes will persist as long as the dune has low vegetation cover so that sand grains can saltate, abrade, and produce fine grains (Figure 2.3). The emission of abrasion-produced dust may be low level, for higher rates of emission there must be some other form of fine grain supply. Sweeney et al. (2023) updated the work of Pye (1989) and showed that low-level dust emission from activated dunes can continue to occur due to aeolian abrasion (Figure 2.3). These low-level, diffuse, and plume-less emissions are difficult to detect through remote

sensing and may be significantly underrepresented in dust models (Okin et al., 2011; Urban et al., 2018). Sweeney et al. (2023) also identified much larger fluxes of dust in the initial stages after reactivation when the resident fines are liberated (Figure 2.3). These large emissions may be observable as plumes of dust which have been recorded from vegetated dune fields in Australia (Figure 2.4; Baddock et al., 2009; Bullard et al., 2008; McGowan and Clark, 2008) and the Kalahari in southern Africa (Eckardt et al., 2020; Vickery et al., 2013). Therefore, vegetated, stabilised dune fields currently exist in a state where environmental factors prevent dust emission. But the stabilised dunes are vulnerable to de-vegetation events which could potentially switch the dunes to becoming large sources of dust.

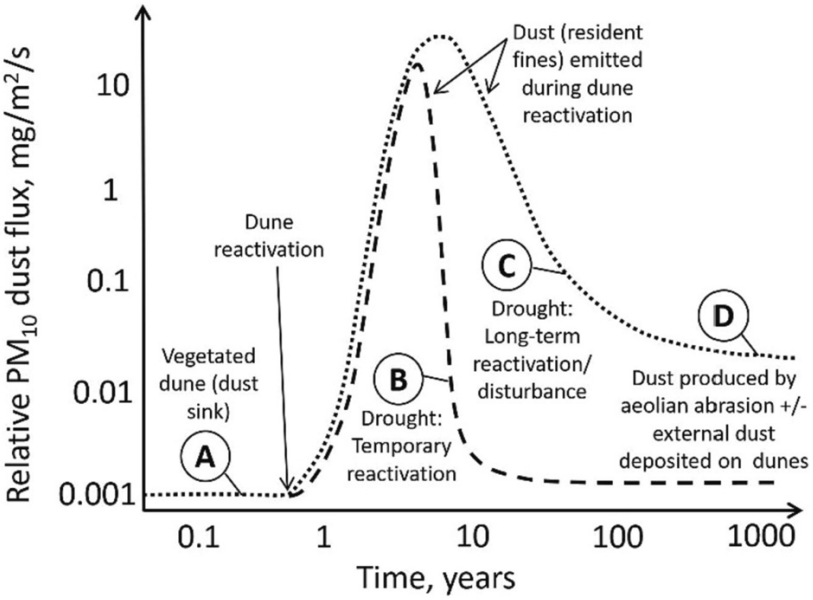

Figure 2.3. The hypothetical transition of a stabilised vegetated dune to an activated dune and potential dust flux. Stabilised dunes are a sink for dust until they are activated when resident fines are rapidly emitted at a high rate. Once the resident fines have been exhausted, dust will continue to be emitted through abrasion - if the dune remains de-vegetated. If the dunes are re-vegetated, dust flux drops to background levels. Figure is from Sweeney et al. 2023, which is adapted from Pye, 1989.

The work of Sweeney et al. (2023) assumes that the rate of abrasion can continue for extended periods of time (Figure 2.3). Yet observations of dust emissions from active dunes are frequently not concentrated or continuous (i.e., diffuse; note that no dune sources are explicitly presented in Figure 2.1). It is likely that there is some form of fine sediment exhaustion resulting from the rare plume emissions that are observed from currently active dune fields (Figure 2.4). The most important factor affecting the number of dust-sized particles produced by natural sand dunes is the presence of clay coatings on the grains (Bullard et al., 2007). These coatings need time to develop and relatively stable, non-erosive conditions to form. Therefore, long periods of stabilised dune environments are needed for these coatings to develop (Busch, 2020). Without the coating the straight abrasion of non-coated, angular sand grains produces much lower rates of dust emission (Bullard et al., 2007; Swet et al., 2020). Further, fine sediment recharge is needed in these systems to provide resident fine material, this can take form of allochthonous dust deposition or pedogenesis, which too will take time and stable conditions to build up. Once built up, these resident fines are expelled quickly after sediment becomes available for wind erosion (Sweeney et al., 2023; Yizhaq et al., 2009). This leads to the emissions characteristics of sand dunes that are observed today - concentrated plumes of dust observed from recently activated systems combined of resident and coated-mineral abrasion fines (Figure 2.4) and low-level diffuse emissions of abraded, non-coated grains from long term active sand dunes.

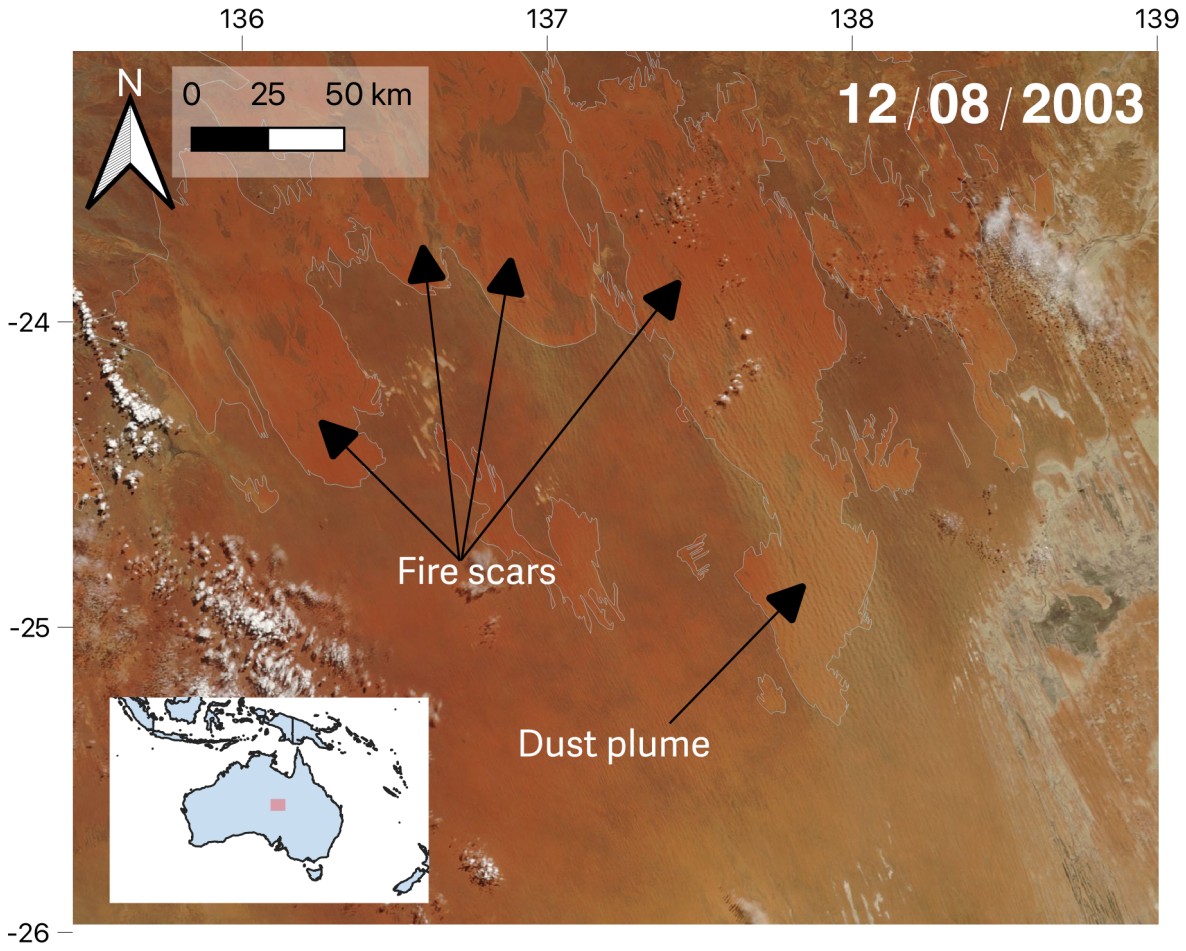

Figure 2.4. Dust plumes from fire scars in the Simpson Desert, Australia captured by MODIS Terra on 12/08/2003. Fire scars are outlined in white.

Dust in the southwest Kalahari dune context

Linear dune systems have been modelled to assess if they are likely to be activated and become potential sources of dust in the future (Ashkenazy et al., 2012; Mayaud et al., 2017b; Thomas et al., 2005). An example of this is the southwest Kalahari dune field where Thomas et al. (2005) forecast enhanced dune activity as early as 2039 through increases in mean wind speed and the development of a negative moisture budget. Bhattachan et al. (2022, 2012) used this notion to investigate the potential of the southwest Kalahari to emit dust and found that potential future dune remobilisation

may lead to dust emissions at a similar level to those observed from major contemporary dust sources in southern Africa.

Bhattachan et al. (2012) highlighted the future potential of the Kalahari as a source of dust. Sediment samples were collected from the dune field and run through an artificial dust generator which found that the interdune dust emission potential of the sediment is around 30% of that of the major dust source pans in the region (Etosha and Makgadikgadi; Bhattachan et al., 2012). Moreover, the fine grains were rich in iron, so that if the material is emitted, it can have significant effects on the ecosystem where it is deposited (Bhattachan et al., 2012). In a further study, Bhattachan et al. (2013) found that the loss of vegetation could lead to a substantial increase in dust emissions from the Kalahari dunes, through exploring in-situ emissions under various land covers. Bhattachan et al. (2022) then went on to examine the efficiency of dust production from the Kalahari soil and found that when accounting for the entire dune field (~87,000 km^2) the potential of the region to emit dust is comparable to other active sources in the region. Recently, Gittings et al. (2024) used a model to back-calculate dust deposited in the Madagascar Sea which was attributed to phytoplankton blooms and found that a source region is the southwest Kalahari following subtropical anticyclonic conditions which draw in westerly winds.

2.3 Factors that affect surface stability on vegetated dunes

Dune fields are found across the globe and form when there is or has been plenty of available sediment and strong enough winds to transport the sediment (Figure 2.5). Classification of sand seas is neither consistent nor clearly defined in the literature, but is based on the current state of the dune which broadly depend upon interactions which include, amongst others, ecological and sediment transport processes (Ballinger et al., 2019; Courrech du Pont et al., 2024; Thomas, 2011). One such classification scheme (Figure 2.5), divides the dunes into three forms: active, probably limited activity, and fixed (Thomas, 2011). Herein, probably limited activity and fixed dunes are referred to as stabilised dunes.

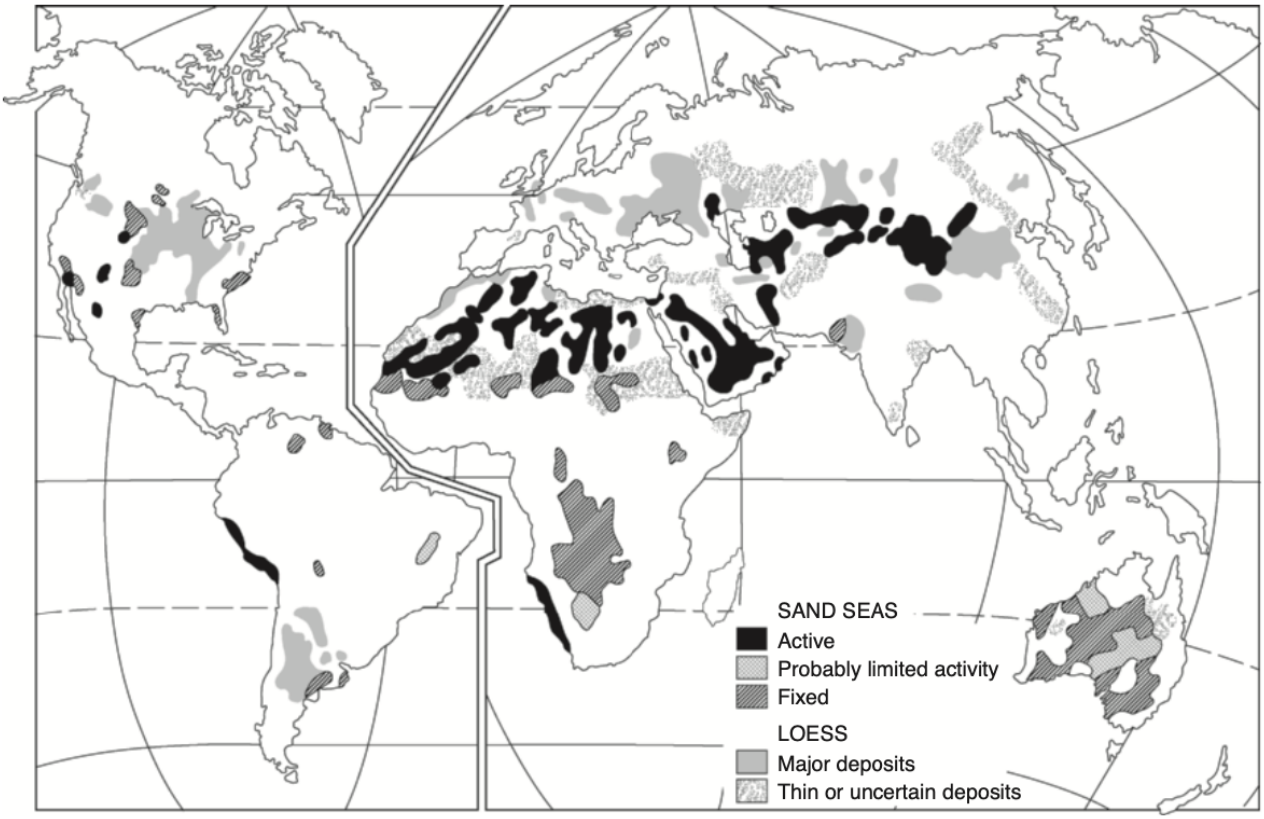

Figure 2.5. The global distribution of aeolian deposits with sand seas divided into active, probably limited activity, and fixed dune systems. Figure from Thomas (2011).

Vegetation

Dunes can be stabilised by spatially extensive vegetation cover (Fisher and Hesse, 2019; Hesse and Simpson, 2006; Wiggs et al., 1995). Vegetation alters the wind flow, providing drag which changes the velocity profile and erosion dynamics at the surface (Leenders et al., 2007; Mayaud et al., 2016a; Suter-Burri et al., 2013; Wiggs et al., 1994; Wolfe and Nickling, 1993). In dryland landscapes, vegetation affects the erosivity of the wind and the erodibility of the surface through three principal methods (Mayaud and Webb, 2017; Wolfe and Nickling, 1993). First, vegetation provides physical sheltering of the surface by covering a portion of the soil and through providing an area of low flow in the wake of plants (Leenders et al., 2007; Mayaud et al., 2016b; Wolfe and Nickling, 1993). Second, vegetation traps sediment which is in transport and promotes localised deposition (Okin et al., 2006; Suter-Burri et al., 2013). Third, vegetation is a form of roughness which increases both the aerodynamic roughness (Z_0) and the zero-plane displacement (d) (Figure 2.6.; Jackson, 1981; Mayaud et al., 2016b; Wiggs et al., 1994). If the vegetation elements is closely spaced such that there is little bare interspace between individual plants, the air flow is displaced upwards so that it skims across the plants (Figure 2.6; Mayaud et al., 2016a; Wiggs et al., 1994; Wolfe and Nickling, 1993), preventing the airflow from reaching the surface and thus limiting aeolian erosion.

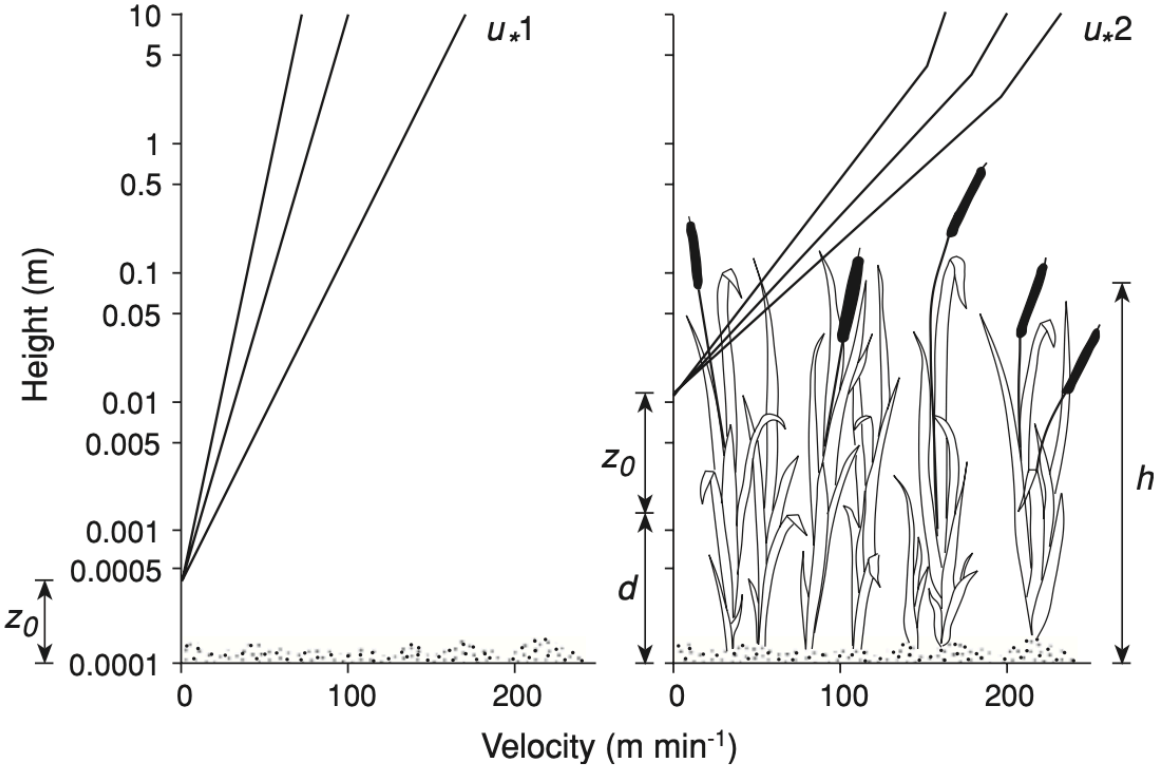

Figure 2.6. Vegetation effect on velocity profile structure: h = mean vegetation height, d = zero-plane displacement. Figure from Wiggs (2011).

Vegetation on dunes is often considered an indicator of dune stability but caution needs to be taken when defining dune fields as simply active or stable (Livingstone and Thomas, 1993). Regarding dune fields in this sense assumes that activity and stability are discrete states. However, stability and activity are just points on a continuum and high vegetation cover does not signify inactivity (Ash and Wasson, 1983; Bullard et al., 1997; Livingstone and Thomas, 1993; Siegal et al., 2013; Wiggs et al., 1995; Wolfe, 1997). The large interannual and spatial variability in precipitation which is characteristic of dryland systems leads to ephemeral and patchy vegetation cover (Bailey, 2011; Wolfe and Nickling, 1993). As a result, periods and patches of aeolian activity can occur within a dune system classified as stable. Activity is

particularly prevalent in partially vegetated dune systems where drier years can result in mass biomass dieback, increased bare surface, and the crest of dunes only offer sparsely populated trees. Evidence of aeolian activity is frequently found in these landscapes (e.g., rippled surfaces or exposed roots; Figure 2.7)

Figure 2.7. Evidence of aeolian activity on a dune crest in the partially vegetated dune field of the southwestern Kalahari. The *Acacia erioloba* tree has exposed roots (A), ripples are present at the dune surface (B), and there is sand deposition in the lee of the log (C).

In dust emission models, emission flux is often estimated by threshold friction velocity, sediment texture, friction velocity, and soil moisture (Kok et al., 2014; Parajuli and Zender, 2017). These are then constrained by other variables which impact

erodibility such as sediment supply and vegetation. Therefore, much research has gone into identifying thresholds of vegetation cover that limit aeolian erosion in dryland landscapes (Ash and Wasson, 1983; Fisher and Hesse, 2019; Lancaster and Baas, 1998; Munson et al., 2011; Wiggs et al., 1995). These estimates of effective cover vary with location, with measurements placing thresholds at 15% at Owens Lake in California (Lancaster and Baas, 1998), 10% in the Colorado Plateau (Munson et al., 2011), 14% in the Kalahari (Wiggs et al., 1995), and 30% in Australia (Ash and Wasson, 1983) which was further refined to 16% by Fisher and Hesse (2019). It is important to note that although cover percentage is an effective measurement for easy model input (Kim et al., 2013; Wu et al., 2016), this method is reductionist in its approach due to other factors such as plant pliability, porosity, and configuration adding significant complexities to wind erosion models (Mayaud and Webb, 2017).

Vegetation is a fundamental control on sediment movement in dune environments, but difficulty arises in quantifying the role of vegetation due to its heterogeneous nature and variability in both space and time, as well as changing pliability and porosity. Work to constrain these parameters and link them back to wind erosion is currently on going (Kono et al., 2025; Kono and Okuro, 2021; Mayaud and Webb, 2017; Shumack et al., 2022; Treminio et al., 2024).

Biological soil crusts

Another ecological factor that influences surface stability on sand dunes is biological soil crusts (BSCs or biocrusts; Figure 2.8). Globally, biocrusts cover 12% of land surface and 25% of dryland soil surfaces (Rodríguez-Caballero et al., 2018). Biocrusts are commonly found in the top one centimetre of sediment and are communities of algae, fungi, cyanobacteria, lichens, and mosses (Belnap and Lange, 2001; Büdel et al., 2009; West, 1990). Thomas and Dougill (2007) explored biocrusts in the Kalahari Desert and found that crusted surfaces have a greater compressive strength, higher organic matter, and larger surface roughness than near-by bare ground. Biocrusts fill an ecological niche and have several functions within the Earth system including providing ecological functions that are normally delivered by plants where vegetation is sparse, fixing carbon and nitrogen, and altering the surface albedo (Büdel et al., 2009; Elliott et al., 2019; Thomas and Dougill, 2007). Biocrusts function as an ecosystem engineer through their ability to survive desert daily temperatures and recolonise quickly after grazing disturbance (Elliott et al., 2019), and can alter surface properties such as water infiltration (Bowker, 2007), roughness (Bullard et al., 2018), and strength (Thomas and Dougill, 2007).

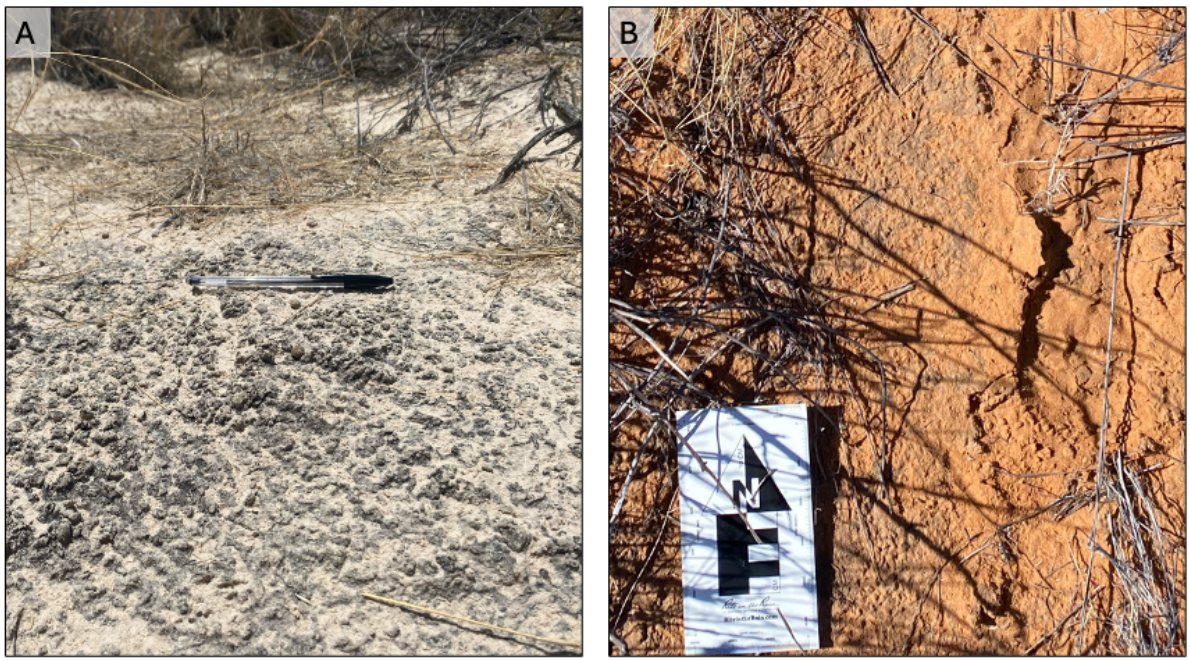

Figure 2.8. Examples of different biological soil crusts in vegetated dune environments. (A) is a biocrust found at White Sand Dunes, USA and (B) is a biocrust found in the Kalahari. Both biocrusts display discolouration to the sediment and create microtopography.

In geomorphology, biocrusts are of particular interest due to the encrusted layer they form on dryland soils. The strong crust is formed through two main mechanisms: filamentous sheath material entangling grains; and the secretion of extracellular polymeric substances (EPS) which agglutinate particles (Figure 2.9; Rodríguez-Caballero et al., 2022; Thomas and Dougill, 2007). Combined these effects create a strong cohesive layer which decreases the erodibility of the surface and suppresses dust emission (Rodríguez-Caballero et al., 2022b). Thomas and Dougill (2007) found that biocrusts have a significant stabilising effect on partially vegetated dunes. In the Kalahari, biocrusts have been recorded covering between 11 and 95% in different locations, occupying bare interspaces between individual plant elements, as well as under shrubs (Thomas and Dougill, 2007). Within the matrix of biocrusts there are

often abundant fine grains due to the trapping of allochthonous dust and soil weathering processes (Figure 2.9; Garcia-Pichel et al., 2016; Verrecchia et al., 1995; Weber et al., 2022)

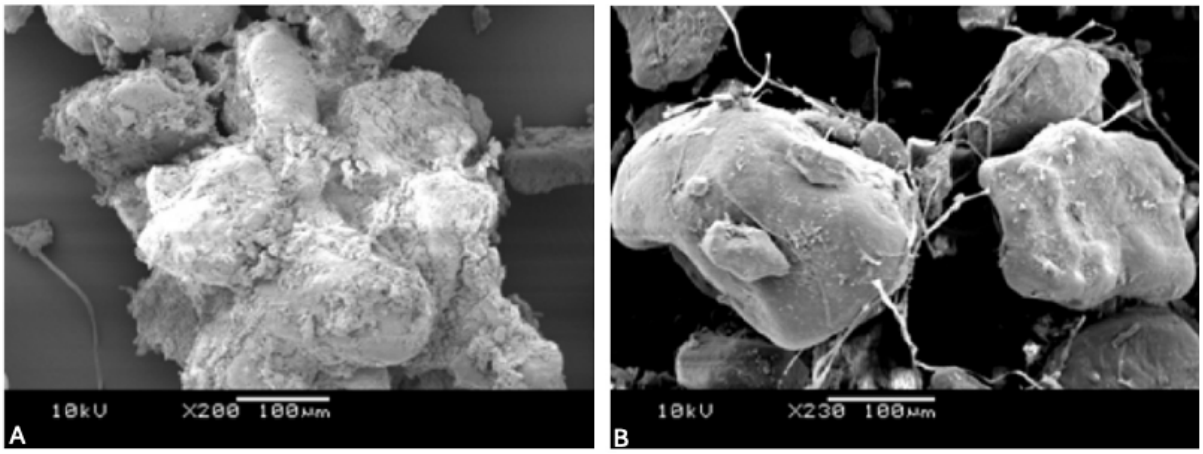

Figure 2.9. Ways in which biological soil crusts agglomerate sand grains. (A) sand grains are bound by extracellular polymeric substances, and (B) sand gains are bound by filamentous cyanobacterial sheath material. Trapped fine grains are visible in the image (B). Scanning electron microscope images from Thomas and Dougill (2007).

The role of biological soil crusts in preventing dust emissions has gained more traction over recent years but it still not completely understood (Pointing and Belnap, 2014; Rodríguez-Caballero et al., 2022b). By influencing dust emissions, biocrusts indirectly impact biogeochemical cycling, ecosystem functioning, and human health (Rodríguez-Caballero et al., 2022b). Rodríguez-Caballero et al. (2022) combined field data and a global aerosol model to estimate that biocrusts reduce global dust emissions by around ~ 60%. The model outputs also showed that future changes in land use and climate will see a 25 to 40% reduction in biocrust cover by 2070, equating to an increase in global dust load of around 5 to 15% (Rodríguez-Caballero et al.,

2022b). This global model used existing data from studies investigating biocrusts effect on threshold friction velocities, but the spatial extent of these studies is limited, with data exclusively coming from the USA, Australia, and China (Rodríguez-Caballero et al., 2022b). At a more localised scale, Fick et al. (2020) used a portable wind tunnel to find that ground which was artificially inoculated with biocrust in Utah, had up to a two-fold reduction in dust emission. The disturbance of biocrusts has been linked to decreased threshold friction velocities in many desert environments including Tengger Desert (Zhang et al., 2008) and Gurbantunggut Desert both in China (Zhang et al., 2006) and Mojave Desert, California (Belnap et al., 2007). Further data are needed on the soil-stabilising role of biocrusts to help constrain the effect of biocrust on reducing wind erosion. Currently, there are no investigations into the role that biocrusts play in limiting dust emissions from the southwest Kalahari dune field.

Wind power

The movement of sand is further affected by the available wind power. For sediment to move, the wind must be strong enough to displace grains, with some researchers concluding that present day dune stability is due to a decline in windiness rather than an increase in precipitation and consequent vegetation cover (Ash and Wasson, 1983; Bullard et al., 1996; Yizhaq et al., 2013, 2007). Low windiness as a factor (amongst others such as vegetation cover and grazing) in dune stabilisation is evidenced by bare dunes coexisting with vegetated fixed dunes under the same climatic conditions. A modelling study by Yizhaq et al. (2007) shows that in environments where wind

power is high or low, dunes remain in one state - active or fixed (stabilised) respectively (Yizhaq et al., 2007).

In moderate wind power environments both dune states can coexist leading to the emergence of bi-stability (Yizhaq et al., 2007). This is the case in the Kalahari, one of the reasons for the current largely stable state of the dunes in the region is low wind energy (Thomas et al., 2005). Yet, wind energy is predicted in increase into the future with global warming as mean wind speeds are expected to double (Thomas et al., 2005). Many models now use the combination of wind power and vegetation to parametrise dune mobility (Baas and Nield, 2007; Mayaud et al., 2017a; Okin, 2008; Yizhaq et al., 2007). By modelling both vegetation and wind power dune mobility models have shown how partially vegetated dunes are bistable with alternative stable states where both bare and fixed dunes will maintain their mobility levels under similar conditions (Bhattachan et al., 2014; D'Odorico et al., 2013).

In partially vegetated dune environments, vegetation, biological soil crusts, and moderate wind power maintains the stable fixed state, but if disturbed beyond a critical level, the system switches to an alternative stable state of bare, active dunes (Bhattachan et al., 2014; D'Odorico et al., 2013), which in turn can lead to dust emissions (Pye, 1989). In partially vegetated dune environments these disturbances tend to be events which remove the protective vegetation cover. Dune fields therefore

have limited resilience; once perturbed the landscape may not necessarily recover and the switch in state can be irreversible (Bhattachan et al., 2014).

2.4 Disturbances on vegetated dunes

Disturbance events on vegetated dunes primarily are where biomass is removed. These events include, but are not limited to, livestock grazing, human habitation, mineral extraction, wood harvesting, recreational use, fire, environmental stochasticity (particularly drought), and predicted long-term climate change (Milton and Dean, 2000; Pointing and Belnap, 2014; Thomas and Twyman, 2004; van Rooyen and van Rooyen, 1998). These events are also not mutually exclusive and often co-occur and interdepend upon one another. For example, water points for livestock grazing is a disturbance in the Kalahari (Perkins, 2018; Thomas and Twyman, 2004) and is an intersection of both livestock grazing and human habitation. This section focuses on the most cited disturbance factors: drought, grazing, and fire.

Drought

Drought is a common occurrence in drylands due to high interannual rainfall variability. Annual grass cover largely depends upon precipitation to germinate and grow (Figure 2.10; Smit et al., 2024). Therefore, in drier spells, when there is not enough precipitation to support grass growth, vegetation also displays marked temporal variability (Smit et al., 2024). Without vegetation to protect the surface (Figure 2.10), increased aeolian activity can occur (Wiggs et al., 1994). Increased

aeolian activity during a dry period has been observed in the Nebraska Sand Hills (Mangan et al., 2004) and Australian Deserts (Hesse and Simpson, 2006). In South Africa, Eckardt et al. (2020) linked drought to dust emissions from sandy soils. Many perennial species of vegetation are adapted to drought conditions with seeds being able to last many years before germinating or plants having large roots to find deep sources of moisture (Aranibar et al., 2004; Bhattachan et al., 2014; Smit et al., 2024; Thomas et al., 2012). Yet currently research has not been conducted to make a link between drought and dust emissions from partially vegetated dune fields.

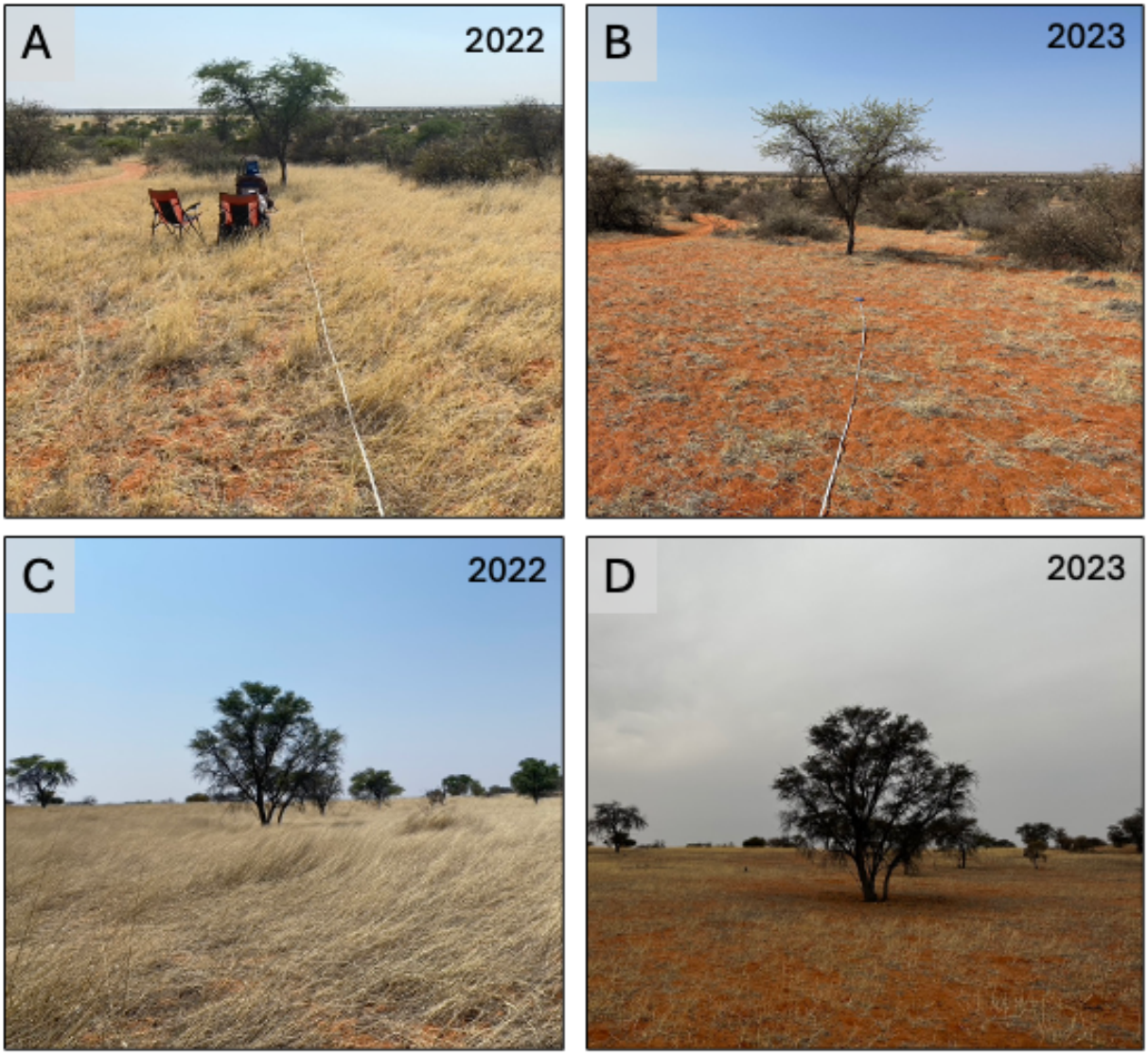

Figure 2.10. The reduction in vegetation cover due to low precipitation. Photos in each row are of the same location on dunes on farmed land in the Kalahari. (A) and (C) were taken in October 2022, and (B) and (D) were taken in September 2023 – a year when the region was experiencing significant drought. In 2023 there is much less surface protection afforded to the surface by vegetation. In both the 2022 images the dominant grass is the annual *Schmidtia kalahariensis,* a largely invasive species that can become dominant in areas of heavy grazing (Bhattachan et al., 2014; Thomas and Twyman, 2004).

Grazing

Grazing is another form of de-vegetation disturbance (Figure 2.11). Animals selectively graze palatable species, which are generally perennial grasses, leading to

the dominance of annual grasses in grazed land (Thomas and Twyman, 2004). These annual grasses keep a high level of cover in wet years, but dieback markedly in the drier years (Figure 2.10). Grazing can alter vegetation structure, with longer term grazing increasing shrub cover (D'Odorico et al., 2012; Eldridge et al., 2011; Thomas et al., 2018). Shrub encroachment has been observed in drylands across the world affecting the dynamics of the system (Archer et al., 2017; Eldridge et al., 2011). For example, in New Mexico, rates of wind erosion can be 20 times higher in shrubland compared to grassland (Li et al., 2022). Biocrusts are easily damaged by grazers, reducing surface coverage (Dougill and Thomas, 2004; Thomas et al., 2018). In the Kalahari, Thomas and Dougill (2007) found an inverse relationship between grazing and biocrust cover, increasing the erodibility of the surface.

Figure 2.11. Localised dust emission during the herding of cattle in the Kalahari.

Fire

Burning of surface vegetation (Figure 2.12) can have a significant impact on sand dune mobility (Fisher and Hesse, 2019). Fire destroys both perennial and annual vegetation, thus plant protective effects are removed (Ravi and D'Odorico, 2009), increasing the wind shear stress on the dune surface (Wiggs et al., 1994). Vegetation removal by fire has been theorised to link to increased dune mobility (Bhattachan et al., 2022, 2012; Mayaud et al., 2017b; Sweeney et al., 2023), dust emissions (Baddock et al., 2009; Bullard et al., 2008; McGowan and Clark, 2008), a reduction in soil nutrients (Okin et al., 2006), and a decrease in air quality (Wiston, 2017). But few field or remote studies have investigated the effect of fire on dryland dune systems. Further, current methods for detecting vegetation fires poorly constrain burned area, leaving gaps in our knowledge of how much land burns (Chuvieco et al., 2022). With climate change and anthropogenic activity, the occurrence of fire on dune fields (and globally) is changing (Sullivan et al., 2022), requiring further detailed investigations.

Figure 2.12. An active fire burning vegetation on the southwest Kalahari dune field. Image: K. Steenkamp.

2.5 Landscape fires

Landscape fires are a natural part of the Earth system where biomass burns. Fires occur in all vegetated parts of the planet and are formed and shaped by underlying geology, vegetation dynamics, and climate (Archibald et al., 2005; Johnston et al., 2024). Landscape fire science covers a wide range of topics, the next section of this chapter discusses two veins of this research: detection and fire in arid to semi-arid drylands.

Detection of burned area

Chuvieco et al. (2018) calculated that an estimated four million square kilometres of global land burns annually. However, this number is most likely a conservative estimate with some calculations placing the true burned areas at 1.8 times that amount (Chuvieco et al., 2019). This discrepancy highlights an ongoing lack of consensus in the fire science regarding burned area estimation and associated trends. The lack of consensus is likely caused by small fires (< 100 ha) which are hard to detect using satellite sensors (Chuvieco et al., 2022, 2019; Khairoun et al., 2024; Ramo et al., 2021; van der Velde et al., 2024), but also due to conflation of terminologies. For example, the recent United Nations Environment Programme (UNEP) report on wildfire cites increasing wildfire occurrence globally (Sullivan et al., 2022), whereas most journal articles find a decreasing trend (Andela et al., 2017; Bowring et al., 2024; Jones et al., 2022). The lack of consensus is likely due to inconsistent use of 'fire' and 'wildfire', where wildfires are unusual or extraordinary free-burning landscape fires which negatively influence social, economic, or environmental values (Sullivan et al., 2022). Herein, burning is referred to as fire, as biomass combustion is a common and natural occurrence in partially vegetated dune systems and cannot be considered unusual or extraordinary (DaSilva et al., 2021; Stavi, 2019).

Globally, the instance of fire has been decreasing for the last quarter century due to agricultural expansion and a reduction in savanna fires (Andela et al., 2017; Bowring et al., 2024; Chen et al., 2023; Jones et al., 2022). Whilst the amount of burned area (BA)

each year is decreasing, the economic and environmental impacts of fire are expected to increase, highlighting complex fire-human-climate interactions (Bowman et al., 2020). This dichotomy between impacts and trends underpins the need to understand the drivers behind fire occurrence and impacts. Many studies have tried to do such, by deducing the impacts of fire-human-climate interactions at both regional (Chuvieco et al., 2022; Pricope and Binford, 2012; Ramo et al., 2021; van Etten et al., 2021) and global (Andela et al., 2019; Burton et al., 2020; Chen et al., 2023; Jones et al., 2022) scales. Drivers of fire have been identified as interdependent factors such as fuel (vegetation) properties including moisture and connectivity (Jones et al., 2022; Kelley et al., 2019; van Etten et al., 2021), humans (Andela et al., 2017; Bowman et al., 2020; Bowring et al., 2024), and climate cycles (Burton et al., 2020; Chen et al., 2017; Shi and Touge, 2022).

One large problem with calculating global fire trends is that there is difficulty in getting an accurate representation of how much land is burning each year. Global BA products are designed to have good agreement over global scale systems, but often perform poorly at local and regional scales (Chuvieco et al., 2019; Giglio et al., 2009). BA detection relies upon remote sensing, but, like the detection of dust, there are multiple limitations in using satellites on a global scale to generate burned area datasets (Chuvieco et al., 2019). Such limitations include overarching sensor problems of cloud cover, over-pass frequency, over-pass timing, and coarse spatial resolution imagery (Chuvieco et al., 2019; Hawbaker et al., 2008; Laris, 2005). With fire detection

specifically the location of the fire has a different spectral signature, requiring sensors to be calibrated at a local scale (Marsett et al., 2006; Poitras et al., 2018). The impacts of fire are not binary (burned/unburned), but instead are a wide range of conditions which vary upon fire behaviour, fire type, and time between the fire extinction and image acquisition (Chuvieco et al., 2019).

Currently, studies are focusing on creating global BA databases that represent the closest to the true burned area (Chuvieco et al., 2019). These methods are continuously being updated and reanalysed. Popular global products include the North American Space Agency's (NASA) MODIS MCD64A1 burned area product (Giglio et al., 2018), the European Space Agency's (ESA) FireCCI51 product (Figure 2.13; Lizundia-Loiola et al., 2020), and the Global Fire Emissions Database (GFED; Chen et al., 2023). It is widely recognised that these global products routinely miss small fires, as well as produce other omission errors (false-negatives) and commission errors (false-positives; Jones et al., 2022).

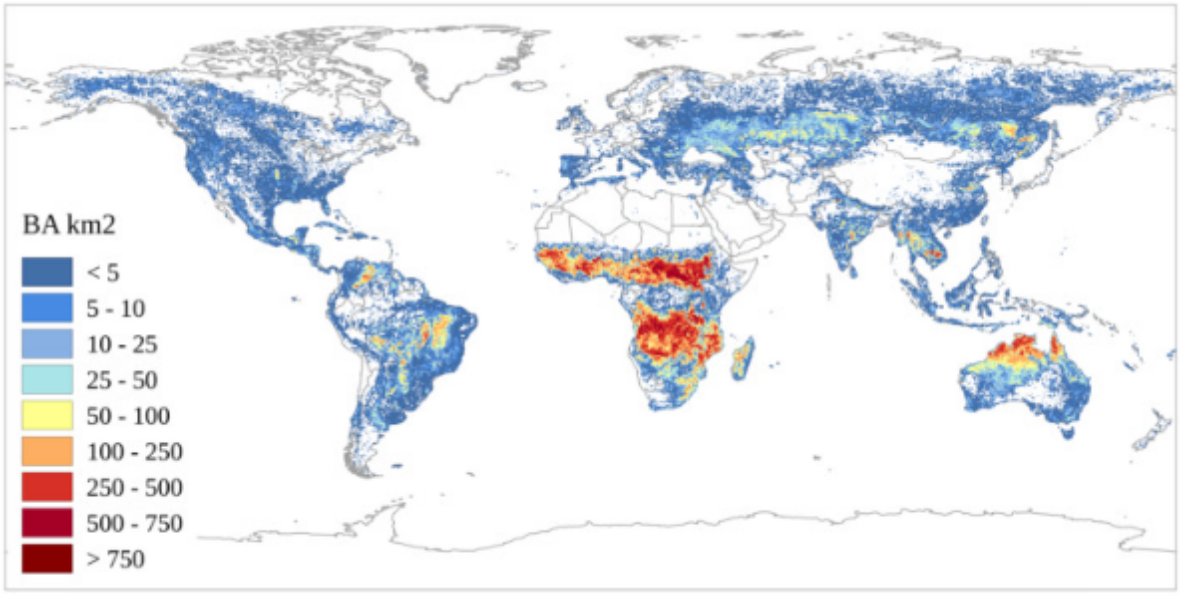

Figure 2.13. Average global burned area 2001 – 2018 using the ESA FireCCI51 product. Figure from Lizundia-Loiola et al. (2020).

Fire in arid to semi-arid drylands

Semi-arid to arid drylands have a distinct context in terms of fire occurrence. They exist in the zone between hyper-arid regions where fire is extremely rare and only occurs after high-rainfall events which enhance fuel loads, and mesic regions where fire regimes are driven by occasional droughts making vegetation more flammable (van Etten et al., 2021). Subsequently, fires in the arid regions are linked to global climate systems such as the El Niño Southern Oscillation (ENSO) which can provide wet conditions for vegetation to grow in drylands (Andela and Van Der Werf, 2014; Chen et al., 2017; Mariani et al., 2016; Shikwambana et al., 2022). Bridging the gap between drought-initiated fires, and precipitation-initiated fires, in arid to semi-arid drylands fire can only occur when fuel has accumulated sufficiently, and fuel loads are spatially connected (Andela et al., 2019; Mariani et al., 2016). The subsequent

timing of fires results from a close interplay between the time since the last fire, and other disturbances such as grazing or human activities that remove vegetation (van Etten et al., 2021). In savanna environments commonly found in arid and semi-arid zones, the fuel structure and climate conditions result in high rates of fire spread (Andela et al., 2019). Fires in savanna regions are quick-burning and the discontinuous vegetation cover results in burns covering relatively small amounts of land (Andela et al., 2019).

In arid to semi-arid drylands, for a fire to spread, conditions must be such that flames can breach the bare interspace between vegetation patches and ignite adjacent patches (Burrows et al., 2009). Once burning, fire pathways are shaped by the landscape, vegetation, topography, and ignition source (McLauchlan et al., 2020; van Etten et al., 2021), and fire severity can vary within a burned area due to variation in fuel type and loads, weather conditions, topography, or maturity of the vegetation (Chuvieco et al., 2023). Fire severity measures the impact of the fire on the local environment and is linked to vegetative cover loss (Lentile et al., 2006). The more severe a burn, the longer lasting the ecological and related geomorphological effects (Lentile et al., 2006). Hence fire severity is important to quantify in relation to the longevity of fire impacts. Fires burn hottest beneath shrubs (>250 °C) and cooler in grass patches (~120 °C) and bare interspaces (<90 °C; Ravi et al., 2009). Weather conditions can play a crucial role in fire spread, with the heat from the fire and corresponding convective updrafts resulting

in major disturbance in the tropospheric wind and temperature fields (Clements et al., 2007; Wagner et al., 2018), and continuing the spread of the fire.

In partially vegetated and vegetated dune fields fire is a normal part of the system, with fires being observed on dune fields around the globe (Figure 2.2). Yet, there is still poor scientific consensus on how fire affects aeolian landscapes. Of the research that has been conducted, many studies have focused on historic fires as an explanation for dune activation (Buckland et al., 2019; Oehler et al., 2024; Patton et al., 2023), rather than looking at changes in surface properties. In investigating contemporary fires Levin et al. (2012) found in the Great Victoria Desert, Australia, that fire is an important factor in controlling dune activity, through the reduction in vegetation and biocrust cover. Fisher and Hesse (2019) expanded upon this in the Simpson Desert, Australia and found the only sites of surface activation were within fire scars, with fire causing significant changes in vegetation cover. In the South African Kalahari, Wiggs et al. (1994) measured near surface winds speeds 200 percent greater in burned sites than unburned sites and suggested greater surface activity at burned sites. No studies have specifically looked at dust emission from burned areas on desert sand dunes.

Research in the cold-steppe desert of the Great Plains in the USA (Kansas and New Mexico) have shown that fire can also reduce the inter-particle cohesion between soil

grains (DeBano, 2000; Ravi et al., 2007; Figure 2.14). The burning of vegetation releases fatty acids onto the soil underneath the plant and these organic compounds condense and wrap around the soil grains, decreasing the strength of interparticle bonding and dynamics of water retention (Ravi et al., 2007; 2009). This leads to increased hydrophobicity of the soil where plants used to grow (DeBano, 2000). Most of the research into the increased hydrophobicity and aeolian activity has taken place in the cold-steppe desert and has not been expanded to different geomorphological features such as dune fields. Differing sediment textures found in different locations impact the water retention capacity of the soil; therefore, soil hydrophobicity properties may vary in differing landscapes.

Fire also has important implications for biological soil crusts. Globally, there is no scientific consensus on the survival of biocrusts after fire, with recorded increases in coverage post-fire in the Columbia basin (Dettweiler-Robinson et al., 2013), New South Wales, Australia (Eldridge and Bradstock, 1994), California (Palmer et al., 2023a), and Oregon (Bowker et al., 2004), decreases in coverage in Utah (Evangelista et al., 2004) and Australia (Levin et al., 2012; Strong et al., 2010), and similar coverages in California (Palmer et al., 2023b) and the Tanami Desert (Nicholas et al., 2009). Palmer et al. (2020) conducted a meta-analysis of studies on biological soil crusts and fire, and found no investigations in southern Africa.

Once a fire removes protective surface vegetation, a feedback cycle may leave the dune in an active state (Figure 2.14). A bare surface is hostile to both vegetation and biocrust regrowth (Strong et al., 2010). Saltating sand grains can abrade and bury biocrusts, resulting in crust mortality (Kidron et al., 2017; Neuman and Maxwell, 2002; Figure 2.14). In the Negev Desert in Israel, Kidron et al. (2017) found distinct erosion 'cirques' on dune surfaces where biocrusts had been buried, died, and subsequently surface sediment had been eroded. Abrasion can impact vegetation regrowth with juvenile vegetation being unable to withstand the constant bombardment of grains (Kadmon and Leschner, 1995; Figure 2.14). By having an active (saltating) surface, dune can maintain their bare state.

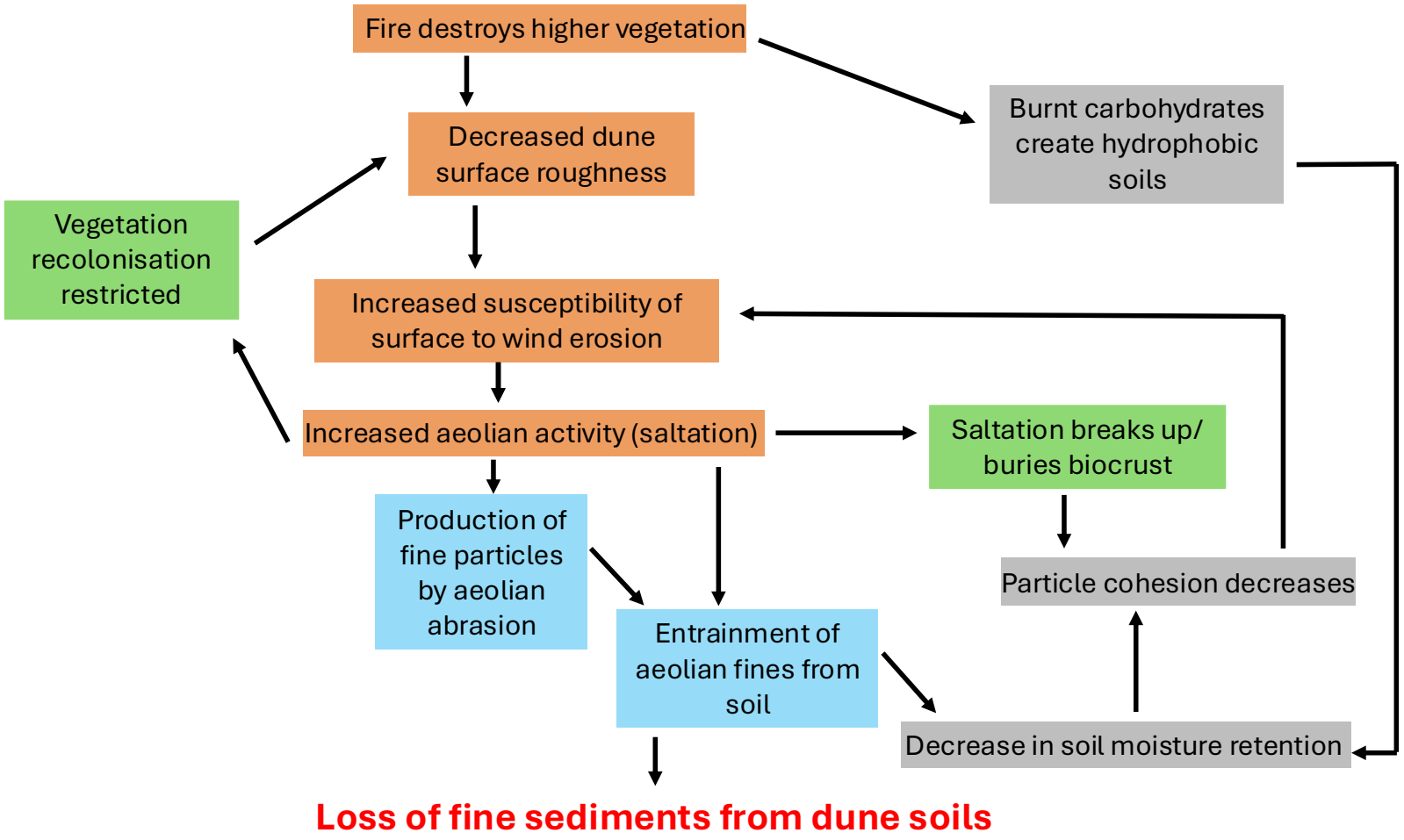

Figure 2.14. The processes behind post-fire dune aeolian activity and destabilisation. Adapted from Strong et al. (2010).

The duration where vegetation remains below threshold cover is therefore the temporal window in which sand movement and dust emission post-fire can occur. Hence, quantifying the ability of a fire to remove the protective vegetation cover and the duration of reduced shelter is an important factor in measuring post-fire surface propensity to dust emissions. Studies in dune fields have placed this recovery period at one to five years in the Great Victoria Desert (Levin et al., 2012), ten years on *Spinifex* dominated dunes in northeastern Australia (Wasson and Nanninga, 1986), and five years has been suggested for the linear dune field in the southwest Kalahari, although this study also included vegetation structure its calculations (Wiggs et al., 1994). While many studies link the duration of reduced cover to precipitation where large rainfall events lead to an increase in vegetative surface cover (Fisher and Hesse, 2019; Levin et al., 2012).

The size of the burn is important as the larger the size of the burned area, the more surface area there is for aeolian action. Mayaud et al., (2016a) investigated in the southwest Kalahari the distance downwind of continuous vegetation cover where the winds reach erosive potential and found that the winds return to equilibrium within 12 -20 heights of the height of the continuous vegetation cover. This buffer zone around the edge of fires is extremely small in relation to the size of the fire and may only impact narrow fire paths.

2.6 Research context summary

Mineral dust is an important and poorly quantified aspect of the Earth system. Current methods of remote sensing struggle to detect small spatial scale, diffuse, quasi-permanent, or transient sources of dust, including dust emissions from fire scars. Sand dunes have been found to emit dust through aeolian abrasion. These emissions are often diffuse and are poorly constrained, particularly using remote sensing. Disturbance events, such as fire have led to easily identifiable plumes of dust being emitted from sand dunes, but these infrequent events have not been the focus of many dust emission studies.

Factors that impact the amount dust potential of burned dune systems are poorly constrained. This includes the size of burned area on arid zones is underestimated due to different vegetation types and post-fire surface spectral changes. The duration of reduced vegetation cover also varies globally and has not been investigated under a variety of climatic conditions. Further, the role of biocrusts in preventing the emission of dust relies on a few spatially explicit studies and is not investigated in southern Africa. Combined with the lack of data on whether biocrusts survive fire, little is known about how biocrusts may help prevent erosion post-fire.

Some research has been conducted in on the above topics, but little research has been conducted in southern Africa. The impact of fire is predicted to increase with anthropogenic induced climate change, further necessitating the need to quantify if dunes emit dust post-fire.

Chapter 3 – Research Approach and Methods

A fence dividing different farms with varying grazing pressures in the Namibian Kalahari.

To reduce overlap with the chapters that are written in academic paper format, some aspects of the methodology elements are discussed in depth in Chapters 4, 5, 6, and 7. The aim of this chapter is to introduce and justify the methods used and include methods that are not fully discussed in the further chapters of the thesis. The first part of this chapter details information on the study region including site justification. Next, the methodological approaches used to address the research questions of this thesis are detailed.

3.1. Study Region

3.1.1 Study region context

The southwestern Kalahari linear dune field (Figure 3.1) study region covers over 120,000 km^2 in South Africa, Namibia, and Botswana. The linear dunes in this region cover the western portion of the Kalahari Sand Sea in eastern Namibia (Figure 3.1 and 3.2), the Northern Cape of South Africa, just branching into Botswana before degrading to dune-like patterns resembling barchanoid ridges to the east (Bullard et al., 1995; Garzanti et al., 2022; Thomas and Wiggs, 2022). The most common dune form in the study area is classified as vegetated linear dunes which extend mainly NNW to SSE (Thomas and Wiggs, 2022). Near river valleys and pans dune patterning is less regular and more complex (Bullard et al., 1995). The dune crests are spaced 0.2 to 2 km apart with heights ranging from 5 to 25 m (Bullard and Nash, 1998). The dunes consist of unconsolidated aeolian sands of mainly quartz and feldspar (Garzanti et al., 2022; Lewis, 1936; Thomas and Wiggs, 2022) with the distinctive red colour of the Kalahari

sediment a result of thin iron coatings on the grain surfaces (Lewis, 1936). These coatings are relatively rich in soluble iron, an important micronutrient for ocean productivity, should the sediment be mobilised as dust (Bhattachan et al., 2012).

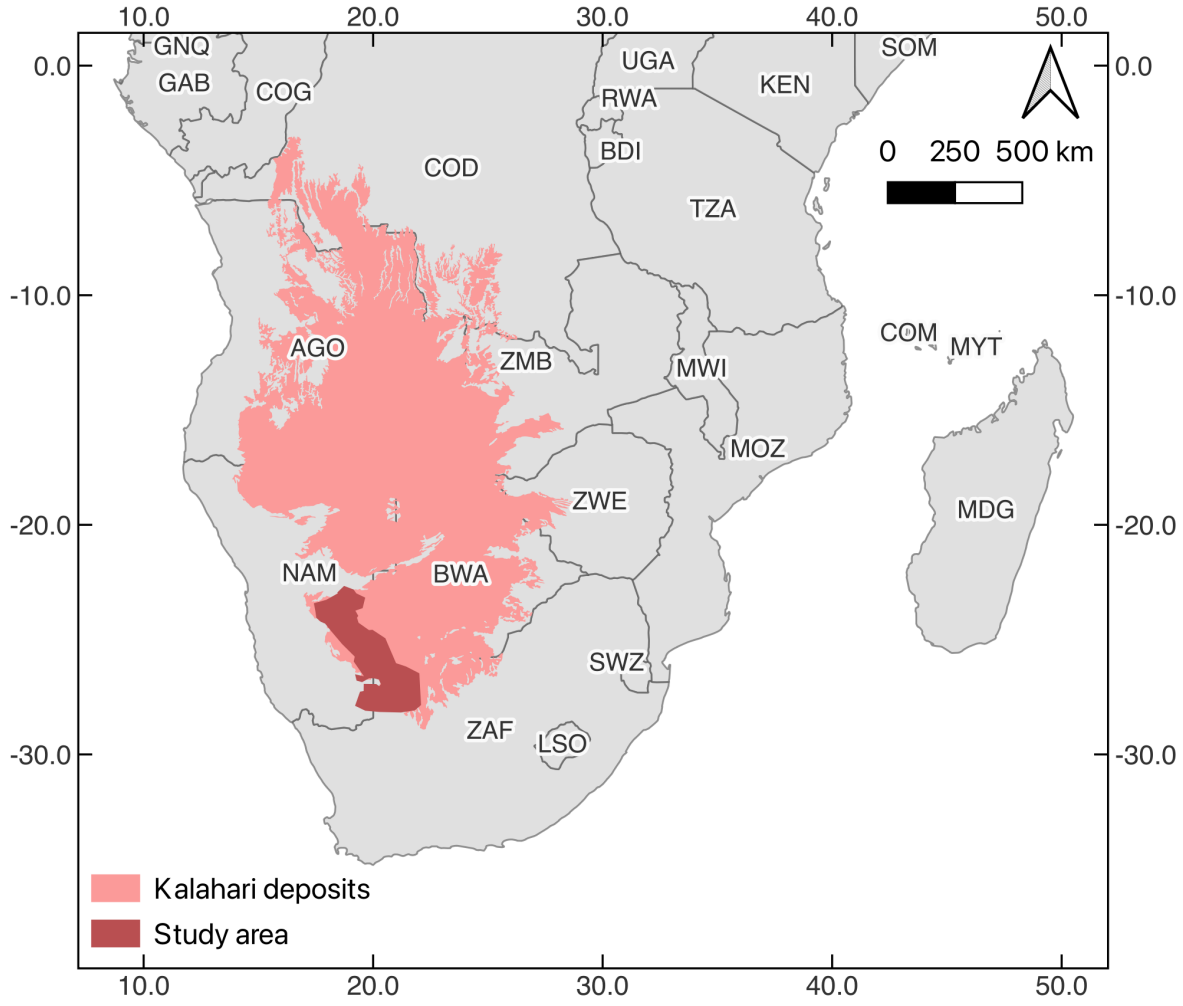

Figure 3.1. The geographic location of the Kalahari linear dune system and the study area within southern Africa and the Kalahari sand sea based on geology data from the South African Council of GeoSciences.

Figure 3.2. Partially vegetated linear dunes near Hoachanas, Namibia in August 2022. The image is taken from a tall dune crest with other linear dunes in the background. The dunes support mixed vegetation cover with the interdunes being well covered in grass species (*Schmidtia kalahariensis)* and a few trees (*Acacia haematoxylon).* The bare dune crests have occasional perennial grasses (*Stripagrostis amabili)* and shrubs *(Grewia flava)*.

The southwestern Kalahari linear dune system experiences a strong north to south precipitation gradient (Figure 3.3). Additionally, there is an east-west variation in precipitation with the western edge of the dune field receiving less precipitation than the east (Figure 3.3). The region experiences a mean annual rainfall of 150 to 450 mm (van Rooyen and van Rooyen, 1998) and precipitation is often highly variable in both space and time. As with most dryland regions, in any given year there can be significantly more (e.g., 2006, Figure 3.3) or less (e.g., 2023, Figure 3.3) precipitation with a high interannual variability of 50% (Figure 3.3; Bhattachan et al., 2014; Thomas and Leason, 2005; Thomas and Wiggs, 2022). Rainfall occurs most often in the summer months December to March.

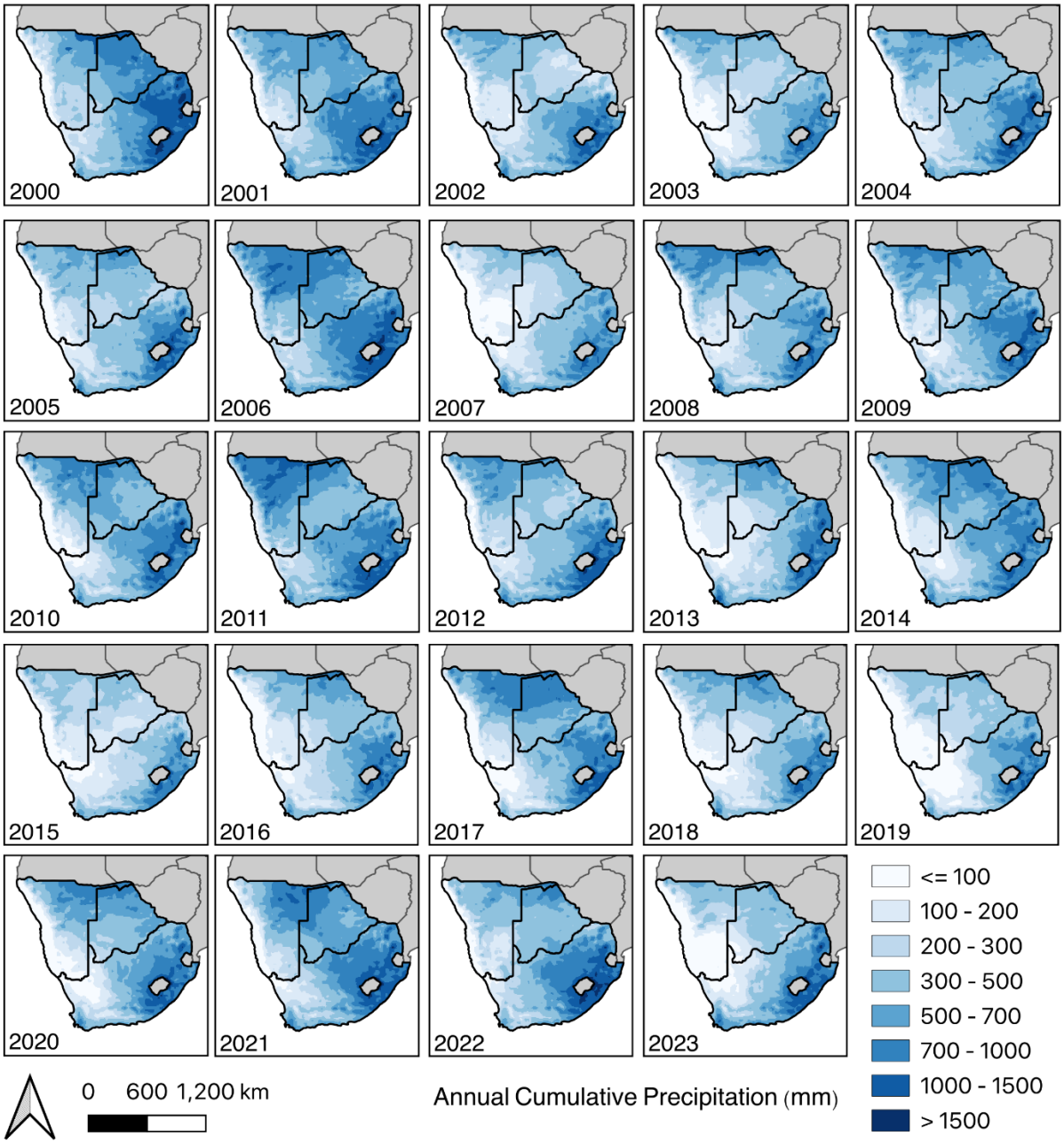

Figure 3.3. Annual cumulative precipitation (mm) in Namibia, Botswana, and South Africa using ERA5-Land reanalysis data from 2000 - 2023 (Muñoz-Sabater et al., 2021). Dry years, (2003, 2007, 2013 – 2016, 2018 - 2020, and 2023) although less common, often indicate drought conditions such as the 2018 to 2020 southern Africa drought. Whereas wet years (2000 – 2002, 2004 - 2006, 2008 - 2012, 2017, and 2021 - 2022) are more frequent but range in cumulative precipitation. For example, there was an extremely yet season in 2006 and a more moderate wet season in 2008.

There is enough water in the southwest Kalahari dune system to support partial vegetation cover on the dunes (Figure 3.2). Vegetation is highly dependent upon precipitation for increases in biomass, with drought periods reducing the vegetation cover (Smit et al., 2024). The typical vegetation in the study area is Kalahari Xeric Savanna (van Rooyen and van Rooyen, 1998), which is controlled by current and historic land use (Bhattachan et al., 2014). Vegetation primarily consists of a mix of trees (e.g., *Acacia haematoxylon;* Figure 3.4f), perennial shrubs (e.g., *Grewia flava* and *Acacia mellifera*; Figure 3.4b), perennial grasses (e.g., *Eragrostis lehmanniana*), and annual grasses (mainly *Schmidtia kalahariensis;* Figure 3.4a). Other types of vegetation such as forbs and creepers (Figure 3.4e) are also observed. In farmed land, vegetation mainly consists of annual grasses such as *Schmidtia kalahariensis,* the lack of perennial grasses has been linked to the overgrazing of land (Bhattachan et al., 2014; Thomas and Twyman, 2004).

Biological soil crusts (biocrusts or BSCs; Figure 3.5) are ubiquitous with the Kalahari landscape and can be found in both naturally grazed and farmed lands. Thomas and Dougill (2007) observed biocrust cover of between 11 and 95% and found that the biocrusts are concentrated under woody and thorny shrubs likely due to the protection the vegetation provides from grazers. Mager (2010), found presence of biocrusts in both grassy interspaces and under shrubs. However, Elliott et al. (2014) recorded that grass interspaces were dominated by cyanobacterial crusts but rarely found biocrusts under shrubs or trees. Additionally, constant burial by sand forces

biocrusts to restrict crust development forcing the crusts to mostly stay unconsolidated or in early successional stages in the dunes (Thomas and Dougill, 2007). But micro-topographical features, can indicate biocrusts at a later development stage (Figure 3.5; Thomas and Dougill, 2007).

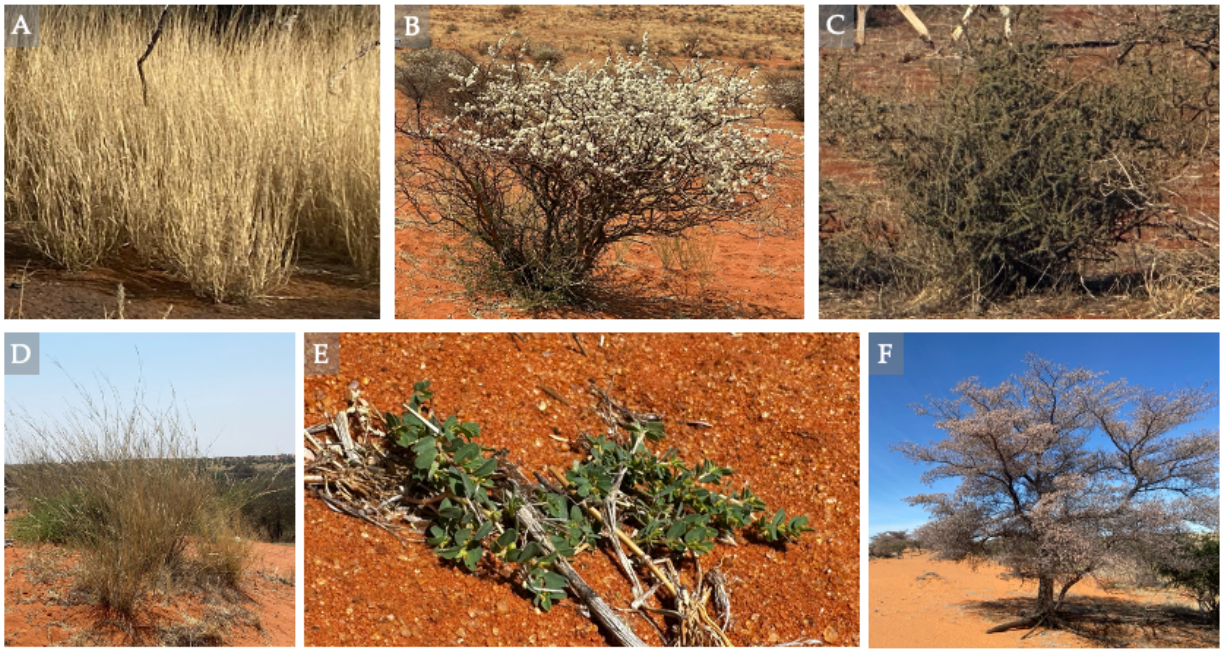

Figure 3.4. Common vegetation found in the study area. (A) *Schmidtia kalahariensis* an annual grass. (B) *Acacia mellifera* a shrub. (C) *Lycium hirsutum* a shrub. (D) *Stripagrostis amabilis* a perennial grass. (E) *Requienia sphaerosperma* a forb. (F) *Acacia haematoxylon* a tree.

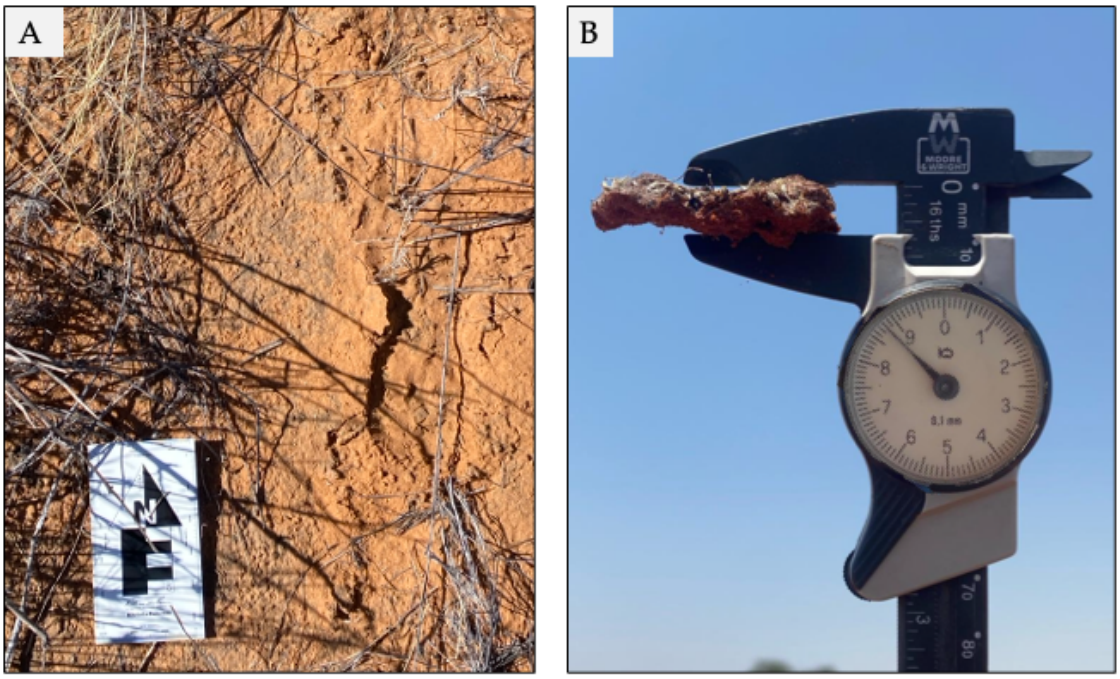

Figure 3.5. Biological soil crust in the Kalahari. (A) An undisturbed biocrust that has created microtopography and discoloured the surface. (B) The thickness of a biocrust sample at 0.88 mm.

The classification scheme developed by Thomas and Dougill (2004), identifies three stages of biocrust in the Kalahari: a weakly consolidated crust with evidence of extracellular polymeric substances (EPS) and filamentous sheaths, but no surface discolouration (Type 1); A more consolidated crust with a speckled black or brown surface (Type 2); and a crust with microtopographical features which is black or brown at the surface (Type 3; Figure 3.6).

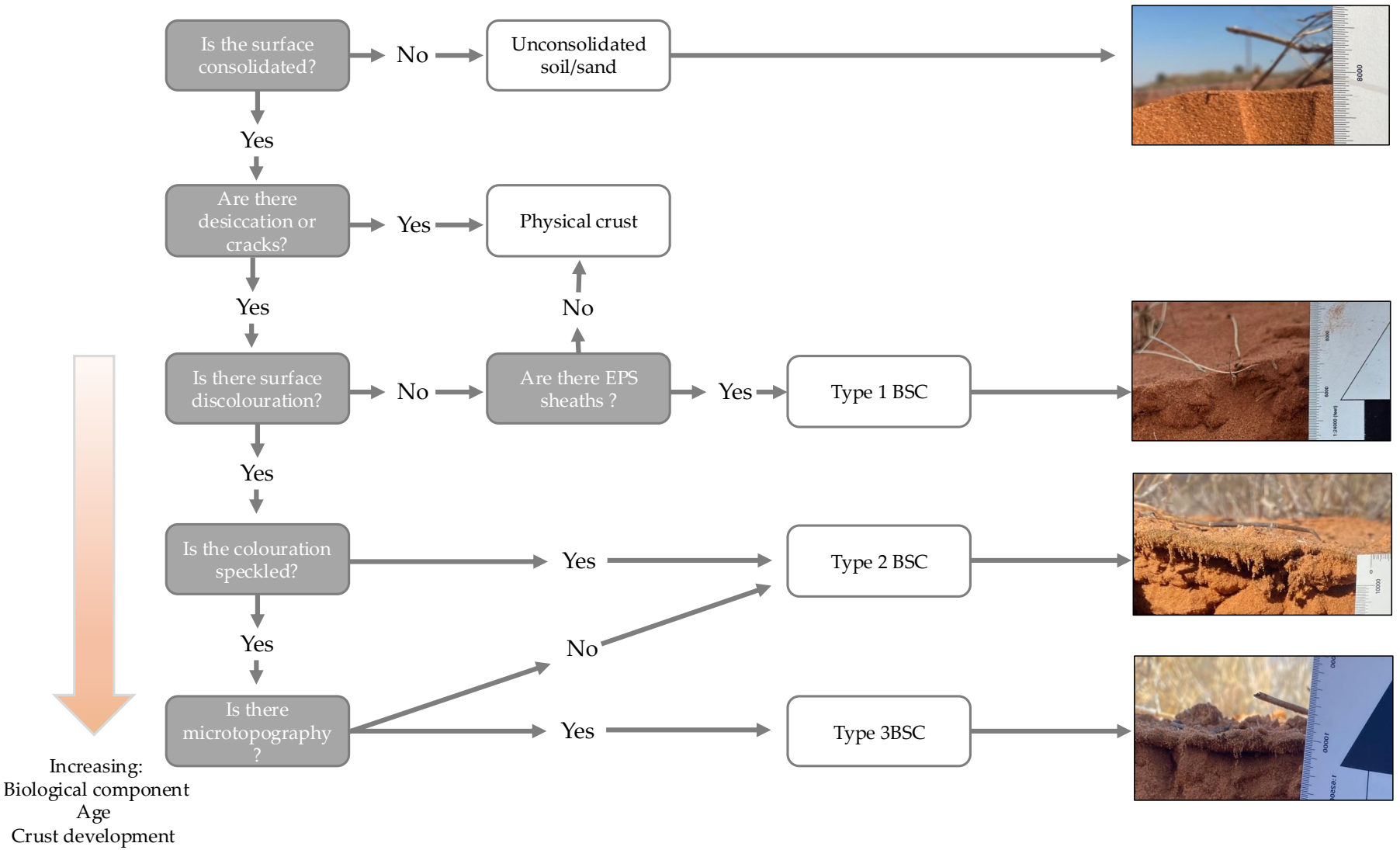

Figure 3.6. Biological soil crust classification based on crust colour and morphology. Adapted from Thomas and Dougill (2004).

Present day vegetation cover, precipitation, and low wind energy limit aeolian activity in the southwest Kalahari linear dune field (Bullard et al., 1997; Wiggs et al., 1995, 1994). This notion can be further broken down by the topography of the dunes where, on the lower flanks and interdune areas, sediment transport is controlled mainly by low ambient wind energy (i.e. erosivity limited), while on the upper dune slopes and crests above ground biomass limits aeolian activity (i.e. erodibility limited; Wiggs et al., 1995). Multiple field-studies have observed evidence of geomorphological activity in the dune field including sand ripples, slip faces, and sharp dune crests (Figure 3.7; Bhattachan et al., 2022; Bullard et al., 1997; Thomas and Twyman, 2004; Wiggs et al., 1995, 1994).

Figure 3.7. Ripples on the crest of a sand dune in the Kalahari

Currently, much of the southwest Kalahari linear dune field (Figure 3.8) consists of agricultural land, which is either community-administered or privately owned and used for livestock production, which is the case for all the Namibian portion of the study area. However, much of the South African study area consists of the Kgalagadi Transfrontier Park (KTP) located in the Northern Cape of South Africa and into Botswana. Differing fire management policies are found in each of the land uses. The KTP Management Plan outlines how fires within the Park that burn in the rainy season should be allowed to burn to their fullest extent, unless life or infrastructure is threatened (Spies et al., 2016). On the primarily private land the fire policy since colonial times has been to avoid fires. Although this policy has been changing more recently (e.g., MET, 2016 in Namibia), the policy is still enforced amongst local landholders in the study region, as fire can have devastating effects for agriculture, property, and grazing (Humphrey et al., 2021; Mayr et al., 2018).

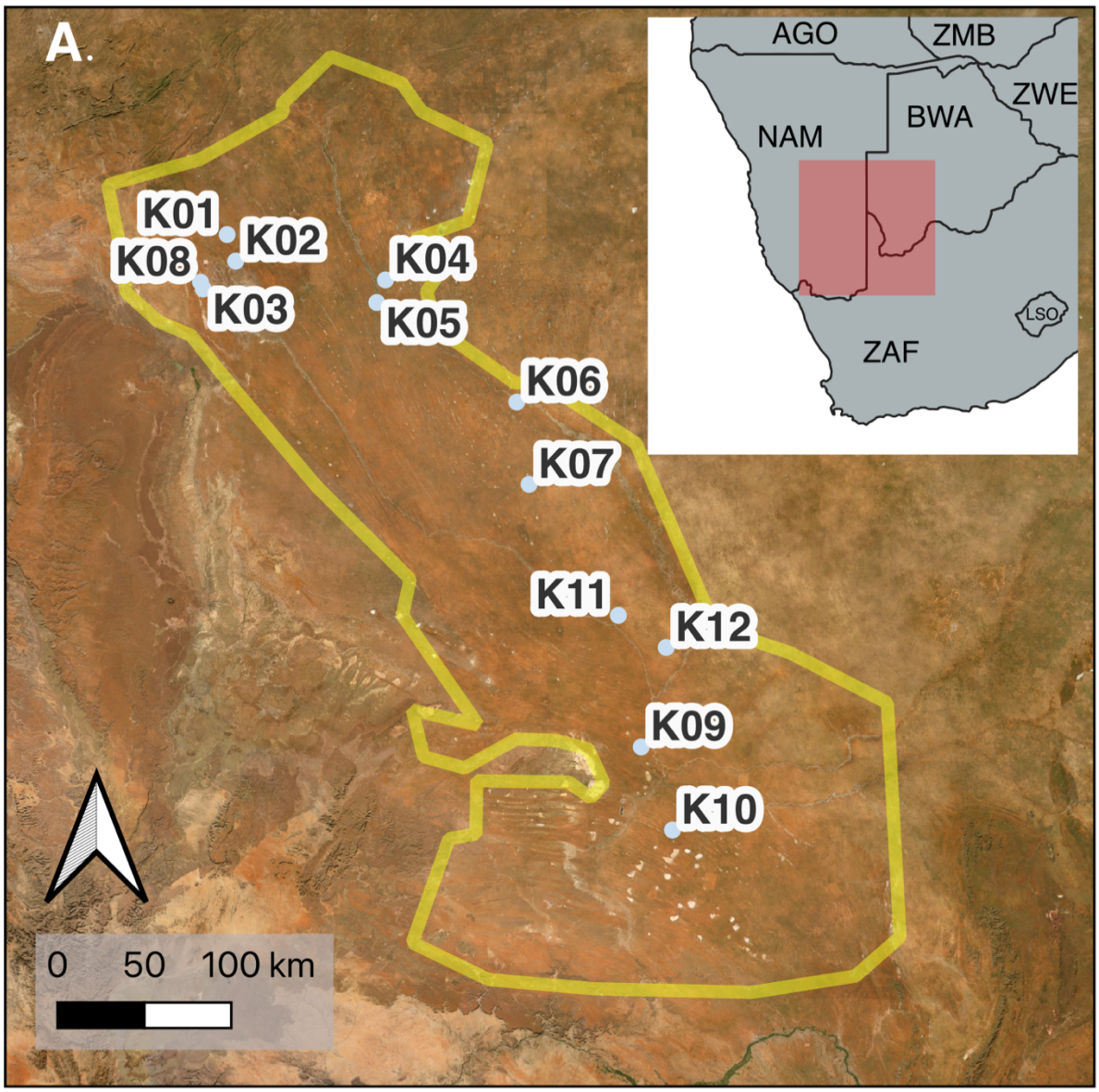

Figure 3.8. The location of the linear dune study area in Namibia, Botswana and South Africa with the field sites visited. The vegetated linear dune study area is outlined in yellow.

The presence of dust in the Kalahari dune system has long been examined. McDonald (1938) recorded increases in haze off the coast of southwestern Africa which was attributed to dust from both the Namib and Kalahari Deserts, although not specifically the dunes. Modern satellite imaging has also enabled plumes of dust to be tracked back to the dunes. Vickery et al. (2013) found two plumes originating from the

southwest Kalahari dunes between 2005 and 2008. Eckardt et al. (2020) traced four plumes to dune origins between 2006 and 2016. Gittings et al. (2024) used back trajectory modelling to find that dust from the southwest Kalahari can be linked to algal plumes in the Madagascar Sea.

Bhattachan et al. (2022, 2012) showed that the dunes of the southwest Kalahari have the potential to emit dust when de-vegetated by investigating dune sedimentological properties. Alongside a potential to emit dust, Bhattachan et al. (2012) also found high levels of soluble iron within the Kalahari dune sediment. Fallout of the eroded Kalahari dust, consisting of iron-rich fine sediment (Dansie et al., 2017a), has the potential to affect ocean productivity in the south Atlantic (Dansie et al., 2017b), the Madagascar Sea (Gittings et al., 2024), or the Southern Ocean (Bhattachan et al., 2012), and ultimately the land-ocean-atmosphere system.

Fire is an integral and normal part of the Kalahari ecosystem. Fires are thought to reburn an area of land every 11 years when they are allowed to occur naturally and frequently happen in the summer months associated with lightning storms (Spies et al., 2016). Studies in the region have investigated the effect of fire on vegetation (Gillespie et al., 2024; Scholes et al., 2002; Van Der Walt and Le Riche, 1984), on surface albedo (Dintwe et al., 2017; Saha et al., 2019), and on wind erosion (Wiggs et al., 1994).

No studies investigating dust emissions because of fire have been investigated in the region.

3.1.2 Study region justification

Research into transient, low concentration dust emissions from fire scars is timely as quantifications of Earth systems (such as the cycle of mineral dust) are needed for more robust predictions of future climate. The Kalahari sands offers a unique chance to study these factors, the sand sea is the largest on Earth, is vulnerable to reactivation under future climate change, burns regularly, and has been proposed as a future source of dust (Bhattachan et al., 2012; Thomas et al., 2005). Dust that could potentially be emitted from the large dune field could be of global significance with consequent iron nutrification of the Madagascar Sea, south Atlantic, and Southern oceans (Bhattachan et al., 2012; Dansie et al., 2017b; Gittings et al., 2024). The southwest Kalahari is geomorphologically and ecologically similar to vegetated dunes where dust emissions have previously been observed, such as the Simpson Desert in Australia (Bullard et al., 2008; Yu and Ginoux, 2022), yet there have been no studies monitoring post-fire dust emissions in the Kalahari. Therefore, the Kalahari provides a unique location to explore the potential of post-fire dust emissions from dune landscapes.

In addition, the southwest Kalahari has several logistical benefits with the study area having easy access to the sites, with multiple fire scars close to accessible roads and

established connections with local landowners. In the timeframe where fieldwork was able to be conducted (2022 - 2023) there were multiple widespread fires in the study area. Further, the process relationships between erosivity and erodibility in the region are well understood as the southwest Kalahari dunes have been subject to numerous surface process and activity studies (e.g., Livingstone et al., 1999; Mayaud et al., 2016; Nield and Baas, 2008; Wiggs et al., 1994). The current research aims to enhance this body of literature by adding an understudied disturbance variable, burning.

3.2 Remote sensing methods

Space-based remote sensing methods were utilised in this thesis to quantify dune field scale vegetation, fire and dust dynamics, which directly links to RSQ 1 – *what is the pattern, frequency, and timing of fire in the Kalahari dune landscape* and RSQ3 - *what is the impact of fire on dune surface properties*. To answer these questions, inventories of burned area (2000 - 2023; section 3.2.1) and dust (2020 – 2024; section 3.2.4) were conducted across the whole study area. The burned area data was combined with vegetation indices (section 3.2.2) and meteorological data (section 3.2.3) to identify patterns, trends, and the timing of fire in the study area. The vegetation data from 17 fire scars additionally provided insight into the impact of fire on the dune surface property of surface cover.

3.2.1 Burned area estimation

In order to answer Research Question 1, the frequency and extent of burning in the area must be quantified through creating a robust inventory of fires on the southwest Kalahari linear dunes. The inventory was then used to identify trends in occurrence and extent of burning alongside identifying impacts of land use (farmed or National Parks) and El Niño Southern Oscillation (ENSO) cycles in the region.

Since the launch of the Landsat sensors, satellites have been used to map burned area (Chuvieco et al., 2018; Chuvieco and Martin, 1994; Hitchcock and Hoffer, 1974). Satellites provide higher frequency and larger spatial range than ground surveys can achieve, and ultimately remotely sensed satellite data was the principal data source in Chapter 5. There have been multiple efforts to create a record of burned area (BA) using remote sensing. These efforts have mainly been spearheaded by the National Aeronautics and Space Administration (NASA) and the European Space Agency (ESA). NASA's Moderate Resolution Imaging Spectroradiometer (MODIS) provides daily imagery of the Earth surface and has been utilised for many of the BA estimates, including its own burned area product (MCD64A1), the ESA's FireCCI51 product (Lizundia-Loiola et al., 2020), and the Global Fire Emissions Database (Chen et al., 2023; GFED). More recently Sentinel-3 has been applied to calculate BA (FireCCI311; Lizundia-Loiola et al., 2022), and long-term data from the Advanced Very High Resolution Radiometer (AVHRR) has been used to supplement MODIS data (FireCCILT11; Otón et al., 2021; Figure 3.9).

However, satellite detection of burned areas is often conservative with both commission and omission errors misrepresenting the actual areas burned (Chuvieco et al., 2022, 2019). One of the main drivers behind these errors is coarse resolution sensors used to estimate BA (Chuvieco et al., 2019; Laris, 2005; Ramo et al., 2021; van der Velde et al., 2024; Figure 3.9). Between different BA products there are large discrepancies. For example, Roteta et al. (2019) used a Sentinel-based burned area detection algorithm in southern Africa and found 1.8 times more BA than estimates derived from MODIS. Due to these large discrepancies, the selection of product or workflow used for making a robust inventory of BA in the southwest Kalahari needs to be carefully considered and is discussed further in Chapters 4 and 5 of the thesis.

The main data source used to create the inventory of burned area in this research is the MODIS MCD64A1 product (Giglio et al., 2018). MCD64A1 was subsequently assessed against ENSO oscillations from the National Oceans and Atmosphere Administration's (NOAA) Climate Prediction Center (CPC; Huang et al., 2017) and land use information from South African National Parks. A detailed description of the MODIS MCD64A1 product is given in Chapter 5, but initially multiple products were assessed to determine which was most appropriate for this research. This initial assessment was conducted using the products or workflows from Planet Labs imagery, ESA Product FireCCIS311, and Sentinel-2 imagery between 2019-2022 and this process is outlined in Chapter 4.

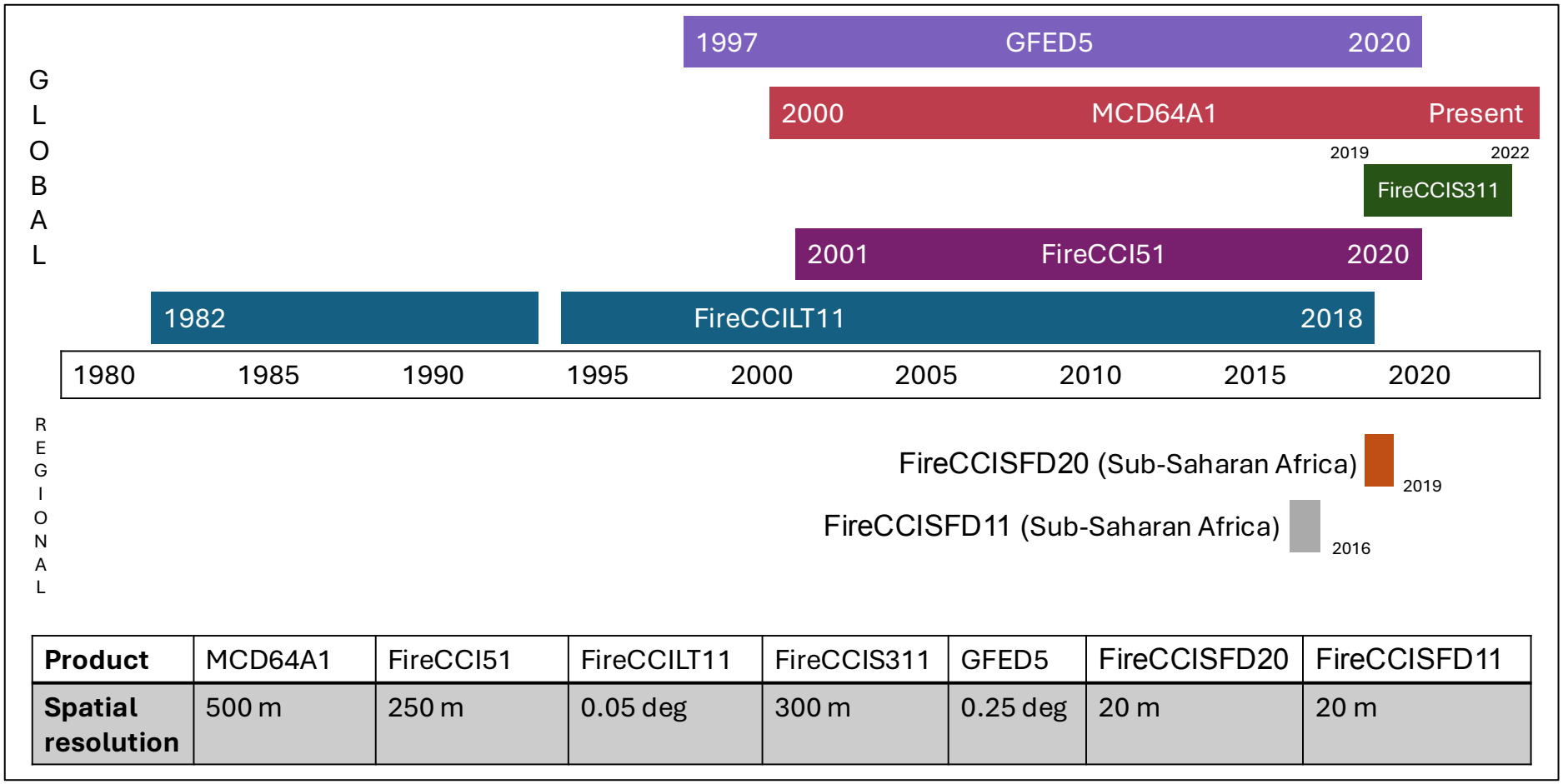

Product	MCD64A1	FireCCI51	FireCCILT11	FireCCIS311	GFED5	FireCCISFD20	FireCCISFD11
Spatial resolution	500 m	250 m	0.05 deg	300 m	0.25 deg	20 m	20 m

Figure 3.9. Timeline of select burned area products and their spatial resolution. The FireCCI products are produced by the ESA, GFED5 and MCD64A1 are produced by NASA. All global products except of FireCCI311 and FireCCILT11 use MODIS data to estimate burned area.

3 m red, green, and blue (RGB) daily imagery from PlanetScope sensors (Planet, 2017) was used to manually digitise fire scar boundaries from 2019-2022. Digitisation of fire scars is a common technique used in BA studies (e.g., Blackwood et al., 2022; Greenwood et al., 2022; Milczarek et al., 2023; van Etten et al., 2021), and was used to denote the most accurate representation of fires in the study area. However, manual digitisation is a labour-intensive task. Therefore, a workflow was established to semi-automate BA detection using 10 m Sentinel-2 imagery. Monthly differenced raster images were employed for the detection of areas where large changes in the Near Infra-Red (NIR) band were observed. This method, named Sentinel-NIR, highlighted issues with differentiation between burned or grazed and agriculturally disturbed areas and produced large variance in overlap with the manually digitised burned area.

Additionally, the ESA's most recently published BA product, FireCCIS311, was used. The FireCCIS311 product utilises the Visible Infrared Imaging Radiometer Suite (VIIRS) and shortwave infrared (SWIR) data from Sentinel-3 to create a daily estimate of burned area at 300 m resolution. In the 4-year preliminary study there was a 7.12% overlap between the FireCCIS311 product and the digitised BA. The lowest recorded overlap with the digitised burned area by the MCD64A1 product only had a marginally higher overlap at 11.12% and hence MCD64A1 was chosen going forward.

The MODIS MCD64A1 is the most popular tool for BA detection (e.g., Bowman et al., 2020; Harris et al., 2021; Jones et al., 2022; Roy et al., 2008; Zheng et al., 2021), and the product was downloaded for 2000 - 2023 for the whole study area. MCD64A1 gives daily BA at 500 m resolution in pixilated form. The data were then assessed to remove any obvious false positive returns and to merge connecting pixels and calculate the duration of each burn. This daily inventory was then compared to land use classes and ENSO oscillation extreme phases from NOAA CPC (Huang et al., 2017). A more detailed description of the burn inventory and statistical analyses used to determine influence of land use classes and ENSO oscillations on fire in the southwest Kalahari are given in Chapter 5.

3.2.2 Vegetation indices

To quantify the impact of fire on dune surface properties - an integral part of RSQ 3 - *what is the impact of fire on dune surface properties,* vegetation cover was tracked post-fire. 17 MODIS BA-identified fire scars on the dunes which burned in different years, in varying seasons, and across the whole latitude of the study area. These scars were paired with co-located unburned control plots which were tracked using various remote-sensing based vegetation indices to assess which index provided the best representation of surface cover. These fires represent a wide range of variables, including antecedent rainfall, land use, and fire time of year to identify the annual trends and season spatiotemporal distribution of fires (RSQ 1). Therefore, these 17 scars are different to the 12 field sites to account for older fires (pre-2012) and rainfall

conditions. The percentage cover of above ground vegetation was estimated using the minimum and maximum values of the Soil-Adjusted Total Vegetation index (SATVI) to calculate Total Vegetation Fractional Cover (TVFC). A detailed description of the processing of SATVI and the tracked burned area are given in Chapter 5.

Multiple vegetation indices were tracked on burned and co-located control sites to quantify the impact of fire on vegetative cover post-burning. These included the Normalised Differenced Vegetation Index (NDVI; Huete et al., 1994; Tucker, 1979), the Enhanced Vegetation Index (EVI; Huete et al., 1994), Soil-Adjusted Vegetation Index (SAVI; Huete, 1988), and SATVI (Marsett et al., 2006). All indices were calculated from MODIS imagery and amassed into 16-day resolution. The only index that recorded a sharp decrease in vegetation cover post-burning was SATVI (Figure 3.10). SATVI has enhanced detection of non-photosynthesising vegetation which can be attributed to the index utilising SWIR bands (Marsett et al., 2006). By detecting both senescent and green vegetation, SATVI is able to provide a more complete idea of changes to above ground biomass in arid environments (Marsett et al., 2006; Poitras et al., 2018).

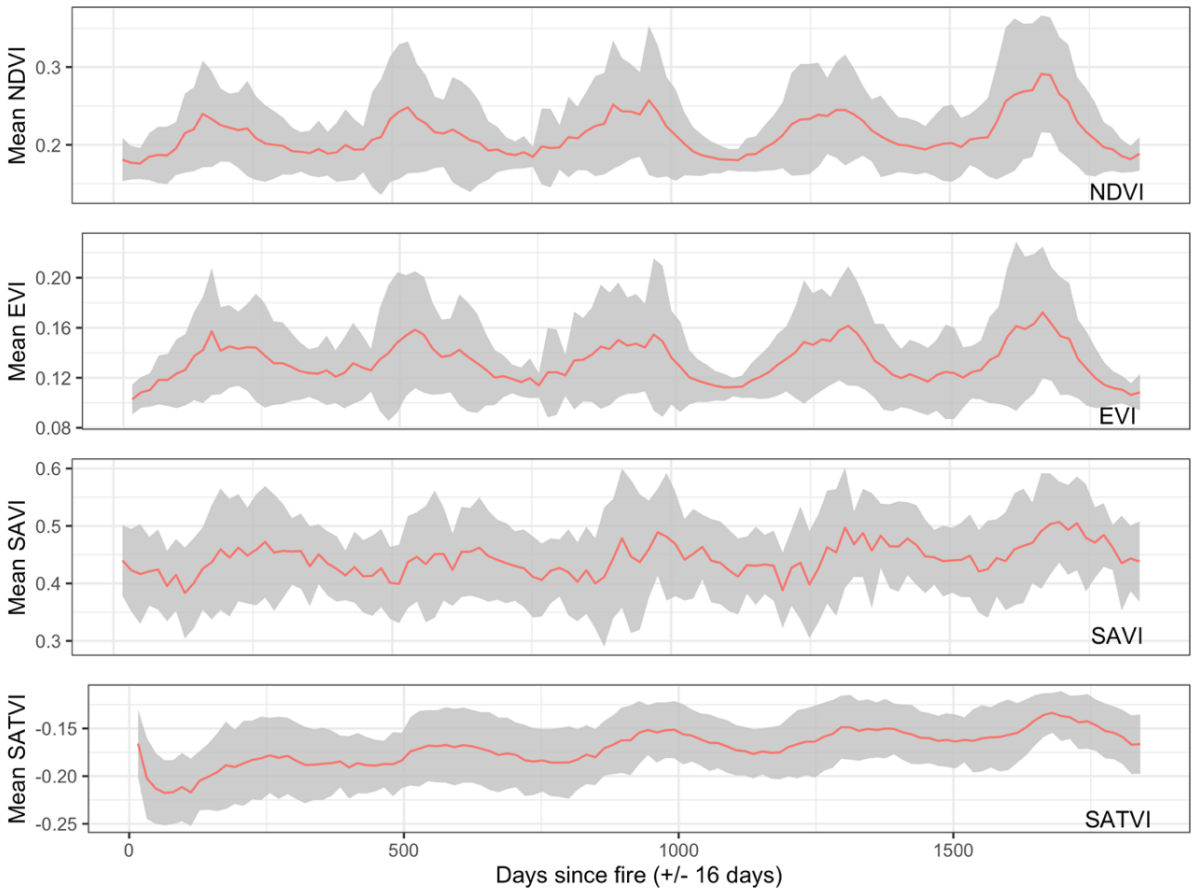

Figure 3.10. Four vegetation indices (NDVI, EVI, SAVI, and SATVI) tracked from 17 fire scars for 2000 days after burning. The mean of all the first scars is displayed in red and the standard deviation in grey. Only SATVI detected an immediate decrease in vegetative cover post-burning.

3.2.3 Meteorological data

Meteorological data are needed to assess the trends in fire occurrence (RSQ1) and post-fire vegetation recovery (RSQ 3), and this is an integral part of this thesis. There are sparsely situated meteorological stations in the southwest Kalahari. Initially, Southern African Science Service Centre for Climate Change and Adaptive Land Management (SASSCAL) meteorological stations were recognised for identifying atmospheric processes and land surface conditions which could lead to fire or dust

emissions. However, the SASSCAL stations in the research area were not continuously online for the duration of the project and the use of SASSCAL data was ultimately excluded.

Due to the lack of ground-based meteorological observations in the southwest Kalahari, modelled climatic parameters were consequently utilised from the European Centre for Medium-Range Weather Forecasts (ECMWF) Fifth Generation European REanalysis Land (ERA5-Land) climate model (Muñoz-Sabater et al., 2021). ERA5-Land provides high spatial resolution data 0.1° at hourly, daily, and monthly estimates from 1950 to the present day and is available to be downloaded from the Copernicus Climate Change Service Data Store (https://cds.climate.copernicus.eu/datasets). The ERA5-Land data was primarily used to obtain wind speed, wind gusts, and precipitation data to track post-fire vegetation recovery and climatic trends. ERA5-Land data is a commonly used method for reanalysis of southern African climate (Chikoore et al., 2024; Gadal et al., 2022; Mwangala et al., 2024; Parsons et al., 2022; Roffe and van der Walt, 2023).

3.2.4 SEVIRI Dust RGB

High temporal resolution (15-minute) image data from the Spinning Enhanced Visible and InfraRed Imager (SEVIRI) based on the geostationary 0° Meteosat Second Generation (MSG) satellite were used to detect dust plumes over the Kalahari. The SEVIRI Dust Red-Green-Blue (RGB) composite utilises the SEVIRI channels IR8.7,

IR10.8, and IR12.0 (Schepanski et al., 2007). The resulting image shows dust in pink to magenta (Banks et al., 2019; Figure 3.11). These images were manually examined for dust plume identification from 01/09/2020 – 01/09/2024. The manual dust source detection technique from Eckardt et al. (2020) was utilised, where identified pink plumes were temporally backtracked until source pixels were located. These plume origins were assessed to identify if they were within a fire scar from the burned area inventory created in Chapters 4 and 5. Using SEVIRI data allowed for high temporal resolution dust plume identification and evolution, but the method is limited by high cloud that can obscure dust plumes underneath.

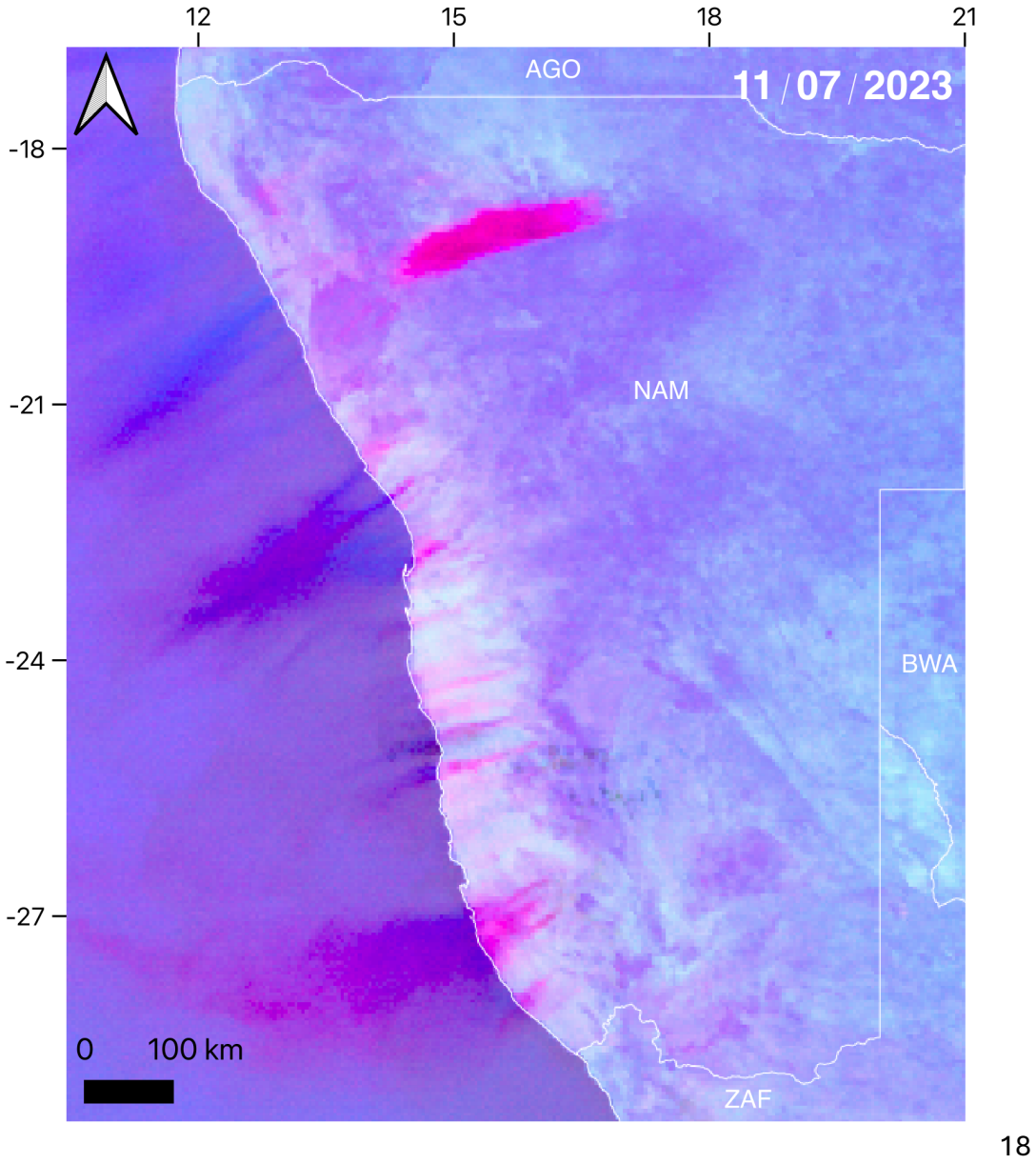

Figure 3.11. An example SEVIRI Dust RGB composite effectively highlighting pink dust plumes in southern Africa. The image is taken on 11th July 2023 at 11:00 UTC displaying significant dust plumes in southern Africa. Airborne dust displays as pink to magenta, the warm desert surface is blue, and purple represents dry hot air. Dust plumes in this image originate from coastal ephemeral river valleys and Etosha Pan, none originate in the Kalahari.

3.2.5 Fire Severity

Fire severity measures the impact of the fire on the local environment and is linked to vegetative cover loss (Lentile et al., 2006). The more severe a burn, the longer lasting

the ecological and related geomorphological effects (Lentile et al., 2006). Hence fire severity is important to quantify in relation to the longevity of fire impacts in the study area (Research Question 4). The Normalised Burn Ratio (NBR; Equation 3.1) was developed to monitor the fire severity on landscapes and to monitor vegetation recovery (Key and Benson, 2006).

$$NBR = \frac{NIR - SWIR}{NIR + SWIR}$$

Equation 3.1

NBR was then used to create the differenced (or delta) NBR (dNBR; Equation 3.2) where pre-and post-fire indices are compared to assess the impact of fire on areas (Miller and Thode, 2007).

$$dNBR = prefireNBR - postfireNBR$$

Equation 3.2

These indices are a measure of the absolute difference between the amount of chlorophyll and water content of vegetation and soils pre- and post-fire and relates to the amount of canopy consumed (Miller and Thode, 2007). As much vegetation in drylands is senescent for much of the year the reliance on chlorophyll detection is not robust and the relativised dNBR (RdNBR; Equation 3.3) was developed (Miller and Thode, 2007).

$$RdNBR = \frac{dNBR}{\sqrt{ABS(\frac{prefireNBR}{1000})}}$$

Equation 3.3

RdNBR better accounts for diverse vegetation types, variations in soil conditions, and pixels where vegetation cover is low before a fire (DaSilva et al., 2021; Miller and Thode, 2007). Both dNBR and RdNBR has been used in desert environments, but RdNBR features more commonly due to its ability to account for the discontinuous vegetation cover (DaSilva et al., 2021). Both dNBR and RdNBR were calculated from Landsat data using the methods in Parks et al. (2018). In the study area, RdNBR was found to be much more effective than dNBR at displaying burned area.

Fire severity can be measured in multiple time steps. In this study three time steps (1 month, 6 month, 12 months post-fire) were chosen to assess fire severity on the 12 studied burned sites on the ground. The results for the surface strength measurements are presented and discussed in appendix C.

3.3 Ground-based methods

Ground-based field methods were utilised in this thesis to quantify plot-scale surface dynamics, which directly link to RSQ 2 – *does fire affect dust emission potential* and RSQ3 - *what is the impact of fire on dune surface properties*. To answer these questions, fire scar sites were identified for experimentation and monitoring in both Namibia and South Africa. At each of these sites there was six sub-plots where three were unburned control plots and three were burned. At each subplot, measurements of surface strength (both shear and compressive), ground cover, soil hydrophobicity (section 3.3.3), and sediment grain size distribution (section 3.3.4) were taken. By comparing

the control to the burned plot, the impact of fire on the surface properties were able to be determined. Further, at the seven Namibian field sites, wind erosion thresholds and emission flux were established using portable wind tunnel experiments (section 3.3.2) to ascertain if fire affects dust emission potential (RSQ 2).

3.3.1 Identification of field sites

In order to determine the potential dust emissions and identify controls on surface erodibility, fieldwork was conducted on the sand dunes in the southwest Kalahari in August to September 2022, July 2023, and September 2023. Accessible burned sites on sand dunes were identified using satellite imagery and discussions with local landowners. Ultimately, twelve fire scars were identified as sites to investigate, each burn had differing time since fire (TSF) varying from 3 days to 127 months (Table 3.1). The sites were then further divided into study plots which were characterised by the topography of the dune, consisting of interdune, flank, and crest (Table 3.1). All burned plots were paired with a co-located unburned control plot. Where possible the plot pairs were close to each other on the same dune, or one interdune across (for example at K11 and K12 one side of a road had burned and the other not). Therefore, all study sites, where access allowed, were broken down into six study plots of three burned and three control plots based on topography (Table 3.1 and Figure 3.12).

Table 3.1. Information on the sites used in this study

Site	Land use	Latitude	Longitude	Date of fire	Cause of fire	Measurement TSF (months)	Topographies measured
K01	Farm	-23.723	18.11	01/09/2022	Humans	0, 1, 12	C*, F, ID
K02	Farm	-23.861	18.150	26/07/2022	Humans	1, 2, 13	C, F, ID
K03	Farm	-24.042	17.981	18/06/2022	Humans	3, 4, 15	C, F, ID
K04	Farm	-23.982	19.017	29/11/2021	Humans	10, 22	C, F, ID
K05	Farm	-24.116	18.996	16/11/2021	Lightning	10,11, 22	C*, F, ID
K06	Farm	-24.688	19.822	27/10/2020	Lightning	25, 37	C, ID
K07	Farm	-25.185	19.895	28/02/2012	Lightning	127	C*, ID
K08	Farm	-23.996	17.960	18/12/2021	Lightning	9, 21	ID
K09	Farm	-27.221	20.740	21/01/2023	Lightning	6	C, F, ID
K10	Farm	-26.735	20.556	18/10/2022	Unknown	10	C, F, ID
K11	NP	-25.957	20.421	27/12/2021	Unknown	18	C, F, ID
K12	NP	-26.146	20.703	09/09/2022	Unknown	10	C, F, ID

*Control only
NP = National Park, C = Crest, F = Flank, ID = Interdune.

Upon arrival at a site visual evaluations of land use were performed. Evidence of animal activity (e.g., scat, holes, and paths) was recorded and, where possible, discussions with local landowners occurred to understand grazing practices in the area for the last few years.

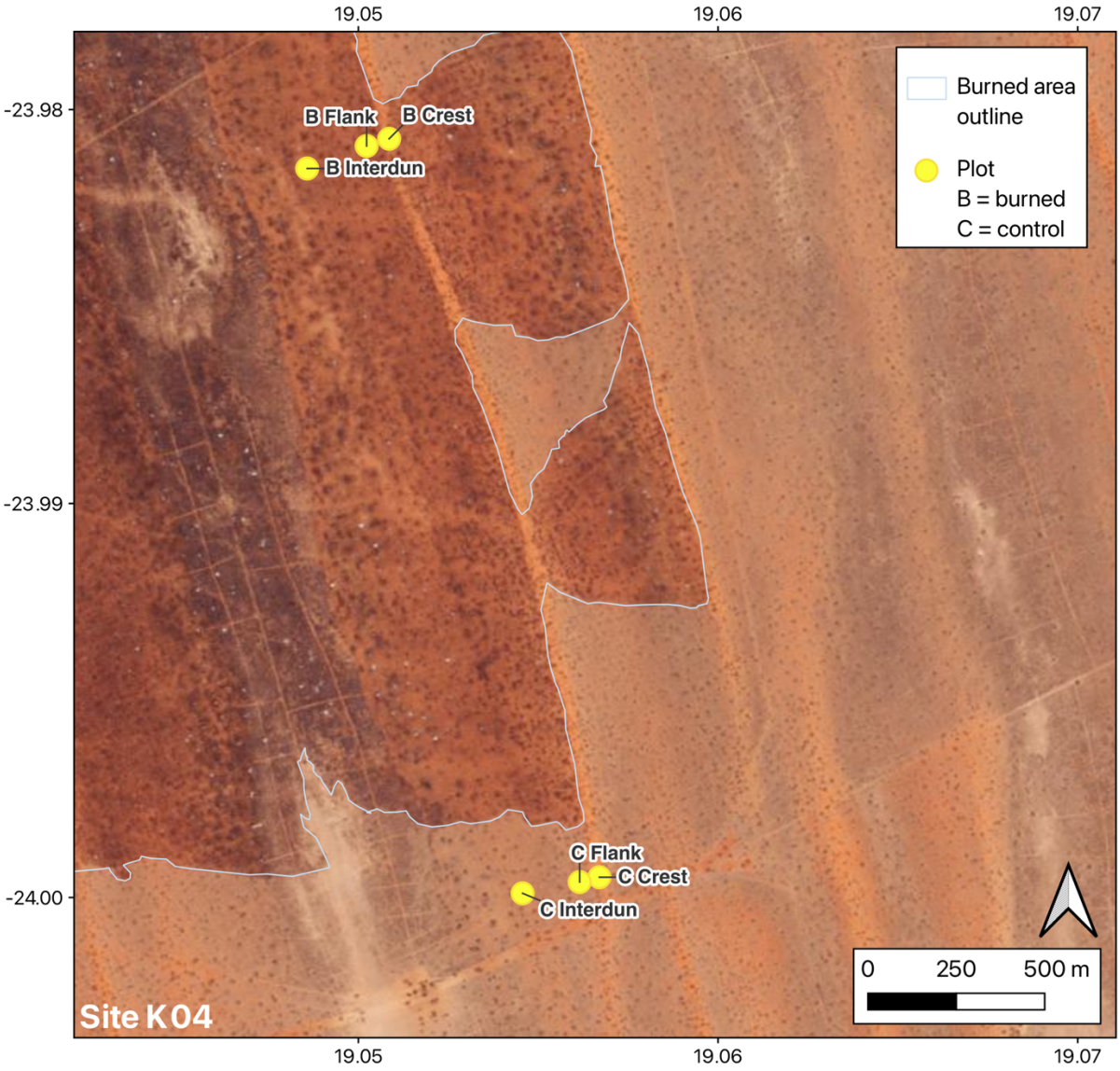

Figure 3.12. An example of the experimental set up at site K04, where six experimental plots were established. Background image © 2022 Planet Labs PBC.

3.3.2 Measurements of dust

To answer Research Questions 2 and 3, both in-situ and experimental ground-based measurements of dust concentrations were made. These measurements were split into two categories, experimental dust emissions measuring dust erosion thresholds and emission flux using a portable wind tunnel (Ob 2.1 and 2.2) and in-situ dust emissions from burned sites (Ob 3.2).

Potential dust emission measurements

In order to answer Research Question 2- *Does fire affect dust emission potential,* potential emission rates were measured using the Portable In-Situ Wind Erosion Laboratory (PI-SWERL ®; Desert Research Institute, Las Vegas, NV, USA; Etyemezian et al., 2007) The PI-SWERL (Figure 3.13) has been used since its conception in 2007 to provide an index for potential dust emissions from anthropogenic and natural landscapes under varying environmental conditions. Now the PI-SWERL is a widely used technique for field studies of wind erosion (Bacon et al., 2011; Cui et al., 2019; Dickey et al., 2023; Fick et al., 2020; Smits et al., 2024; Sweeney et al., 2023; van Leeuwen et al., 2021; von Holdt et al., 2021; Vos et al., 2021; Wang et al., 2025). The instrument consists of a flat, annular ring inside a closed chamber (height 25 cm and width 57 cm) rotating near the surface which exerts shear stress on the surface and entrains particles. The emitted particles are measured by a DustTrak ® II model 8530 nephelometer to measure concentration of dust in the chamber per second in mg m^{-3}. Fresh air is pumped into the chamber at a rate of approximately 0.1 m^{-3} s^{-1}. The PI-SWERL can be pre-programmed to run at a variety of rotation rates per minute (RPM) which translate into specific friction velocities (u_* m s^{-1}). The relationship between RPM and u_* is determined by surface roughness and defined as:

$$u_{*eff}(RPM) = C_1 \cdot \alpha^4 \cdot RPM^{C_2/\alpha}$$

Equation 3.4

Where C_1 and C_2 are constants 0.000683 and 0.832 respectively. α is a value calculated based on surface roughness using the look-up table in Hartshorn et al. (2023) An α value of 0.98 was chosen for the dune surfaces which represents loose unconsolidated sand with less than 2.5% gravel cover. As a result, a maximum shear velocity of 0.64 m s^{-1} was used in this study. Errors in association with alpha value determination are discussed at length in Etyemezian et al. (2014) and are thought to be around 7 to 20% of the typical threshold RPM range between 1000 and 3000 RPM. To assess its impact on calculated shear velocity $u_{*\text{eff}}$ a midpoint uncertainty of 15% (±0.297) was propagated through the model equation. This results in an estimated uncertainty in $u_{*\text{eff}}$ of ±0.297, or approximately 44% of the calculated value.

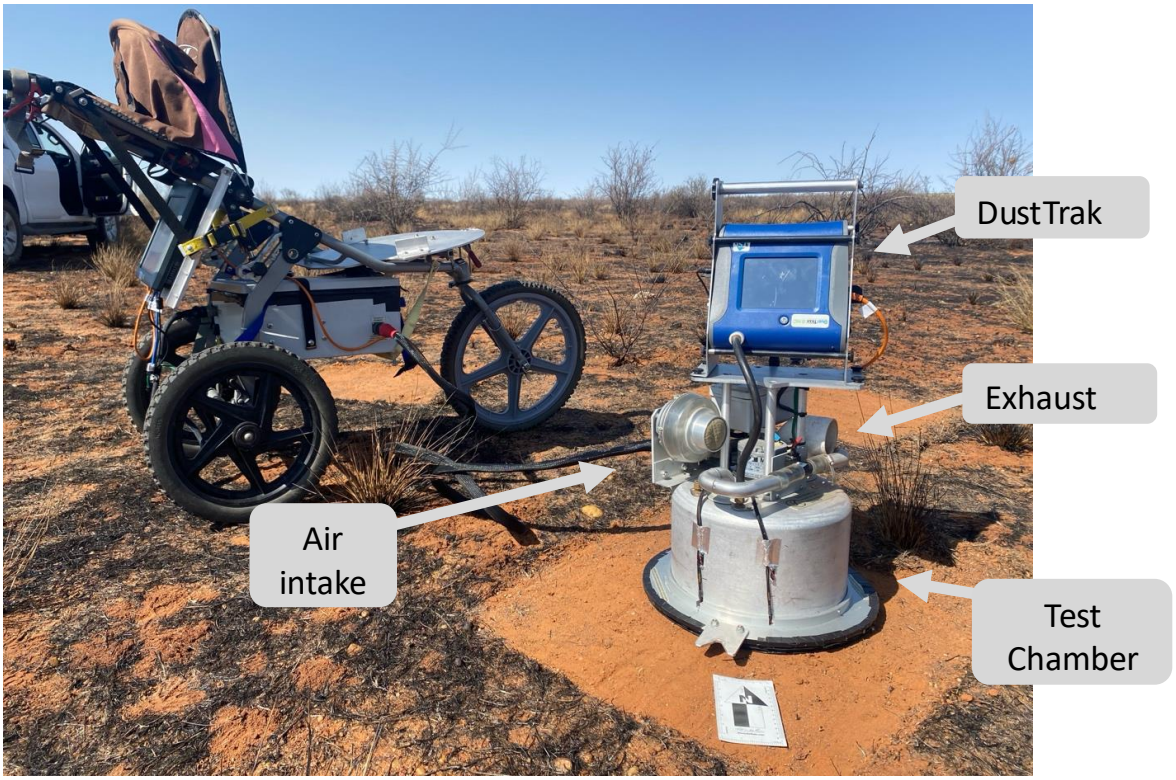

Figure 3.13. The PI-SWERL deployed on a mechanically disturbed patch at plot K01 burned interdune.

RPMs can be increased either continuously at a constant rate (ramp test: e.g., Gillies et al., 2022; von Holdt et al., 2021; Vos et al., 2020, 2021) or incrementally at distinct stages (step test: e.g., Bacon et al., 2011; Fick et al., 2020; Kavouras et al., 2009; King et al., 2011; Sankey et al., 2011; Sweeney et al., 2023). In this study, a ramp test was conducted to determine if the surface is capable of emitting dust and to observe any changes in the emission threshold between the burned and unburned surfaces. By maintaining the maximum RPM for 90 seconds, it was possible to further analyse factors controlling emissions and to calculate flux from a single specific u_* value. The ramp test contrasts with the step test, in which dust flux is calculated at multiple u_* values, a method more commonly applied at sites known to be consistently emissive.

At the start of each measurement, a 60 second clean air flush was run to flush remaining particles in the chamber, the RPM was then increased from 0 to 3500 RPM over 90 s, held at 3500 RPM for 120 seconds, the blade was then stopped and slowed down alongside a clean air flush for the final 60 seconds of the test (Figure 3.14). To reduce contamination between each run, the chamber was brushed down to remove any visible sediment. In addition, after concluding measurements at each plot, three cleaning cycles were run, with the PI-SWERL at maximum RPM for 180 seconds, to flush the system of any contaminating sediment.

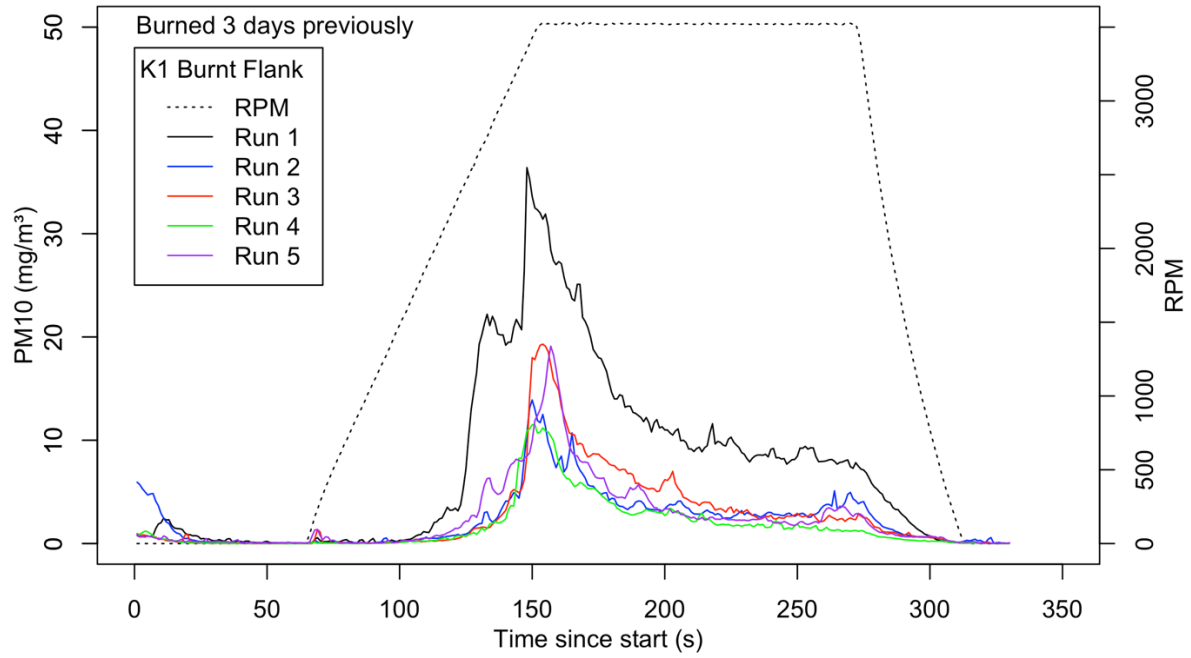

Figure 3.14. Multiple example runs of a PI-SWERL at each measurement plot, displaying the programming used for each measurement.

The first recording where the PM_{10} concentration began to consistently increase for ten or more seconds is determined as the threshold of emission (u_{*T}; Cui et al., 2019). The threshold RPM was then converted into u_* using the Equation 3.5. The PM_{10} flux was calculated using the equation:

$$E_i = \frac{\sum_{begin,i}^{end,i} C \cdot F}{\left(t_{end,i} - t_{begin,i}\right) \cdot A_{eff}}$$

Equation 3.5

where C is the measured PM_{10} concentration (mg m^{-3}), F is the airflow rate (L s^{-1}), t is the duration (s) of step i, and A_{eff} is the effective area (m^2) of the PI-SWERL (Etyemezian et al., 2014). The flux was used to compare emission fluxes to other measurements and PI-SWERL results.

In-situ dust and meteorological measurements

The most recently burned fire scar sites K01 (a three-day old burn scar in an interdune) and K02 (a one-month-old burn scar in an interdune Figure 3.15) were chosen for measurement of in-situ aerosol concentrations. These sites were selected as they had the lowest vegetation cover at the time and therefore thought to be most likely to emit dust. Measurements were recorded from 04/09/2022 to 03/10/2022 to identify any in-situ dust emissions from burned dune areas which directly address Objective 3.2 – *establish in-situ dust emissions*. DustTrak DRX (TSI Inc) aerosol monitors (Wang et al.,

2009) were mounted on a tripod at 1.8 m height and located at least 500 m from the edge of the burned area. The DustTrak nephelometer uses a light-scattering laser photometer to measure real-time aerosol concentration corresponding to particulate matter and is commonly used in aeolian research (Bhattachan et al., 2022; Dansie et al., 2017b; Mockford et al., 2018; Preston et al., 2020; Wiggs et al., 2022). Average aerosol concentrations (mg m^{-3}) were recorded at two-minute intervals at PM_1, $PM_{2.5}$, and PM_{10}. In conjunction with the DustTrak sensors, horizontal wind velocity and direction was determined using a Vector instruments cup anemometer (A-100LK) and wind vane (W-200P) at site K02, both positioned at a height of 1.8 m. The sampling frequency of the anemometers was two minutes for 29 days in September 2022.

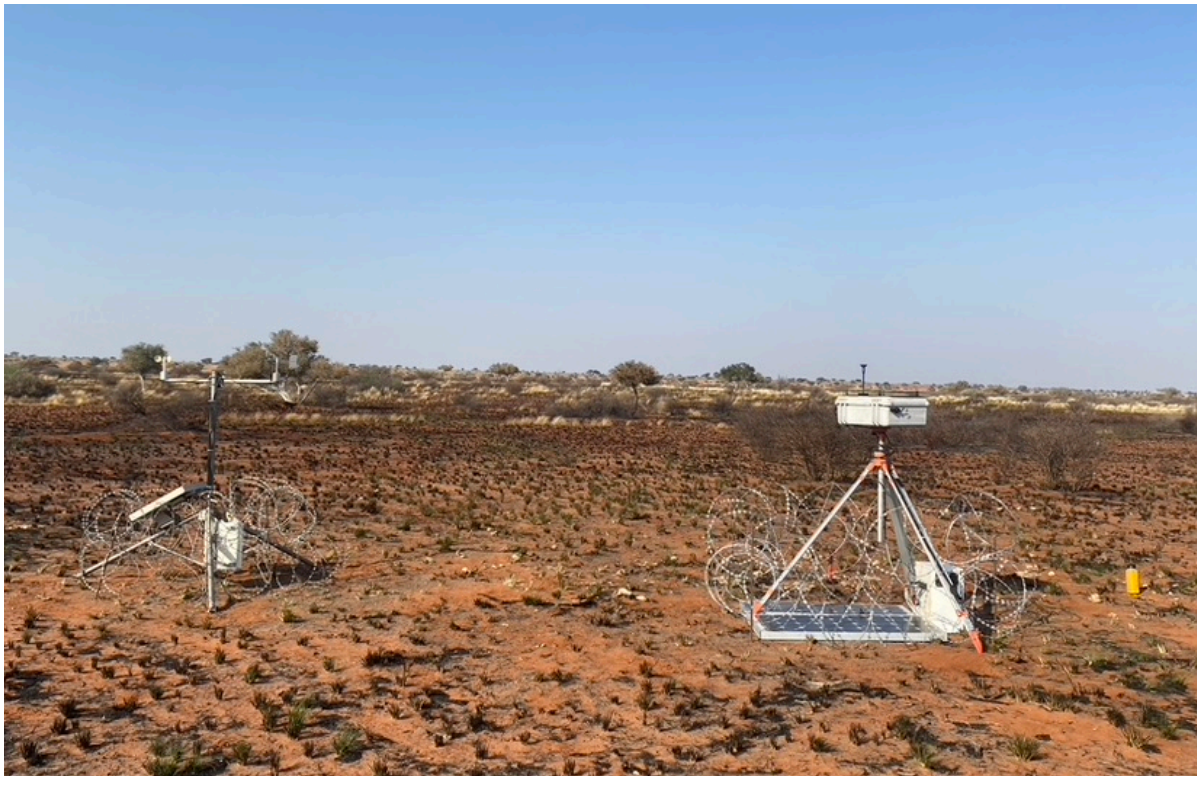

Figure 3.15. In-situ measurements of dust using a DustTrak monitor and meteorological station at site K02, burned interdune, in September 2022.

Big Spring Number Eight traps

Big Spring Number Eight (BSNE; Custom Products and Consulting, Big Spring, TX) traps were also used to measure in-situ horizontal sediment fluxes from the burned and co-located control sites. Three pairs of passive sediment collectors were located within two fire scar sites (K01 and K02) and one unburnt control plot (K01) in September 2023 using BSNE sediment trap at 15 cm and 50 cm height (Figure 3.16). BSNEs are a common technique to measure horizontal sediment flux in post-fire aeolian research (Miller et al., 2012; Ravi et al., 2012, 2009a; Sankey et al., 2009; Vermeire et al., 2005; Wagenbrenner et al., 2013). Due to the lack of fires in the Namibian portion of the study area in the 2022 to 2023 fire season, the four BSNE traps were placed in one year old fire scar sites at the same locations as the DustTrak sensors described in the above section. An additional two traps was placed in a nearby unburnt interdune.

Figure 3.16. In-situ measurements of dust using two BSNE traps at site K02 burned interdune in September 2023 – 12 months after burning.

3.3.3 Surface properties

Grain size distribution, surface strength, surface cover, and soil hydrophobicity were measured to ascertain the extent to which they are modulated by fire, the effect they had on the emissivity of each plot, and to quantify the persistence of the effect of burning on the landscape to address Objective 3.1. These surface properties have been heavily utilised in other studies of wind erosion (Bhattachan et al., 2012; Hesse and Simpson, 2006; Sweeney and Mason, 2013; von Holdt et al., 2019) and fire research (DeBano, 2000; Tinebra et al., 2019).

Ground cover surveys

Previous studies show that vegetation coverage below 14% on the Kalahari dunes leads to an increase in aeolian activity (Wiggs et al., 1995). To quantify the longevity of the impact of fire at the plots, how this varies between plots, and the duration that the surface is below this threshold, ground cover surveys were conducted at each site. The range in time since fire (TSF) for each site provided an opportunity to assess the longevity of the impact of fire on surface coverage. The surveys involved measuring, along 10 m transects (Figure 3.17 and 3.19a), surface coverage for every centimetre and noting surface items or conditions (Brun and Box, 1963; Canfield, 1941; Etchberger and Krausman, 1997; Hesse and Simpson, 2006). The factors that were recorded were:

- Bare ground (including cyanobacterial and algal crusts which were not easily distinguishable from bare ground)
- Vegetation height, width, and class (perennial grass, annual grass, shrub, forb, tree)
- Biocrust presence (visually obvious biocrusts with presence of darkening and microtopography)
- Litter
- Burned detritus

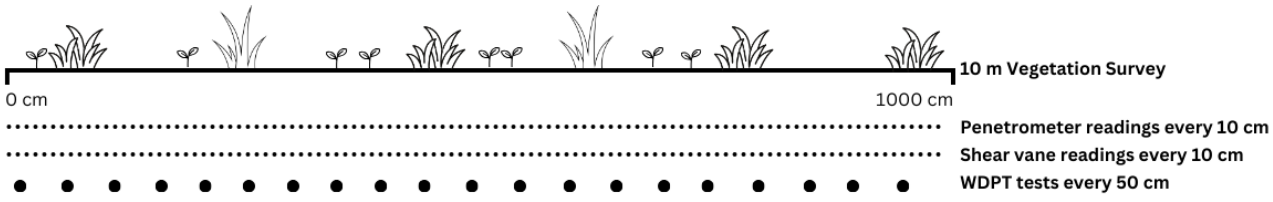

Figure 3.17. An example of the ground surface cover transects and experimental procedure at each field plot.

Surface strength

The strength of the surface can be an indication of its erodibility (Feng et al., 2013; Goossens, 2004; Vos et al., 2021) and crust strength can signify soil resistance to saltation impact (Neuman and Maxwell, 2002). Surface strength was assessed in two ways. Compressive strength (i.e., the force required to break the surface) was measured using a pocket penetrometer (ELE International) in kg cm^{-2} (Figure 3.18a). Surface shear strength (i.e., the resistance of the surface to shearing forces) was measured using a Torvane pocket shear vane (ELE International) in kg cm^{-2} (Figure 3.18b). Measurements were made at 10 cm intervals along each 10 m transect, providing 100 measurements per plot (Figure 3.17). The results for the surface strength measurements are presented and discussed in appendix C.

Water drop penetration time

To assess any post-fire sediment hydrophobicity, a water drop penetration time (WDPT) test was conducted at each site (Doerr, 1998; Ravi et al., 2012, 2009a; Tinebra et al., 2019). Using a pipette held approximately one centimetre above the surface, a drop of water was placed on the ground and the time required for the drop to penetrate the surface was recorded. Measurements were taken every 50 cm (20 measurements in total) along each transect (Figure 3.17).

Figure 3.18. Measurements of surface properties recorded at 10 cm intervals along the 10 m transect at each field plot. (A) surface strength measured using a pocket penetrometer and (B) surface strength using a Torvane pocket shear vane.

Sediment profile trenches

To assess the presence of biocrust and ascertain if individual biocrusts had survived being burned, 10 cm deep pits were dug at each plot. The pits were used to describe the surface and the structure of the top few centimetres of the interdune and dune sediments, and to ascertain any surface crusting through identification of agglomerations of sediment (Figure 3.19b). Digging the pits proved a useful means of assessing biological crust presence, particularly in areas where the crust was weakly consolidated and showed no surface discolouration and therefore difficult to decern from above.

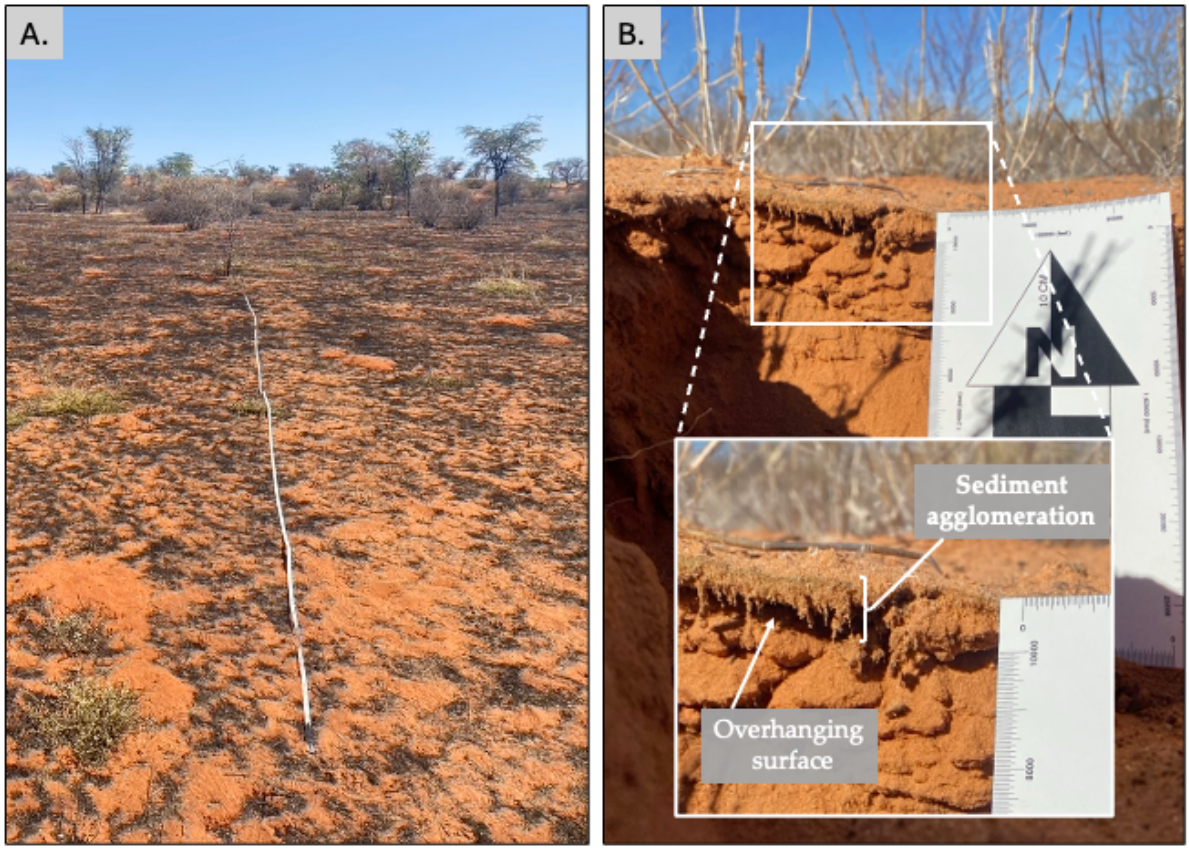

Figure 3.19. (A) An example 10 m transect at site K01 burned flank. (B) An example pit with biological soil crust presence in the top 1 cm of sediment at site K11 unburned interdune. Highlighted are surface properties typical of a biological soil crust.

Sediment sampling

Surface sediment samples that were exposed to the wind (i.e., the top two cm) were collected at each experimental plot. These samples were stored in plastic zip-locked bags and transported back to the University of Oxford where grain size analyses and loss on ignition tests were conducted within six months of collection.

3.3.4 Laboratory analysis

Sediment analyses were conducted to ascertain if there is any dust sized material (< 62.5 μm) within the dune sediment that, when exposed to the wind, can be eroded.

Subsequently the grain-size distributions are critical to answering Research Questions 2 and 3.

Loss on ignition

Nine samples were chosen for water and organic content to be estimated through loss on ignition (LOI) tests at 105°C and 550°C (Heiri et al., 2001). LOI is a standard method for characterising sediments (Heiri et al., 2001). Samples were dried at 105°C for ~ 12 hours and at 550°C for four hours. The percentage of organic content is calculated using Equation 3.6.

$$LOI_{550} = \frac{DW_{105} - DW_{550}}{DW_{105}} * 100$$

Equation 3.6

Where DW_{105} is the dry weight of the sample at 105°C and DW_{550} is the dry weight of the sample at 550°C. The results of the LOI tests are displayed in Table 3.2 and show low organic contents in all the samples.

Table 3.2. Loss on ignition result for nine select samples.

			Sample weight (g)			
Farm	Type	Topography	Pre-processing	DW_{105}	DW_{550}	% organic
K06	Burned	Crest	16.5	16.48	16.46	0.121
K04	Control	Interdune	21	20.98	20.94	0.191
K01	Burned	Interdune	16.55	16.55	16.51	0.242
K01	Control	Crest	14.28	14.28	14.26	0.140
K01	Burned	Flank	15.4	15.42	15.38	0.259
K07	Control	Crest	20.2	20.27	20.25	0.099
K07	Control	Interdune	14.43	14.43	14.41	0.139
K02	Burned	Interdune	16.87	16.87	16.82	0.296

Particle size distribution

Grain size distribution measurements were conducted using a Malvern Mastersizer Hydro 2000MU laser diffraction particle size analyser. Samples were tested to determine if organic material and test procedure impacted on particle size distribution. Nine samples were selected for this analysis and the particle size distribution of the samples was derived from the samples without any pretreatment (Figure 3.20 in yellow – no pretreatment). Next, tests were conducted on samples where the organic material was removed by using LOI or digestion, and with or without the ultrasonic (US) probe. Subsequently, four types of pretreatments were tested which included samples which were free from organics by LOI (Figure 3.20 in black - LOI), samples that were free from organics using digestion with hydrogen peroxide without US dispersion (Figure 3.20 in blue – digest), digested samples with US dispersion (Figure 3.20 in green – digest w/ US), and no pretreatment with US dispersion (Figure 3.20 in red – US only). Results are shown in Figure 3.20. As the effect of the digestion treatment and LOI was found to be minor, it was concluded to be unnecessary to remove organic material before analysis. Therefore, the remaining sample were measured using the no pretreatment with US dispersion protocol.

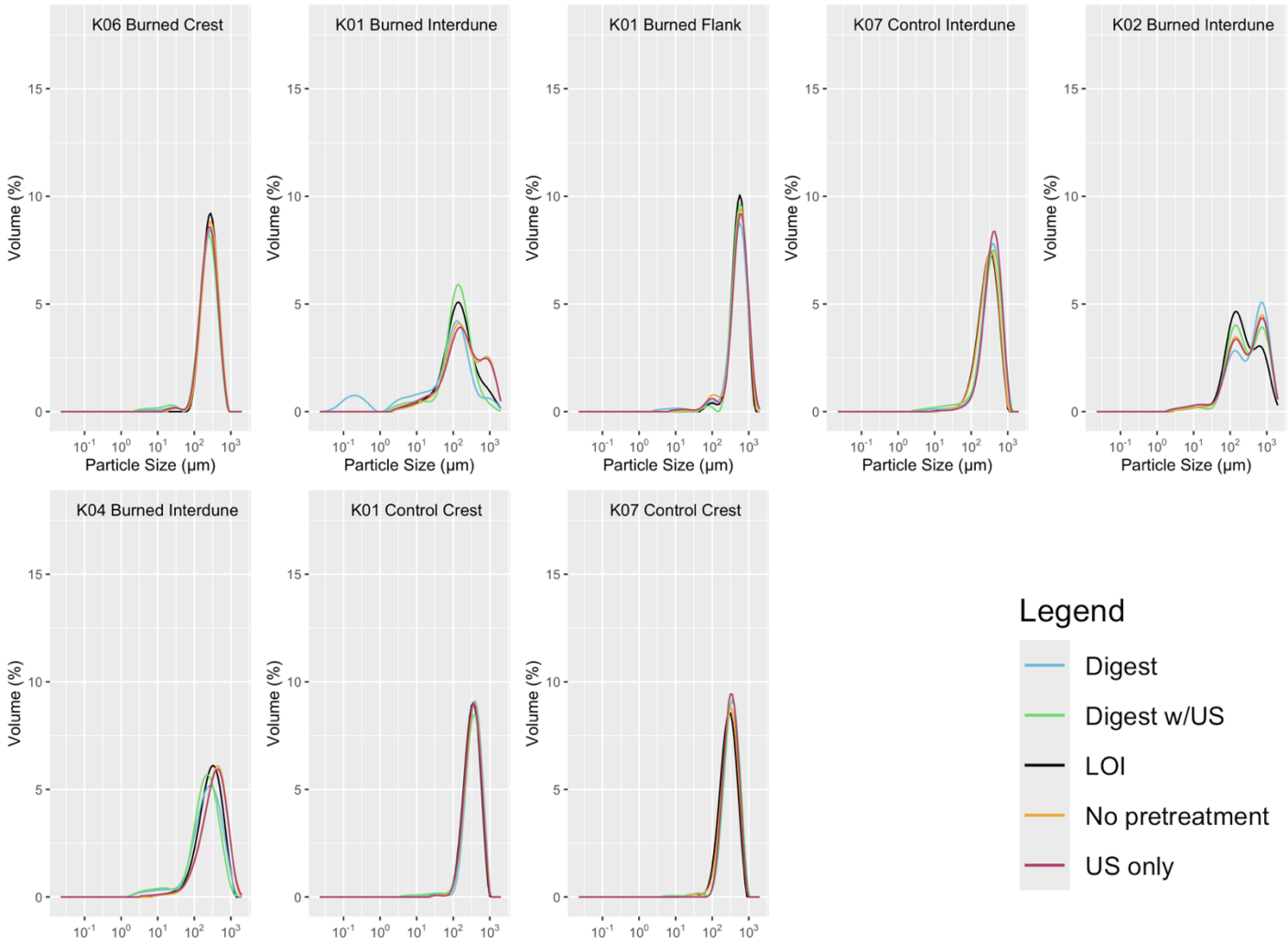

Figure 3.20. Comparison of the grain size distribution with prior and post removal of organic matter.

Chapter 4 -

Towards a True Burned Area Inventory for the Southwest Kalahari: Comparing Manual and Automated Methods

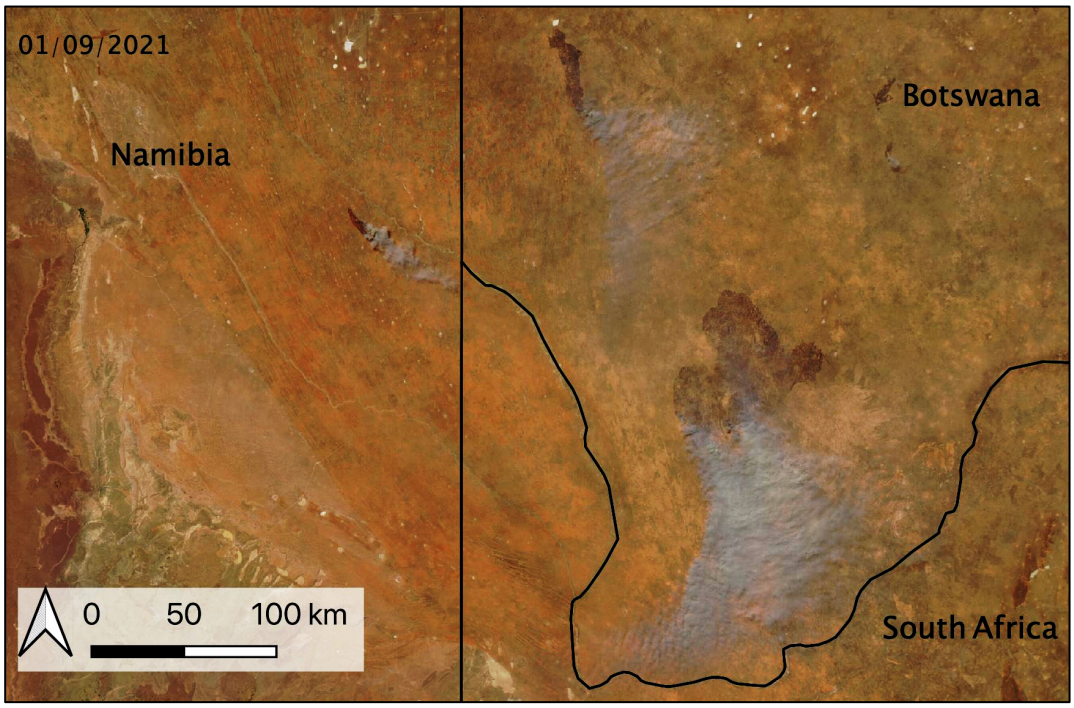

Multiple fires burning in the Kalahari. Image: NASA

Summary

This chapter addresses **research question one** – *what is the pattern, frequency, and timing of fire in the Kalahari dune landscape?* To answer this question, first an inventory of burned area (BA) needs to be collated and subsequently the efficiency of different BA detection methods needs to be established. This chapter seeks to better understand the detection rates and limitations of satellite products or workflows to identify the best method to create the BA inventory from 2000 – 2023 and associated fire trends which will be used in Chapter 5. The main findings are that spaced-based automated products perform poorly in the region. This is largely due to small fire being missed.

Abstract

To effectively assess the impact of fire on dust emissions in the Kalahari, it is crucial to evaluate whether burned area (BA) products accurately represent the actual extent of land burned. Most BA products are calibrated to have good agreement over global scales but struggle to accurately detect BA locally. The aim of this analysis is to create a true four-year inventory of the burned area for the arid southwest Kalahari, by comparing four datasets that estimate burned area for 2019-2022. We use two manual approaches using digitisation of burned area and change detection using Sentinel Near infra-red (NIR) and two frequently used automated datasets, NASA's MODIS burned area product and ESA's Sentinel CCI burned area pixel tool. Overall, the automated datasets struggle to detect all BA, the minimum amount of overlap with the digitised burned area was 7.12%. Like many global fire products, the coarse resolution of MCD64A1 (500m) and the FireCCIS311 product (300m) has resulted in all fires under 1 km^2 being missed by these products. We show that small fires can contribute a significant proportion of the total burned area in some dryland regions (up to 48% in the South African study area). Therefore, efforts should be made to recognise the role of small fires in burned area studies and improve algorithm detection. Our findings reinforce prior research which queries the accuracy of global fire products, drawing particular attention to the misrepresented region of the southwest Kalahari.

4.1 Introduction

Over the last 40 years, estimates of global burned area (BA) have improved in line with advances in the availability and both spatial and temporal resolution of remotely sensed technologies (Chuvieco et al., 2019). But challenges with remote sensing BA detection remain in areas with different climatic conditions, notably in semi-arid and arid regions that cover over 38.45% of the global land area (Hardtke et al., 2015; Zomer et al., 2022). Ultimately the undercalculation of BA in semi-arid and arid environments leads to the erroneous representation of these regions in fire trend studies which are important to our understanding of the Earth's system and future environmental changes.

Quantifying BA is crucial for fire ecology (Bowman et al., 2020; Harris et al., 2021; Neves et al., 2024), atmospheric (including carbon) emissions (Ramo et al., 2021; Van Der Werf et al., 2010; Yu and Ginoux, 2022), land management and deforestation (Khairoun et al., 2024; Noojipady et al., 2017), and human livelihoods (Moritz et al., 2014). The aim of this analysis is to create a true four-year inventory of burned area for the arid southwest Kalahari, by comparing four datasets that estimate burned area for 2019-2022. This is achieved through using two manual approaches of digitisation of burned area and change detection using Sentinel Near infra-red (NIR) and two frequently used automated datasets, NASA's MODIS burned area product and ESA's Sentinel CCI burned area pixel tool.

Accurate detection of BA remains complicated by vegetation type and spatially variable biomass fuel loads, resulting in diverse post-burn spectral and radiative signals (Tansey et al., 2008). As a result most products detect BA using dynamic thresholds (Chuvieco et al., 2019; Giglio et al., 2009) and are catered towards having good agreement over global scale ecosystems. However, the products have significant limitations in distinguishing BA in specific land cover types, such as semi-arid and arid environments (Hardtke et al., 2015). This complication is compounded by well-known remote sensing limitations of satellite over-pass time and frequency, cloud cover, and spatial resolution resulting in many burned area estimates being conservative (Chuvieco et al., 2020). The arid southwest Kalahari is known to experience regular fires (Andela et al., 2019; Chen et al., 2023) yet appears to be underrepresented in most global BA assessments.

Traditionally, most common space-based products estimate BA through detection of changes in spectral signature over a series of consecutive periods (Chuvieco et al., 2019). Many BA products now use a combination of changes in spectral images after the fire and active fire detection, where infrared (IR) imagery detects signals from currently burning fires (Chuvieco et al., 2019). The combination of IR radiative signature and ground spectral change was introduced to reduce false positive detection when other rapid changes in spectral signature (e.g., flooding) resulted in false positives and now is common technique for BA estimation used in MODIS and CCI products (Giglio et al., 2018; Lizundia-Loiola et al., 2020).

Numerous indices rely upon red and near infra-red (NIR) bands to detect vegetation from space (Bannari et al., 1995) and BA products utilise these indices to estimate burned area (Chuvieco et al., 2008; Giglio et al., 2018). However, accurately mapping vegetation cover in drylands has major limitations through using NIR and red bands (Marsett et al., 2006; Poitras et al., 2018). In semi-arid and arid environments there is a lack of a strong green vegetative cover, confusion between non-photosynthesizing vegetation and the bare ground, discontinuous coverage, and high coverage of senescent vegetation (Marsett et al., 2006; Poitras et al., 2018; Tueller, 1987). As a result, after burning there is a relatively small change in the spectral reflectance in semi-arid regions, influencing detection rates (Roy and Boschetti, 2009). The most widely used BA product, MODIS MCD64A1, incorporates the NIR band into its burned area detection algorithm (Giglio et al., 2018, 2009).

Globally the fastest moving fire fronts are found in semi-arid and arid grasslands where fuel structure and climate conditions result in high rates of fire spread (Andela et al., 2019). However, limited fuel availability and connectivity results in short fire durations (Andela et al., 2019). These two characteristics of dryland fires further complicate BA detection, fires burn for a short time and only over small areas. If a satellite sensor over-pass does not coincide with the rapidly moving fire front, the low-fuel fire scar does not retain enough radiative energy to be detected as burned after the fire has passed over (Hardtke et al., 2015; Hawbaker et al., 2008).

The southwest Kalahari also has rapid surface brightening after a fire which differs from wetter regions where soils darken for longer periods post-burn (Saha et al., 2019). Initially, the ash and burned debris of the fire lowers the albedo (darkens) of the desert surface and it remains darker than unburned areas for an average of 31 days (Figure 4.1 panels A and D; Saha et al., 2019), but can often be for a much shorter period of time. However, this debris is eroded away, and the removal of the biomass results in the BA having a higher albedo (brighter) than the surrounding surfaces (Figure 4.1 B,E, and F; Saha et al., 2019). Saha et al. (2019) observed that in the Kalahari the brightening of the land can last for around a year after fire. In more temperate environments where there is high soil moisture, different soil composition, and lower soil albedo, burn scars do not observe this same albedo temporal patterning on burned land (Lobell and Asner, 2002; Saha et al., 2019).

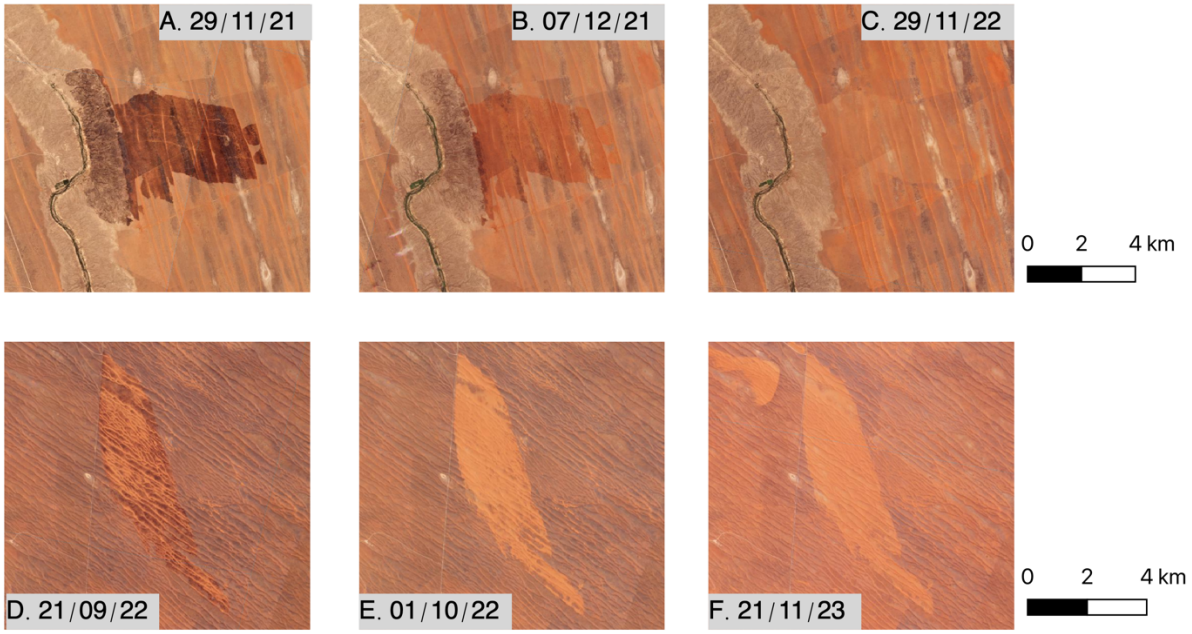

Figure 4.1. PlanetScope imagery showing the change in surface reflection (from dark to bright) for two burned area in the southwest Kalahari. Panels A to C contain a fire scar that burned in 2021 and panels D to F a fire that burned in 2022 at the start of a drought period. The landscape is dominated by an extensive area of vegetated linear sand dunes. Image © 2022 Planet Labs PBC.

Fire regimes in the arid southwest Kalahari have been under-represented in global and Africa-wide fire assessments. These omissions can include data cleaning and subsequent figures (for example Figure 4.2a) which are calibrated to focus on the wetter mid-sub Sarhan Africa (SSA), that omit still flammable areas (Andela and Van Der Werf, 2014). Additionally, many studies measure only a single year, which does not capture the full extent of oscillations in the burning regime (Figure 4.2b and Chuvieco et al., 2022; Khairoun et al., 2024; Ramo et al., 2021; van der Velde et al., 2024)

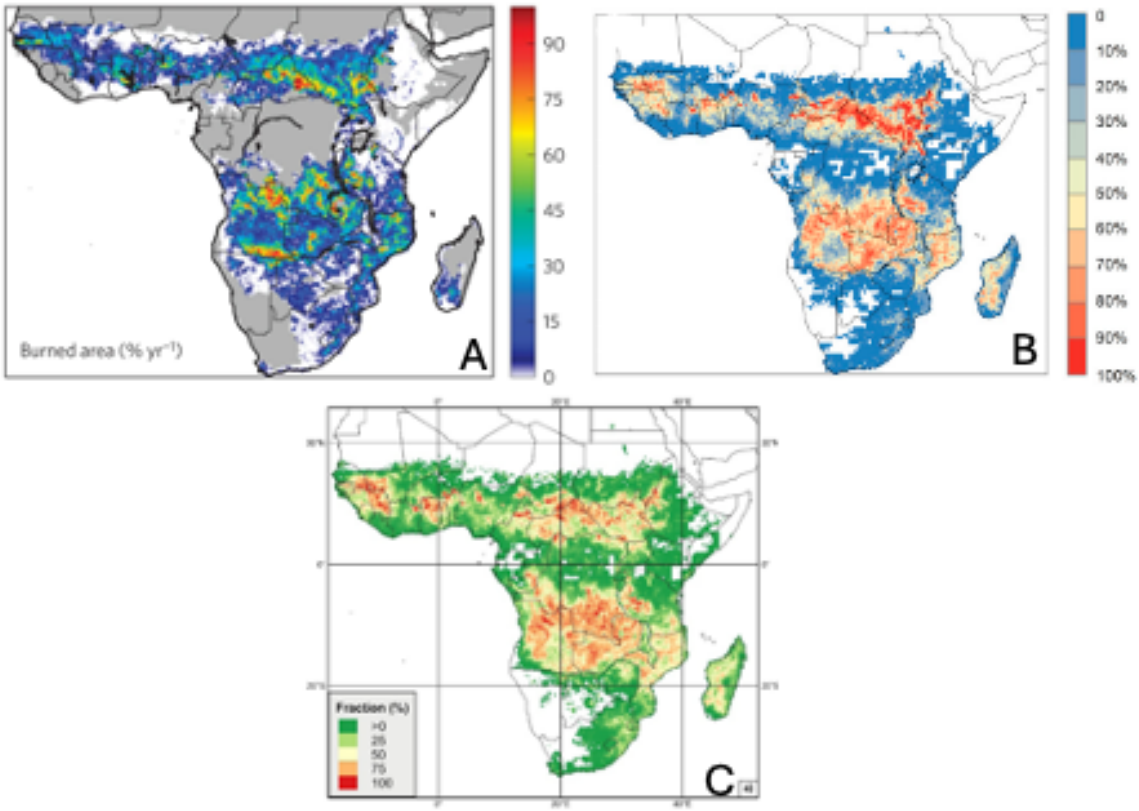

Figure 4.2. Example studies of fire in Africa that suggest that the southwest Kalahari does not burn. (A)The omission of the southwest Kalahari from savanna burned area in Andela and van der Werf, (2014) due to the removal of regions which receive under 400 mm a^{-1} precipitation. (B) burned area in 2016 only as the percent of each 0.25 degree grid cell using FireCCISFD11 in Ramo et al. (2021). (C) Burned fraction in a 0.25 degree cell for the whole sub-Saharan Africa in 2019 only from Chuvieco et al. (2022).

Most existing BA products rely on coarse spatial-resolution (> 250 m) images (Hall et al., 2016; Khairoun et al., 2024; Ramo et al., 2021). However, the use of coarse-resolution imagery leads to the omission of fires with a smaller coverage (Laris, 2005). For example, Ramo et al. (2021) used Sentinel-2's 20 m high resolution imagery to create a burned area inventory for Sub-Saharan Africa (SSA). In the study, small fires (< 100 ha) accounted for up to 41% of the total burned area in SSA, but the coarse resolution MODIS BA only returned 5% of small fires (Ramo et al., 2021).

The purpose of this chapter is to explore the current state of the burned area detection in the study region, through using two pilot study regions and conclude which method is best for BA delineation. In essence, this chapter is an extension of the methodology but reveals some novel findings regarding automated burned area detection in the Kalahari and therefore warrants its own chapter. The overall aims are to:

1. Establish BA detection rates using different methods
2. Identify factors that affect BA detection rates in the southwest Kalahari

4.2 Methods

4.2.1 Study area

Two study areas were chosen for this analysis with both in the livestock farming dominated linear dune landscape of the southwest Kalahari. The characteristic vegetation in the area is Kalahari Xeric Savanna (van Rooyen and van Rooyen, 1998) is primarily composed of grasses (such as *Schmidtia kalahariensis* and *Eragrostis lehmanniana*), but also with sparsely distributed trees (e.g., *Acacia erioloba*) and patches of shrubs (e.g., *Grewia flava*). Interspersed in the dune field are seasonally flooded basins, commonly known as pans, which are typically unvegetated (Goudie, 1991). Research region of interest (ROI) one is located around the settlement of Hoachanas in the north-western area of the dune field and ROI two is located on the dunes south of Askham in South Africa (Figure 4.3).

In the southwest Kalahari, mean annual precipitation is 150 – 200 mm but, typical of dryland regions, interannual variability is high at 50% (Thomas and Leason, 2005; Figure 2.3) and strongly influenced by ENSO cycles (Manatsa and Reason, 2017). 2019 and 2020 were dry El Niño and neutral years, but 2021 and 2022 were wet La Niña years (Figure 4.3), so here we can assess different BA detection rates during different precipitation conditions. From global long term fire maps, it is evident that the two research areas have burned over the last 20 years (Andela et al., 2019; Chen et al., 2023) and that large fires typically follow after La Niña periods (Chen et al., 2017).

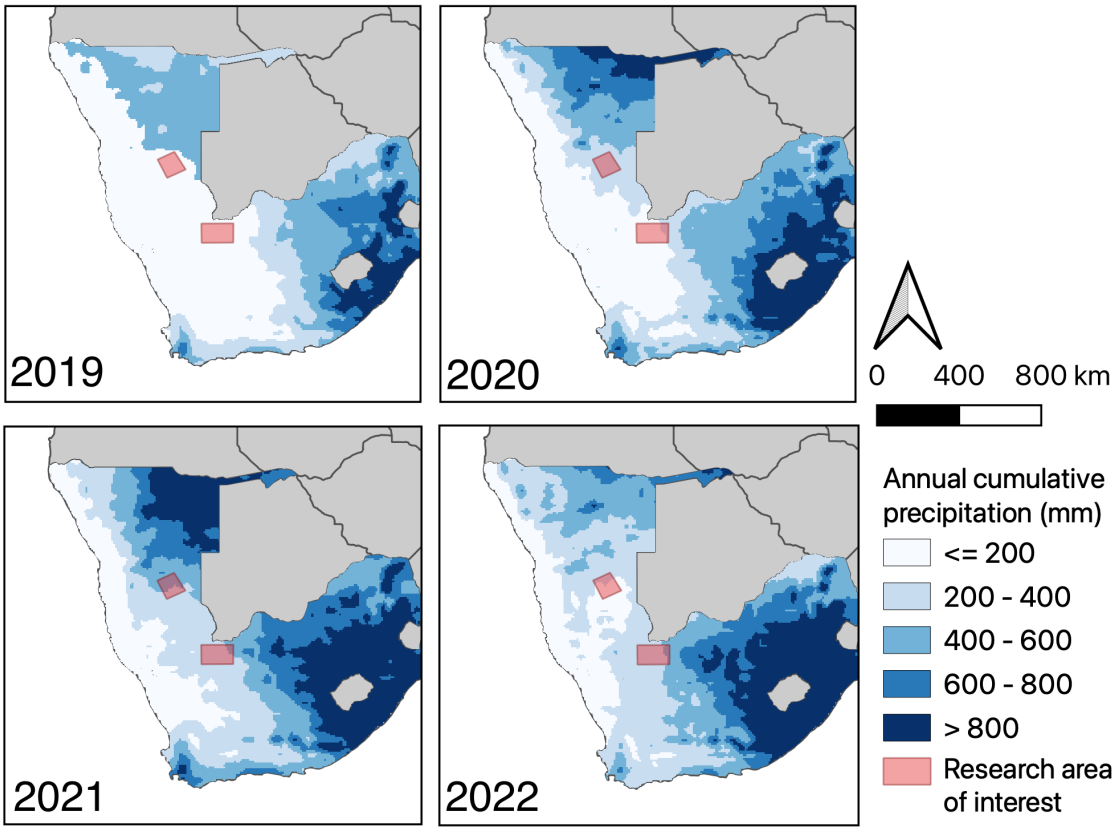

Figure 4.3. Annual cumulative precipitation (mm) for Namibia and South Africa from 2019 to 2022 calculated from ERA5-Land reanalysis data (Muñoz-Sabater et al., 2021). The Namibian research area of interest (ROI1) is the northern most pink box, whilst the South African research area of interest (ROI2) is the southern pink box.

4.2.2 Manual approaches

Digitising

In the past decade, there has been a growth in miniaturised, multi-platform satellite constellations known as CubeSats. These provide high spatial resolution (3 – 5 m) data at a daily to sub-daily rate. One such constellation is Planet Labs Dove satellites which are each equipped with a PlanetScope sensor that collects images in four bands (Red, Green, Blue, and NIR) at 3 m resolution (Planet, 2017). Manual digitisation of fire boundaries is long-standing and common practice in fire studies (Blackwood et al., 2022; Burrows et al., 2006; Burrows and Christensen, 1990; Greenville et al., 2009; Greenwood et al., 2022; Kharuk et al., 2007; Milczarek et al., 2023; van Etten et al., 2021), and here we utilised the PlanetScope images (Planet, 2017) of the study areas to visually identify burned areas that, post burn, had brightened (see Figure 4.1). The perimeter of fires identified in this manner were then manually digitised in QGIS and labelled with the day of the year when the burn scar was first visible on the PlanetScope imagery, creating a daily burned area record. The resulting inventory provided an accurate representation of the true burned area in the southwest Kalahari, although it was time and labour-intensive. Throughout the rest of the project, the manually digitised burned area scars are used as an estimate of the true burned area.

Sentinel-NIR

A semi-automated workflow to identify burned areas at monthly resolution was established using the near infrared band of Sentinel-2. Sentinel-2 provides five-day

temporal resolution imagery at 10 m spatial resolution. A differenced-based approach was adopted, where the mean NIR measurements for the last seven days of each month were subtracted from the mean NIR of the previous month. The NIR band was originally chosen, as this workflow was originally intended for the PlanetScope imagery. However, high computing power was required to process the three metre PlanetScope images in this workflow which was not available and the NIR band in Sentinel-2 still provide the most readily accessible band which showed changes in biomass and soil cover. The resulting differenced raster image highlighted areas that had seen change in the NIR value over the course of the month (Figure 4.4).

The observed changes in NIR are not however solely due to fire, as intense grazing and rapid vegetation growth can also lead to NIR change being detected. Therefore, multiple thresholds for the difference in NIR were trialled to assess which provided the most accurate burned area perimeter. The differenced-NIR outputs were assessed by using the PlanetLabs monthly true colour base map to identify burned area and a visual assessment if the NIR perimeter matched. The threshold that produced the closest match to the burned area perimeter was change that was outside the first 20% of the maximum differenced NIR (e.g., for a maximum difference of 1100 result over 220 were used) and first 20% of the minimum differenced NIR (e.g., for a minimum difference of -1100 result under -220 were used). Choosing high- and low-differenced values accounted for both ash-darkened surfaces from recent fires and brightened surfaces where the fire debris had eroded away. Areas where the differenced NIR was

within the threshold were then manually reviewed with reference to the PlanetLabs monthly base map and returns that were not fires (for example, ploughed land) were removed from the dataset (Figure 4.4). This workflow (Figure 4.4) still required a high amount of supervision and was still a labour-intensive task.

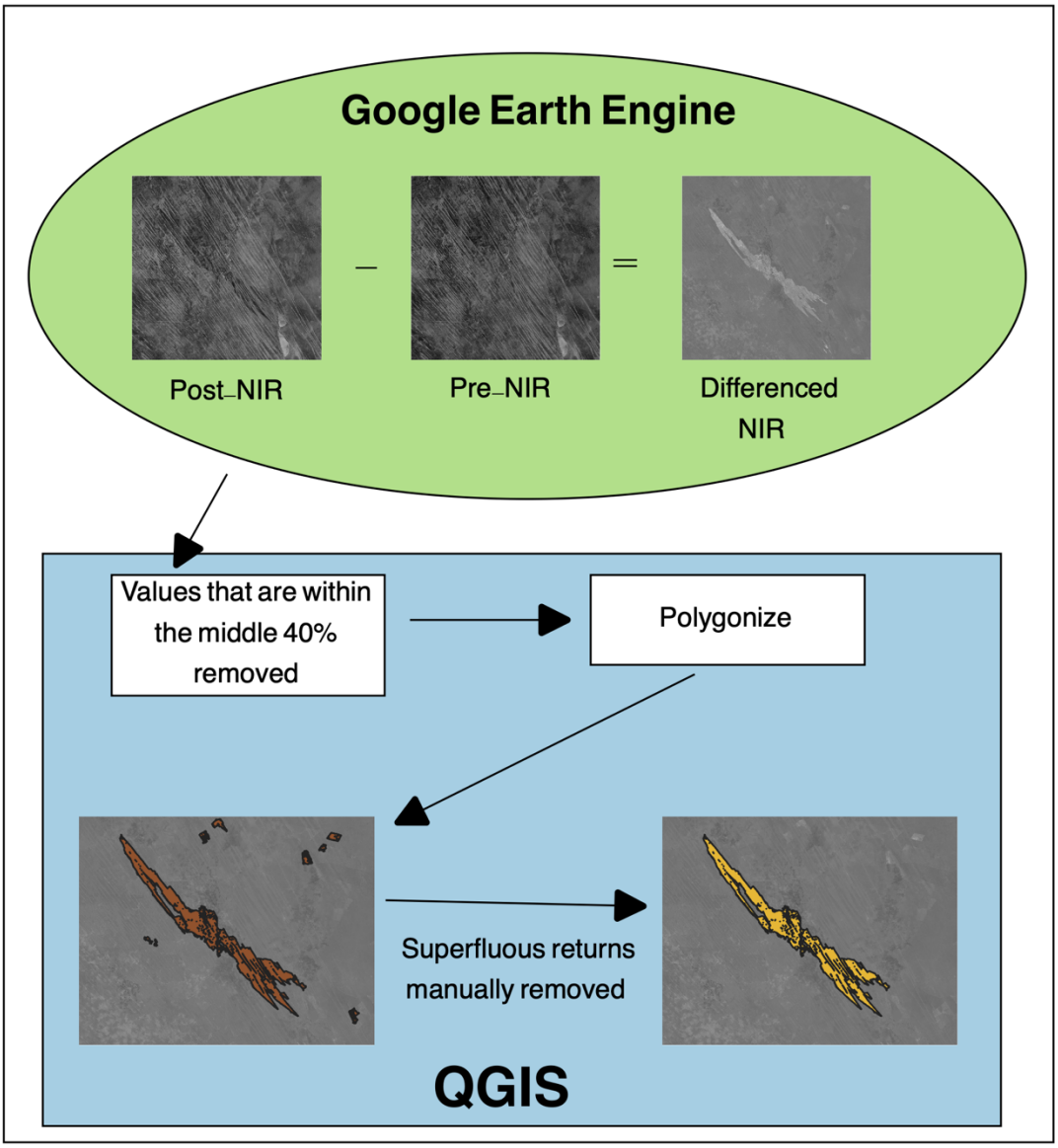

Figure 4.4. A graphical workflow for the Sentinel-NIR differenced dataset.

4.2.3 Automated approaches

Both automated approaches (MODIS MCD64A1 and ESA's FireCCIS311) follow similar overall methods for the detection of burned area which are outlined for each product below. Once the products were downloaded, the pixels were examined to identify individual fires. The classification was conducted through identifying pixels that shared borders and had burned on successive days. Creating an individual fire inventory aided in the accurate calculation of the area of each individual fire, recreating a fire count which is representative of each burn which match the format of the digitised fire scars. The BA from the automated approaches were then analysed to assess for the percentage of overlapping burned area with the digitised dataset. The overlap metric was used to assess if the automated approaches were detecting the same BA as the digitised dataset.

MODIS BA

The MODIS Burned Area Product (MCD64A1 Version 6.1; Giglio et al., 2018) is a popular tool for the detection of burned land area (e.g., Bowman et al., 2020; Harris et al., 2021; Jones et al., 2022; Roy et al., 2008; Zheng et al., 2021). The product estimates the daily burned area through rapid darkening in daily surface reflectance and dynamic thresholds of a burn sensitive vegetation index in the MODIS shortwave infrared and NIR bands (Giglio et al., 2018). The reflectance data is then combined with the 1 km MODIS active fire product to provide data on detection date and confidence level at 500 m resolution globally from the year 2000 to the present (Giglio

et al., 2018). If burning is detected in a pixel, the whole pixel is assumed to have burned.

Sentinel CCI

The Sentinel-3 SYN Fire CCI version 1.1 (FireCCIS311) pixel is the latest burned area product of the European Space Agency's (ESA) Fire CCI working group (Lizundia-Loiola et al., 2022). This product was chosen over other ESA products as it accounted for more fires than the ESA MODIS based algorithms (FireCCI51), as well as covering a larger time series than higher spatial resolution ESA products (FireCCISFD20 and FireCCISFD11; Lizundia-Loiola et al., 2020). The FireCCIS311 product utilities shortwave infrared (SWIR) from Copernicus Sentinel-3 (S3) Synergy data and the active fire detection from the Visible Infrared Imaging Radiometer Suite (VIIRS) to estimate global burned area at roughly 300 m. The dataset is only available for the years 2019 to 2022. Here we used the pixel product which was downloaded from the CEDA Archive (https://data.ceda.ac.uk/neodc/esacci/fire/data/burned_area/Sentinel3_SYN/pixel/v1.1/uncompressed/2019/01 last accessed 20/05/25) and which gives data on the date of detection, confidence level, and land cover in the pixel detected as burned. If burning is detected in a pixel, the whole pixel is assumed to have burned. The FireCCIS311 product is relatively new, having only been available to download in early 2024.

4.3 Results

In this study we used the manually digitised burned area to represent the highest accuracy of burned area detected (Figure 4.5). The digitised data returned the highest burn counts on all years and detection methods in both ROI1 and ROI2 (Tables 4.1 and 4.2). Each of these fires was individually verified to have burned by assessing true colour imagery around the date of the fire, and therefore the digitised database was taken to be the closest to the true BA. Overall, 148 burns were detected burning 1,264.52 km^2. Of the digitised burns, 45.81% (or 72 burns) were small fires which burned under an area of 1 km^2.

The burn count and burned areas detected by each method had some notable differences that impact upon the ability to establish the true impact of fire on the landscape (Figure 4.5). In 2019, a year without any fires, methods agreed and did not detect any false positives. In 2020 to 2022, when many fires were detected, the estimation of burn data differed substantially according to the method used. Across all metrics the automated methods performed poorly during high burn years. One comparative method utilised in this study was to assess the percentage of overlapping burned area with the digitised burned area. Here, MCD64A1 reports an intersection of 44.8% in ROI1 and 11.1% in ROI2 compared to FireCCIS311 reporting an overlap of 44.5% in ROI1 and 7.1% in ROI2 (Tables 4.1 and 4.2). The fire counts were also compared and for the MCD64A1 were 25% (ROI2) and 45% (ROI1) and for the FireCCIS311 23% (ROI2) and 29% (ROI1) of the digitised BA (Tables 4.1 and 4.2). Here,

the MCD64A1 product slightly outperforms the FireCCIS311 product in relation to the digitised burn count and overlapping BA.

The semi-automated Sentinel-NIR method fared better than the two automated methods producing an 81.66% overlap in ROI2 and an 33.04% overlap in ROI1. The Sentinel-NIR differencing method also detected a larger number of burns than the automated products at both study sites.

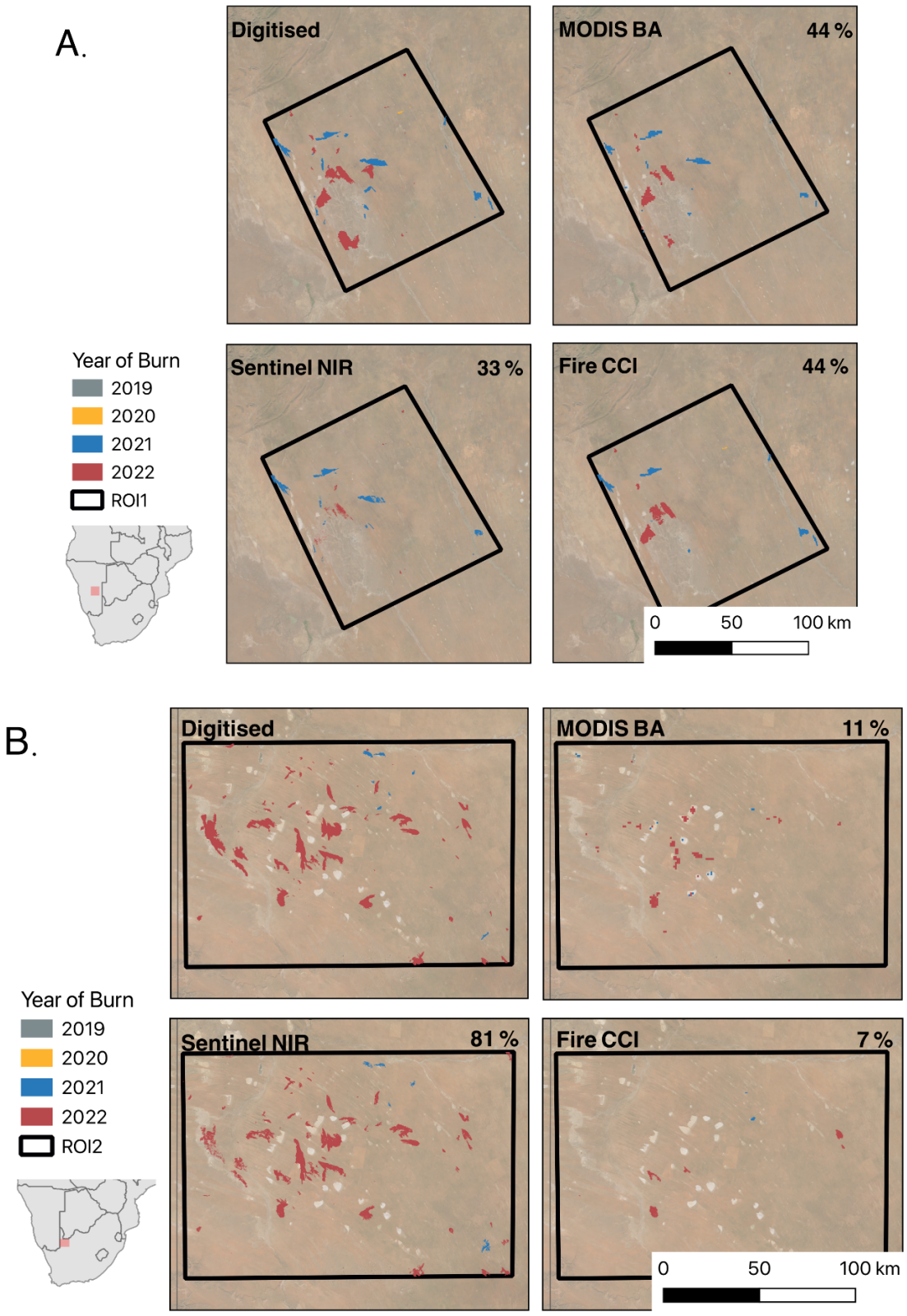

Figure 4.5. The burned area derived from each product, with the (A) panels in ROI1 and the (B) panels in ROI2. Burned area from in 2020 are in yellow, 2021 in blue, and 2022 in red, no fires were recorded in 2019. Amount of BA overlap with the digitised burned area are indicated in the top right corner. Image © 2022 Planet Labs PBC.

Table 4.1. Summaries of total burned area, fire count, overlap of BA, and percentage of small fire for ROI1 and method of BA detection.

ROI1		Digitised				Modis BA				Fire CCI				Sent NIR		
Year	Total Burned Area (km^2)	Fire count	Overlap %	% small fires	Total Burned Area (km^2)	Fire count	Overlap %	% small fires	Total Burned Area (km^2)	Fire count	Overlap %	% small fires	Total Burned Area (km^2)	Fire count	Overlap %	% small fires
2019	0	0	n/a	n/a	0	0	0	n/a	0	0	0	n/a	0	0	0	n/a
2020	0	0	n/a	n/a	0	0	0	n/a	2.88	2	0	50	0.44	1	0	100
2021	203.37	25	n/a	48	126.13	13	49.3	30.77	105.04	7	44.82	12.5	137.83	13	**62.9**	30.77
2022	331.77	22	n/a	31.82	157.39	9	41.9	11.11	179.61	5	**45.44**	0	49.93	10	14.69	40
4-year	535.14	47	n/a	40.43	283.51	22	44.76	22.73	287.51	14	**45.25**	14.29	203.37	24	33.04	37.5

Table 4.2. Summaries of total burned area, fire count, overlap of BA, and percentage of small fire for ROI2 and method of BA detection.

ROI2	**Digitisation**				**Modis BA**				**Fire CCI**				**Sent NIR**			
Year	Total Burned Area (km^2)	Fire count	Overlap %	% small fires	Total Burned Area (km^2)	Fire count	Overlap %	% small fires	Total Burned Area (km^2)	Fire count	Overlap %	% small fires	Total Burned Area (km^2)	Fire count	Overlap %	% small fires
2019	0	0	n/a	n/a	0	0	0	n/a	0	0	0	n/a	0	0	0	n/a
2020	0	0	n/a	n/a	0	0	0	n/a	0	0	0	n/a	0	0	0	n/a
2021	24.90	8	n/a	12.5	11.49	9	4.57	66.7	3.89	2	12.15	50	25.61	1	**66.73**	0
2022	701.37	99	n/a	50.51	112.14	18	11.35	27.8	51.82	23	6.95	82.61	644.03	70	**82.23**	31.43
4-year	726.27	107	n/a	48.15	123.63	27	11.12	40.74	55.71	25	7.12	80	863.23	71	**81.66**	30.99

4.4 Discussion

Satellite data are critical to mapping global burned area and each year upgraded algorithms are released that improve our understanding of global burn estimates and fire regimes. In this study we utilise four different remote sensing methods to compare relative mapping approaches for detecting burned area on an under-studied landscape of the southwest Kalahari. In general, we found that all forms of detection produced highly different results to the manually digitised burned area.

4.4.1 Time series

All the products showed large heterogeneity in the yearly fire count, with zero burns being recorded in 2019 and 99 being recorded in ROI2 in 2022. The range in burn counts over both research areas highlights the interannual variability of fires in the region. It is highly likely that there were no burns in the areas in 2019, but in other years such as 2022 there are multiple, widespread fires. Presenting one year of fire data is a common occurrence in the literature and has been used to present new fire products (Chuvieco et al., 2022; Roy et al., 2008; Tansey et al., 2004) and to calculate product error (Khairoun et al., 2024; Ramo et al., 2021). We show that such an approach, for highly variable arid regions at least, cannot be a full characterisation of the fire regime. Therefore, careful consideration needs to be taken with fire studies that present data for only one year, as the data (see figure 4.2) may not be representative of the regional fire regime and give the false impression that fire does not burn in certain regions. This present study is limited in its representation of the

regional fire regime as the analysis only utilises the four years of data available with the FireCCIS311 product.

4.4.2 Method comparison

Manual digitisation of fire scars has been used to validate burned area estimates (Milczarek et al., 2023; Silva et al., 2005) and therefore taken to be the closest representation of the true burned area in this study. The regions of interest were examined at a monthly resolution to identify any changes in surface reflection and then each fire scar was verified at the daily level at three metre resolution to ensure burning evidence at the site. However, this method was not without limitations. Only the boundaries of each fire scar were digitised to create this dataset. Some fires burned incompletely resulting in partial burning within the scar boundary, in these cases the digitised BA is an overestimation. Manually digitising using PlanetScope imagery is a time and labour heavy task, and the imagery is somewhat limited for automated mapping of burned area by recording at only four bands (Red, Green, Blue, and NIR). However, recent efforts have been made to use the PlanetScope sensors to estimate burned area (Azami et al., 2022; B. Kim et al., 2024).

The different frequency of fires in ROI1 and ROI2 could be a possible explanation for the observed difference in detection rates between the platforms and research areas. ROI2 had more than double the fire count than that of ROI1, allowing for a higher chance for fires to be missed by the lower resolution assessments. Both automated

products rely on active fire products to supplement the detection of burned area and it is well established this approach is not the best method to map burned area (Chen et al., 2023; Neves et al., 2024; Van Der Werf et al., 2017). Daily over-pass time affects active fire detection, with both the MODIS and VIIRS satellites over-passing twice a day. Fires in the southern Africa burn quickly (Andela et al., 2019) and often do not coincide with a sensor over-pass and therefore the active fire product misses the fire occurrence. Burning and over-pass mismatch error is heightened in arid environments where the low fuel load does not retain heat after the fire front has moved through and lacks the post-fire radiative energy to be classified as an active burn (Andela et al., 2019; Hardtke et al., 2015; Hawbaker et al., 2008).

Over the 4-year study period, ROI1 and ROI2 observed different patterns of burned area detection. Both the automated methods performed poorly in ROI2, with only 11.12% overlap with the digitised burned area for MCD64A1 and 7.12% for FireCCIS311 products. This low rate of detection suggests some burns in ROI2 occurred under cloud cover and resulted in the active fire product not being triggered (Giglio et al., 2013; Justice et al., 2002; Schroeder et al., 2014). Cloudiness was observed in the MODIS imagery on 24/10/2022 and 30/11/2022 when the highest frequency of burn counts was measured. For example, a large fire (68.5 km^2) burned under cloud cover in ROI2 on 30/11/2022 (Figure 4.6) and was not detected by either VIIRS or the MODIS active fire products. By the next day the surface had brightened in comparison to the surrounding area. This suggests that the combination of cloudiness with the

rapid and unusual pattern of surface brightening post-fire fails to trigger the surface reflectance change detection in automated BA products.

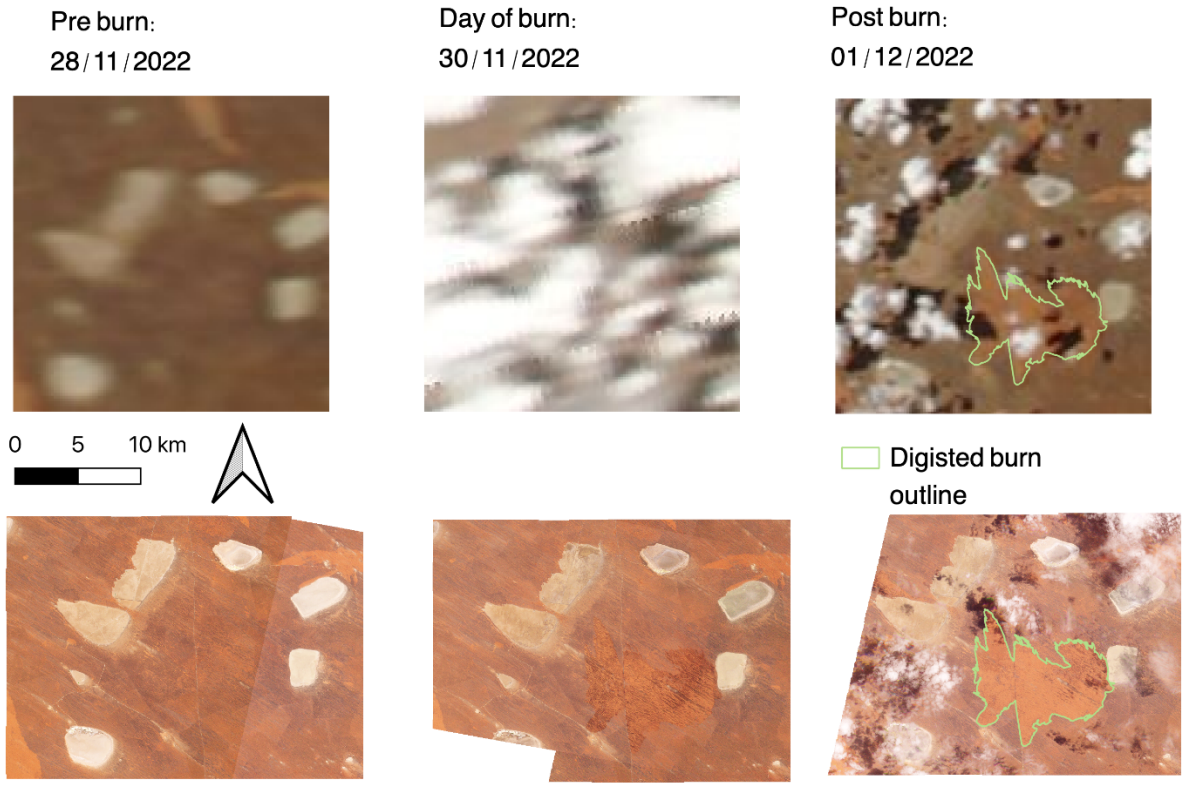

Figure 4.6. MODIS Aqua true colour imagery (top row) and PlanetScope RGB imagery (bottom row) displaying the same burn scar in South Africa over 3 days in 2022. Cloud can be seen obscuring the burn during the MODIS over-pass. The Planet Scope imagery reveals the surface only remained darkened for one day after the burn. Image © 2022 Planet Labs PBC.

In ROI2 the Sentinel-NIR differenced workflow performed better than the automated products. Here the averaging of the month enables a cloud-free surface change detection to take place that was catered towards both the brightening and darkening changes in surface reflection, therefore capturing the quick brightening of the burned areas (Figure 4.6). The high detection rate came at the cost of lower temporal resolution: the Sentinel-NIR differencing method recorded monthly. Additionally, by

capturing both increase and decrease in NIR over a month, several false positives were detected, and the outlines of the fire were often inflated using the Sentinel-NIR workflow.

MCD64A1 can be particularly affected by using a vegetative index to detect BA. Although this vegetation index makes use of the NIR band 5 and SWIR band 7 on MODIS satellites, vegetation in semi-arid and arid areas often have different spectral signals than that in more temperate locations (Marsett et al., 2006; Poitras et al., 2018) and the reliance of the product on changing vegetation spectra can result in an under detection of burning. The Kalahari is covered in lots of annual grasses which for most of the year are senescent and therefore NIR-based indices may not be best for the detection of burning in this region.

Additionally, the MCD64A1 product produced more commission errors than the FireCCIS311 product. These errors were particularly evident in ROI2 where there are multiple pans. The MCD64A1 detected fires on the pans on multiple occasions accounting for 1.7% and 25.4% of returns in ROI1 and ROI2 respectively (Figure 4.5). It is unlikely that these MCD64A1-detected BA burned due to the low vegetation cover, however the pans have rapid change in reflectance (and darken) when they flood, which can trigger the false-positive record. Despite this, the MCD64A1 product still had the highest overlapping BA with the digitised burned area, indicating the product was more accurate than the FireCCIS311 product at mapping true fire scars.

ROI2 had more than double the number of burn counts than that of ROI1 but only had 26.3% more burned area. The number of smaller fires could account for the lack of BA detection as it is well documented that the coarse spatial resolution of MCD64A1 and precursors of the FireCCIS311 products struggle to detect BA under 100 ha (Laris, 2005; Ramo et al., 2021). Yet, 40.43% (ROI1) and 48.15% (ROI2) of the digitised BA were under 1 km^2 and both the FireCCIS311 and MCD64A1 products reported the detection of small fires. Whilst only a small proportion of the FireCCIS311 product were small fires the MCD64A1 product reports high percentages of fires under 1 km^2 (Tables 4.1 and 4.2). Upon further investigation 90% of the small fires detected by MCD64A1 in ROI2 in 2022 were located within pans and therefore discounted as commission errors. Both automated products record 0% overlapping BA in ROI1 and ROI2 with the digitised dataset for fires under 1 km^2. Therefore, the two automated products are failing to detect the true burned area under 1 km^2 in the southwest Kalahari. Chevico et al. (2022) produced a small fire database for SSA but this database is only available for 2019, the year in which there was no fire in the study area, and therefore this study is not useful to verify compared to a higher spatial resolution product.

The Sentinel-NIR differencing technique proved useful in ROI2, but converted much less burned area in ROI1, particularly when compared to the automated methods. This discrepancy in consistency of the workflow resulted in doubts in its viability moving

forward. Differencing data at 10 m resolution for 48 months required a vast computing power, and the manual deletion of superfluous returns also required a lot of human discretion over what was BA or not. It was often found that burned area outlines were combined with areas where the differencing has highlighted changes in NIR which were not fire, and so the workflow often produced an overestimation of burned area. However, the tool was useful at identifying gaps inside burned areas that the manual digitisation did not account for. Ultimately the high computing power, labour-intensive cleaning of the data, and high amounts of exaggerated burned area resulted in the decision not to roll out this workflow over a longer time-series. Exploring the SWIR band and using that to identify fires may also be a useful way to estimate BA in semi-arid or arid environments, but at present was outside the scope of this study.

4.5 Conclusions

We compared four burned area datasets in the southwest Kalahari. In general, we found that annual variations in fire trends leads to the under-representation of fire in this region in many large global fire studies that only use a single years' worth of burned area data. Detection from both the MCD64A1 and FireCCIS311 product was low, the minimum amount of overlap with the digitised burned area was 7.12%. Detection of burned area is also hampered by the low biomass and differing vegetative spectral reflectance that is observed in arid environments. Like many global fire products, the coarse resolution of MCD64A1 (500 m) and the FireCCIS311 product (300 m) has resulted in all fires under 1 km^2 being missed by these products. We show

that small fires can contribute a significant proportion of the total burned area in some dryland regions (up to 48% in the South African study area). Therefore, efforts should be made to recognise the role of small fires in burned area studies and improve algorithms detection. Additionally, the 3-meter resolution of the Planet Scope satellites provides useful imagery for burned area detection, with sometimes sub-daily temporal resolution and could be utilised in the future for burned area detection.

Chapter 5 -

Post-fire vegetation recovery and human activity limits the scale of fire disturbance on a partially vegetated dune landscape – the southwest Kalahari linear dune system.

Status: Submitted to *Science of the Total Environment* in May 2025.

Fire burning on the dunes in 2022. Photo: K. Steenkamp.

Summary

This research paper addresses **research question one** – *what is the pattern, frequency, and timing of fire in the Kalahari dune landscape?* - through creating an inventory of burned area in the southwest Kalahari over 2000-2023. From the inventory the spatial and temporal scale, as well as patterns and trends in fire occurrence are determined. Fire is common in the region with 11% of the study burning, but fire occurrence and size is significantly impacted by land use, with the National Park having the longest burning and largest fires. Vegetation post-fire also recovers quickly in under two years.

Abstract

Fire is often cited as a major disturbance that can induce increased aeolian activity on vegetated sand dunes due to the removal of protective plant cover. This study investigated the spatial and temporal dimensions of burning as an agent of disturbance in partially vegetated linear dunes in the southwest Kalahari. The region is often omitted as a burn-prone area in continental and global burned area studies due to its aridity and proximity to intense temperate zone fires. The MODIS burned area product was used to create an inventory of burned area from 2000-2023 to identify trends in burned area extent and occurrence. In addition, MODIS-derived Soil Adjusted Total Vegetation Index (SATVI) was used to calculate vegetation recovery post-burn. Over the 24-year study period 13,310 km^2 of the southwest Kalahari dune field burned; 11.1% of the total area. Land management regime significantly impacts on fire occurrence ($p < 0.001$) and size ($p < 0.001$), with more burns occurring on privately owned land but larger burns within the National Park, and duration ($p < 0.001$) with the National Park having longer duration burns. Vegetation recovery is swift after burning, with cover returning to control levels within two years of being burned. The implications highlight how the Kalahari linear dune field is neglected in burned area studies but burns regularly. However, the temporal and spatial disturbance effect of the fire is limited by anthropogenic modulation of the fire regime and rapid vegetation recovery post-burn.

5.1 Introduction

In desert dune environments, aeolian processes dominate sediment distribution and are a fundamental factor in biogeochemical cycles and geomorphological patterns (Field et al., 2010; Okin et al., 2006; Ravi et al., 2011; Wiggs, 2022). Vegetation on dunes can affect the ability of the wind to move sediment by reducing the erodibility of the surface through physical sheltering or binding of sediments, and by reducing the erosivity of the wind by increasing the aerodynamic roughness (Leenders et al., 2007; Ravi et al., 2011; Wiggs et al., 1995). Consequently, landscape-scale dune surface activity has been framed according to vegetation cover (Livingstone and Thomas, 1993): 'active' dunes are often bare or with low vegetation density, and have high levels of aeolian erosion; 'fixed' or 'inactive' dunes have higher vegetation densities and are considered stabilised with limited aeolian erosion. Consequently, both states will stay in equilibrium unless disturbed (Bhattachan et al., 2014).

Disturbance events are classed as events which cause an perturbation to a component of the system (Rykiel, 1985) and in vegetated dunes include the loss of stabilising vegetation through drought, grazing, or fire amongst other factors. Wiggs et al., (1995) found a non-linear relationship between mean vegetation cover and surface activity in the southwest Kalahari and noted that when cover falls below 14% on the crest and upper flanks of the dune then surface activity increases markedly. Although there is no simple threshold of vegetation cover below which surface activity begins as transport can happen at high surface coverage (especially under high wind stress), the

effective threshold of 14% surface cover is a useful indicator for surface activity at the dune scale (Wiggs et al., 1995). Once vegetation is disturbed beyond a critical threshold, positive feedback mechanisms can push a system that was previously stable to an alternative stable state (i.e., from inactive to active), which can be an irreversible switch (Bhattachan et al., 2014; Yizhaq et al., 2009). Vegetated or partially-vegetated dune systems are a significant feature of many dryland landscapes (Hesse and Simpson, 2006; Siegal et al., 2013), and fire is considered to be a significant mechanism for vegetation destruction and increase in wind-erosion in dryland environments (Mayaud et al., 2017a; Miller et al., 2012; Wasson and Nanninga, 1986).

Once a sand surface has become activated, bombarding sediment can cause mechanical injury to vegetation, increasing vegetation mortality and limiting the regrowth of plants (Kadmon and Leschner, 1995; Strong et al., 2010). Dunes can become taller and steeper (Hesse and Simpson, 2006), and surfaces may become active dust sources (Sweeney et al., 2023), which can have detrimental effects on local air quality and human health (Goudie, 2014). In the immediate aftermath of a fire, the incineration of vegetation releases previously trapped sediment and modulates airflow which can lead to an increase the erosivity of the wind (Okin et al., 2009). Additionally, fire changes the erodibility of the surface through inducing soil hydrophobicity (Ravi et al., 2009b). The duration of increased aeolian activity is linked to the length of time in which vegetation can recolonise the burned area. In the linear dune systems of the Kalahari and Simpson Deserts the recovery time has been posited

to be around five and over six years respectively (Strong et al., 2010; Wiggs et al., 1994) but some estimates place recovery times to be as high as 25-30 years (Levin et al., 2012). Therefore, defining the magnitude, both spatially and temporally, of state-changing vegetation disturbances can allow a better quantification of the significance of the disturbance on a landscape.

Climate oscillations and weather are important controls on fire activity (Pricope and Binford, 2012; Swetnam and Betancourt, 2010, 1990). For significant burning to occur fires require biomass accumulation, atmospheric conditions conducive to burning (e.g., dry and windy), and an ignition event (Lehmann et al., 2014; Moritz et al., 2012, 2005). Over short timescales, precipitation can limit fire ignition and extent, and over longer periods climatic oscillations can lead to biomass accumulation in the wet season and increased fuel accumulation for burning during drier periods (Pricope and Binford, 2012).

In the vegetated linear dune system, extended dry seasons, predominantly grass ecosystems, combined with the arid environment, leads to surfaces being vulnerable to burning. Furthermore, fire occurrence, extent and severity are affected by a mixture of both natural, and anthropogenic factors. For example, fires are ignited through both natural (e.g., lightning) and anthropogenic (e.g., cigarette stubs, vehicle sparks) causes and, under the right conditions, can spread quickly.

For decades, mapping burned area and quantifying the impact of burning on the environment at a range of scales has been a focus for interdisciplinary studies (Barbosa et al., 1999; Chen et al., 2023; Chuvieco et al., 2018; Chuvieco and Martin, 1994; Giglio et al., 2018; Tansey et al., 2004). These studies are often conducted at global to continental scale, and burned area representation in figures often highlights the intensity of fire in more woodier or temperate regions (e.g., Andela and Van Der Werf, 2014; Khairoun et al., 2024; Xiang et al., 2023) or over short timescales (e.g., Chuvieco et al., 2018, 2022). As a result of these scaling decisions there is frequent omission of some arid areas as burn-prone regions (Andela and Van Der Werf, 2014; Jones et al., 2022).

A growing body of research addresses post-fire aeolian erosion in arid environments (Dukes et al., 2018; Ravi and D'Odorico, 2009; Roehner et al., 2020; Sankey et al., 2012, 2011; Wang et al., 2019; Whicker et al., 2002). Research has also addressed some drivers of disturbance on vegetated linear dunes including increased aridity (Thomas et al., 2005) and grazing pressure (Bhattachan et al., 2014). Fire is often cited as being a major disturbance that can induce increased aeolian activity on sand dunes (e.g., Hugenholtz and Wolfe, 2005; Mayaud et al., 2017b; Nield and Baas, 2008). There has, to date, been little assessment of the scale of fire as a disturbance factor on vegetated sand dunes. Here, we aim to investigate the scale of burning as an agent of disturbance in partially vegetated dunes in the southwest Kalahari. This aim is achieved through creating an

inventory of fire from 2000-2023 to identify trends in burned area extent and occurrence.

5.2 Study area

The southwestern Kalahari dune field (Figure 5.1) covers ~120,200 km^2 in South Africa, Namibia, and Botswana. The linear dunes in this region cover the western portion of the Kalahari Sand Sea in eastern Namibia, the Northern Cape of South Africa and just branching into Botswana before degrading to dune-like patterns resembling barchanoid ridges to the east (Bullard et al., 1995). The most common dune form in the study area is classified as vegetated linear dunes which extend mainly NNW to SSE (Thomas and Wiggs, 2022).

Today much of the southwest Kalahari linear dune field comprises agricultural land, which is either privately owned or community-administered and used for livestock production, herein 'primarily private farmland' (PPF). The exception is the Kgalagadi Transfrontier Park (KTP), located in the Northern Cape of South Africa and across the border into Botswana (Figure 5.1). The two different land uses have differing fire management policies. Since colonial times the Namibian national fire policy has been to avoid fires, a policy still enforced amongst local landholders as fire can have devastating effects for agriculture, property, and grazing (Humphrey et al., 2021). The Kgalagadi Transfrontier Park fire policy dictates that fires that burn in the dry season are allowed to burn until they self-extinguish (Spies et al., 2016).

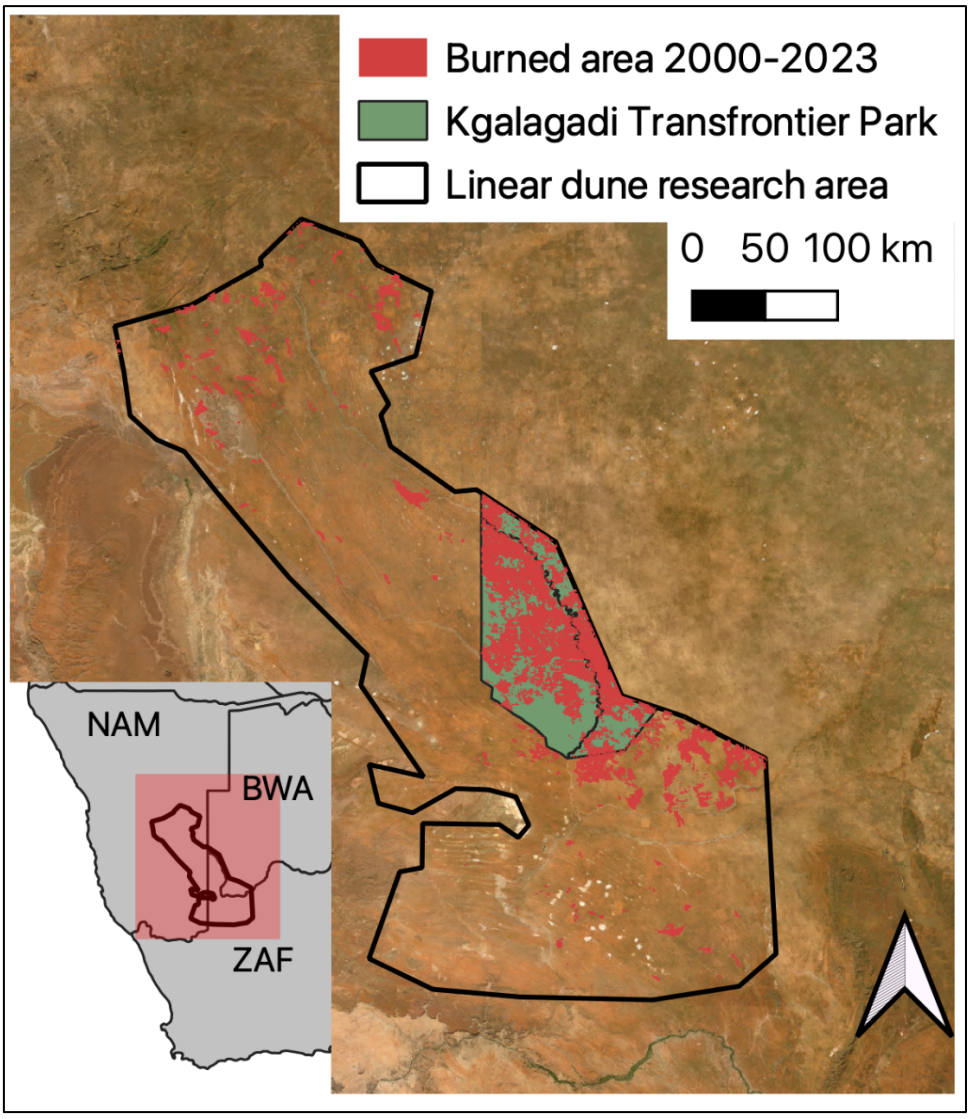

Figure 5.1. Fire in the southwest Kalahari dune field. The study area of interest outlined in black and all burned land delineated by the MODIS BA product from 2000 to 2023 are displayed in red. The Kgalagadi Transfrontier National Park is highlighted in green. Image © 2023 Planet Labs PBC (Planet, 2017).

The typical vegetation in the study area is Kalahari Xeric Savanna (van Rooyen and van Rooyen, 1998), a mix of annual grasses (mainly *Schmidtia kalahariensis*), perennial grasses (e.g., *Eragrostis lehmanniana*), shrubs (e.g., *Acacia mellifera)* and sparsely populated trees (e.g., *Acacia erioloba*). The dominance of annual grasses, particularly in

the farmland, leads to an annual build-up of dead and dry vegetation that are easily combustible. The vegetation is very sensitive to changes in climatic and physical conditions and therefore coverage is dynamic in both time and space through complex relationships between sediment, plants, temperature, grazing pressure, and wind erosion processes (Bailey, 2011; Smit et al., 2024). The ephemerality of vegetation cover provides a unique biogeomorphological landscape on which fires can develop. The ability of a fire to spread laterally is restricted by the vegetation state of the dune crests, as fire often cannot spread across large unvegetated inter spaces of the crests (Burrows et al., 2009).

The study area today exhibits a strong north-south precipitation gradient (Figure 5.2), with the northern region receiving more precipitation linked to the seasonal movement of the Inter-Tropical Convergence Zone (Kaseke et al., 2016). The region has large interannual variability in precipitation but generally the year can be classified into three seasons: cold and dry in May to August, hot and dry in September to December, and hot and wet in January to April (Mills and Retief, 1984; Stapelberg et al., 2008; van Rooyen and van Rooyen, 1998). Herein we refer to the cold and dry and the hot and dry seasons as the 'dry season' and the hot and wet season as the 'wet season'. In wet years biomass can build up, whereas in dry years without disturbance biomass will remain constant or reduce. The El Niño-Southern Oscillation (ENSO) modulates precipitation patterns over differing oscillations to induce drought or intensify wet season rainfall which can further build biomass and affect interannual

variability in fuel load and subsequent burning (Andela and Van Der Werf, 2014; Le et al., 2022; Swetnam and Betancourt, 1990). In southern Africa, ENSO influence on surface temperature is strong and is triggered by the sea surface temperatures in the Indian Ocean the preceding December (Manatsa and Reason, 2017). Therefore, water resources in the region fluctuate with ENSO oscillations with extreme cycles resulting in El Niño and La Niña phases (Manatsa and Reason, 2017). El Niño phases have been linked to a decrease in precipitation, drought, and a reduction in vegetation (Hao et al., 2020; Nicholson et al., 2001) and La Niña phases have been linked to increased precipitation (Mphale et al., 2014) in the region.

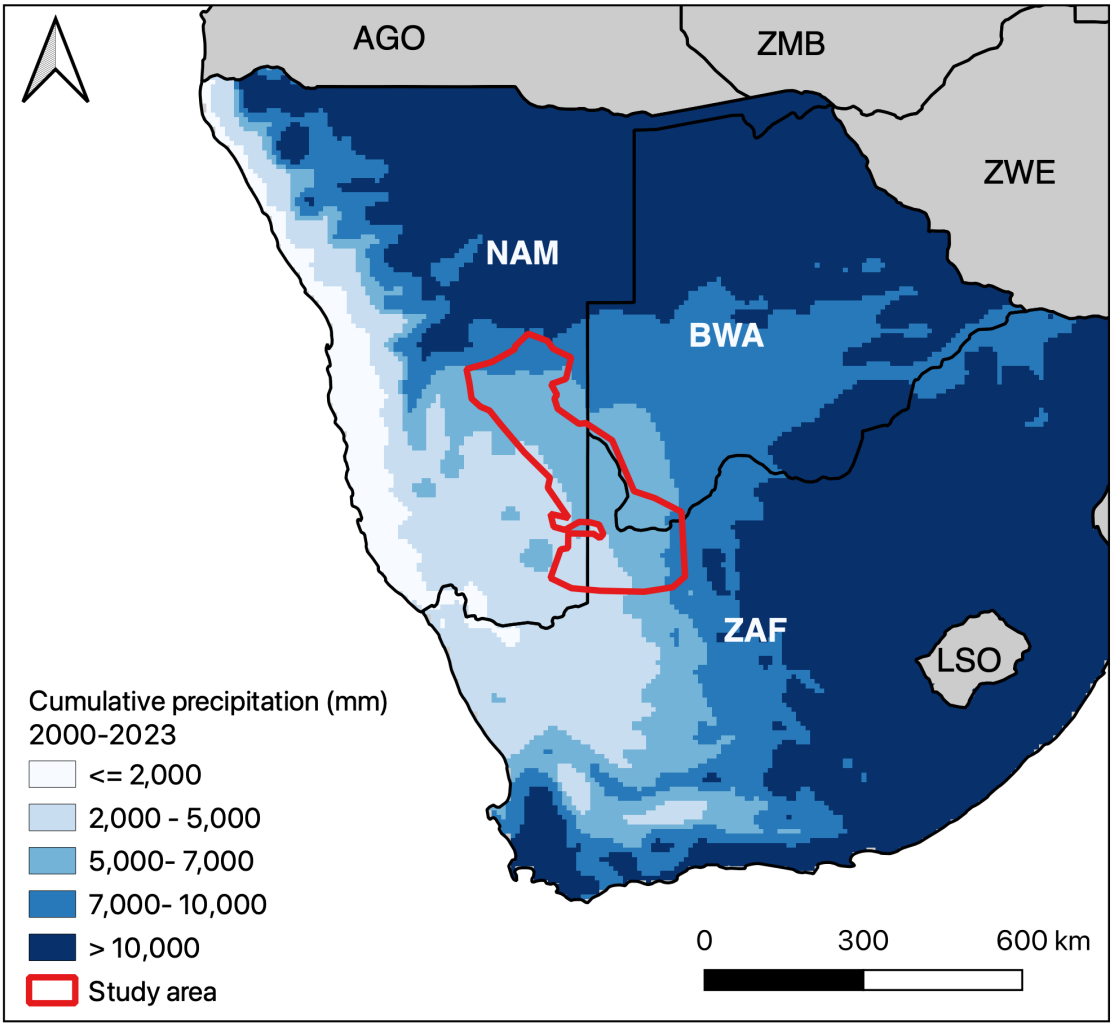

Figure 5.2. Cumulative precipitation (mm) in South Africa, Botswana, and Namibia from 01/01/2000 – 31/12/2023 using ERA5-Land reanalysis daily total sum precipitation (Muñoz-Sabater et al., 2021). The study area is outlined in red.

5.3 Methods

5.3.1 Burned Area

The MODIS Burned Area (BA) Product (MCD64A1 Version 6.1; Giglio et al., 2018) is a popular tool for the detection of burned land area (Bowman et al., 2020; Harris et al., 2021; Jones et al., 2022; Roy et al., 2008; van der Velde et al., 2024; Zheng et al., 2021). The product estimates the daily burned area through rapid changes in daily surface reflectance at 500 m resolution globally from the year 2000 to the present (Giglio et al.,

2018). The MODIS BA tool has been useful for global fire trend studies (e.g., Giglio et al., 2013; Jones et al., 2022; Van Der Werf et al., 2010) to build a picture of fire occurrence, controls, and trends. But, like many satellite-derived measurements, the MODIS BA product still has a variety of limitations (Chuvieco et al., 2019). These can lead to commission errors (false-positives) and omission errors (false-negatives) and may form due to satellite over-pass frequency and diurnal timing, cloud cover, and the low spatial resolution of the algorithm (Jones et al., 2022). These errors do not occur uniformly across the globe, due to cloud cover and over-pass frequency, and detection rates in southern Africa sit at approximately 85% of the true burned area (Archibald et al., 2009). Another known limitation is coarse-resolution BA products, such as MODIS BA, struggle to detect small fires < 500 m^2, which leads to an underestimation of the true burned area (Boschetti et al., 2019; Campagnolo et al., 2021; Khairoun et al., 2024). Despite these limitations, the MODIS BA product provides a succinct fire detection tool for the last 24 years, particularly in hard-to-access areas, which can give useful insights into fire that could not be achieved with local inventories of fire activity (Jones et al., 2022). Here, we use the MODIS BA product to achieve an overall image of fire activity on the Kalahari linear dunes for the last 24 years to assess trends in occurrence and extent.

To mitigate the effect of any commission errors within the fire count, each burn recording from the MODIS BA data was individually assessed for the possibility of the MODIS BA algorithm returning a false-positive. For example, a high number of

pixels identified as burned were found in pans (deflation basins that can have seasonal inundation of surface water, but which are usually dry; Goudie,1991) in the South African area of the study. Burn pixels that were found within pans were removed due to the low likelihood that they represented fires, as many pan surfaces have less than 10%, and often zero vegetation cover (Leistner, 1959) but can experience rapid changes in surface reflectance when they flood, potentially triggering the MODIS algorithm to detect fire on the pans.

Once the commission errors were removed, these data were then assessed for fires that were burning in multiple fronts or over many days which returned numerous unconnected pixels and increasing the total burn count. The fires that were burning on multiple fronts were classed as one burn in the count, determined by looking at the previous day's burned pixels and assessing if the current day's pixels were connected. However, each individual day the continuing fire burned was counted as a new burn in the count. Following this method causes large size burns to only count as a singular burn, leading to difficulty differentiating between large and small burns which can have vastly different effects in terms of scale of disturbance. Therefore, to quantify the spatial and temporal scale of fire as a disturbance effect on the landscape, a combination of both daily burn count, daily burned area, and burn duration was used in this study.

Data were then gridded to 0.5° by 0.5°. The count for each grid cell with overlapping burned area was then calculated to compile how many separate days over the study period the cell burned. The shortest gap between burn years for each cell was used to estimate reburn time. Each grid cell covers ~113 km^2, and there is the possibility that the two separate fires that are counted as reburning do not have any overlap. Further, by scaling reburn at a yearly scale, fires that burned in the same fire season (for example December 2021 and January 2022) would count as a reburn. If fires are large and burn slowly for an extended period, then they may be detected as reburned areas. The majority of the pixels that have a less than 5-year reburn time, burned in two separate fires in September 2022 and September 2021. These two fires burned within the same pixel, but not necessarily the same area on the ground.

5.3.2 Climate data

Globally there is a link between vegetation fire occurrence and ENSO extreme phases (Andela and Van Der Werf, 2014; Burton et al., 2020; Cordero et al., 2024; Fuller and Murphy, 2006; Harrison and Meindl, 2001; Mariani et al., 2016). To assess any relationship between fires and ENSO extreme phases in the study area, monthly ENSO occurrence data was downloaded from the National Oceans and Atmosphere Administration's (NOAA) Climate Prediction Center (CPC; dataset available at https://origin.cpc.ncep.noaa.gov/products/analysis_monitoring/ensostuff/ONI_v5.php). Each month was classified into El Niño, La Niña, or no occurrence. Due to the non-normality of the data, Kruskal-Wallis rank sum tests were performed to assess the

statistical relationships between the ENSO and the burn count, burned area, and burn duration for the whole study area, the Kgalagadi Transfrontier Park, and the primarily private farmland.

5.3.3 Vegetation indices

To investigate how long the surface is devoid of protective vegetation (both alive and dead) after fire, 17 fire scars were selected to track throughout the study period. Each burn required an area larger than one kilometre to be tracked and there needed to be no evidence of previous burning (verified through the MODIS BA product for fires after 2009 or Google Earth before 2009). The coordinates of each fire scar are listed in Table 5.1. Each of these scars were then co-located with an adjacent unburned (termed control) area for comparative purposes. These corresponding 17 control locations are situated more than 500 m outside of the fire scar to ensure they were in a different pixel of MODIS imagery.

MODIS Surface reflectance product (MOD09GA) provides daily, 500 m resolution surface reflectance for MODIS bands 1- 7. To obtain consistent above-ground biomass estimates for the sites, we calculated the Soil Adjusted Total Vegetation Index (SATVI; Marsett et al., 2006) for each daily MOD09GA image. SATVI is calculated as:

$$\mathrm{SATVI} = \frac{\mathrm{SWIR1} - \mathrm{R}}{\mathrm{SWIR1} + \mathrm{R} + \mathrm{L}} (\mathrm{I} + \mathrm{L}) - \frac{\mathrm{SWIR2}}{2}$$

Equation 5.1.

Where SWIR1 = MODIS shortwave infrared Band 6, R = MODIS Red Band 1, and SWIR2 = MODIS shortwave infrared Band 7. L is a soil-adjustment factor between 0 and 1. The L value of 0.5 was used in this study, representing a moderate vegetation coverage. The SATVI index returns a value between -1 (no vegetation) and 1 (green vegetation).

SATVI has been shown to detect changes in vegetation than more commonly-used vegetation indices, such as the Normalised Differenced Vegetation Index (NDVI) or the Enhanced Vegetation Index (EVI), were unable to detect (Goirán et al., 2012). This enhanced detection can be attributed to SATVI utilising shortwave Infrared (SWIR) bands which are sensitive to both green and senescent vegetation, as opposed to NDVI and EVI which rely on near infrared for green vegetation only. The sensitivity to non-green vegetation cover has made SATVI a useful tool in arid environments where vegetation is senescent for much of the year (Marsett et al., 2006; Poitras et al., 2018). NDVI and EVI calculated with MODIS MOD09GA 16-day tool for each tracked fire scar were originally calculated for this study as well, but ultimately were excluded due to the lack of sensitivity to changes in vegetation in arid environments. However, the workflow for the data was established whilst still including NDVI and EVI data. To match MODIS product EVI and NDVI sample temporal resolution, the SATVI data were reduced to 16-day mean reflectance.

The percent cover of both green and senescent vegetation can be estimated using the maximum and minimum SATVI values to calculate the Total Vegetation Fractional Cover (TVFC; Villarreal et al., 2016). Here, the maximum and minimum value of each burned pixel was used to calculate the SATVI-TVFC which ranged from -0.2852 to -0.0729. SATVI-TVFC is calculated as:

$$SATVI - TVFC = \frac{SATVI - SATVI_{min}}{SATVI_{max} - SATVI_{min}} X\ 100$$

Equation 5.2.

Table 5.1. The 17 tracked fires and corresponding control coordinate and date of fire.

Fire	Year	Fire Day Of Year	Date of fire	Burned Coordinates	Control Coordinates
1	2001	283	10/10/2001	-23.886108, 18.27055	-23.88191, 18.32897
2	2006	199	18/07/2006	-23.80115, 18.581572	-23.79735, 18.544
3	2006	278	05/10/2006	-23.47634, 18.34874	-23.43737, 18.41622
4	2007	263	20/09/2007	-24.525542, 18.712428	-24.53783, 18.68606
5	2007	295	22/10/2007	-24.983461, 20.024239	-24.98885, 20.080366
6	2007	25	25/01/2007	-27.075864, 20.619525	-27.06651, 20.64863
7	2009	258	15/09/2009	-24.985778, 20.246531	-24.917485, 20.331255
8	2010	280	07/10/2010	-27.690119, 21.335681	-27.65235, 21.37921
9	2011	204	23/07/2011	-23.589586, 18.6381	-23.5826, 18.68335
10	2011	254	11/09/2011	-24.885406, 18.864719	-24.8703, 18.88918
11	2011	270	27/09/2011	-25.306547, 20.199558	-25.25766, 20.21641
12	2012	306	01/11/2012	-23.178489, 18.533536	-23.21355, 18.62934
13	2012	262	18/09/2012	-26.09055, 20.597092	-26.19015, 20.52438
14	2013	56	25/02/2013	-27.818025, 21.595753	-27.86208, 21.60531
15	2017	228	16/08/2017	-23.976797, 18.532275	-23.9993, 18.4908
16	2017	206	25/07/2017	-27.4131, 20.608086	-27.379528, 20.574417
17	2018	299	26/10/2018	-27.065808, 20.642625	-27.072131, 20.666761

5.4 Results

5.4.1 Spatial

Over the 24-year study period 13,310 km^2 of the southwest Kalahari dune field burned, 11.1% of the total area. When including land that reburned, 16,125 km^2 burned in 240 individual burn events over 417 days. Figure 5.3 illustrates the highly concentrated spatial organisation of fire on the linear dunes. There are few cells where only single burns occur; if a fire is detected within a grid cell 66% of the time either the burn continues for more than one day or has multiple burn events over the study period. Of the overall burned area, a substantial portion, 10,625 km^2 (65.8%), burned in the Kgalagadi Transfrontier Park. Fires within the Kgalagadi Transfrontier Park burned for a median time of six days compared to two days on the primarily private farmland. These long duration burns are combined with the multiple fires in different years and result in the high number of burn days in the Kgalagadi Transfrontier Park (Figure 5.3). The highest density of burns occurred along the Nossob River, which is the boundary between South Africa and Botswana and main road in the Kgalagadi Transfrontier Park. There is also another small cluster of burned area in the wetter (see Figure 5.2) northern part of the research area, where burns were observed multiple times within the 0.5° pixels.

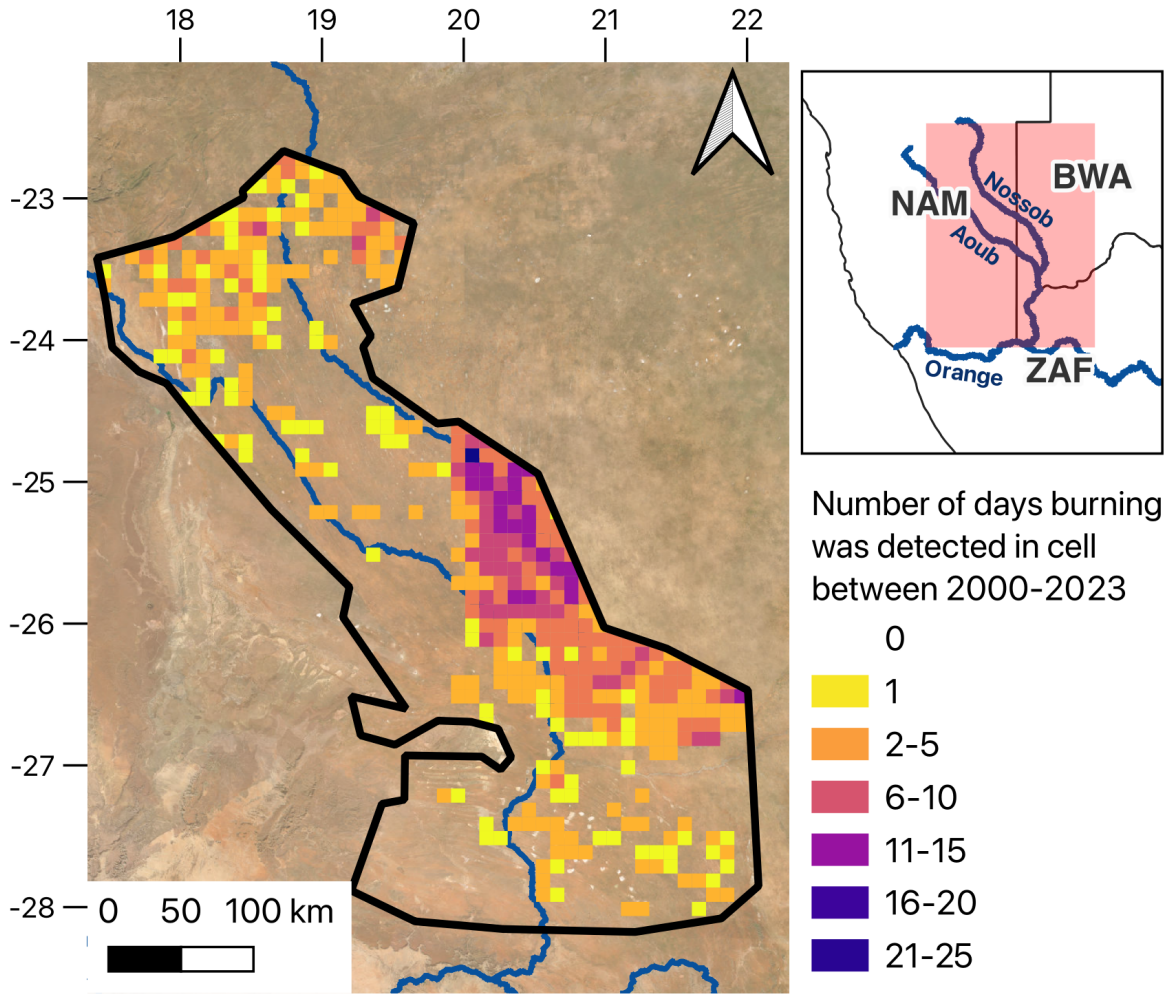

Figure 5.3. Number of days burning was detected in the 0.5° cell between 2000 - 2023. Background image © 2023 Planet Labs PBC, river data from (Lehner and Grill, 2013).

5.4.2 Temporal

There is marked interannual variability in burn counts (Figure 5.4), with the highest total number of burns in both land use classifications recorded in 2022, with 77 burn days compared to no burns at all being recorded in 2004, 2005, and 2016. No obvious regular cycle is evident, with peaks occurring in 2012, 2021, and 2022. The largest number of burns in a month was recorded in September 2021 with 28 burning days.

At the monthly scale, the maximum burned area and burn counts tend to cluster around September in the early dry season (Figure 5.4). Wet season burns make up only 25% of the burning days.

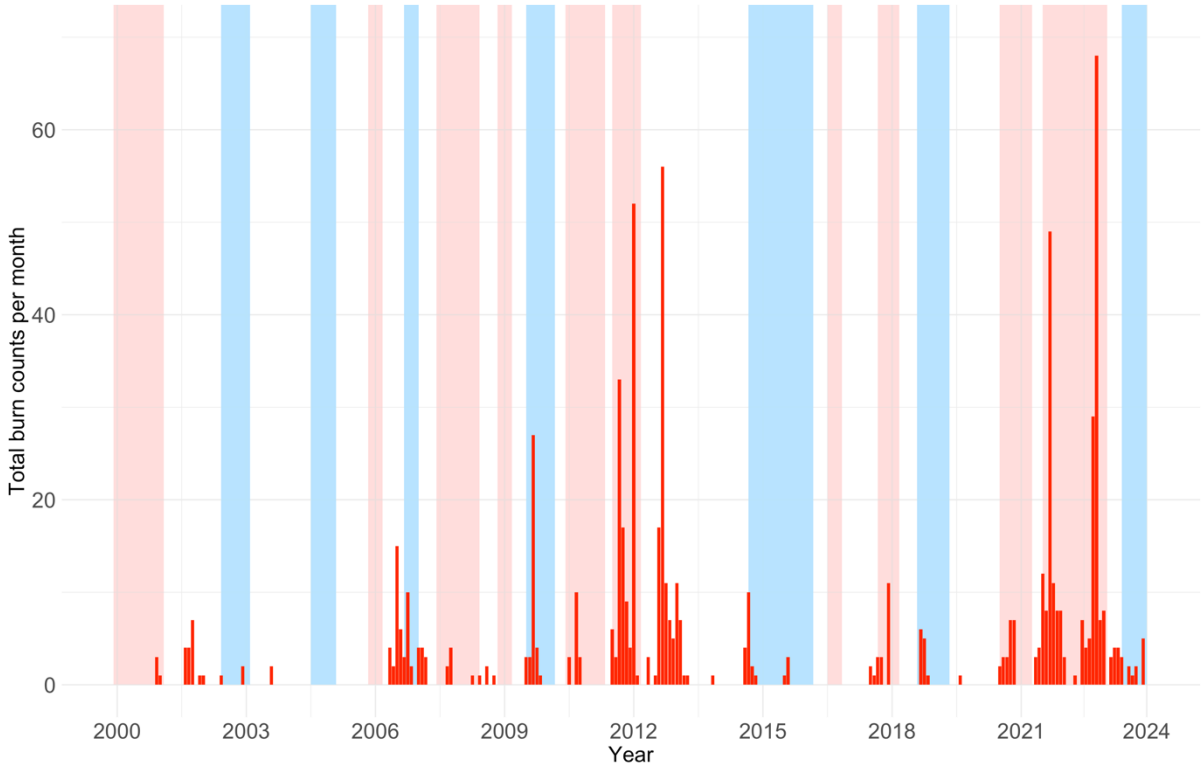

Figure 5.4. Total burn counts per month over the 24-year study period for the whole study area. Overlayed are the ENSO periods, with El Niño months in blue, and La Niña months in red.

Figure 5.5 illustrates the importance of representing both burn count and burned area, as different land management regimes display opposing trends. The Kgalagadi Transfrontier Park has a relatively low daily burn count, but a large, burned area. Contrastingly, the primarily private farmland has a high burn count, but these burns are small. These are not the only difference in patterns observed between the two land management regimes. The primarily private farmland has more isolated burn

incidences throughout the year, with the highest frequency of burning occurring in September which is the middle of the dry season (Figure 5.5). However, sporadic burns still happen throughout the wet season. Conversely, burns in the Kgalagadi Transfrontier Park observe a distinct fire season, which peaks in September through to October but tends to be limited in number, burn for a longer time, and over a larger area. There is also a second fire window in late January, where fires have burned on multiple years.

Kruskal-Wallis tests showed that there was significant difference between the Kgalagadi Transfrontier Park and the primarily private farmland in the monthly burn count ($p < 0.001$), monthly burn duration ($p < 0.001$) and monthly burned area ($p < 0.001$).

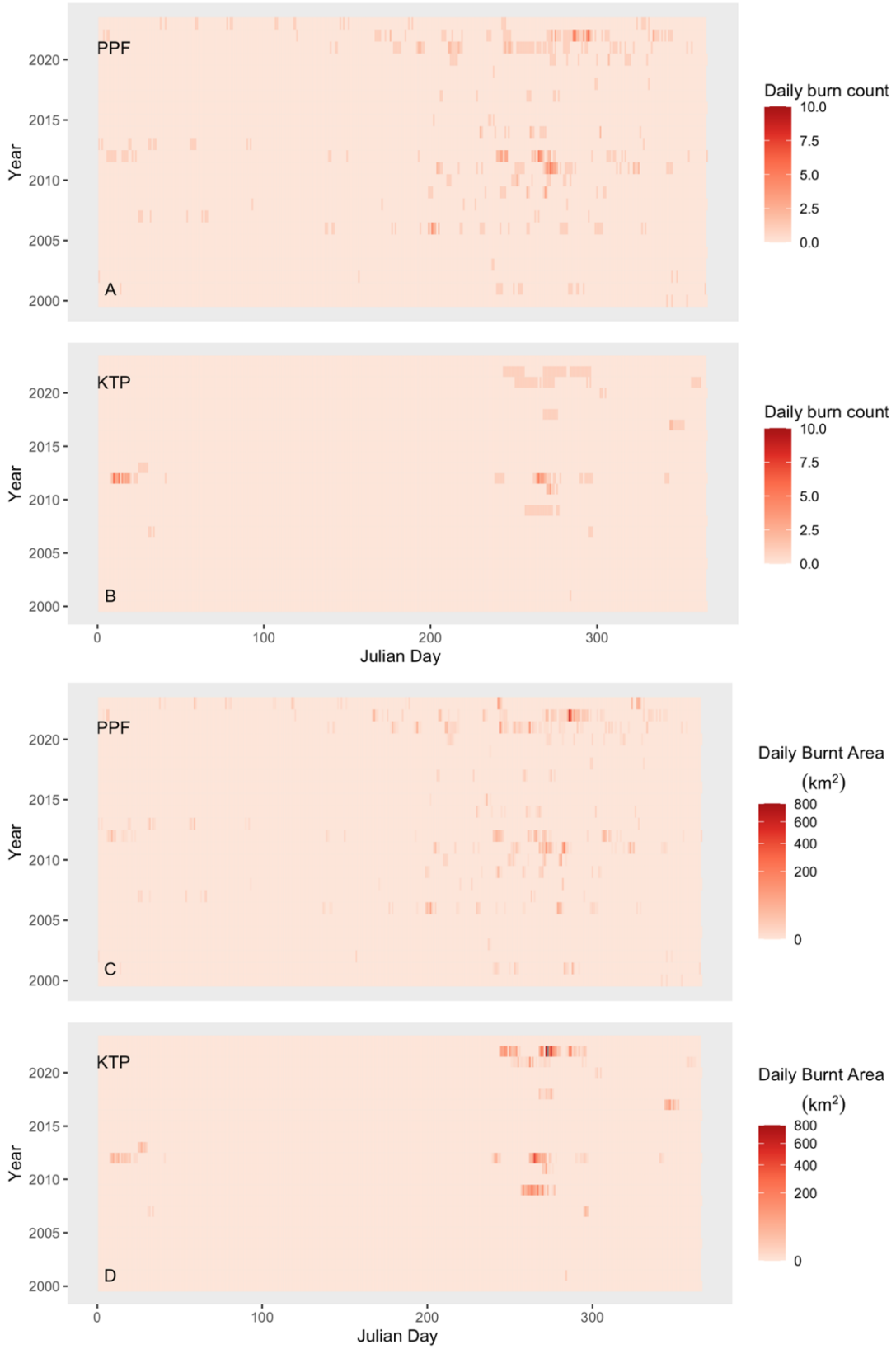

Figure 5.5. Daily burn count (Panels A&B) and burned area (Panels C&D) from 11/01/2000 to 31/12/2023 using cleaned MODIS burned area product in research area (see Figure 5.1) for the primarily private farmland (PPF; Panels A&C) and the Kgalagadi Transfrontier Park (KTP; Panels B&D).

5.4.3 ENSO phases

Fires burned in all ENSO phases (Figure 5.4). Multiple, successive months of burn counts are observed in neutral ENSO months in 2002 and 2012, in El Niño conditions in 2014 and 2019, and during La Niña phases of 2012, 2021, and 2022. Fire counts peak in October 2022 and January and September 2012 which are all in La Niña months. The largest fires do not burn after long periods without a La Niña extreme phase (Figure 5.4). Years with the highest fire counts often occur after two consecutive La Niña phases.

Overall, fires occur more frequently and burn a larger area during La Niña conditions (Figure 5.6). However, burns within land management systems also display different trends within the ENSO oscillations (Figure 5.6). Sensitivity to ENSO is particularly evident in the Kgalagadi Transfrontier Park burn trends, which can be considered an emulation of a more 'natural' cycle of fire in the area. Within the Kgalagadi Transfrontier Park, there is a delayed onset from the beginning of a La Niña phase and the occurrence of burns. Land outside of the Kgalagadi Transfrontier Park has a higher number of burns occurring in the neutral ENSO months, but this is not reflected in the burned area, suggesting small frequent burns. There is no significant effect of ENSO on all the assessed pairs ($p > 0.05$; Table 5.2).

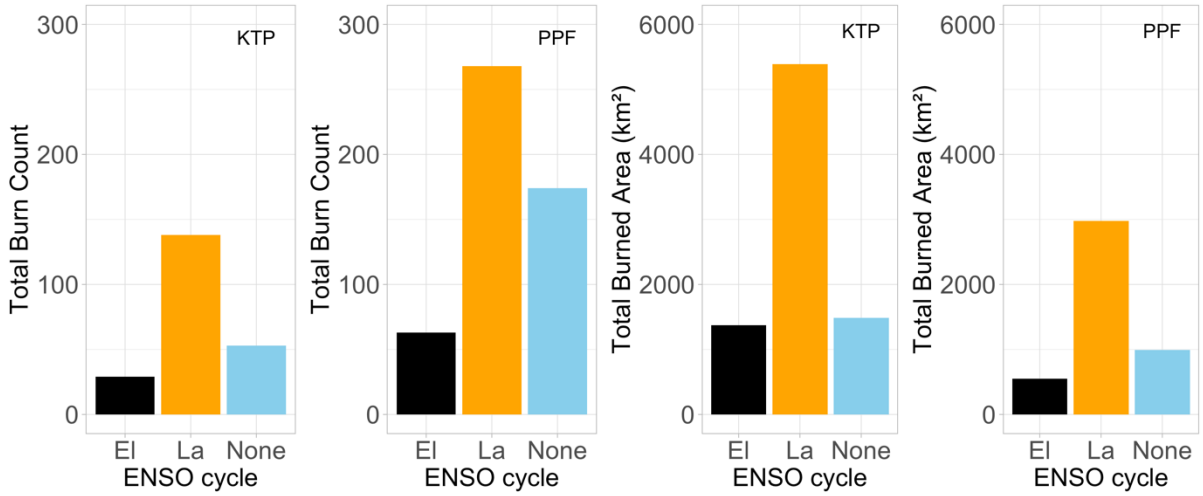

Figure 5.6. Total burn count and total burned area for the Kgalagadi Transfrontier Park (KTP) and primarily private farmland (PPF) under different ENSO oscillations. El Niño conditions are in Black, La Niña conditions are in orange, and neutral is in blue.

Table 5.2. Kruskal-Wallis rank sum test results testing against ENSO phases in the whole study area, Kgalagadi Transfrontier Park, and primarily private farmland against the monthly burn count, burned area, and burn duration.

K-W test	Whole study area	Kalagadi Transfrontier Park	Primarily Private Farmland
Burn count	$p > 0.05$	$p > 0.05$	$p > 0.05$
Burned area	$p > 0.05$	$p > 0.05$	$p > 0.05$
Burn duration	$p > 0.05$	$p > 0.05$	$p > 0.05$

5.4.4 Reburning

The areas that reburn are clustered within the Kgalagadi Transfrontier Park, where some areas reburned after less than a year. The less than a year reburning mainly occurred in the 2020/21 and 2021/22 dry seasons when two large fires swept through the Kgalagadi Transfrontier Park in successive years. However, 73.6% of the pixels in the Kgalagadi Transfrontier Park burned over multiple incidences, Figure 5.7 only displays the shortest time to a reburn in a pixel. Most of the Kgalagadi Transfrontier

Park reburned in the study period in less than 10 years. Outside the Kgalagadi Transfrontier Park, some areas reburned, but there was a large variability in time between burns. There is a concentration of reburned areas in the wetter north of the linear dune system. There are a few isolated incidents of reburning on farmland in the South African portion of the linear dunes.

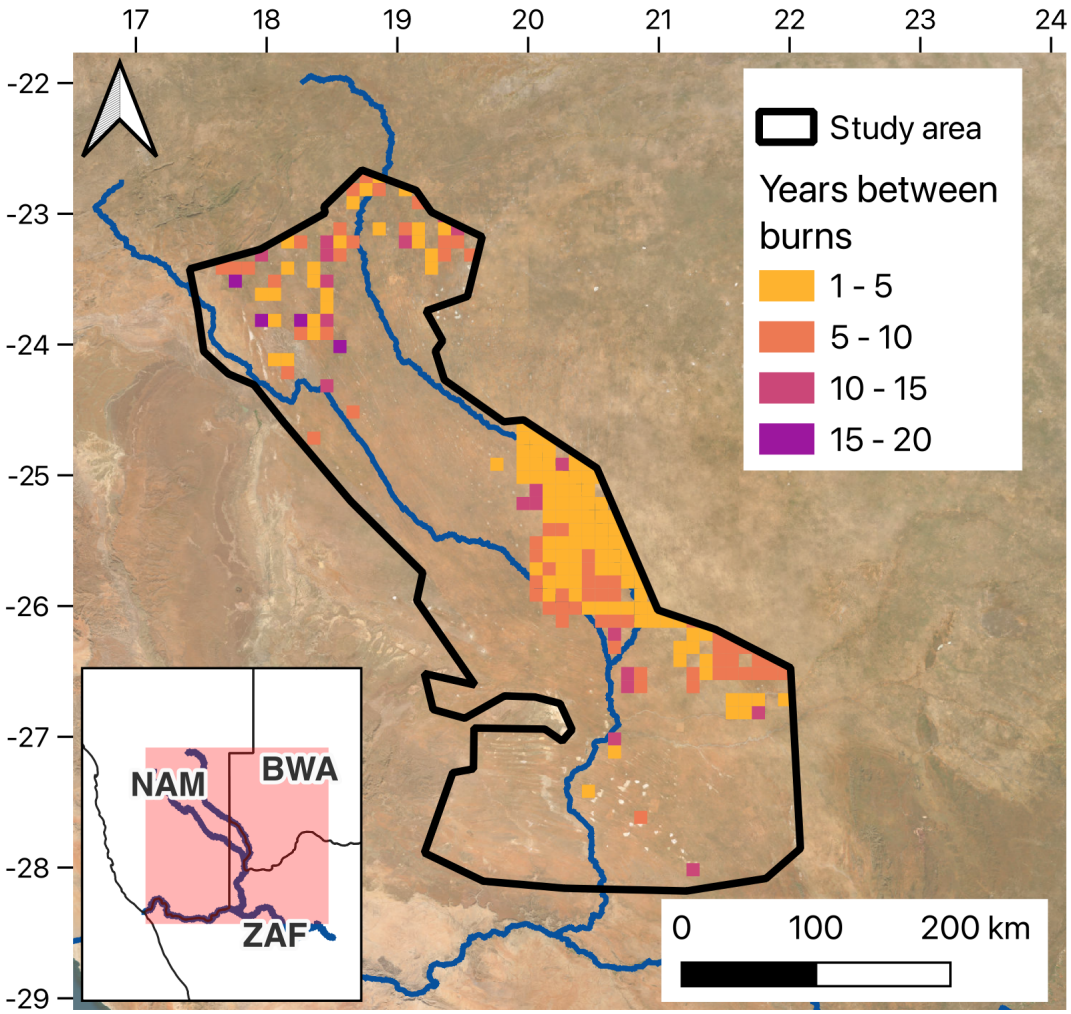

Figure 5.7. The shortest number of years between burning detected in each 0.5° cell between 2000- 2023. Background image © 2023 Planet Labs PBC, river data from (Lehner and Grill, 2013).

5.4.5 Vegetation indices

The annual fluctuations in SATVI provide context for the spatial and temporal magnitudes of a disturbance whether this be drought or fire. Additionally, the annual and seasonal fluctuations in SATVI at the control sites provide rich information on vegetation response to global and local climate cycles (Figure 5.8). Maximums in vegetation cover are observed in April 2011 and April 2022, whereas the minimum mean cover are found in November 2019 (Figure 5.8). At this minimum time, mean vegetation cover was below the 14% threshold for sediment transport for 112 (±16) days.

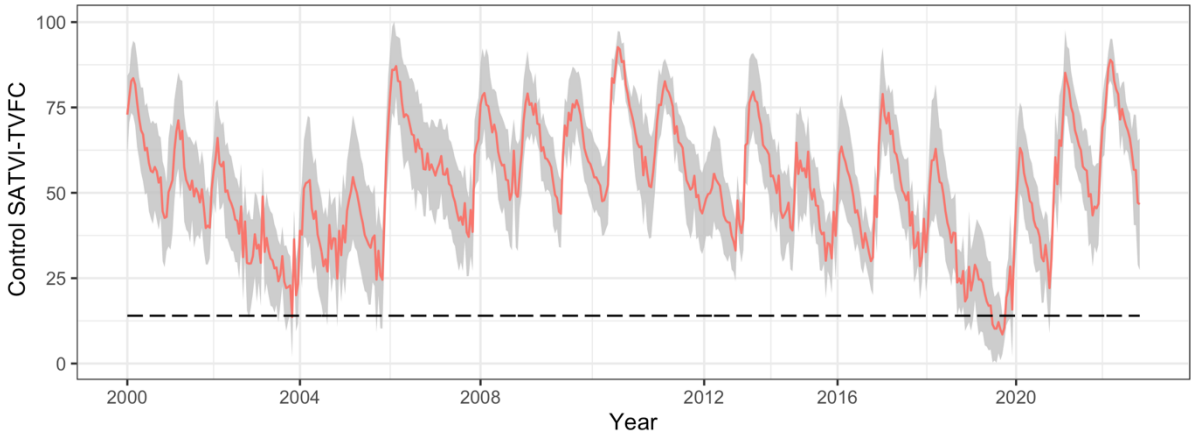

Figure 5.8. SATVI-TVFC for the control (unburned) pixels from 2000-2023. The one standard deviation is shown in grey and mean in red. The dotted line delineates the 14% vegetation cover for sediment movement from Wiggs et al. (1995).

SATVI mean Total Vegetation Fractional Cover (SATVI-TVFC) for the burned pixels show strong annual and seasonal fluctuations on the linear dunes in the research area (Figure 5.9a). Fire acts as a disruption to these fluctuations, reducing the mean TVFC

by 54 (±17) % (Figure 5.9a). However vegetative cover was only completely removed at five sites, and the mean cover minimum only drops to 19 (±16)%. 13 of the 17 tracked fires drop below the 14% coverage posited for sediment movement by Wiggs et al. (1995) within one year of being burned. Of the fires that dropped below the 14% threshold cover, the median time under that threshold was 112 (±16) days.

When compared to the control pixels, burned site recovery time varies (Figure 5.9b). The quickest time to achieve no difference between the burned and control site was 400 (±16) days which was recorded at three fires burned in 2007 and 2011. The longest time to recover was 2528 (±16) days (around seven years) after a fire in 2013. The median time to return to a positive difference with the matched control site was 608 (±16) days.

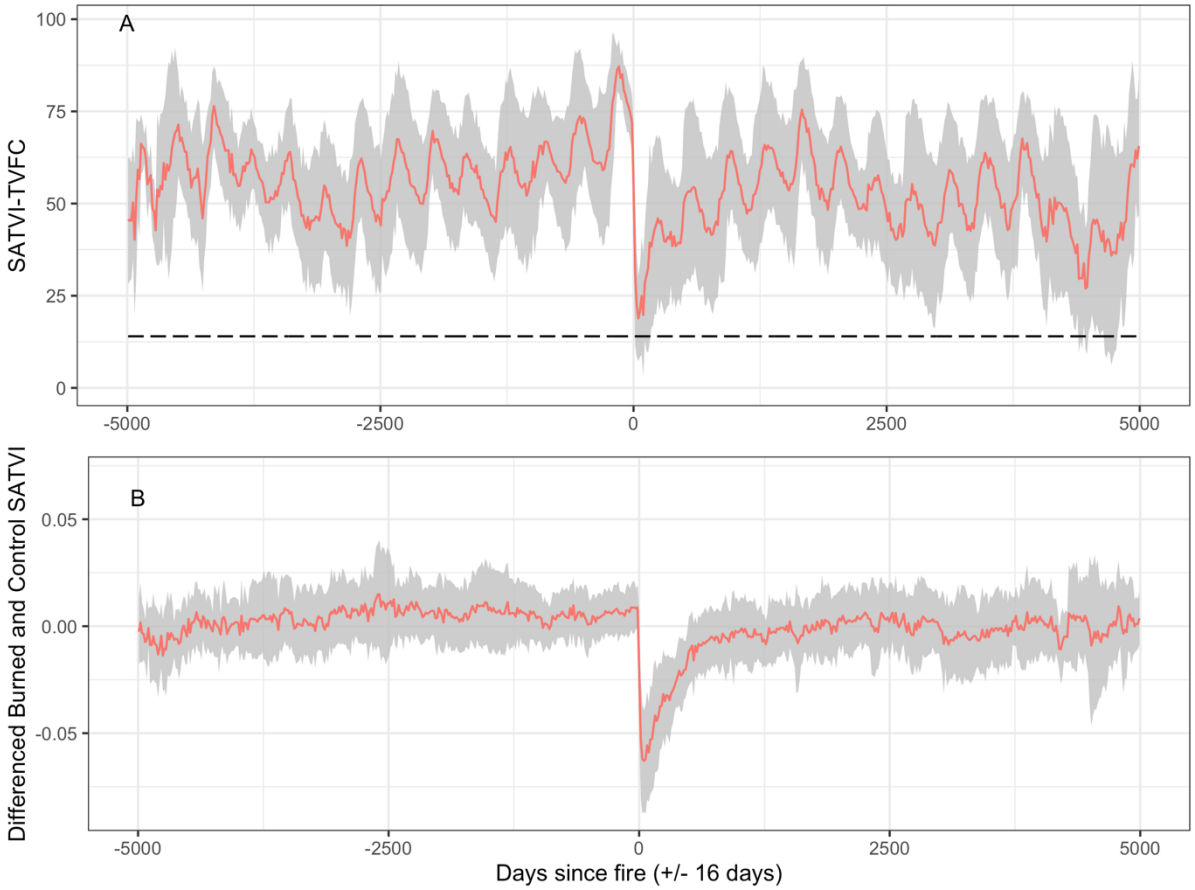

Figure 5.9. SATVI derived measurements of vegetation for 5000 days before and after fire. (A) displays SATVI-TVFC in the burned pixels before and after the 17 tracked fires. +/- one standard deviation is shown in grey and mean in red. The dotted line delineates the 14% vegetation cover for increased sediment movement from Wiggs et al. (1995). (B) displays the difference in SATVI index between each paired burned and control pixel before and after fire.

5.5 Discussion

This study used MODIS burned area product to create an inventory of fire occurrence on an often-overlooked landscape, the Kalahari's southwest vegetated linear dunes. Scaling decisions in previous studies have resulted in this region being omitted from global and continental-scale studies of burn-prone ecosystems (Archibald et al., 2009; Lizundia-Loiola et al., 2020; Ramo et al., 2021; Roy et al., 2008; Strydom and Savage, 2018; Yu and Ginoux, 2022). For example, Andela and Van Der Werf, (2014), excluded

areas receiving less than 400 mm mean annual precipitation from their analysis of burn potential in African savannas. We show here that fires can be an important part of ecosystem dynamics, even in dryland dune regions. However, we also show that vegetation mostly recovers under two years and in much of the study area fire was either triggered or suppressed by anthropogenic activity. As a result, fire as a disturbance effect, is limited both temporally and spatially and is not great enough to switch the system from a vegetated stable state to a de-vegetated stable state. These findings align with modelled scenarios for the Kalahari where, infrequent fire (10 years + reburn time) results in dune reactivation only 4% of the time (Mayaud et al., 2017b).

5.5.1 The effect of fire on vegetation cover

By comparing SATVI-TVFC values from burned and unburned control sites, we gained information on post-fire recovery times across different years. Overall, the effect of fire on vegetation cover is short-lived: vegetation recovers quickly, returning to control site levels on average under two years after being burned (Figure 5.9). All the sites returned to control levels of vegetation, indicating that the de-vegetated state was not a persistent change. The short period of reduced vegetation cover limits the temporal window in which aeolian erosion can occur and is much shorter than the previous disturbance window, of five years, suggested by Wiggs et al. (1994). However, Wiggs et al. (1995) also investigated vegetation structure as well as percent surface cover and accounted for this in the five-year recovery timeline. Although five

years is a useful indicator it is not all encompassing, for example, high wind speeds may provide enough energy to remobilise sediment when surface cover is above 14%. Indeed, Wiggs et al. (1995) found evidence of surface activity at up to 40% vegetation cover, although these were at low levels. The quick vegetation recovery time indicates that the saltating sand grains are not at a sufficient scale to abrade resprouting vegetation and create positive feedback mechanisms which limit vegetation recolonisation (Bhattachan et al., 2014; D'Odorico et al., 2013; Strong et al., 2010). The lack of saltating grains may be due to vegetation cover not reducing enough to be sufficient for increased sediment transport (discussed below). Alternatively, other factors, such as the baking of the ground surface or biological soil crusts surviving being burned may leave the erodibility of the surface unchanged (Palmer et al., 2020; Stavi et al., 2017). Additionally, the period of reduced vegetation cover may not have coincided with any high windspeed events that were strong enough to remobilise sediment, and thus the sites may also be erosivity limited in the immediate post-fire period.

Not all fires resulted in vegetation cover reduction below the approximate threshold of 14% for increased aeolian activity at the dune scale (Wiggs et al., 1995). Over the period measured in this study (2000-2023) burned land that does drop below 14% cover only does so for a maximum of 320 (±16) days (Figure 5.9). The resulting temporal window of erosion opportunity linked to a fire disturbance event is limited to the time the surface is below the 14% cover. Additionally, the temporal window of

erosion opportunity would have to match up with climatic conditions conductive to aeolian erosion, dry and windy (Lehmann et al., 2014; Moritz et al., 2012, 2005).

It is also important to note that the region suffered an El Niño induced drought from 2014-2020, which was the longest and most intense drought of the last 60 years (Kolusu et al., 2019; Smit et al., 2024). During the final stages of this drought, in 2018-2019, the SATVI-TVFC of the control sites dropped below 14% cover for a median 112 (±16) days which is the same duration of reduced cover because of fire disturbing the landscape (Figure 5.8). Therefore, over this time period, fire and drought are a similar magnitude disturbance on the system.

5.2 Implications of anthropogenic controls on occurrence, size, and duration

In the southwest Kalahari vegetated dune field, land management systems have a significant effect on fire occurrence and burn duration. This finding collaborates previous results from southern Africa (Andela and Van Der Werf, 2014; Archibald et al., 2010, 2009; Cochrane and Barber, 2009; Shikwambana et al., 2022). One important finding is the comparison between the primarily private farmland and the Kgalagadi Transfrontier Park, the latter of which has a policy that naturally ignited fires are allowed to burn to their fullest extent (Spies et al., 2016). The policy results in fires that often have long durations and burn in multiple directions (Figure 5.3; Spies et al., 2016). In contrast to the Kgalagadi Transfrontier Park, the agricultural lands in

Namibia and South Africa have a high volume of fire counts, but a much smaller burned area (Figure 5.5). One explanation may be due to land users actively fighting the fires and having fire control methods in place to reduce the affect that fire may have on agricultural potential and livelihoods (Humphrey et al., 2021). A clear demonstration of these different fire policies is the Namibian and South African border in the Kgalagadi Transfrontier Park where a clear line has developed displaying how the fire is prevented for traversing into neighbouring regions (Figures 5.3 and 5.7).

The anthropogenically modified fire regime in southwest Kalahari dune field severely limit the ability of fire to trigger dune activation. This is twofold. Firstly, the small fire size reduces the area of sediment available to be moved. With only small patches available to be eroded, the length is not sufficient to generate a large amount of erodible material to produce significant surface activation (Miller et al., 2012). Localised surface activation may occur, but this is limited by the continuing vegetation and debris cover discussed above. Secondly, even though a quarter of burns occur in the wet season, these fires do not have the right atmospheric or ecological conditions to propagate (Jones et al., 2022), resulting in small fires that are often restricted to a single day (Figure 5.5).

It is of interest that the highest number of fire days (Figure 5.3) and reburned pixels (Figure 5.7) are recorded in the Nossob valley, where grass is much more limited than

on the dunes themselves (Leistner, 1959). The ephemeral river valley may act as a natural fire break and prevent the burn spread. Fires burning the north and the southeast side of the river often stop at the river valley. However, many of the pixels that cover this region encapsulate both sides of the river and therefore return frequent fires in that area. The river valley is also the main road through the park and some burns originate in the valley, therefore, may be triggered anthropogenically. The river valley also has a higher concentration of trees than the surrounding dunes (Leistner, 1959). The trees provide optimal lightning strike features and can burn for longer durations than grasses.

Additionally, fires occur most commonly during La Niña conditions (Figure 5.6). In arid regions, fuel quantity and continuity generally govern fire regime (Andela et al., 2019; Archibald et al., 2009; Wright et al., 2021). As such, large fires only occur after precipitation has been sufficient to promote biomass build up and continuity (Andela and Van Der Werf, 2014). During La Niña phases, southern Africa has wetter conditions (Mphale et al., 2014) which provides the moisture for biomass to accumulate. In the data this evidenced with the peaks in SATVI-TVFC during La Niña conditions in 2006, 2011, and 2022 (Figure 5.8) which coincide (± one year) with peaks in burn counts (Figure 5.4).

The relationship between fire occurrence and ENSO oscillations, however, is mostly not statistically significant (Table 5.2) and the break down in significance could be

evidence of anthropogenic impacts on burned area. It is well known that humans influence fire regime (Andela et al., 2017; Andela and Van Der Werf, 2014; Kelley et al., 2019). In this region anthropogenic influences act to both suppress and ignite fires. The accidental ignition of fires are evident in the wet season fires, which would not occur naturally (Spies et al., 2016). However, the relatively small burned area of fires, even in the dry season is evidence of human suppression. If the Kgalagadi Transfrontier Park is taken as an example of a "natural" fire regime, fire will burn for longer and over a larger area than what we observe in the primarily private farmland. These anthropogenic influences add noise to the data and lead to different from trends with ENSO that have been observed over a larger southern-African scales (Andela and Van Der Werf, 2014; Pricope and Binford, 2012; Shikwambana et al., 2022). This finding highlights the importance of assessing the impact of fire and associated effects at both small and large spatial scales.

5.6 Conclusions

Our aim was to establish the scale of fire as a disturbance event on vegetated linear dunes by creating an inventory of burned area from 2000-2023 and quantifying post-fire vegetation regrowth. Overall, fires occur on all but three years and burn a significant amount of area on the vegetated dunes, but these burned areas are often limited to within the Kgalagadi Transfrontier Park and the wetter northern areas. We found that burn count and fire duration differs significantly between the Kgalagadi Transfrontier Park and primarily private farmland, which can be attributed to the

differing fire management regimes, modulating the spatial scale of the burn disturbance. In the primarily private land small, quick burning fires occur regularly, whilst in the National Park fires burn for longer, over larger areas, and more rarely. Vegetation regrowth also occurs rapidly after fire, limiting the temporal window for which post-disturbance sediment transport, and thus sediment activation, can occur. The temporal and spatial effect of the fire as a disturbance factor is limited by anthropogenic modulation of the fire regime and rapid vegetation recovery post-burn. Due to the lack of representation of the southwest Kalahari dunes in fire studies, other vegetated dunes systems should also be reassessed and explored to understand fire dynamics and impacts upon these landscapes.

Chapter 6 -

Quantifying the impact of fire events on dust emission potential from partially vegetated dunes in the south-west Kalahari

Status: Submitted to *Aeolian Research* in May 2025

PI-SWERL measurements on a bare dune crest.

Summary

This research paper addresses **research question two** – *does fire affect dust emission potential?* – through using a portable wind tunnel to investigate PM_{10} erosion thresholds and emission fluxes of dust from control and burned surfaces. Further, grain size distribution from the dunes is examined to determine if there is resident fine material available for erosion. The findings from this chapter highlight how post-fire the dunes of the southwest Kalahari remain availability limited, rather than supply-limit as previously thought. This limitation is most likely due to biological soil crusts surviving fire and armouring the surface against erosion.

Abstract

The removal of stabilising vegetation from sand dunes by fire has been widely linked to increases in aeolian sediment transport and dune movement. However, substantial gaps exist in our knowledge of whether de-vegetated dunes are also at greater risk of emitting dust. To explore relationships between vegetation, fire, and dust emission on desert sand dunes, 180 measurements of dust emission on differing dune surfaces were carried out using a portable wind tunnel (PI-SWERL) in the Namibian Kalahari Desert. Data were analysed to compare erosion thresholds and dust emission flux on adjacent burned and unburned sites. Our data suggest that dune crests, flanks and interdunes have lower dust emission potentials compared to other desert landscape features such as ephemeral river valleys or pans. Whilst we found no significant difference in dust emission flux on burned and de-vegetated (but undisturbed) control surfaces (Kruskal-Wallis, $p > 0.05$), there was evidence of significantly higher erosion thresholds on burned surfaces (T-test, $p < 0.01$). The data strongly suggest that, even when devoid of vegetation, the Kalahari linear dune system is fine grain sediment-availability limited. This is likely explained by the persistence of biological soil crusts (biocrusts) on the dune surfaces, agglomerating sediments and significantly limiting dust emissions even after a fire. Where the surface had been mechanically disturbed, our data suggest that dust emission fluxes can exceed 77 times those of unburned vegetated surfaces. This finding indicates the importance of biocrusts in preventing dust emission from the Kalahari dune field.

6.1 Introduction

Accurately quantifying mineral dust emissions from diverse landscapes is crucial for understanding atmospheric dust loading and its climatic and environmental impacts (Field et al., 2010; Gill, 2018; Kok et al., 2023; Schepanski, 2018). However, current atmospheric models are not in agreement on the sources and emission flux of existing atmospheric dust (Chappell et al., 2023; D. Kim et al., 2024; Kok et al., 2021a; Mahowald et al., 2024). Models rely on field studies to quantify surface controls on emissions and satellite data to estimate the amount of dust in the atmosphere (Haustein et al., 2015; Klose et al., 2019; Webb and Strong, 2011). There are several uncertainties in the data on dust flux and source locations used in the atmospheric models including: low-resolution remote sensing imagery often fails to detect emission sources (Urban et al., 2018; von Holdt et al., 2019); challenges in characterising surface properties of key emission sources (Webb and Strong, 2011); and the miscalculation of coarse dust in the atmosphere (Adebiyi et al., 2023). Another key uncertainty in dust and atmospheric modelling is the accurate quantification of low-concentration or infrequent emission dust sources, which are difficult to capture due to their irregularity and the limitations of remote sensing technologies (Okin et al., 2011; Sweeney et al., 2023; Urban et al., 2018; Wagenbrenner et al., 2017).

The entrainment of dust from the Earth's surface is a complex interaction of factors that influence either the erosivity of the wind and/or erodibility of the surface (Webb et al., 2021; Wiggs et al., 2022). For dust particles to be eroded, wind speed must exceed

a critical shear velocity threshold, though this threshold is influenced by numerous surface characteristics (Field et al., 2010; Kok et al., 2012; Reynolds et al., 2007; von Holdt et al., 2019). These surface features are highly variable in time and space and include sediment size, surface moisture, presence of a surface crust (both biological and physical), surface roughness, agglomeration of soil grains, surface geochemistry, and vegetation cover (Dickey et al., 2023; Engelstaedter et al., 2003; Langston and McKenna Neuman, 2005; Nield et al., 2011; Sweeney et al., 2011). Particle size is especially important in dust emission, as it dictates both the force required for entrainment and the potential distance particles can travel (Kok et al., 2012). Consequently, low-lying landforms filled with fine sediment, such as paleolake basins and ephemeral river or lake beds, represent some of the largest dust sources globally (Bullard et al., 2011; Ginoux et al., 2012; Parajuli and Zender, 2017; Prospero et al., 2002).

Sand dunes are not typically considered to be significant sources of atmospheric dust as they generally contain less than 5% silt and clay (Prospero et al., 2002). However, some studies have suggested that active dunes can emit dust through aeolian abrasion processes (Amit et al., 2014; Bullard et al., 2004; Bullard and White, 2005; Cui et al., 2019; Sweeney et al., 2022). Vegetated dunes are often excluded from dust emission studies because plants act to stabilise the surface preventing sediment movement and abrasive interactions. Plant architecture increases surface roughness and provides physical sheltering, but also traps allochthonous dust particles and allows a finer

fraction of sediment to build up (Gonzales et al., 2018; Suter-Burri et al., 2013). However, there is evidence to suggest that such stabilised dunes can yield larger fluxes of dust in comparison to active dunes where the surfaces have suffered recent disturbance (such as grazing, drought, or fire; Bullard et al, 2011; Sweeney et al., 2023).

It has been hypothesised that if vegetated dunes were to lose their vegetation cover and become more geomorphologically dynamic (e.g., Wiggs et al., 1995), they could potentially become large sources of dust into the future (Bhattachan et al., 2022, 2012; Pye, 1989; Sweeney et al., 2023). One of the key mechanisms by which vegetated desert dunes may become denuded of vegetation and act as low concentration emission sources of dust over short timescales is fire (Bullard et al., 2008; McGowan and Clark, 2008; Yu and Ginoux, 2022).

In 'stabilised' vegetated linear dune systems, vegetation both extracts momentum from the wind, and provides physical surface protection (Wiggs et al., 1995, 1994), as a result few dust emissions are observed in these regions (Bullard et al., 2011). But vegetated dune fields often have a higher percentage of fine grain-sized material than active dune systems and also are capable of generating fine grains through abrasion (Baddock et al., 2013; Bullard et al., 2004; Bullard and White, 2005; Sweeney et al., 2023). Fine grains accumulate in the surface sediment as vegetation traps wind-blown dust from further afield (Yan et al., 2011). Further, fine sediment is produced as sediment in many vegetated dune systems round the globe are coated in iron oxide

rich clay which can rapidly be abraded to emit fine grains. For example, abrasion studies using sediment from the vegetated dunes of the Simpson Desert in Australia found that the iron-rich clay coating of sand grains can be rapidly winnowed into smaller particles (Baddock et al., 2013; Bullard and White, 2005). The Kalahari Desert in southern Africa also contains a fine fraction within its sediment that has high concentrations of soluble iron in its fine material (< 45 μm; Bhattachan et al., 2012). The iron oxide is noteworthy as, if deposited in the marine system, it can have significant influence on ocean productivity (Bhattachan et al., 2015; Dansie et al., 2022; Jickells et al., 2005). The combination of fine sediment trapped at the surface and the abrasion produced dust in vegetated dune fields has led to current research challenging the assumption that vegetated desert dunes are not emitters of dust (Bullard et al., 2008; Sweeney et al., 2023, 2022). Further, disturbance events that remove the protective vegetation cover can liberate the sediment, meaning that currently stabilised vegetated dune fields have the potential to be large emitters of dust (Pye, 1989; Sweeney et al., 2023).

Burned surfaces in other desert landscapes often exhibit higher emissivity rates due to volatilised fatty acids from vegetation, which condense onto nearby sediment and form a hydrophobic coating on grains, thereby reducing interparticle cohesion by altering the contact angle of the grains (Ravi et al., 2006; Sankey et al., 2012). In the arid shrubland of the USA, Sankey et al. (2012) found that burned surfaces emitted three times more sediment than unburned areas. Yet, there have been no field studies

investigating the emissivity of burned vegetated dune fields. To understand the complexities of the impact of de-vegetation on vegetation reestablishment , it is crucial to examine the de-vegetation–aeolian erosion feedback mechanisms on dune environments after different disturbances, such as burning.

There is some evidence for post-fire dust emissions from sand dune systems. For example, Yu and Ginoux (2022) used Moderate Resolution Imaging Spectroradiometer (MODIS) data (deep blue aerosol product and burned area product) and found that at the global scale wildfires lead to enhanced dust emissions. This included dust emissions from vegetated dune systems in Australia, the Sahel, and Argentina, but there are notable gaps in emission from the southwest Kalahari linear dune system (Yu and Ginoux, 2022). Further, Bullard et al. (2008) and McGowan and Clarke (2008) used remote sensing methods to detect dust plumes originating from fire scars in the Simpson Desert in Australia. But emission potential from the southwest Kalahari dune field has been poorly constrained. The Kalahari is ecologically and geomorphologically similar to the Simpson Desert in Australia (Buckley, 1981) and burns frequently (Andela et al., 2019). The Kalahari is often suggested as being a source of dust if it were to become spontaneously de-vegetated (Bhattachan et al., 2012). Yet, no research has investigated post-fire dust emissions in the region. This research aims to fill the knowledge gap of whether the vegetated dunes of the southwest Kalahari have the potential to emit dust into the atmosphere because of fire destroying their protective vegetation cover and decreasing particle

cohesion. Fire surface sedimentology is examined to determine changes between burned and co-located unburned plots to establish if, (1) there is fine material typical of dust in the sediment texture, and (2) if fire impacts the grain size distribution. Next, the emission potential between burned and unburned plots is quantified using a portable wind tunnel. The research can be broken down into three aims which are to:

1. Characterise the sediment texture at burned and control plots
2. Quantify emission flux potential from de-vegetated southwest Kalahari linear dunes
3. Establish if there are different emission thresholds for burned surfaces in comparison to undisturbed (control) plots

6.2 Methods

6.2.1 Study area

The research was conducted on the vegetated linear dunes (Figure 6.1) in the arid southwest Kalahari in Namibia in September and October 2022. The dunes consist of unconsolidated aeolian sands of mainly quartz and feldspar (Garzanti et al., 2022). There is no statistical difference in grain sizes on the east or west flank of the dunes (Lancaster, 1986): therefore, sediments in this study were collected from either face of dune. The dune crests are spaced 0.2 to 2 km apart with heights which range from 5 to 25 m (Thomas and Leason, 2005). In this study a crest is the highest point of the dune, a flank is 3 - 5 m down the side from the crest of the dune, and an interdune is classed as the area where the slope of the dune has become undetectable by eye.

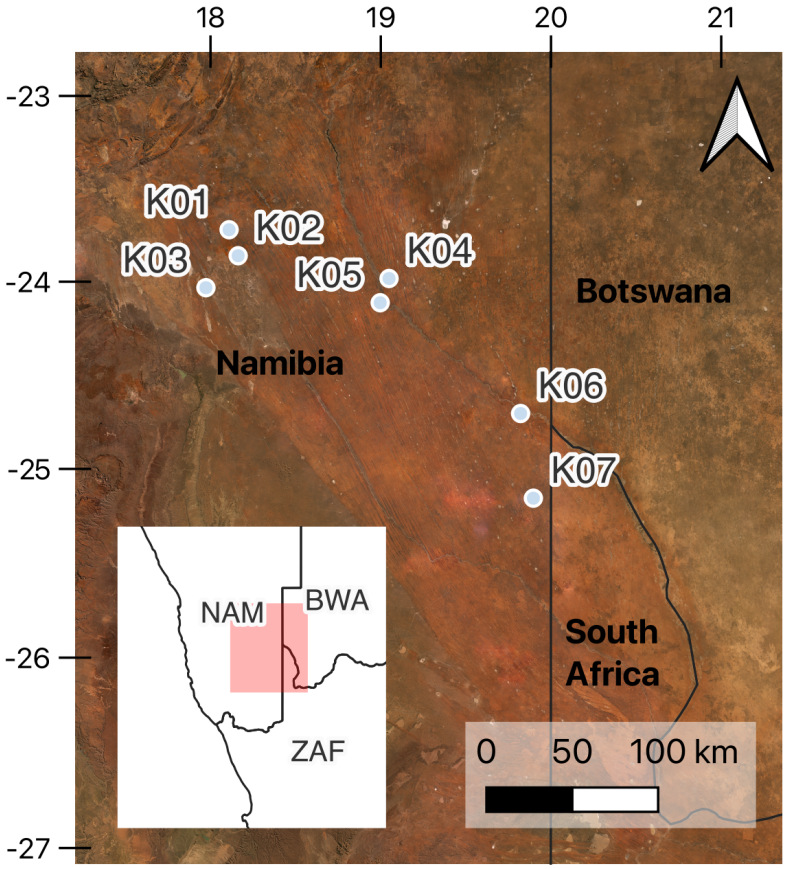

Figure 6.1. Locations of sites in the southern African context. Background imagery © 2023 Planet Labs PBC.

The linear dune system lies within the southern Africa summer rainfall zone and has a mean annual precipitation of 150 – 300 mm but, characteristic of dryland regions, interannual variability is high at 50% (Bhattachan et al., 2014; Thomas and Leason, 2005). The rain generally falls between November and April; accordingly, September and October represent the end of the dry season. Additionally, the dry season also coincides with the windiest months. In the 12 months preceding September 2022 when measurements were made the sites received an average of 201 mm precipitation.

The typical vegetation in the study area is Kalahari Xeric Savanna (van Rooyen and van Rooyen, 1998), with varying surface coverage depending on land use history. The vegetation composition on the dunes is a mix of annual grasses (mainly *Schmidtia kalahariensis*), perennial grasses (e.g., *Stipagrotis amabilis*), prostrate creepers (e.g., *Aptosimum elongatum*), patches of shrubs (e.g., *Lycium hirsutum)* and sporadically populated trees (e.g., *Acacia haematoxylon*). All measurements were conducted on farmland which is either sheep, goat, or cattle grazed. Most of the unburned farmland had a high coverage of annual grasses.

Fires in the region are limited by vegetation, which provides both fuel and affects the connectivity of the burnable surface. Vegetation mass and extent is strongly linked to precipitation amounts and to land use (Andela et al., 2019). Consequently, like precipitation, fires have a high interannual variability, and occur regularly after wetter La Niña periods which provides the moisture for biomass build up (Chen et al., 2017). The fire season peaks in September but can continue into the early wet season

6.2.2 Experimental set-up

Seven burned sites, with different fire ages (Time Since Fire: TSF), were identified using remote sensing, followed by conversations with local landowners (Table 6.1). Each burned site was co-located with a nearby unburned control site. Where possible the plot pairs were close to each other on the same dune, or one interdune across (for example at K04 measurements were taken on the same dune 2 km apart).

The sites were then further divided into plots to investigate the effect of the dune morphological unit (crest, flank, and interdune) on emission potential with particular focus on the dune crest and interdunes (Figure 6.2). The different morphological positions of the plots on the dune surfaces are summarised in Table 6.1. The accessibility of the area burned limited the ability to record at all the dune topographies. Within each plot a 10 m transect was randomly place along which PI-SWERL experiments were conducted. To compare the impact of mechanical disturbances on potential dust emissions, at each plot the surfaces were mechanically disturbed by scraping the top two centimetres of sediment using a spade, and additional measurements made (Figure 6.2). Subsequently, the maximum number of experimental plots each site was nine- the burned crest, flank, and interdune, with co-located control plots and additional mechanically disturbed interdune, flank, and crest plots.

Table 6.1. Location, date of fire, and plot position for each burned site

Site	Latitude	Longitude	Date of fire	TSF (months)	Dune morphology measured
K01	-23.722675	18.109997	01/09/2022	0 and 1	C*, F, ID
K02	-23.8606	18.1507	26/07/2022	1	C, ID
K03	-24.04225	17.98124	18/06/2022	4	C, ID
K04	-23.98248	19.01717	29/11/2021	10	C, F, ID
K05	-24.1159	18.99656	16/11/2021	10	ID
K06	-24.68887	19.82227	27/10/2020	25	C, ID
K07	-25.185	19.8947	28/02/2012	127	ID

C – Crest, F – Flank, ID – Interdune
**Control only*

	Burned	Control
Crest		
Flank		
Interdune		
Mechanical disturbance (scraped)		

Figure 6.2. Examples of PI-SWERL measurement locations on different topographies.

6.2.3 PI-SWERL measurements

Emission flux was measured using the Portable In-Situ Wind Erosion Laboratory (PI-SWERL ®; Desert Research Institute, Las Vegas, NV, USA), now a widely used technique (Bacon et al., 2011; King et al., 2011; Kolesar et al., 2022; Sweeney and Mason,

2013; von Holdt et al., 2019; Vos et al., 2021; Walker et al., 2023; Wang et al., 2025). The instrument (as seen in Figure 6.2) consists of a flat, annular ring inside a closed chamber rotating about 6.5 cm above the ground which exerts shear stress on the surface and entrains particles. The emitted particles are measured by a DustTrak ® II model 8530 nephelometer to measure the PM_{10} concentration of dust in the chamber per second in mg m^{-3}. Fresh air is pumped into the chamber at a rate of approximately 0.1 m^{-3} s^{-1}. The PI-SWERL was preprogramed to run at a variety of revolutions per minute (RPM) which translate into specific friction velocities (u_* m s^{-1}). The relationship between RPM and u_* is determined by surface roughness and defined as:

$$u_{*eff}(RPM) = C_1 \cdot \alpha^4 \cdot RPM^{C_2/\alpha}$$

Equation 6.1

where, C_1 and C_2 are constants 0.000683 and 0.832 respectively. α is a value calculated based on surface roughness using the look-up table in Hartshorn et al. (2023). It was deemed that all surfaces consisted of loose unconsolidated sand which was less than 2.5% gravel cover, therefore, the α value of 0.98 was chosen for all sites, equating to a peak u_* value of 0.64 (±0.297) m s^{-1} at 3500 RPM.

The rotation of the flat ring was increased at a constant rate (ramp test). The ramp test was chosen as it enables the determination of (a) if the plot is capable of emitting dust, (b) enables an easy identification of the erosion threshold, and (c) any changes in dust emission flux whilst at a constant rate. At the start of each test, a 60 s clean air run was

undertaken to flush out any remaining particles in the chamber (Figure 6.3). The RPM was then increased from 0 to 3500 RPM over 90 s, held at 3500 RPM for 120 seconds, and then reduced to 0 RPM together with a clean air flush for the final 60 seconds of the test (Figure 6.3). To reduce contamination between each run, the inside of the chamber was brushed down to remove any remaining visible sediment and after concluding measurements at each plot, the PI-SWERL was run at max RPM for three minutes.

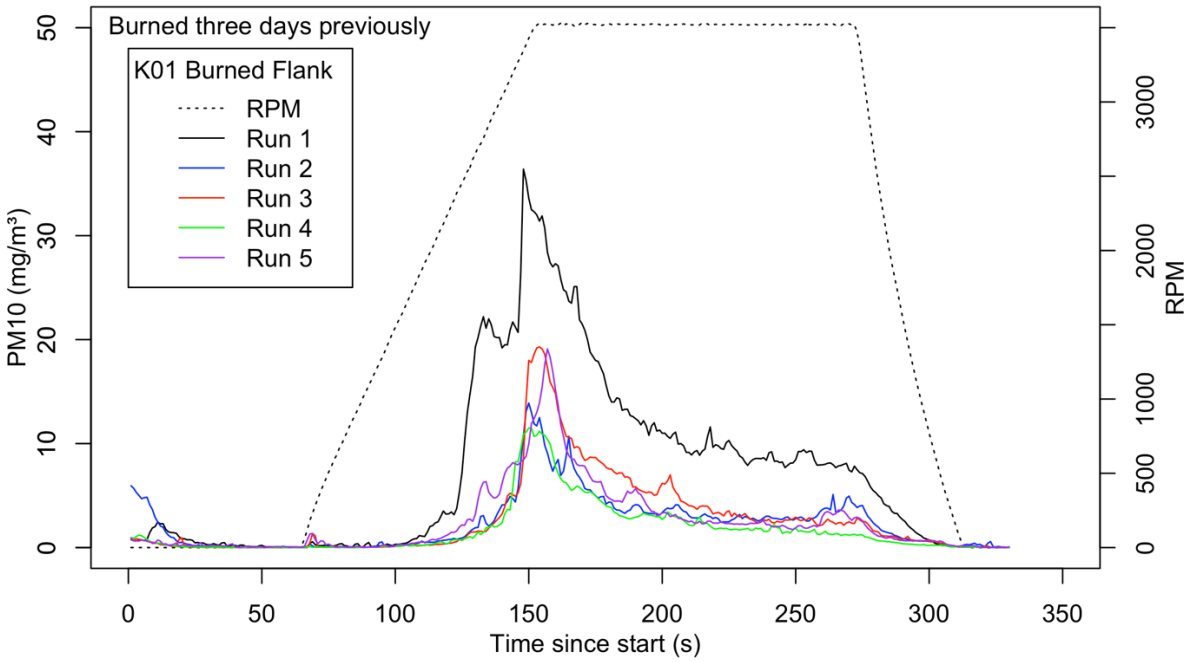

Figure 6.3. Example runs of a PI-SWERL at each measurement plot, displaying the programming used for each measurement.

Many previous experiments with a PI-SWERL have utilised a 'step' test, where the flux of dust is measured at different u_* to assess differing wind velocities (e.g., Bacon et al., 2011; Cui et al., 2019; Sankey et al., 2012). As the aim of this study is to assess the potential for the surface to be emissive, and if there is any change in thresholds with

different disturbances only one maximum velocity is used. This maximum RPM was maintained for 90 s (Figure 6.3), which allows us to calculate flux and identify controls on emission.

Threshold of emission (u_{*T}) was determined using the same process as Cui et al. (2019) where the first recording once the PM_{10} concentration began to consistently increase for ten or more seconds is determined as the threshold. The threshold RPM was then converted into u_* using the Equation 6.1. The PM_{10} flux was calculated using the equation:

$$E_i = \frac{\sum_{begin,i}^{end,i} C \cdot F}{\left(t_{end,i} - t_{begin,i}\right) \cdot A_{eff}}$$

Equation 6.2

where C is the measured PM_{10} concentration (mg m^{-3}), F is the airflow rate (L s^{-1}), t is the duration (s) of step i, and A_{eff} is the effective area (m^2) of the PI-SWERL (Etyemezian et al., 2014). The flux was used to compare emission fluxes to other measurements and PI-SWERL results.

Within each plot, a ten metre transect was set out and a PI-SWERL measurement was taken every two metres along the transect. To test further mechanistic disturbance effects other than fire, at each plot the top two centimetres of the surface was removed

at a plot away from the transect for further PI-SWERL measurements to be conducted. By removing the top two centimetres, the surface was mechanically disturbed and any biological soil crusts were removed from the surface. One to six measurements were performed at each plot to get a representative characterisation of the surface (Table 6.2). Where there was grass and creeper coverage, to ensure that the vegetation did not interfere with the rotating blade, vegetation was trimmed using shears to surface level (Figure 6.2), taking care not to disturb the surface. In total, 180 Pi-SWERL measurements were conducted at seven sites during September and October 2022 (Table 6.2).

Table 6.2. Measurements made at each site. C denotes a control plot and B denotes a plot which has burned. Scraped surfaces are where the top 2 cm of the surface was removed. K01 was visited twice, three days after burning and then 1 month after burning.

	K01 (3 Days)	**K01 (1 month)**	**K02**	**K03**	**K04**	**K05**	**K06**	**K07**
Interdune (C)	5		5	5	5	5	5	4
Interdune (B)	5	5	5	5	5	3	5	5
Flank (C)	5				5			
Flank (B)	5	5			5			
Crest (C)	3		5	5	5		6	
Crest (B)			5	5	5		4	
Scrape -Interdune	3	2	3	4	6		6	1
Scrape -Flank	6							
Scrape -Crest							3	

The PM_{10} threshold and flux data were analysed to determine statistical differences based on dune morphological unit (dune morphological unit, i.e., crest, flank, and interdune) and condition (burned or control). The choice of statistical test depended

on the data distribution and number of groups compared. Kruskal-Wallis chi-squared tests were used to assess differences in emission flux across topographies and status (i.e., control, burned, or mechanically disturbed), while Welch Two Sample t-tests were applied to threshold data for the same factors. Additionally, for variations in measurements taken at different dune morphological units, Kruskal-Wallis chi-squared tests were used for emission flux, and Analysis of Variance (ANOVA) was applied to threshold data.

6.2.4 Grain size distribution

Grain size distribution measurements for samples were conducted using the wet (no pre-treatment) dispersal method with a Malvern Mastersizer Hydro 2000MU laser diffraction particle size analyser. Before analysis, samples were oven dried overnight and sieved to under 2 mm and exposed to 10 s of ultrasonic dissolution. Samples were then classified by type where clay is <2 μm, silt is 2 μm to 50 μm, and sand is 50 μm to 2000 μm. In addition, sediment was further classed into particles which are inhalable under 10 μm and using recent evidence of more coarse dust under 62.5 μm (Adebiyi et al., 2023). Kruskal-Wallis chi-squared tests were used to assess any statistical differences between the different morphological units where measurements were taken on the dune (i.e., crest, flank, and interdune) and grain size distribution.

6.3 Results

6.3.1 Sediment Size distribution

88.4% of the samples have a soil texture of sand, the remaining 11.6% is classified as sandy loam. Only 5.78% contained any clay sized (< 2 μm) material and 92.8% containing silt sized (2 - 50 μm) material. Differences can be observed when assessing the topographical location of the sediments. 30% of crest plots contained sediment smaller than 10 μm, whilst all the interdune plots has higher percentage of sediment under 10 μm (with a maximum content of 8.9% at K01 burned interdune plot).

Sediment finer than 62.5 μm is typically considered to be able to be suspended in the atmosphere (Adebiyi et al., 2023). The proportion of sediment under 62.5 μm differed significantly with the different dune morphological unit (Kruskal-Wallis $p < 0.0001$). Interdunes had the largest mean proportion of sediment < 62.5 μm at 9.8 (±6.9)%, whilst the flanks had 4.3 (±2.7)% and the crests had 1.65 (±2.1)% on average (Table 6.3).

Table 6.3. Grain size data for samples from the study plots.

		% of sample																			
		Clay				Silt				Sand				< 10 μm				< 62.5 μm			
		x ~	Max.	Min	SD	x ~	Max.	Min.	SD	x ~	Max.	Min.	SD	x ~	Max.	Min.	SD	x ~	Max.	Min.	SD
Burned	C	0	0	0	0	2.562	7.321	1.322	1.918	97.438	98.678	92.679	1.918	0.556	1.976	0	0.643	3.210	9.511	1.323	2.575
	F	0	0	0	0	2.641	3.174	1.432	1.493	97.359	96.826	95.209	1.493	1.432	1.729	0.245	0.622	4.213	6.873	1.951	1.960
	ID	0.011	0.090	0	0.024	9.244	25.254	1.577	6.891	90.744	98.423	74.655	6.912	2.870	8.907	0.182	2.316	11.408	29.965	2.068	8.165
Control	C	0	0	0	0	0.350	0.796	0	0.306	99.651	100	99.204	0.306	0	0	0	0	0.617	1.356	0	0.419
	F	0	0	0	0	3.546	6.962	0	2.770	96.453	100	93.038	2.770	1.213	2.781	0	1.091	4.403	8.178	0	3.443
	ID	0	0	0	0	5.964	11.928	0.963	2.978	94.035	99.037	88.072	2.978	1.768	3.386	0.062	1.028	7.594	14.722	1.360	3.658

C- Crest, F- Flank, and ID - Interdune

6.3.2 The impact of dune topography on emission threshold and flux

There was great variance in both u_{*T} and emission flux with the location of the plots on the dune (Table 6.4). The dune morphological unit is highly significant for both the u_{*T} (ANOVA, $p < 0.01$) and the flux of dust (Kruskal-Wallis test, $p < 0.01$). Of the undisturbed surfaces, interdunes had the largest peaks in emission, with the unburned interdune at K07 recording a PM_{10} peak concentration of 65.5 mg m^{-3}. Yet, on average the flanks of the dunes have the largest flux of dust (Figure 6.4b). However, surfaces where the upper 2 cm of sand was removed consistently saw the highest fluxes of dust (Figure 6.4), recording a peak concentration of 173 mg m^{-3} observed at K02 scraped interdune.

Table 6.4. Descriptive statistics of measured threshold velocities (m s^{-1}) and emission flux (mg m^{-2} s^{-1}) for each dune morphological unit and disturbance type.

Dune morph. unit	Disturbance	n	Threshold (m s^{-1})				Flux at 0.64 m s^{-1} (mg m^{-2} s^{-1})			
			Mean*	SD*	Min	Max	Mean*	SD*	Min	Max
ID	B	38	0.308	1.305	0.187	0.551	0.190	3.363	0.005	1.892
	C	34	0.221	1.610	0.038	0.462	0.281	3.061	0.005	1.587
	M	25	0.167	2.670	0.187	0.409	1.105	2.033	0.862	6.305
Flank	B	15	0.264	1.228	0.202	0.417	0.403	1.942	0.129	1.251
	C	10	0.175	2.525	0.013	0.391	0.447	2.397	0.069	0.999
	M	6	0.266	1.218	0.202	0.310	1.949	1.815	0.500	2.538
Crest	B	19	0.303	1.298	0.179	0.489	0.467	1.430	0.029	0.723
	C	24	0.282	1.414	0.178	0.424	0.253	2.428	0.238	0.960
	M	3	0.288	1.601	0.210	0.495	0.942	1.026	0.923	0.970

**Geometric Mean and Standard Deviation*

B = Burned, C = Control, and M = Mechanical (Scraped)

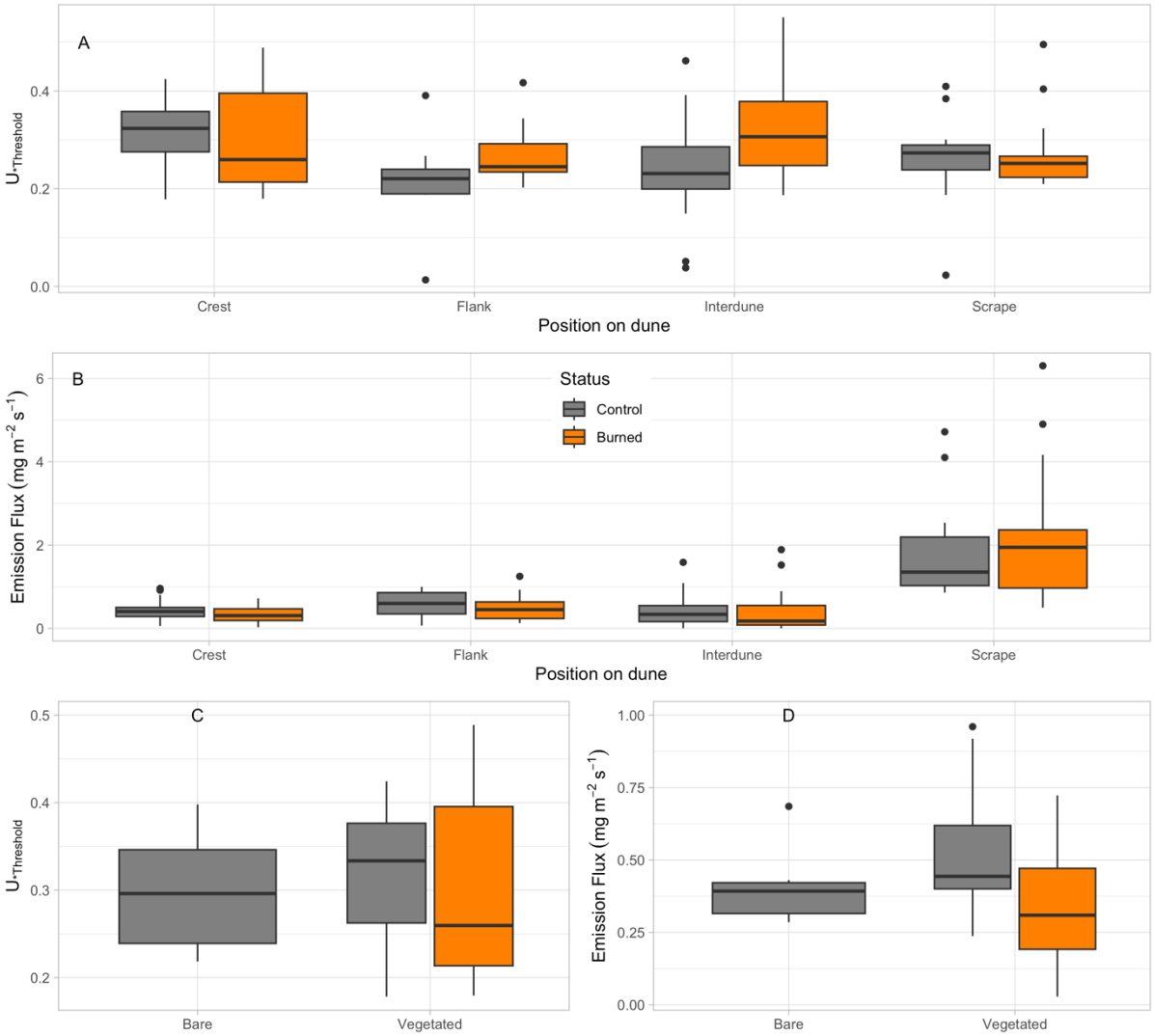

Figure 6.4. Panels A and B: u_{*T} and emission flux for the crests, flanks, interdunes, and scraped (mechanical) surfaces across all the measurement plots. Panels C and D: u_{*T} and emission flux for the crest plots only subdivided into bare and vegetated crest plots. Burned plots are in orange and control plots are displayed in grey.

6.3.3 Inter-plot comparisons

Each plot investigated has different surface properties that impact the ability to emit dust, and there is a significant difference in the emission flux between each control interdune plot (Kruskal-Wallis test, $p < 0.01$). Emission fluxes from each experimental plot are reported in Table 6.5. All control plots showed similar u_{*T} values (Figure 6.5), which are not significantly different from one another (ANOVA, $p > 0.05$) in contrast

to the emission flux. There was no significant difference in the flux between the control crests and flanks between the sites.

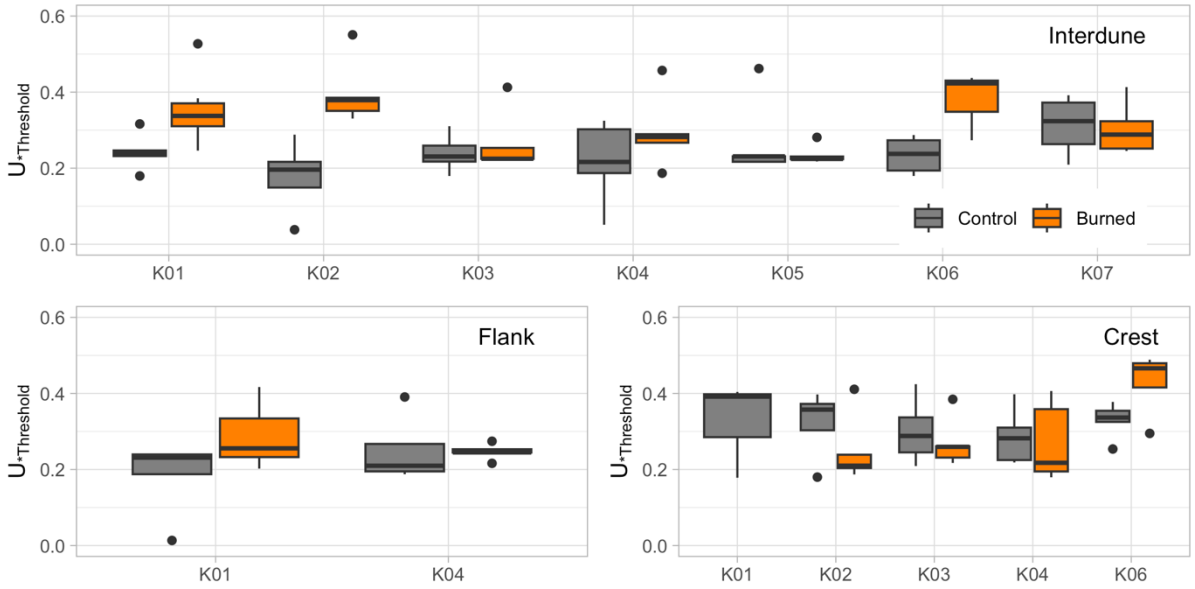

Figure 6.5. u_{*T} at each site on the interdune, flank, and crest plots.

6.3.4 The effect of burning on emission threshold and flux

The magnitude of difference in dust flux between the burned and control plot varies with site (Figure 6.5). In the interdunes, four plots had higher emission flux in the control plot and four had higher emission flux in the burned area (Figure 6.6). The difference between the burned and control plots are minimal as four plots have overlapping standard deviations (Figure 6.6 – panel C, D, E, H).

Table 6.5. Emission flux for each experimental plot measured.

	Emission flux (mg m^{-2} s^{-1}) (geometric mean ± geometric standard deviation)							
	K01 (3 Days)	**K01 (1 month)**	**K02**	**K03**	**K04**	**K05**	**K06**	**K07**
Interdune (C)	0.936 ± 1.442		0.065 ± 6.192	0.406 ± 1.659	0.237 ± 1.789	0.176 ± 2.324	0.303 ± 1.529	0.487 ± 1.514
Interdune (B)	0.108 ± 1.570	0.035 ± 3.249	0.221 ± 3.108	0.653 ± 1.235	0.197 ± 1.711	0.273 ± 1.897	0.065 ± 1.509	0.575 ± 3.336
Flank (C)	0.713 ± 1.340				0.280 ± 2.840			
Flank (B)	0.268 ± 1.691	0.322 ± 1.792			0.756 ± 1.489			
Crest (C)	0.893 ± 1.095		0.454 ± 1.318	0.449 ± 1.085	0.353 ± 1.210		0.451 ± 1.486	
Crest (B)			0.367 ± 2.290	0.384 ± 1.246	0.297 ± 1.495		0.078 ± 2.862	
Scrape - Interdune	2.245 ± 1.167	4.400 ± 1.104	5.007 ± 1.247	1.747 ± 2.021	1.732 ± 1.306		1.052 ± 1.119	1.872
Scrape - Flank	1.105 ± 2.033							
Scrape - Crest							0.942 ± 1.026	

The burned and control surfaces had significantly different u_{*T} (T-test, $p < 0.01$) on all topographies, with burned sites having a higher threshold for erosion. In contrast, burning does not have a significant impact on the emission flux on all topographies (Kruskal-Wallis test, $p > 0.05$). The largest average difference in the flux between the burned and control plots at the same site was found at the interdune K01 where the

difference between the geometric means was 0.901 mg m^{-2} s^{-1} with the control plot having a larger dust flux.

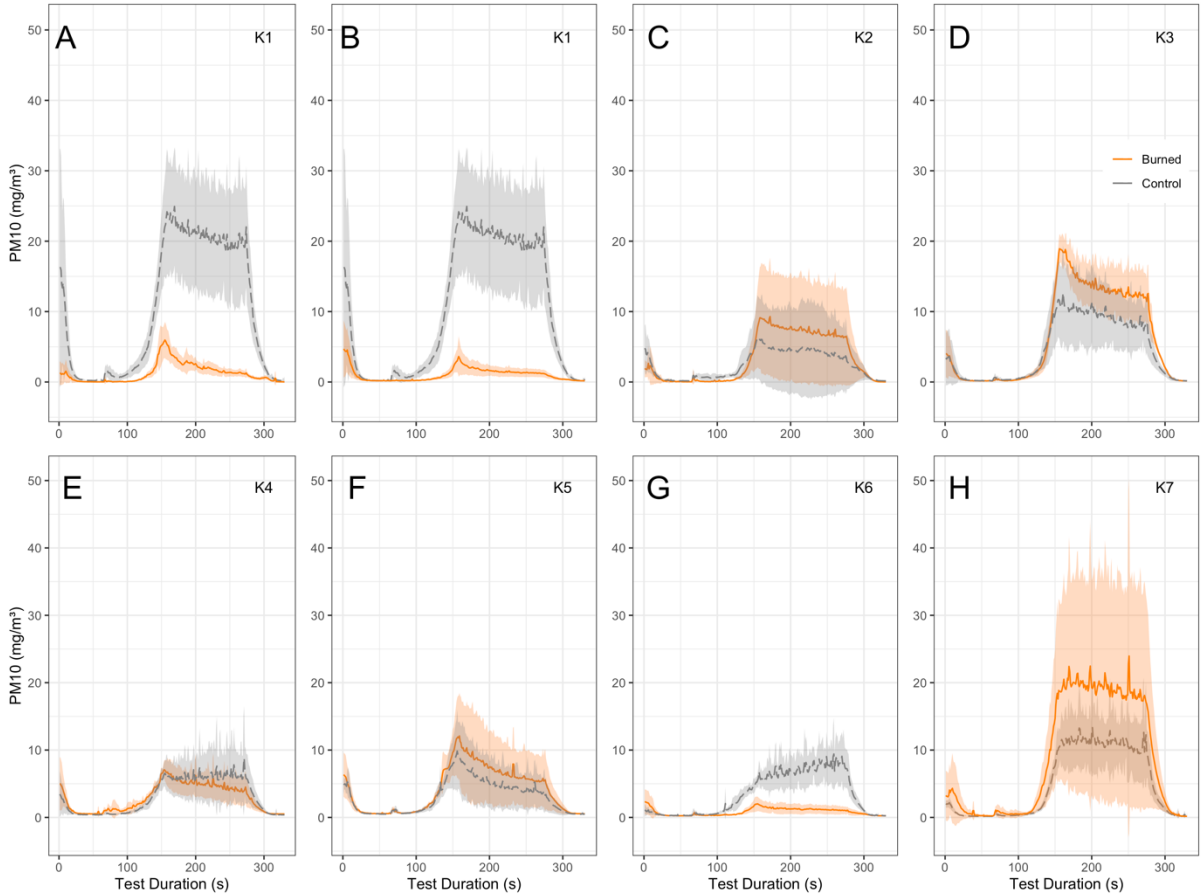

Figure 6.6. PM_{10} emissions for the burned and control plots at each interdune plot. Mean PM_{10} is the solid line with one standard deviation shaded. The burned plots are in orange and the control plots are in grey. In A the area was burned three days before measurement and in panel B the plot was remeasured one month after burning, the same control plot data was used for both measurements.

6.3.5 The effect of mechanical disturbance on emission threshold and flux

Surfaces which were mechanically disturbed constantly reported the highest fluxes of dust (Table 6.5 and Figure 6.4b) but similar threshold for emissions (Table 6.4 and Figure 6.4a). The largest difference between the control and mechanically disturbed plots measured was at site K02 where the geometric mean of flux from the control plot

was 0.065 (±6.19) mg m^{-2} s^{-1} whereas the mechanically disturbed plot had a geometric mean flux of 5.007 (±1.25) mg m^{-2} s^{-1}, 77 (CV of 82.4%)times greater than the control plot. The largest flux of dust from any one measurement was recorded on a mechanically disturbed surface with a peak flux of 6.305 mg m^{-2} s^{-1} at the burned interdune plot at site K02.

6.3.6 Summary of results

The Kalahari sediment has dust sized (< 10 μm) grains (up to 8.9%) particularly in the interdune areas. When tested using a portable wind tunnel, all sites displayed some PM_{10} emission, but the threshold for erosion and emission flux varied with the surface status (control/burned/mechanically disturbed), site, and the morphological unit of the dune. The dune crests emitted the lowest flux of dust with an average emission of 0.253 mg m^{-2} s^{-1} whereas the flanks reported the largest dust fluxes with an average emission of 0.447 mg m^{-2} s^{-1}. The results of this study show that there is fine sediment found in most of the dune experimental plots and this material should be available to be eroded by the wind once the vegetation has been burned (Table 6.3). Yet, burning increases the erosion threshold from Kalahari sand dune surfaces but does not significantly impact the flux of emitted dust (Table 6.4). However, once the surface has been mechanically disturbed by the top 2 cm being removed, fluxes of dust are up to 77 (CV of 82.4%) times greater than the control or burn-disturbed surfaces.

6.4 Discussion

In this study a wide range of variables (dune morphological unit, burning, and mechanical disturbance) were tested to assess their impact on dust emission from the

southwest Kalahari dune system. Characterisation of emission potential of vegetated dune fields and factors that modulate the baseline emissivity are important to quantify for global emissivity/erodibility maps and models of dust flux, both now and into the future (Kok et al., 2021b). This study presents a broad dataset of potential PM_{10} emissions and estimated threshold velocities from vegetated linear sand dunes and further explores within-dune landscape variations and different disturbance pressures. Overall, results indicate that potential emission of mineral dust is low across all sites in the southwest Kalahari linear dune system regardless of whether the dunes have burned or not, but mechanistic disturbance of the surface results in higher emission fluxes (up to 77 times greater) of dust.

6.4.1 Fine sediments within dune compositions

Grain size analysis shows that there is fine material (< 62.5 μm) within the sediment composition (ranging from 0% to 30%) at most plots measured. Fine grain presence indicates that if the dunes become de-vegetated the fine grains should be available to be eroded by the wind. The finding of fine material substantiates work by Bhattachan et al. (2012) that the Kalahari has the potential to emit dust once de-vegetated.

6.4.2 Emission from the southwest Kalahari linear dunes compared to other PI-SWERL tests

Previous PI-SWERL experiments have found that undisturbed bare sand dunes have a low emission potential when compared to landforms such as dry washes or playas (King et al., 2011; Sweeney et al., 2016) but higher emissions than many other surfaces such as desert pavements and alluvial fans (Dickey et al., 2023). The dust flux measured from the partially vegetated linear dunes in this study is frequently lower than those from dunes in other geographic locations. For example, Sweeney et al. (2023) found a PM_{10} max of 18.985 mg m^{-2} s^{-1} from sand from a stabilised dune in Arizona. This is an order of magnitude higher than the maximum undisturbed flux of 1.89 mg m^{-2} s^{-1} which was recorded at K07 burned interdune plot, however Sweeney et al. (2023) exerted a much higher shear velocity of 0.82 m s^{-1} on the surface compared to this study's 0.64 (±0.297) m s^{-1}. Higher emission fluxes were also observed from dunes in the Salton Sea, USA where an average flux of 2.30 mg m^{-2} s^{-1} was measured at a u_* of 0.73 m s^{-1} (Table 6.6; Dickey et al., 2023). Other studies have measured similar levels of emission flux to this study, for example in northern China Cui et al. (2019) at a slightly higher u_* of 0.69 m s^{-1} and in the southwest USA by King et al. (2011) at a lower u_* of 0.56 m s^{-1} (Table 6.6).

Table 6.6. Measurements of dust flux from sand dunes in previous PI-SWERL studies. If the study reports where on the dune measurements are made the topography is reported, otherwise the terminology used in the study is used. Many studies did not report the α value, if the value is not mentioned a hyphen is used in place. Where studies have multiple measurements of the same surface at different u_* then the closest two u_* values to the current study (0.64 ±0.297 m s^{-1}) are used.

Study	Topography	u_* (m s^{-1})	α value	Emission flux (mg m^{-2} s^{-1})	Metric
Bacon et al., 2011	Crest	0.69	-	4.21 ± 4.72	Geometric mean ± Standard Deviation
Cui et al., 2019	Interdune	0.55	0.96-0.90	~1	Geometric mean
Dickey et al., 2023	Interdune	0.73	0.9	2.30 ± 0.81	Geometric mean ± Standard Deviation
King et al., 2012	Interdune	0.56	-	0.269 ± 1.252	Geometric mean ± Standard Deviation
King et al., 2013	Interdune	0.56	-	0.279 ± 1.511	Geometric mean ± Standard Deviation
Kolesar et al., 2022	Active dune	-	-	0.20 ± 0.11	Mean ± Standard Deviation
Sweeney et al., 2018	Coppice	0.7	0.98 - 0.92	~2	Median
Sweeney et al., 2016	Stabilised	0.7	0.98 - 0.92	<0.5	Median
Sweeney et al., 2011	Dune	0.56	-	0.1443	Geometric mean
Sweeney et al., 2022	Vegetated	0.6	-	0.356 ± 0.241	Geometric mean ± Standard Deviation
Sweeney et al., 2022	Interdune	0.6	-	0.033 ± 0.063	Geometric mean ± Standard Deviation
Sweeney et al., 2022	Interdune	0.7	-	0.070 ± 0.193	Geometric mean ± Standard Deviation
Sweeney et al., 2022	Active	0.6	-	0.048 ± 0.059	Geometric mean ± Standard Deviation
von Holdt et al., 2019	Dune	-	-	0.0640 ± 1.199	Geometric mean ± Standard Deviation
Wang et al., 2025	Active	0 – 0.69	-	0.25	Average
This study	**Interdune (undisturbed)**	**0.64**	**0.98**	**0.281 ± 3.061**	**Geometric mean ± Standard Deviation**
This study	**Crest (undisturbed)**	**0.64**	**0.98**	**0.253 ± 0.238**	**Geometric mean ± Standard Deviation**

Comparison of the PI-SWERL data between studies must take account of the respective u* values used. Only one study used the same u* (0.64 m s^{-1}) as this study

and used emission fluxes on a variety of different landscapes in the Salton Sea, USA (Dickey et al., 2023). However, all dune measurements by Dickey et al. (2023) reported higher emission flux measurements than both the burned and control plots in the current study. These higher fluxes included surfaces which typically would be expected to have lower flux such as sand with gravel lag (Dickey et al., 2023). However, fluxes of dust from the scraped surfaces were of similar magnitude to highly emissive surfaces such as dry washes (King et al., 2011), smooth playas (Dickey et al., 2023) and Wadis (Cui et al., 2019) although the u* values used in these studies ranged from 0.55 to 0.73 m s^{-1}. The similar fluxes indicates that if the Kalahari surface is mechanically disturbed, emission fluxes can be similar to those reported from frequently dust producing topographies.

Notably, there is a wide range of α values used to account for different surface roughness and to calculate u_* used in all PI-SWERL studies. Of the above-mentioned studies, α values range from 0.9 – 0.96 on sand dune surfaces, which affect the u_* value and cross-study comparison. These values were chosen based on a table in Etyemezian et al. (2014). The u_* value is sensitive to the choice in α value. For example, the peak RPM of 3500 was used in this study with a resulting u_* value of 0.64 (±0.297) m s^{-1} at an α value of 0.98, if the α value is changed to 0.9 the u_* value becomes 0.85 m s^{-1}. Recently a visual look up table was created by Hartshorn et al. (2023) and this table was used in the selection of 0.98 as the α value for this study. The new look-up table

should reduce the discrepancy in assigning α values and thus u_* estimates into the future.

6.4.3 Disturbance effects

Factors that are frequently cited as disturbance agents in the arid zone context include drought, fire, and grazing (e.g., Hesse and Simpson, 2006; Mayaud et al., 2016; Nield and Baas, 2008; Wasson and Nanninga, 1986). Drought and fire do not produce any mechanistic changes in sediment distribution at the surface, only grazing reorganises the sediments through hoof action. In this study we investigate two types of disturbance, mechanical (scraped surfaces) and environmental (burned surfaces). In previous studies, disturbance has been an umbrella term to show that disturbed surfaces produce a higher flux of dust (Bacon et al., 2011; Cui et al., 2019). The current study shows an increased flux for mechanical disturbance only (Figure 6.4b). At plots where the top two centimetres of the surface had been removed, fluxes were larger (geomean 1.654 (± 1.90) mg m^{-2} s^{-1}) than undisturbed (geomean 0.314 (±2.76) mg m^{-2} s^{-1}) and fire disturbed (geomean 0.240 (± 2.91) mg m^{-2} s^{-1}) plots. The mechanically disturbed plots have dust fluxes similar to highly emissive landscapes such as dry washes and playas (King et al., 2011) and other generalised disturbed surfaces (Cui et al., 2019). The higher flux from the mechanically disturbed plots suggests that sediment availability limits dust emissions in the Kalahari, even when the surface is bare.

Sediment availability limitation is through agglomeration of sediment at the surface, likely by biological soil crusts (biocrusts or BSCs). Biocrusts are widespread throughout the Kalahari, with coverage ranging from 11 to 95% (Thomas and Dougill, 2007) and were frequently observed in the study area but it was often hard to differentiate between a crusted and un-crusted surface. The presence of crusts has previously been shown to limit PI-SWERL-generated dust flux (Fick et al., 2020; Vos et al., 2020) and globally biocrusts are thought to reduce dust emissions by around 70% (Rodríguez-Caballero et al., 2022b). Studies in other locations have found that the amount of fine grains is often increased within and below biocrusts, due to weathering processes and allochthonous dust entrapment (Garcia-Pichel et al., 2016; Weber et al., 2022), but no investigations have been conducted in the Kalahari. The removal of the surface through scraping removed any biocrust present and left the finer sediment exposed. The uncovering of this fine sediment and the loss of the biocrusts protective effect can result in subsequent higher emissions (Figure 6.4b). This is a significant finding, if the biocrust from the Kalahari is removed (for example through drought induced mortality), then large amounts of dust have the potential to be emitted. The system will shift from an availability-limited system, where fine sediment is unavailable as it is locked up in biocrusts, to a supply-limited system, where emission is limited by the number of fine grains.

The presence of biocrusts might explain why there is no statistical difference in the potential emission flux between the burned and control plots. Currently, there is no

quantitative consensus on biocrusts response to fire (Palmer et al., 2020) and fire in the Kalahari burns fast, due to the high combustibility of the vegetation (Andela et al., 2019). The rapid combustion of vegetation reduces the amount of heat transferred to the surface sediment, allowing some biocrust to withstand fire (Lentile et al., 2006; Palmer et al., 2020). Even if the heat transfer is fatal to the biocrusts they do not initially lose their protective effects. Biocrust toleration to fire has been found in the USA and Australia (Brianne et al., 2020) but at present there are no studies in southern Africa. Our data suggest that biocrusts still offer protective coverage to the surface after fire, reducing the emission flux.

Moreover, there is a significant difference between the threshold for emission between the burned and control plots (Figure 6.5). In the first two months after fire in the interdune plots, the threshold for erosion is higher than the collocated control plot (Figure 6.5). In comparison, on the dune crests in the first year after fire, the threshold for erosion is lower than the control plots. Biocrusts were not found on the more active crests of the dunes whereas in the interdunes where the biocrusts are widespread, and thresholds were higher.

The higher u_{*T} post-burn is in contrast to previous findings where PI-SWERL measurements in semi-arid shrubland has shown that desert surfaces have higher emissivity after fire (Sankey et al., 2012, 2011). The emissions recorded in Sankey et al., (2012) were concentrated in hotspots under shrubs and were likely due to burn-

induced soil hydrophobicity under the shrub canopies (Ravi et al., 2007, 2006). The experimental design for the current study intentionally did not conduct wind tunnel tests under shrubs due to woody vegetation burning incompletely, increasing the surface roughness, and subsequently the shrubby areas would likely not emit dust (see Figure 6.7).

Figure 6.7. An example of a burned formerly shrubby area three months after fire at K03. The remaining shrubs increase surface roughness and reduce the likelihood of the site emitting dust.

6.4.4 The impact of the dune morphological unit on emission flux

The dust flux, erosion threshold, and grain size differ significantly with the dune morphological unit (Figures 6.4 and 6.5, Tables 6.3, 6.4, and 6.5), consequently results were divided into the morphological units of crest, flank, and interdune. Overall, the PI-SWERL emission flux results suggest that all morphological units have the potential of emitting low level dust emissions (Table 6.4). The minimum flux of dust

recorded in this study was 0.005 mg m^{-2} s^{-1} at the burned interdune of site K01 one month after burning (Table 6.4), demonstrating that, even though this is low, the surface can emit some PM_{10}. The interdunes had the largest range of emission flux, and the highest maximum flux of the dune morphological units (1.892 mg m^{-2} s^{-1} at the burned interdune K07 plot), but this was not reflected in the geometric mean where the emissions were mostly lower than the flanks and crests (Table 6.4). In previous work in the Kalahari, Bhattachan et al. (2012) discounted the crests of the dunes from being dust-emitting surfaces. Instead, the results from this study suggests that both the flanks and crests have some capacity to emit dust and should be included in dune-field scale estimates of dust emission flux.

On the crests, there was a 1.85 ± 18.58 times greater emission flux from the average burned (0.467 ± 1.43 m s^{-1}) than the control (0.253 ± 2.43 m s^{-1}) plots. The higher flux for emission on burned dune crests is likely an indicator of sediment size distribution rather than the effect of fire. In the Kalahari, many dune crests are not vegetated, if a crest burned it must have had vegetation cover sufficient to allow the spread of fire. Therefore, as vegetation traps allochthonous dust and allows some pedogenesis (Garcia-Pichel et al., 2016; Garzanti et al., 2022; Gonzales et al., 2018; Weber et al., 2022), the burned crest have some finer sediment fraction available to be eroded by the wind. Finer material in burned crests was reflected in our sediment size distributions as the burned crest plots had an average of 2.562% silt content whereas the control crest plots had an average of 0.349%. This finding substantiates previous

work which has highlighted that vegetated dune fields have a higher potential to emit dust, if denuded of vegetation, than active dune fields (Bullard et al, 2011; Sweeney et al., 2023).

6.5 Conclusions

The aims of this study were to (1) characterise the sediment texture at burned and control plots; (2) quantify emission flux potential from southwest Kalahari linear dunes; and (3) establish if there are different emission thresholds for burned surface to control plots. Our principal findings from this study are:

1. All fluxes of dust from the Kalahari dune surfaces were low, with an average flux of 0.336 mg m^{-2} s^{-1} compared to more prevalent dust-emitting landscape such as dry washes or playas which experience fluxes above 1 mg m^{-2} s^{-1} (King et al., 2011; Sweeney et al., 2016). The low emission fluxes recorded in this study were at a u_* of 0.64 (±0.297) m s^{-1} and remained low independent of whether the surface had burned or not. However, the measured fluxes of dust in this study are similar to other dune dust fluxes from different locations such as the USA (King et al., 2011; Sweeney et al., 2022) and China (Cui et al., 2019; Wang et al., 2025).

2. The dust flux varies significantly between the different morphological units on the dune. The emissions are highest from the dune flanks and interdunes, with crests recording the lowest emission potential (Table 6.4). However, all surfaces are capable of emitting dust, even if this is low in concentration. Subsequently future estimates of dust flux from the entire southwest Kalahari should use a more nuanced approach of

first calculating the proportion of vegetated crests and including these in emission estimates.

3. Emissions from burned crests were 1.8 ± 18.58 times greater than the flux from the control crest plots on average. This finding, alongside a higher proportion of fine material in the crests, supports previous work indicating that vegetated dune fields have a higher capacity to emit dust when initially de-vegetated than currently active dune fields (Bullard et al, 2011; Sweeney et al., 2023).

4. A key finding from this study is the identification of the role that different surface disturbances may play in dust emission. Fire alone does not produce a significant effect on the flux or lower thresholds for erosion at all the morphological units on the dune. This is likely due to biological soil crusts surviving fire and armouring the surface against erosion. Therefore, dust emissions are unlikely to occur after burning on the Kalahari linear dunes. But mechanical disturbance and the removal of biocrust from the surface produces large fluxes of dust which are comparable with other highly emissive landscapes such as playas (King et al., 2011). This again indicates the importance of biocrusts in preventing dust emission from the Kalahari dune field, substantiating previous studies worldwide (Rodríguez-Caballero et al., 2022b).

Future work should aim to try and understand the complexities highlighted in the data reported in this study. There should be a focus on quantifying the impact of fire on biological soil crust survival and quantify biocrusts protective effects on the surface

in southern Africa. Furthermore, running longer PI-SWERL experiments to understand the role of abrasion on low lying dust emissions may be beneficial.

Chapter 7 -

The southwest Kalahari dune field does not emit dust post-fire despite lack of vegetation and above-threshold winds

Status: Submitted to *Earth Surface Processes and Landforms* in May 2025

Meteorological station and dust track.

Summary

This research paper addresses **research question three** – *what is the impact of fire on dune surface properties?* – focusing on erosivity and erodibility controls on dust emission after fire through measurements of in-situ wind and dust, grain size distribution, and ground cover surveys. Findings suggest that there is little emission of dust despite a fine grain component. This is due to infrequent strong winds and high surface cover post-fire. Further, biological soil crusts were found at 100% of interdune sites, increasing surface strength and subsequently protecting the surface from wind erosion.

Abstract

Sand dunes are not typically considered to be large sources of dust, due to coarse grain sizes and high vegetation cover. Yet plumes of dust have been observed from dune fields and wind tunnel experiments show the potential for interdunes to emit dust. The southwest Kalahari is one such dune field which has been posited as a potential future dust source. In this study we exploit the post-fire de-vegetated state of 11 interdunes to investigate the dust emission potential and erodibility controls on emission. Findings suggest that there is little emission of dust despite a fine grain component (up to 30% of resident < 62.5 μm) and a lack of vegetation, despite high velocity wind events (> 7 m s^{-1}) post-fire. Suitable wind events were less frequent compared to other dust producing regions, with wind speeds generally under 7 m s^{-1}. Five high wind speed events over 7 m s^{-1} were recorded in September 2022, the month immediately following burning, but even then, only one event had a concurrent increase in aerosol concentration. This is indicative of other erodibility factors limiting dust emission. These include high burned debris cover in the immediate post-fire period and biological soil crusts surviving burning and protecting the surface for the duration of decreased vegetation cover. Combined, the general low wind speeds, high initial surface cover, and the protective effect of biocrusts result in the low possibility of the southwest Kalahari emitting dust post-fire. However, fine grain sizes and low vegetation cover under drought and high grazing may lead to conditions conducive for dust emission.

7.1 Introduction

Windblown dust is the most abundant atmospheric aerosol and is a critical component of the Earth's land-atmosphere-ocean-biosphere system (Adebiyi et al., 2023; Kok et al., 2017; Schepanski, 2018). Whilst airborne, dust has influences on the Earth's radiation balance and atmospheric chemistry, alongside issues for human health and air quality (Goudie, 2014; Hilly et al., 2025; Kok et al., 2023; Schepanski, 2018). Once deposited, it can be an important nutrient source for both terrestrial (Dong et al., 2020; von Suchodoletz et al., 2013; Winton et al., 2024) and marine (Dansie et al., 2022; Gittings et al., 2024; Jickells et al., 2005) ecosystems. Yet current understanding of the factors driving changes in the emission of dust, including the relative roles of wind speed, soil properties, changes in land use, sediment supply, and vegetation cover is poor (Bryant, 2013; Kok et al., 2023; Mahowald et al., 2024). These uncertainties have led to significant challenges in parameterising the amount of dust in the atmosphere and thus future climate conditions (Kok et al., 2023; Mahowald et al., 2024).

Vegetated dune fields are not typically considered to be large sources of dust, mainly due to low fine material (< 100 μm) content and high surface roughness due to vegetation cover which stabilises the dunes but also reduces near surface wind velocities and promotes deposition (Hesse and Simpson, 2006; Strong et al., 2010; Wiggs et al., 1994). However, vegetated sand dunes have resident fine grains (< 62.5 μm) in the sediment composition due to limited surface movement (Bullard et al., 2004). This stability allows for weak pedogenesis which occurs over geologic time

scales increasing the fine-grain content of the dune field (Bhattachan et al., 2013; Bullard et al., 2008; Hesse, 2016). In addition, established vegetation and biological soil crusts (biocrusts) trap allochthonous sediment further enhancing the fine portion of the dune field sediment texture (Garcia-Pichel et al., 2016; Hesse, 2016; Zhao and Lei, 2025). Currently it is thought that biocrusts, communities of bacteria and algae in the top few millimetres of the soil, stabilise the surface and reduce global atmospheric dust emissions by around 60% (Rodríguez-Caballero et al., 2022b). Subsequently, when these systems are disturbed and de-vegetated, there are portions of fine sediment available to be eroded by the wind (Pye, 1989; Sweeney et al., 2023).

Furthermore, there has been a recent growth in the recognition that super-coarse grains ($10 \leq$ diameter < 62.5 μm) make up a large part of suspended dust, indicating that source regions are producing coarse dust grains (Adebiyi et al., 2023; Adebiyi and Kok, 2020; Ratcliffe et al., 2024; Ryder et al., 2018; Weinzierl et al., 2017). Moreover, both laboratory and field-wind tunnel studies have shown that although sand dunes comprise of coarse grains, the saltation process can abrade sediment and generate fine material (Baddock et al., 2013; Bullard et al., 2004; Bullard and White, 2005; Sweeney et al., 2023). For example, Bullard et al. (2004) used sand from the central Australian Deserts and a 'test-tube' glass chamber to simulate an abrasive environment and found that continuous abrasion over 16 hours lead to sediment under 10 μm dominating the distribution. More recently, Sweeney et al. (2023) used a portable wind

tunnel to find that up to 40% of the dust flux from various natural sand surfaces came from aeolian abrasion.

Within vegetated dune systems the interdune locations are primarily considered to be the most likely source of dust due to vegetation canopies trapping aerosols being advected across the dune field (Garcia-Pichel et al., 2016; Hesse, 2016; Zhao and Lei, 2025) and larger proportions of fine sediment compared to the dune crests or flanks (Bhattachan et al., 2013, 2012; Lancaster, 1986; Strong et al., 2010). In the southwest Kalahari interdunes frequently have a thin sand cover over extensive calcrete duricrusts which are exposed in some places and a source of fine grained material in the surface sediment matrix (Lancaster, 1988; Mabbutt, 1957; Nash, 2022). Bhattachan et al. (2012) used a dust impact generator in the partially vegetated dunes of the southwest Kalahari and found that only the interdune locations have the potential to emit dust. Interdunes were also posited to be the only dust-producing portion of the dune field by Strong et al. (2010) in the Simpson Desert, due to grain size and vegetation establishment.

Fires are common on vegetated dune landscapes and pose a disturbance event that triggers de-vegetation which exposes large portions of bare surface to the wind. Subsequently, post-fire dust emission events are becoming more frequently observed and investigated globally (Li et al., 2021; Wagenbrenner et al., 2013; Yu and Ginoux, 2022). Fire can further increase the erodibility of the surface through reducing inter-

grain cohesion (Ravi et al., 2009b, 2006). This occurs through the volatilisation of the organic component of plants when burned, which is then transported into the soil through strong temperature gradients, condensing around sand grains creating a hydrophobic coating (DeBano, 2000; Ravi et al., 2009a, 2007).

Yet, few studies have reported post-fire dust plumes from interdune locations. Bullard et al. (2008) and McGowan and Clark (2008) both recorded dust events in the Simpson Desert in late 2003 using MODIS imagery where one plume with origins within a dune field fire scar had a recorded size of 85,700 km^2. Yu and Ginoux (2022) used MODIS based dust optical depth (DOD) to identify increases in aerosols above burned land. The study observed increases over burned vegetated dune systems globally, but the events were rarely observed as distinct plumes of dust (Yu and Ginoux, 2022). Furthermore, Strong et al. (2010) measured higher than average total annual dust concentration at a meteorological station downwind of large fire scars seven years after burning in the Simpson Desert. The above-mentioned observations of post-fire dune dust emission all have difficulty in pinpointing the exact origins of these emissions within the dune landscape.

The Kalahari Desert in southern Africa is ecologically and geomorphologically similar to the post-fire dust-producing Simpson Desert (Buckley, 1981) and also burns frequently. Yet, post-fire dust emissions have not be observed in the region despite some evidence of dust plumes originating from within the dune field (Eckardt et al.,

2020; Vickery et al., 2013). Vickery et al. (2013) and Eckardt et al. (2020) both used the Meteosat Second Generation - Spinning Enhanced Visible and Infrared Imager (MSG – SEVIRI) to identify only six plumes originating from the southwest Kalahari dune field over 13 years of observation, but none of these plumes were explicitly linked to burned area. Dust emitted from the dune field can be of global consequence, with the iron-rich fallout providing nutrients to the south Atlantic (Dansie et al., 2017b), the Madagascar Sea (Gittings et al., 2024), or the Southern Ocean (Bhattachan et al., 2012). This study investigates the post-fire environment of burned interdunes in the southwest Kalahari Desert to answer the research questions: what is the potential to produce dust and what are the controls on dust emission post-fire.

7.2 The southwest Kalahari linear dune field

The arid dune field in the southwestern Kalahari is characterised by long, linear dunes that stretch from northwest to southeast (Lancaster, 1986; Thomas and Wiggs, 2022). Dunes consist of unconsolidated aeolian sands, primarily composed of quartz and feldspar (Garzanti et al., 2022). Previous studies have found that there is fine material within the dune sediments, with fine silt and clay content ranging from 0 – 7% (Bhattachan et al., 2013; Livingstone et al., 1999; Stone and Thomas, 2008; Telfer, 2011).

The vegetation in this region is a mixture of trees, shrubs, and grasses. Interdunes are dominated by the annual grass *Schmidtia kalahariensis*. Wiggs et al. (1995) identified that the litter component of ground cover has much greater importance in protecting

the surface from wind erosion than rooted vegetation. Fires in the region are limited by vegetation cover and are therefore linked to precipitation (Andela et al., 2019). Wet years allow for the build-up of biomass which senesce generating a lot of dry flammable material in the subsequent dry season (Chen et al., 2017). Further, biocrusts are dominated by cyanobacteria in the region, and provide additional protection to the surface through the filamentous sheath material entangling grains and the secretion of extracellular polymeric substances which agglutinate particles (Thomas and Dougill, 2007). Biocrusts cover is between 11 to 95% of the surface of the Kalahari dune field (Thomas and Dougill, 2007).

7.3 Methods

In order to answer the research questions of what is the potential to produce dust and what are the controls on dust emission post-fire, a primarily field-based study was conducted in the region to identify evidence of in-situ emissions and any potential factors that could limit erosion. Measurements were conducted in three periods in September 2022, and July and September 2023 (Figure 7.1). In-situ monitoring of wind speeds and dust emissions were collected in September 2022. September, at the end of the dry season, was chosen as the primary measurement month due to the high likelihood of fire and conditions most conductive to wind erosion (dry and windy). A comparative methodology was established, where burned plots were co-located with nearby unburned plots for a total of 22 interdune plot measurements (11 within fire scars and 11 co-located unburned interdunes).

The investigation is divided into two subsections: (1) what is the potential for dust emission? and (2) are there erodibility controls on dust emission? To answer the first question, surface sediment samples were collected to establish fine-grain components and any loss of fine grains from the burned plots and compared with samples from co-located control (unburned) plots. Wind speeds were measured on the ground and compared to longer term reanalysis data to establish if wind strength was a factor in limiting dust emissions. Additionally, in-situ dust emissions were measured using a DustTrak aerosol monitor. To address how post-fire erodibility controls dust emission the same comparative methodology was utilised to identify controls on emission through quantification of surface and biocrust cover, alongside measurements of soil hydrophobicity. Each measurement in section two was conducted at plots with varying burn ages to investigate the persistence of the impact of burning on the surface, which is another potential control on emission.

Study sites

To investigate what limits dust emission from the southwest Kalahari, measurements were conducted in three periods at 22 interdune plots (11 within fire scars and 11 co-located unburned interdunes; Figure 7.1). To ensure that the breadth of the linear dune field was represented, sites were selected at different locations in the dune field (Figure 7.1) and each site had varying burn age (Table 7.1). Fire leaves a distinct mark, or scar, on the surface and this was used to identify sites using remote sensing imagery in addition to conversations with local land administrators.

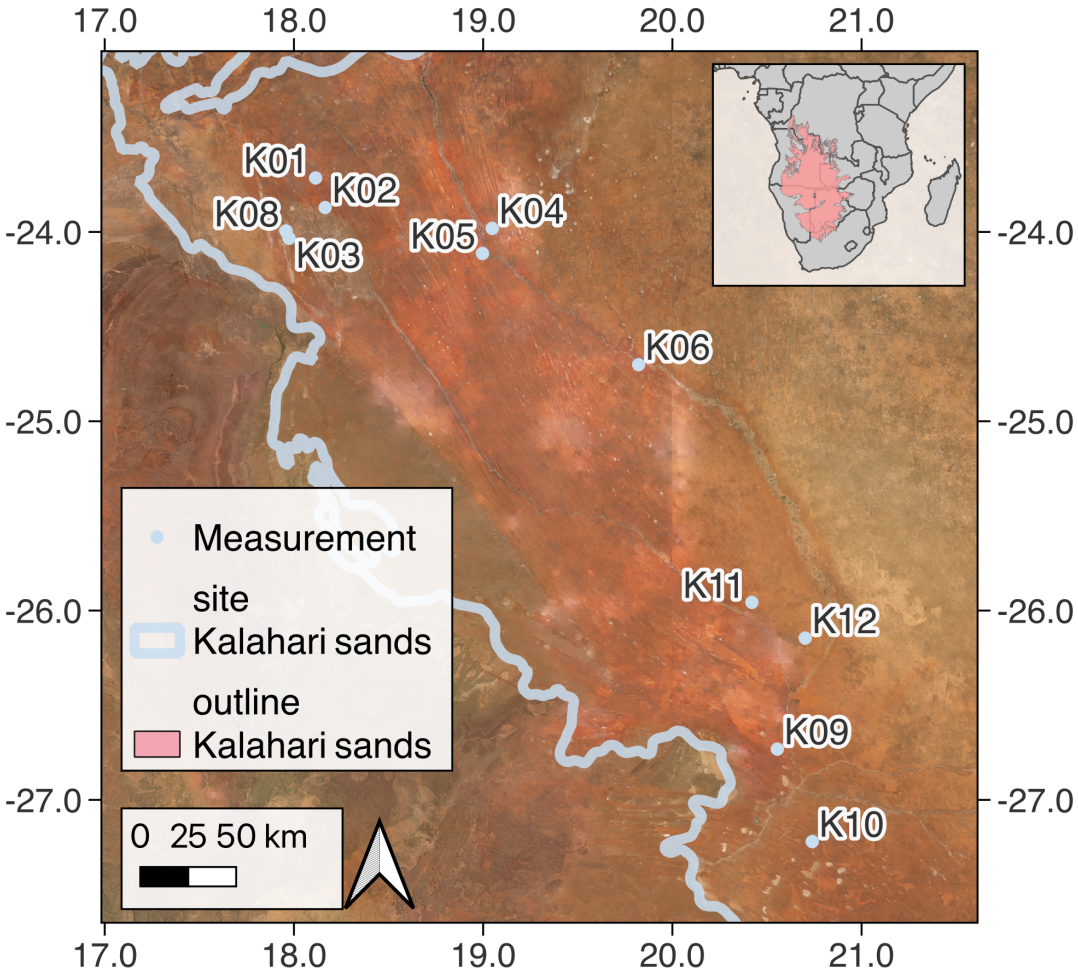

Figure 7.1. The location of the study sites in southern Africa and the Kalahari sand sheet. Background image © 2023 Planet Labs PBC (Planet, 2017).

The use of co-located control and burned plots aimed to remove variations through differences in surface properties at each site (e.g., soil type or grazing density). By utilising the co-located plots, the differences between them are controlled. Accordingly, the control and burned measurements aimed to be conducted on the same dune or one dune across from another and on farmed sites within the same fenced area. Sites that were first visited in September 2022 were remeasured in September 2023 upon revisiting. The most recently burned sites (K01 and K02) were

measured one month after the initial measurements when the recording equipment was dismantled (Table 7.1).

Table 7.1. Locations of measurement sites on the Kalahari linear dunes. Measurement Time Since Fire (TSF) also reveals the number of measurements made at each site.

Site	Land use	Burned interdune latitude	Burned interdune longitude	Date of fire	Measurement TSF (months)
K01	Farm	-23.7227	18.1100	01/09/2022	0*[3],1*,12
K02	Farm	-23.8606	18.1507	26/07/2022	1*,2*,13
K03	Farm	-24.0422	17.9812	18/06/2022	4*, 15
K04	Farm	-23.9825	19.0172	29/11/2021	10*, 22
K05	Farm	-24.1159	18.9966	16/11/2021	10*, 22
K06	Farm	-24.6889	19.8223	27/10/2020	25*, 37
K08	Farm	-23.9961	17.9593	18/12/2021	9*, 21
K09	Farm	-27.2211	20.7403	21/01/2023	6
K10	Farm	-26.7354	20.5562	18/10/2022	10
K11	NP	-25.9571	20.4206	27/12/2021	18
K12	NP	-26.1460	20.7030	09/09/2022	10

*Surface cover survey only
[3] Site K01 was initially recorded three days after burning
NP = National Park

Wind speed

To examine wind strength and erosive capability, horizontal wind velocity and direction were determined using a Vector Instruments cup anemometer (A-100LK) and wind vane (W-200P) at the burned K02 plot at a height of 1.8 m (Figure 7.2). The burned K02 plot was chosen as it was the most recently burned site visited at the start of the measuring period and subsequently could record the longest duration. The sampling frequency of the anemometers was two-minutes in September 2022.

Figure 7.2. In-situ measurements of dust using a DustTrak monitor and meteorological station at site K02 burned interdune plot in September 2022.

To contextualise the month-long meteorological station data in the context of the wider wind regime in the region, daily mean wind speeds and wind gust data from 01/01/2000 – 31/12/2023 were obtained using ERA5-Land reanalysis daily aggregate data (Muñoz-Sabater et al., 2021). Wind gusts (m s^{-1}) are defined as the maximum value, within the hourly observation period, and were chosen for analysis due to previous research finding good correlation between wind gusts and dust emission (Engelstaedter and Washington, 2007). ERA5-Land data is a commonly used method for reanalysis of southern African climate (e.g., Chikoore et al., 2024; Mwangala et al.,

2024; Parsons et al., 2022; Roffe and van der Walt, 2023), with Gadal et al. (2022) finding that ERA5-Land can reliably be used for wind speed analysis in southern Africa.

Grain size distribution

Surface sediment samples were collected from each burned and control plot to establish (1) if there were resident fines contained within the interdunes and (2) if dust was being emitted from the surface. Resident fine material, is described by Bullard et al. (2004) as particles under 125 μm that are released as dust during saltation and surface remobilisation. In this study, sediment under 62.5 μm is considered as the resident fine material benchmark as this size bin is a key component of dust (Adebiyi et al., 2023; Sweeney et al., 2023). Grain size distribution of the samples was conducted using the wet (no pre-treatment) dispersal method with a Malvern Mastersizer Hydro 2000MU laser diffraction particle size analyser. Before analysis, samples were oven dried overnight and sieved to under 2 mm and exposed to ten seconds of ultrasonic dissolution. Samples were determined using the classification system of the United States Department of Agriculture (USDA) where clay is <2 μm, silt is 2 μm to 50 μm, and sand is 50 μm to 2000 μm. In addition, sediment was further classed into particles which are typically considered to be the inhalable size of dust under 10 μm and using recent evidence of super-coarse dust under 62.5 μm (Adebiyi et al., 2023; Sweeney et al., 2023).

Lancaster (1986a) investigated sediment size characteristics of the southwest Kalahari and concluded that the interdunes have more fine material than the dune crest due to the differential movement of grains of different sizes. Subsequently, should the resident fine material be emitted from the surface as dust, then a coarsening in grain size between control to burned surfaces could be indicative of dust emissions from the plots. This assumes the interdunes are fine grain supply-limited, which is likely the case for the Kalahari due to the lack of large recharge events replenishing supply (Bhattachan et al., 2012). Yet some interdune sand layers are so thin that they interact with the underlying calcrete, providing some fine material. These calcrete-influenced interdunes are characteristically lighter than the unconsolidated red sands, and sediment was not sampled in this study. Subsequently, we assume that the interdune sediment is supply-limited and Wilcoxon rank-sum tests were chosen to assess for any statistical differences between the burned and control plots, due to the paired and skewed nature of the dataset.

Aerosol concentration

To identify any dust events that are not recorded by satellite remote sensing, aerosol concentrations were measured at the two most recently burned plots K01 (3-day old fire scar) and K02 (one month old fire scar) during September 2022. DustTrak DRX (TSI Inc) aerosol monitors (Wang et al., 2009) were mounted on a tripod at 1.8 m height and located at least 500 m from the edge of the burn. Average aerosol concentrations (mg m^{-3}) were recorded at two-minute intervals at PM_1, $PM_{2.5}$, and PM_{10}.

Ground cover surveys

10 m transect line ground cover surveys were conducted at each interdune area to quantify the proportion of the surface available for wind erosion using the line-intercept method (Canfield, 1941). This method is an established technique to assess ground cover (Brun and Box, 1963; Canfield, 1941; Etchberger and Krausman, 1997; Hesse and Simpson, 2006) with Etchberger and Krausman (1997) finding that the line-intercept method was the most close estimate to the real census of vegetation in the Sonoran Desert. The line-intercept measurement regime was chosen to accommodate the need for instantaneous measures of both surface cover and bare ground without instrumentation of the plots. At each plot a tape measure was placed on the surface and for each centimetre in contact with the tape recorded. This included: bare ground (including cyanobacterial and algal crusts which were not easily distinguishable from bare ground), vegetation height, class (for example perennial grass, annual grass, shrub, forb, tree), basal cover, litter, burned vegetation, and burned detritus.

Sediment profile trenches

The visual delineation of biocrusts is difficult, many biocrusts in the Kalahari are early successional stage cyanobacterial crusts which do not have any surface discolouration. Therefore, mapping their cover from above is hard. To circumvent this problem, 10 cm deep pits were dug at each plot when measurements were made in 2023 to describe

the surface, the structure of the top few centimetres and ascertain any surface crusting through identification of conglomerations of sediment (Figure 7.3).

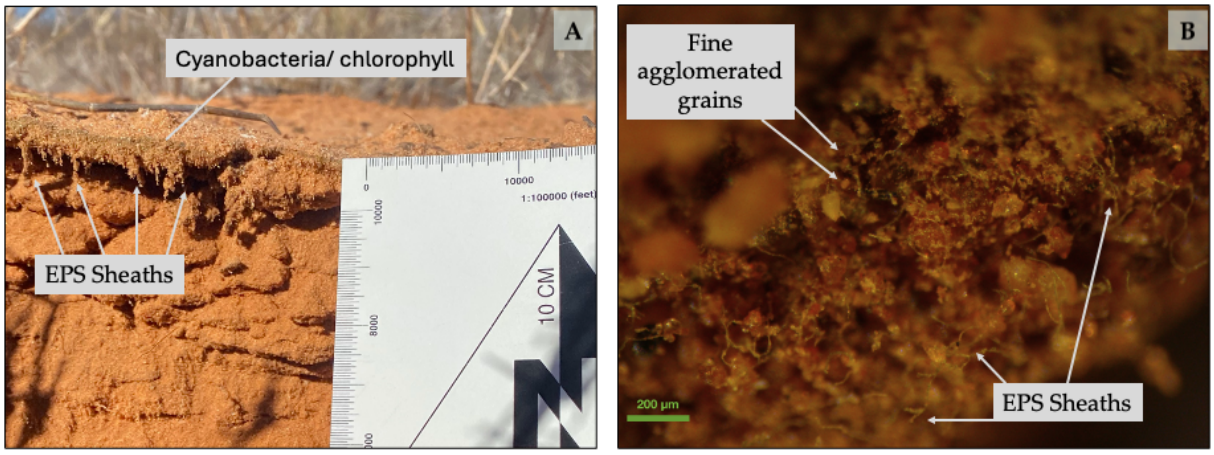

Figure 7.3. Biological soil crusts in the Kalahari. (A) A sediment profile trench at control interdune plot K11 where biological soil crust is present. Extracellular polymeric substances (EPS) and greened cyanobacteria/chlorophyll are highlighted. (B) Microscopy of a biological soil crusts displaying the EPS and the diverse grain sizes present within the crust.

7.4 Results

Wind conditions

The 24-year ERA5-Land reported an above average mean wind speed of 4.29 (±1.5) m s^{-1} for September 2022. The wind gust data is present in Figure 7.4 and shows September 2022, with wind gusts of 6.81 m s^{-1} was an above average month for wind gusts for the month of September in 2000-2023. However, January, October, November, and December with average wind gusts of 6.64, 6.92, 7.07, and 7.19 m s^{-1} respectively proved to be windier months in general (Figure 7.4). Examining the hourly ERA5-Land 10 m wind speed data for the recording month of September 2022 there were eight high wind speed days that reached over 7 m s^{-1}. ERA5-Land and meteorological station data correlated well with an R^2 value of 0.326 and can be used

comparatively. Data from the meteorological station, with a temporal resolution of two minutes, recorded five high wind speed days during the recording period where winds surpassed 7 m s^{-1}.

In-situ aerosol concentrations

Despite events with wind speeds greater than 7 m s^{-1}, there were a limited number of coincident increases in aerosol concentration measured by the DustTrak. Figure 7.5a shows aerosol concentration at the burned plots K01 and K02 from the 04/09/2022 - 03/10/2022 alongside the meteorological station wind speed. In the recording period there were four events where the relationship between wind speed and aerosol concentration increased concurrently (07/09/22, 13/09/22, 14/09/22 and 29/09/22). Yet there were also days that recorded the strong wind speeds but had no increase in aerosols (16/09/22). Other days experienced minor increases in wind speed (<4 m s^{-1}) with no aerosol concentration increase (e.g., 12/09/22 and 21/09/22), or aerosol increased without recent (in the previous 3 hours) wind speed increase (24/09/22 and 25/09/22). These results suggest no relationship between wind speed and aerosol concentration and, when tested, the R^2 values were 0.036 and 0.029 at K01 and K02 respectively (Figure S1).

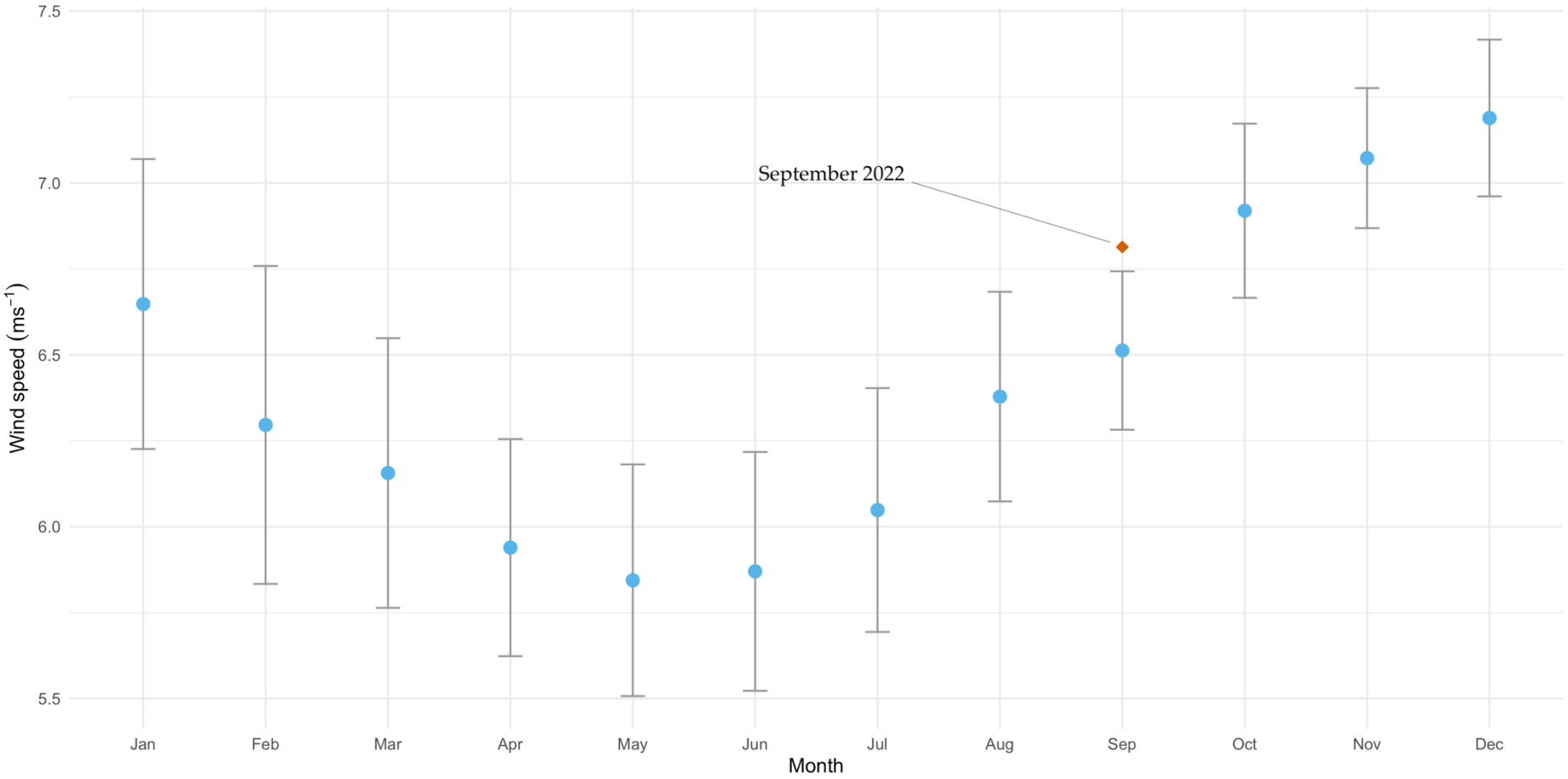

Figure 7.4. Monthly mean wind gusts (m s^{-1}) from 2000 - 2023. Mean values are reported in blue with ± one standard deviation. The ground survey month (September 2022) is highlighted in the orange diamond and had higher than average wind gusts than other Septembers in the measuring period.

The four days where aerosol concentration increased with wind speed were deemed potential dust emission events (Figure 7.5 b,c,d,e). These events on the 07/09/22, 13/09/22, 14/09/22 and 29/09/22 occurred in the early morning, approximately 3 hours after sunrise, where wind speeds were above 6 m s^{-1} for 0, 2, 12, and 66 minutes respectively reaching maximum 2-minute wind speeds of 4.19, 6.56, 6.585, 7.414 m s^{-1}. In these events the aerosol concentration remained low, peaking at 0.0636 mg m^{-3} at K01 and 0.072 mg m^{-3} at K02 both on 29/09/2022.

Sediment particle-size characteristics

Grain size distribution data for the study site sediments are presented in Table 7.2. The median D_{50} grain size for the sediment was 249 μm, indicating that the sediments were largely sand-sized, as expected for a dune field. Fine-grained sediments (< 62.5 μm) were present (mean: 8.74% range: 1.36 to 29.97%) at all the measured interdunes, with the highest proportion (29.9%) at the burned K01 plot. When comparing the control and burned plots, there was no overall coarsening in grain size and any difference between the pairs of data was not significant ($p > 0.05$) when the data are tested using a Wilcoxon rank-sum test.

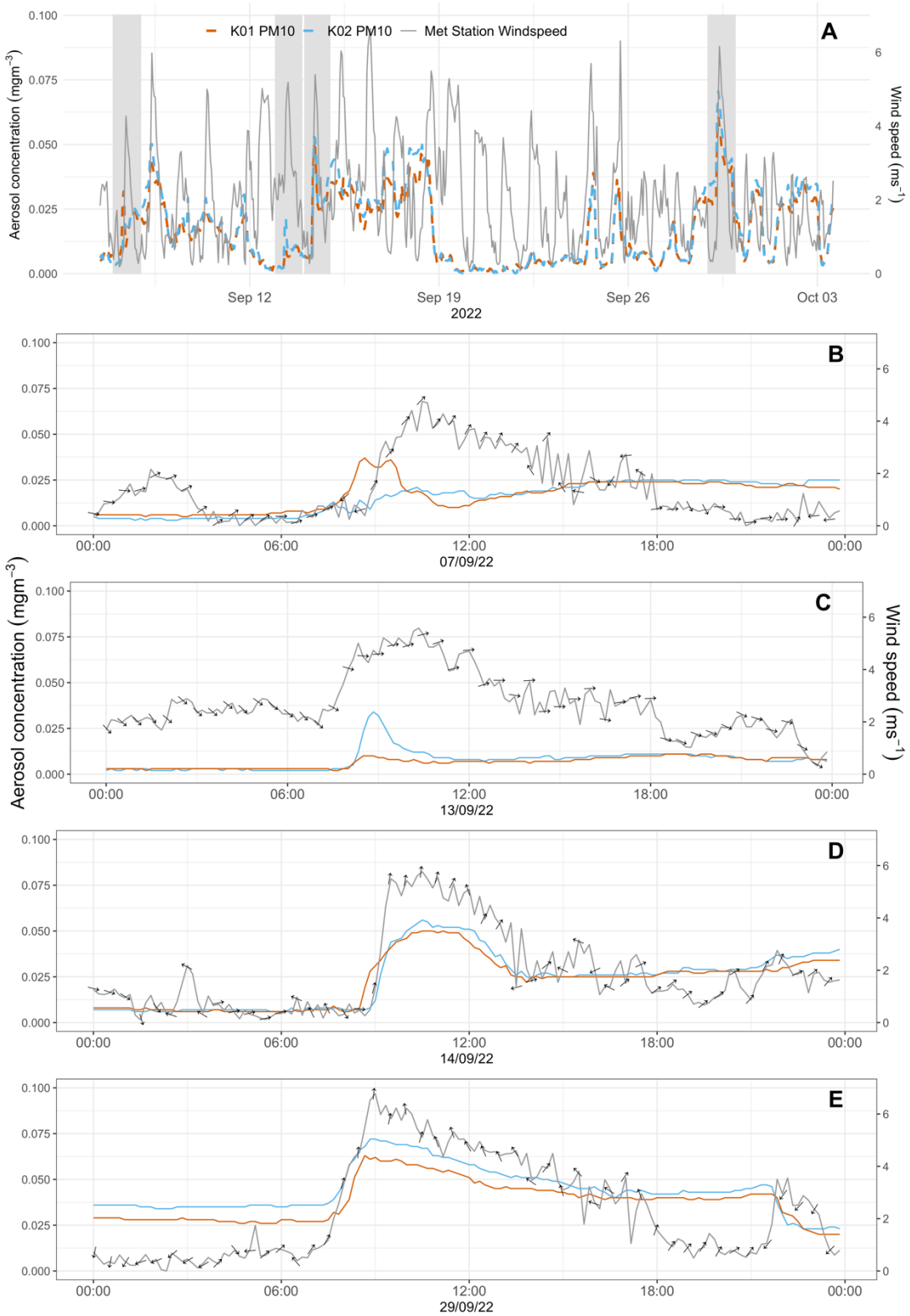

Figure 7.5. 24-hour time series of measured aerosol concentration (PM_{10}, mg m^{-3}) with measurements from plot K01 in blue and K02 in brown. Panel (A) is throughout the full monitoring period, with the grey background denoting periods of increased aerosol concentration with coincidental increases in wind speed. Details of these events over 24 hr periods are shown in panels B,C,D, and E which include ten-minute weighted average wind speed (m s^{-1}) displayed with arrows indicating the 30-minute median wind direction where the wind is going to.

Table 7.2. Grain size data for samples from the study plots.

	% of sample																			
	Clay				Silt				Sand				< 10 μm				< 62.5 μm			
	x ~	Max.	Min	SD	x ~	Max.	Min.	SD	x ~	Max.	Min.	SD	x ~	Max.	Min.	SD	x ~	Max.	Min.	SD
Burned	0	0.090	0	0.022	5.466	25.254	1.446	6.656	94.534	98.554	74.655	6.674	1.688	8.907	0.155	2.244	6.873	29.965	2.068	7.928
Control	0	0	0	0	5.381	11.928	0.963	2.872	94.619	99.037	88.072	2.872	1.649	3.386	0.062	1.021	6.637	14.722	1.360	3.563

Patterns of surface cover

Analysis of the ground cover surveys can be divided into the initial post-fire period (0-4 months) and then the remaining post-fire measurements (6 months onwards). The data presented in Figure 7.6 shows the initial post burn period in 2022 and the subsequent plot measurements made in 2023 when the region was experiencing a drought. Initially, after burning there is a high cover of burned debris. Three days after fire at the burned K01 plot, burned debris cover was 70.4%. This cover then reduces to the lowest cover observed at the burned K02 plot two months after fire with 3.8% of the surface covered. Of the control plots, litter (which mainly consisted of the dead annual grass *Schmidtia kalahariensis*), provided the most surface cover. The older burned plots (6-37 months) measured lower surface cover than the co-located control plots, but cover is again dominated by litter. The lower coverage on burned plots indicates that these plots have difficulty retaining cover under the drought conditions of the measurement period.

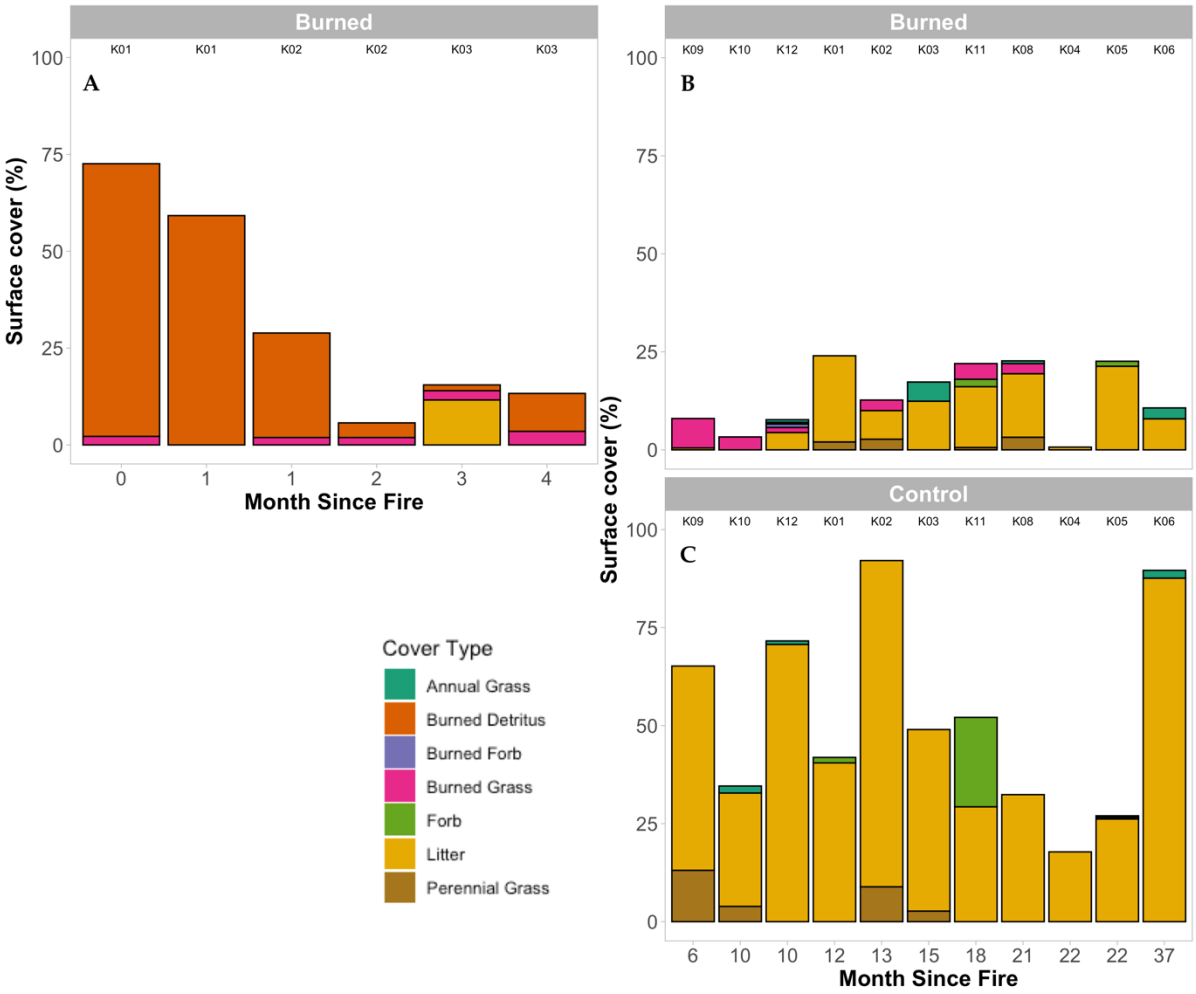

Figure 7.6. Surface cover of burned and control plots. (A) displays the immediate post-fire period (0-4 months) where surface cover is dominated by burned material, which is gradually translocated. (B) and (C) are measurements from less recently burned plots measured during a drought in 2023 (6-37 months post-fire). Here, the surface cover is dominated by litter with the burned plots having much less surface cover than the co-located control plots.

Biological soil crust presence

Biocrusts are ubiquitous with the Kalahari landscape (Thomas and Dougill, 2007) and were identified at 95% of interdune plots and 100% of burned interdune plots when trenches were dug. 65.2% of these crusts were early successional stage crusts with no surface discolouration or micro-topographical changes.

7.5 Discussion

7.5.1 What is the potential for dust emission?

Factors that influence the potential for interdunes in the southwest Kalahari to emit dust are first discussed, through examination of wind speed and grain size distribution. Next, the relationship between dust emissions and wind speed is explored.

Resident fine grains in the interdunes

All interdunes sampled contained resident fine material (<62.5 μm). Grains under 62.5 μm are a key component of dust and having resident material under this size indicates that if the dunes become de-vegetated fine grains should be available to be eroded by the wind. This release of the fine grains once saltation has been initiated has been suggested as a form of dust emission from sand dunes and represents the initial entrainment of sediment before abrasion-produced fine sediment begin to dominate the dust flux (Bullard et al., 2004; Sweeney et al., 2023). The presence of a < 62.5 μm component indicates that the system is not supply-limited in terms of dust emission potential.

Low overall wind speed

Overall, the recorded wind speeds were below thresholds for dust emission compared to other dust producing regions (Allen et al., 2013; Wiggs et al., 2022; Yang et al., 2012). Whilst examining dust emissions at Etosha Pan in Namibia, Wiggs et al. (2022) placed

the modal threshold for erosion (U_t) at 7.25 m s^{-1}. When examining the 2-minute meteorological station wind data recorded in the current study, this threshold was only exceeded in three wind events (16/09/22, 24/09/22, and 29/09/22) and was not sustained for a period longer than 6 minutes. Similarly, in the highly emissive paleolake beds of the central Sahara, Allen et al. (2013) placed the U_t at 8 m s^{-1} which again is higher than the wind speeds recorded by the meteorological station during our measuring period. Yang et al. (2012) investigated dust emissions from an interdune in the Taklimakan Desert using a piezoelectric saltation sensor (Sensit) to calculate an average U_t of 7 m s^{-1}. Due to the low wind speeds during the recording period of this study, it is unlikely that dust emissions would have been observed apart from on 29/09/22.

By contextualising the September 2022 meteorological station data with the 24-year record from ERA5-Land data, it is evident that September is not the windiest month of the year. On average maximum wind speeds are higher in October, November, December, and January. In these months maximum wind gusts frequently exceed 7 m s^{-1}, subsequently the wind speeds in these months may exceed thresholds for erosion and dust may be emitted from the interdune locations. On the 29/09/22 there was an increase in aerosol concentration and concurrent increase in wind speed, which remained above 6 m s^{-1} for 66 minutes and peaked at 7.41 m s^{-1} in the 2-minute recordings. During this event, the recorded increase in aerosol concentration peaked at 0.078 mg m^{-3} and remained above background levels for 14 hours. This increase may

have been the local mobilisation of dust. However, without a camera trap it is not possible to confirm if the increase in PM_{10} recorded by the DustTrak was the local emission of dust, allochthonous aerosol advected across the plot, or the local remobilisation of burned debris. The removal of burned debris was recorded at the plot during the DustTrak monitoring period (discussed below; Figure 7.7). Due to the low correlation between wind speed and dust emission (R^2 = 0.036 and 0.029 at K01 and K02 respectively; Figure S1) and lack of confirmed dust events, thresholds for dust emission were not calculated in this study.

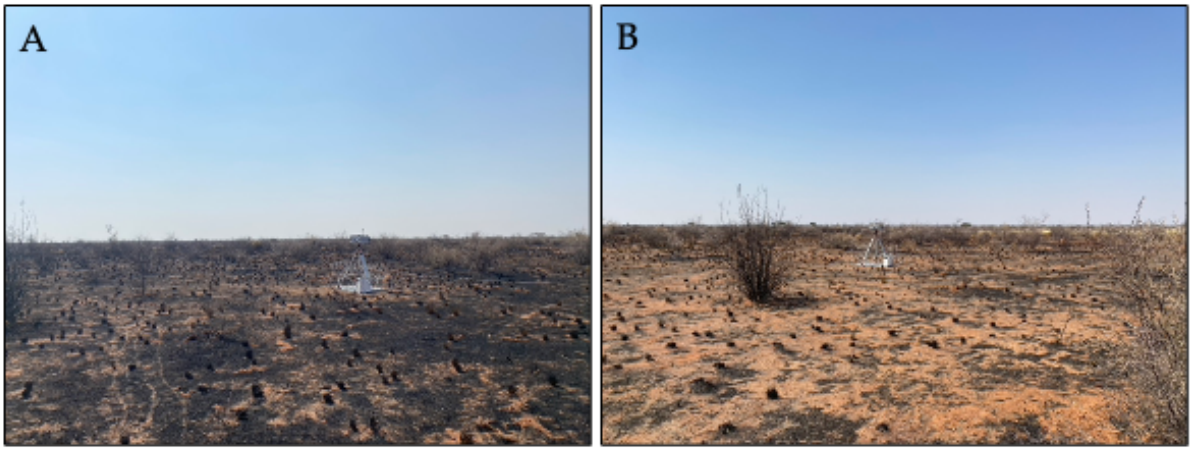

Figure 7.7. Burned plot K01 with the DustTrak (A) three days after burning at the start of the recording period and (B) 32 days after burning before recording ended. In image (A), the surface is largely covered by burned debris and some burned grass stubble. Much of this burned debris had been translocated by the time image B was taken.

No definitive emissions recorded

A coarsening of the surface grain size between control to burned surfaces could be indicative of dust emissions from the plots, removing finer components. No statistically significant difference between the co-located surfaces were measured. In

its unburned state, the Kalahari is an availability limited system as vegetation and biocrusts prevents sediment from being available to be eroded by the wind. When vegetation is removed through burning, deflatable sediment becomes available. The system should switch to become supply limited as there is no recharge of fine grains in the southwest Kalahari dunes unlike areas that have fluvial inflows. Thus, dust sized particles from the dune field should be depleted as the surface is eroded (Bhattachan et al., 2012; Li et al., 2009) and there should be a reduction in fine grains at the burned plot compared to control plots. There was no consistent coarsening in grain size found in the study sites, even in plots which were older. Therefore, it is unlikely that dust has been emitted from the dunes post-fire, even though there is fine material available for erosion.

The relationship between wind speed and aerosol concentration was not strong (Figure S1). Only four events showed distinct increases in aerosol concentrations with an increase in wind power which suggests some form of local emission, but whether this is dust or remobilised burned debris is unknown. Within these four events PM_{10} concentrations remained below previously defined dust concentration thresholds for emission events (Bergametti et al., 2022; Leys et al., 2011; Wang et al., 2008; Wiggs et al., 2022), although threshold concentrations from these studies vary with time averaging. Furthermore, there were four events (24/09/22, 25/09/22, 16/09/22, 15/09/22) where 2-minute wind speeds surpassed 7 m s^{-1} but there were no recorded increases in aerosol concentrations. The breakdown in this relationship between wind speed

and aerosol concentration indicates that other factors are limiting the availability of sediment for erosion. The data suggests that this is not due to a lack of fine material available, instead other factors such as biological soil crusts or surface cover play an important role in suppressing dust emission post-fire in the region.

7.5.2 Are there post-fire erodibility controls on emission?

The duration that a surface can emit dust post fire is inherently linked to the duration of reduced surface cover. Immediately after fire there is a high surface cover due to the production of burned debris. This material is then eroded away (Figure 7.7), most likely by the wind, until 2 months after fire when there is low surface cover. Therefore, in the immediate post fire window, emission of dust may be low. The immediate post-fire period was the same time in which the meteorological and DustTrak stations were monitoring and are an explanation for why (a) there were few instances of increased aerosols recorded and (b) we cannot be certain any aerosol concentration increases were dust emissions but instead could have been the local remobilisation of the burned debris. The photographs of the DustTrak station at the burned K01 plot in Figure 7.6 are evidence that there is remobilisation of this material during the post-fire stage.

Once the burned material has been blown away, the duration in which dust can be emitted is linked to the vegetation regrowth. This regrowth is linked to larger climate cycles which provide moisture to the region (Smit et al., 2024). The ground cover

measurements made in 2023 under drought conditions, show that the burned surfaces are less resilient to drought conditions than unburned surfaces, with plots remaining under 25% surface cover during the drought – regardless of time since fire. There have been very few studies into the response of dune systems to fire and how long the de-vegetated states persist, particularly in relation to levels below which aeolian erosion can occur. Previous work in the southwest Kalahari by Wiggs et al. (1994) found that increased sand activity occurred for five years post burn. In the Great Victoria Desert dune system in Australia, Levin et al. (2012) found that effective vegetation cover returns within one to five years post-fire whilst full recovery occurs within 25 - 30 years. Further, in the Simpson Desert in Australia, dust emission was observed from fire scars 27 months after burning (Bullard et al., 2008; McGowan and Clark, 2008). Bullard et al. (2008) attributed the combination of fire and drought to the causation of the dust event. The data from the current study strongly suggest that dunes recovery is strongly impacted by larger climate regimes, with burned dune surface cover being more vulnerable to drought than unburned surfaces.

During the post-fire low-surface cover period, biological soil crusts likely play a large role in limiting dust emissions. Our data show that biocrusts were found in all of the burned interdune plots, which indicates that biocrusts are able to survive fire and afford protective effects to the surface. The post-fire presence of biocrusts means that even though cover provided by grasses and shrubs is limited, sediment is still not available to be eroded as it is bound together in biological soil crusts. Previous studies

have found that even at low coverage biocrusts can reduce wind erosion in sandy deserts (Belnap and Gillette, 1998, 1997; Zhang et al., 2006, 2008). For example, in the Gurbantunggut Desert in China, Zhang et al. (2006) found a reduction in wind erosion with as little as 20% biocrust surface cover. As biocrusts are present in the Kalahari, it is likely that the crust is reducing the emission of dust too. Globally, there is no consensus on the fate of biocrusts after fire (Palmer et al., 2020), with recorded increases in cover post-fire in the Columbia Basin (Dettweiler-Robinson et al., 2013) and Oregon (Bowker et al., 2004), and decreases in cover in Utah (Evangelista et al., 2004) and Australia (Strong et al., 2010). The data presented in this study show that in the Kalahari, biocrust are withstanding burning and continue to provide protection to the surface.

In general, biocrusts are vulnerable to climate and land use change (Maestre et al., 2015). A modelling study by Rodríguez-Caballero et al. (2022a), showed that until 2070 there will be an ~25 to 40% dieback in biocrust representing and ~5 to 15% increase in global dust emissions. This model was generated using data from nine sites, none of which were in southern Africa and other research has suggested that biocrust response may be more nuanced (Couradeau et al., 2016; Delgado-Baquerizo et al., 2014; Raanan et al., 2016; Rodríguez-Caballero et al., 2022a). For example, in the Negev Desert Raanan et al. (2016) found that some species that contribute to biocrusts are more tolerant to desiccation than others and, as a result, the species composition may shift in response to changing environments. In the Kalahari, biocrusts possess a quick

recovery rate post-disturbance (Elliott et al., 2014; Thomas and Dougill, 2007). Data from the current study suggest that biocrusts survive fire but mortality may increase should a fire be followed by intense drought or higher grazing pressure. The increased mortality of biocrusts was observed at the burned K09 plot which was measured 6 months after burning. At the plot, there was evidence of scoured biocrusts (Figure 7.8) which indicated that the protective effect of the crust survived the initial fire but then was abraded by saltating grains as a result of the slow vegetation recovery during the drought period after the fire.

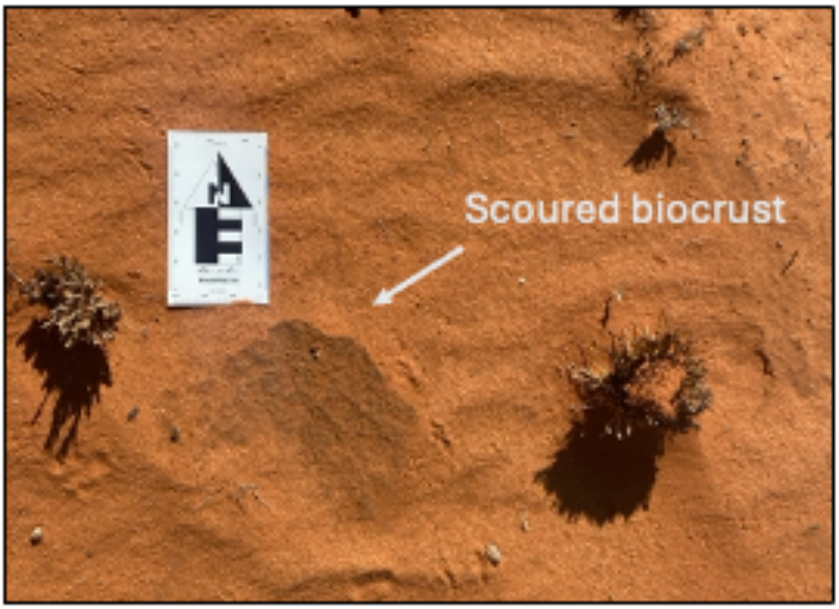

Figure 7.8. Evidence of scouring of biological soil crust at the burned K09 plot.

Surface moisture is another factor that can impact the erodibility of the surface and was not measured during this study. However, soil hydrophobicity was measured, as this phenomenon has been linked to increased rates of soil erosion in other non-dune desert landscapes after fire (Ravi et al., 2012, 2009b). A water drop penetration time

(WDPT) test was carried out, where the time a drop of water remained on the surface was recorded. At all plots measured in 2023 this was conducted 20 times; all measurements were 0 seconds, indicating no soil hydrophobicity. The lack of evidence for soil hydrophobicity, indicated that the volatilised grasses though burning are not transported into the soil and do not envelope the grains. The lack of post-fire soil hydrophobicity is also evidence that the fires in the region burn cool and do not transfer much heat into the ground (Lentile et al., 2006). This offers an explanation as to why the biocrusts are not killed by burning in the southwest Kalahari dune system.

7.6 Conclusions

Previous research suggests that the southwest Kalahari dune landscape should emit dust when de-vegetated (Bhattachan et al., 2022, 2013, 2012), but no dust emissions have been linked to the landscape post-fire. This study aimed to examine why does the southwest Kalahari dune field not produce dust after burning. The findings from this research suggest that there is little emission of dust, despite the lack of vegetation, fine grains, and a few above threshold wind events post-fire.

The results show that the Kalahari does have fine grains within all interdune plots recorded, up to a maximum of a 29.97%, under 62.5 μm, a grain size that is frequently used to denote dust (Sweeney et al., 2023). Disturbance events, such as fire, remove protection afforded to the surface by vegetation which makes large portions of the surface available to be eroded by the wind. The wind speeds recorded in this study

provide a snapshot of the wind regime in the area and show that in the recording month, September 2022, overall wind speed was low compared to other dusty regions of the world, though high for the Kalahari. The limited occurrence of strong winds offers an explanation as to why no dust events were recorded. However, there were four high wind speed events where there were no increases in aerosol concentration. These 'high wind speed but no emission' events alongside the low concentrations of aerosol when there were concurrent wind and aerosol events mean that there may be other factors controlling emission in the southwest Kalahari. The reduction in burned debris indicates that the increases in aerosols recorded cannot be explicitly linked to the emission of mineral dust. Instead, we suggest they could be the local remobilisation of burned material.

The finding of no emissions alongside high wind speeds required the examination of erodibility factors at the plots, including surface crusting and burned debris cover. High burned debris cover was found after fire, limiting the amount of surface available to be eroded by the wind. Biocrusts were recorded at 100% of burned interdune plots, affording protection to the surface for the duration of the reduced vegetation period post-fire. Subsequently, sediment is not available to be eroded by the wind after fire and explains why post-fire emissions are not observed from the landscape. However, evidence has shown that biocrusts are vulnerable to climate and land use change (Rodríguez-Caballero et al., 2022b) should the biocrusts die-back due

to changing environmental conditions, the fine grains found in the interdunes may become available to be eroded by the wind.

The findings from this study are not contrary to the work of Bhattachan et al. (2012). The abundance of resident fine-grains in the dunes indicates that dust should occur when the surface is de-vegetated. However, the importance of wind speed and biological soil crusts should not be overlooked. The Kalahari is predicted to get hotter and drier into the future, with changing patterns in precipitation (Attwood et al., 2024; Dunning et al., 2018; Engelbrecht et al., 2015). This may lead to the dieback of both vegetation and biocrusts (Lawal et al., 2019; Rodríguez-Caballero et al., 2022b) and hence increase the potential for dust emission. Yet, there is no predicted increase in wind speed (Fant et al., 2016; IPCC, 2023) and so the system would be limited to rare above-threshold wind events, when the resident fines would quickly be exhausted. Future work should establish longer term monitoring of post-fire wind and aerosol concentrations in the region. Additionally, further quantification of the role of biocrusts in preventing dust emissions is needed in the Kalahari dune field.

Chapter 8 - Discussion

An 11-month-old fire scar border in the Namibian Kalahari, with the left unburned and the right burned.

8.1 Introduction

The research presented in this thesis provides an evidence base towards understanding the relationship between fire and potential dust emissions from the southwest Kalahari linear dune system. In doing so, the research has focused on three research questions (RSQ):

RSQ1: What is the pattern, frequency, and timing of fire in the Kalahari dune landscape?

RSQ2: Does fire affect dust emission potential?

RSQ3: What is the impact of fire on dune surface properties in relation to the potential emission of dust?

The first part of this discussion chapter will assess how each of these questions have been answered. From answering the research questions, four cross-cutting themes have emerged (Figure 8.1):

1. The window of dust emission opportunity
2. Biological soil crust effect on dust emissions
3. The impact of dune morphological unit on fire spread and dust emissions
4. The impact of drought and human activity on surface erodibility

with the second part of the chapter considering these themes. The cross-cutting themes help address the overall aim of thesis - *to investigate if the Kalahari dunes emit dust after disturbance by burning* - as well as discuss the implication of the thesis findings in the context of the wider literature and consider some potential avenues for future research.

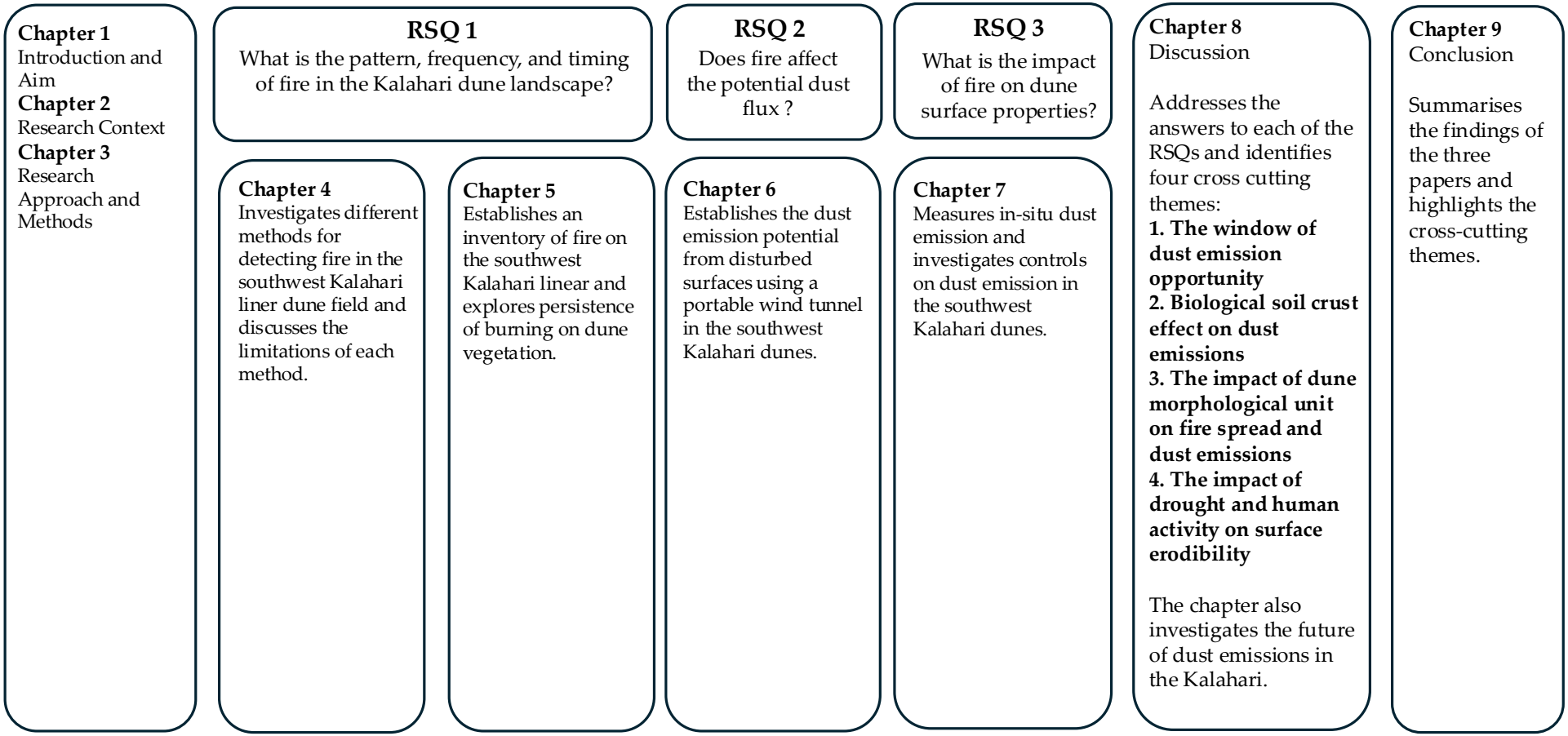

Figure 8.1. A schematic showing the organisation of the thesis and the four emerging themes. Developed with reference to Richards, (2020).

RSQ 1: What is the pattern, frequency, and timing of fire in the Kalahari dune landscape?

Chapter 5 used space-based methods to present a 24-year inventory of fire in the southwest Kalahari dune field. The chapter answers RSQ1, finding that fire frequently occurs in the southwest Kalahari dune field with 13,310 km^2 (11.1% of the dune field) burning in 240 separate fire events. These fires are regularly timed at the end of the dry season (September to January). Furthermore, fires occur most regularly during or one year after La Niña conditions which provides moisture for biomass buildup. Land use is a key factor which determines both spatial and temporal patterns of fire, with burning occurring more frequently and over smaller areas in primarily privately owned land. The Kgalagadi National Park, which comprises 11.4% of the study area, represents a more 'natural' fire regime for the region due to the Park policy of allowing fires to burn to their fullest extent (Spies et al., 2016). Resultingly 65.8% of the Park in the study area burned from 2000 - 2023. Reburn time is also influenced by land use, with burned land reburning more frequently in the National Park. Previous studies have placed the reburn time in the region to be approximately 11 years (Spies et al., 2016) whereas, the results of the inventory suggest that if a site is to reburn it does so quicker than 11 years. For example, 66% of cells that reburned did so under ten years since the first burn. However, only 17.6% of the pixels burned over multiple incidences, indicating that not all land reburns regularly. The implications highlight how the arid Kalahari linear dune field is neglected in burned area studies but burns

regularly. Yet the temporal and spatial disturbance effect of the fire is limited by anthropogenic modulation of the fire regime and rapid vegetation recovery post-burn.

RSQ2: Does fire affect the potential dust flux?

Research considered in Chapter 6 in this thesis used a portable wind tunnel and sediment size distributions to assess the ability of the southwest Kalahari dunes to emit dust and if there are changes in dust emission threshold and flux after burning. Sediment finer than 62.5 μm was present at most sites tested. There was however no significant reduction in grain size between the control and burned plots, suggesting that there is no loss of fines from wind erosion post-fire. Further, there was no significant difference in the flux of dust between the burned and unburned control plots, but significantly higher thresholds for erosion on the burned plot. Therefore, higher wind velocities are needed to move dust-sized sediment on burned land, but once the sediment begins to move, the amount emitted remains similar (around 0.2 mg $m^{-2} s^{-1}$). Thus, fire alone does not affect the dust flux. The data strongly suggest that even when devoid of vegetation, the Kalahari linear dune system is fine sediment-availability limited.

An additional finding from this study is the identification of the role that different surface disturbances may play in dust emission. Surfaces which were mechanically disturbed by the top 2 cm of sediment being removed alongside any biological soil crusts had significantly larger fluxes of dust (1.105 mg $m^{-2} s^{-1}$) than the undisturbed

(0.281 mg m^{-2} s^{-1}) and fire disturbed (0.190 mg m^{-2} s^{-1}) surfaces. These finding display that the Kalahari does have the potential to emit dust, if some event (such as droughts or grazing) removes biocrusts or disturbs the surface.

RSQ3: What is the impact of fire on dune surface properties?

Chapter 7 addressed research question three, finding that fire has varying effects on dune surface properties. To assess the amount of bare surface available to be eroded by the wind, surface cover (which is primarily impacted by vegetation) was measured along transects. The results indicate that the opportunity for dust to be emitted post-fire is short and linked to burned debris cover and vegetation regrowth. Initially after fire the surface has high cover (> 50%) of burned debris, which prevents the wind from reaching the surface. The burned debris is eroded away around two months after fire, leaving a low surface cover and large amounts of the surface available to be eroded by the wind. The duration of this reduced cover is complex and relies on rainfall following the fire, burned surfaces are less resilient to drought than unburned surfaces regardless of time since fire.

To characterise dune surface sedimentological properties, grain size distributions were determined and hydrophobicity tests run. All characteristics displayed no significant difference between the burned and unburned control plots. If sediment was being eroded in the form of dust, there would be preferential removal of fine grains in the burned plot. However, even though there was a coarsening of sediment

in the burned plots, it was marginal, indicating that large quantities of dust are not being emitted from the burned sites. The highest proportion of fine material is found in the interdune areas, yet all burned interdunes had evidence of biocrust presence. The biocrusts increase the cohesivity of the surface, ensnaring the grains, and decrease the erodibility of the surface.

Despite high wind speeds (> 7 m s^{-1}) being measured at sites K01 and K02 during the two-month monitoring period after fire, there were no large increases in aerosol concentrations at the sites. This finding indicates that dust emission at the site is not limited by the wind, instead other factors supress erosion. These limiting factors are likely high burned debris cover immediately (two months) after fire, biological soil crusts when the surface cover is low (between two months and significant precipitation), and then vegetation cover from then onwards.

8.2 Cross-cutting themes

The findings outlined above address each of the overarching research questions of this thesis and in addition four cross-cutting themes have emerged across all the research questions. These themes highlight common findings and address the aim of the thesis - *if Kalahari dunes emit dust after a burning disturbance.* The four themes are:

1. The window of dust emission opportunity
2. Biological soil crust effect on dust emissions
3. The impact of dune morphological unit on fire spread and dust emissions
4. The impact of drought and human activity on surface erodibility

8.2.1 THEME 1 – The window of dust emission opportunity

The Kalahari dune ecosystem is resilient to fires, as the vegetation is adapted to quickly regrow after burning (Gillespie et al., 2024). The persistence of fire as a geomorphic agent of disturbance is constrained by the duration of reduced vegetation cover. Therefore, it is crucial to quantify the period of reduced cover in which aeolian erosion can occur. In this thesis surface cover was quantified in two ways, through satellite derived Soil-Adjusted Total Vegetation Index (SATVI) and ground measurements of surface coverage. Both methods found that vegetation recovers faster than previously thought and highly influenced by broader climate conditions. The SATVI results tracking 17 fires over a 24-year (2000-2023) period showed that fires dropped below the 14% effective cover threshold for just 112 (±16) days (around four months). Whereas the ground cover results found that vegetation can recover within ten months (~ 304 days) post-fire. But surfaces which had previously burned are much less resilient to drought conditions that unburned sites. This increased vulnerability is evidenced through all burned sites dropping below 25% cover in the dry year of 2023, whereas most unburned control plots remained above 25%. Therefore, the temporal window for dust emission opportunity is both short *and* discontinuous, bookended by high burned debris surface cover and live vegetation cover (which relies on precipitation). The results from this thesis show that in the southwest Kalahari, fire disturbance is not great enough to cause of long-term reactivation (or an alternative stable state) as vegetation regrew at all sites. Burned vegetated dunes vulnerability to drought has previously been observed in the Simpson Desert in Australia, where

Bullard et al. (2008) attributed the combination of both fire and below average rainfall as factors that lead to an 87,500 km^2 dust emission event in 2003.

This thesis substantiates work that highlights that post-fire dust emissions do not occur for a continuous window after fire. For example, dust emissions were measured after the Jefferson Fire in the USA by Wagenbrenner et al. (2013). At this site, dust emission was observed from the fire scar after snowmelt, displaying a discontinuous emission window, as emission ceased for the three months the surface was covered in snow (Wagenbrenner et al., 2013). Whilst snow cover is not a factor in the Kalahari, another form of discontinuity in the potential to emit dust found is the combination of fire, partial recovery, and then drought. At sites K04 and K06, annual grasses had regrown and prevented surface erosion in the ten and 21 months respectively since fire. But low precipitation after the subsequent year reduced vegetation cover. Subsequently, measurements of the longevity of the impact of fire on the surface should take this discontinuous recovery period into account when calculating future dust risk from burned areas.

An important finding from this thesis, is that not all fires are significant enough to reduce surface cover to levels where resultant aeolian activity has been observed. Both methods used in this thesis found that not all sites dropped below the 14% effective cover threshold, with four out of the 17 measured SATVI sites and site K03 on the ground cover surveys remaining above 14%. This is a significant finding; fire is not a

significant enough disturber to enable surface cover to drop below the threshold for aeolian activity at all the burned sites. For a few fire scars where surface cover remains above 14% the surface is still availability limited due to high cover.

Defining thresholds of surface cover below which wind erosion has occurred has long been an area of research interest. By identifying a simple numeric cover below which aeolian activity can occur there is easy input into predictions of erosion events and models. This study uses 14% cover identified in the Kalahari by Wiggs et al. (1995). Yet, there are multiple factors that impact the ability of the surface to emit dust. Using simple percentage cover does not account for vegetation porosity, phenological changes, and structure, or the spatially heterogeneous impact of vegetation on erosion thresholds (Mayaud and Webb, 2017). Further, there are many small changes in vegetation dynamics that are hard to account for in both the ground surveys and using remote sensing. Vegetation is frequently not fully incinerated at the study sites (Figures 6.7, 7.7, 7.10, 8.2 and 8.3), and therefore still act as a form of surface roughness. Sub-daily changes in burned vegetation structure as vegetation regrows results in dynamic levels of roughness at the burned sites which is difficult to parameterise. Future work should investigate how the burned stubble impacts the aerodynamic roughness, potentially using methods such as Terrestrial Laser Scanning.

Figure 8.2. Vegetation regrowing at site K02 two months after burning. The regrowth is primarily from burned stubble. As vegetation regrows there are dynamic levels of surface roughness.

Wiggs et al. (1995) highlighted how litter cover in the Kalahari is much more important at protecting the surface from wind erosion than rooted vegetation. The results from this thesis support this finding. After fire, burned debris (litter) leaves a high surface coverage as found at sites K01 and K02. The in-situ monitoring of aerosol concentrations at the burned sites were recording during this period of when the surfaces had high burned litter coverage and little dust was recorded despite strong winds over 7 m s^{-1}. This finding has important implications, as the one remote-sensing global study to date of measured dust from fire scars (Yu and Ginoux, 2022) only

records for two months post-fire. Findings from this thesis show that in the two months after fire, the Kalahari still has high surface coverage in the form of burned debris (Figure 8.3). Wind cannot reach the surface during this time of high burned debris cover. Thus, increase in aerosols measured in the region, both by Yu and Ginoux (2022) and the in-situ DustTrak monitor used in this thesis, are likely not recording mineral dust emission events, but increase remobilised burned material (or ash). Subsequently, the southwest Kalahari dune field is not properly represented in terms of its post-fire dust potential in the Yu and Ginoux (2022) study. Longer term (more than five years) monitoring of fire scar site is recommended for future research.

Figure 8.3. High burned litter cover at site K01 three days after burning.

Due to the burned litter being darker than the surface sediment, it can be tracked using remote sensing. Dintwe et al. (2017) investigated post-fire albedo change in the whole of sub-Saharan Africa (SSA) and found that there was a large decrease in albedo post-fire. These changes in albedo persist for around 140 days (Dintwe et al., 2017). Yet, in a Kalahari focused study, Saha et al (2019) found that the initial post-fire darkening lasted for an average of 31 days before sediment was removed from the surface. The period of darkened albedo indicates the period where surface erosion is limited by burned debris. The difference between the whole-SSA and the Kalahari study highlights how difference processes are dominant in different regions and emphasises the important of spatial scale in remote sensing studies. In the Kalahari, burned debris is moved by being washed or blown away post-fire (as was observed at K01 and K02 field sites), where in other SSA ecosystems the darkened burn scar persists for longer (Dintwe et al., 2017). Regional differences further complicate any calculation of the temporal window of dust emission using remote sensing. Future calculations need to ensure the incorporation of localised albedo changes to find when the surface is bare after the burned litter is removed and vegetation indices to calculate plant-induced roughness limitations on sediment transport potential post-fire.

8.2.2 THEME 2 – Biological soil crusts effect on dust emissions

Fine-grain surface availability limitation can result from several factors, including the 'baking' of the ground surface during burning, infiltration induced sediment sorting, or biological soil crusts (biocrusts or BSCs) that bind sediments together. Several

studies have indicated that surface sediments may undergo thermal alteration or 'baking' following fire (Stavi et al., 2017; Agbeshie et al., 2022). This response is attributed to the presence of finer grain fractions in surface sediments, which are more susceptible to structural disruption and cementation at lower combustion temperatures (Agbeshie et al., 2022). However, this phenomenon remains insufficiently investigated in sandy soil systems. The possible 'baking' of the surface also explains the burned plot higher threshold friction velocity found in Chapter 6.

Similarly, infiltration-driven vertical grain-size sorting occurs in sandy soils, where finer grains accumulate deeper in the sediment profile could account for the higher dust fluxes with mechanistic disturbance (Lei et al., 2017b, a). Again, these processes are insufficiently investigated in sandy soil systems.

Alternatively, biocrusts are widespread throughout the Kalahari and were frequently observed in the study area but it was often hard to differentiate between a crusted and un-crusted surface. In this thesis we attribute biocrust survival of fire as the main factor which is limiting dust emissions in the region. The importance of biological soil crusts (biocrusts) in preventing wind erosion from bare soils is becoming increasingly understood (Bullard et al., 2022; Elliott et al., 2019; Rodríguez-Caballero et al., 2022b; Thomas and Dougill, 2007). Findings from this thesis support that these communities of bacteria and algae are integral in preventing dust emissions in the Kalahari. The evidence for the role of biocrusts in suppressing emissions in this thesis include:

biocrusts were identified at 88% of sites and when the top 2 cm of the surface had been removed there was significantly different dust flux potential from the undisturbed surfaces. The filamentous sheaths and glue-like substance that biocrusts secrete to create a three-dimensional matrix which binds individual grains together (Figure 8.4), creating a more cohesive surface that is stronger and more resistant to erosion (reduction in flux).

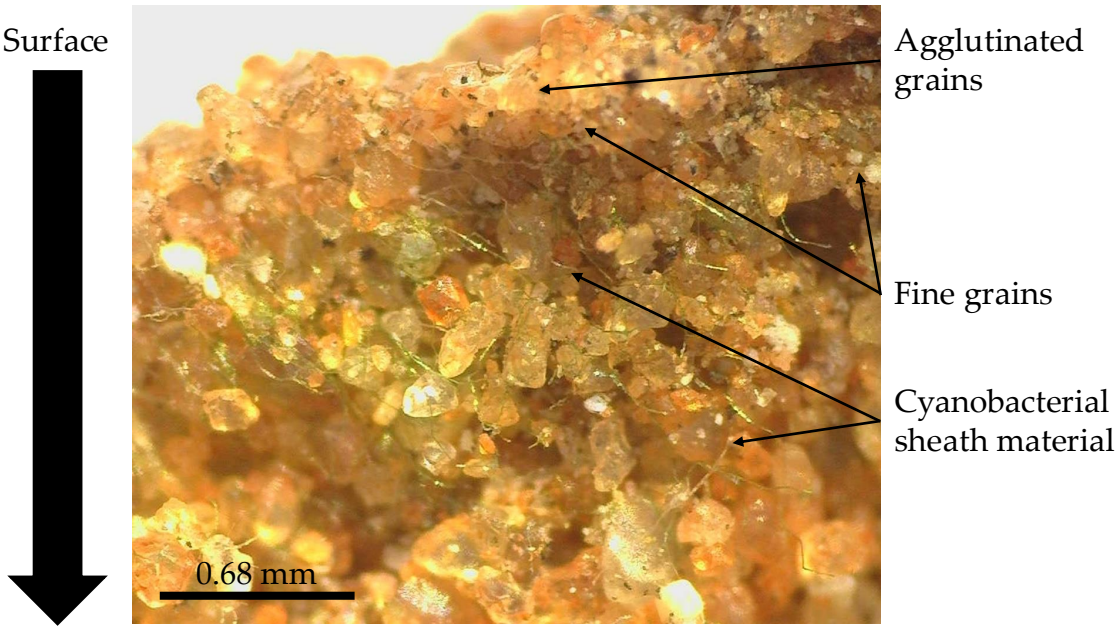

Figure 8.4. Field microscopy of a cross-section of biological soil crust from site K11.

Findings from this thesis suggest that the protective effects of biocrusts survive fire and continue to protect the surface. Survival of biocrust after fire is determined by the type and composition of the biological soil crust (Palmer et al., 2020; Pressler et al., 2019). Taxonomic analyses suggest that the biocrusts are dominated by cyanobacteria in the Kalahari (Thomas and Dougill, 2006). Cyanobacteria has been found to have high mortality post-fire, with reduction in cover observed in Australia (Strong et al.,

2010) and Utah, USA (Aanderud et al., 2019). Aanderud et al. (2019) found however that two months after fire, some crusts remained attached, and upon returning to the same site one year after fire found that only bare ground existed. The authors attributed this loss of protective biocrust to wind erosion (Aanderud et al., 2019). The Utah findings, match outcomes from this thesis, some biocrust communities may still provide surface protection after fire. The continued protection may be due to fires burning relatively 'cold' (i.e., the quickly combustible material does not transfer much heat into the surface) in the Kalahari. The lack of heat transfer to the surface may increase biocrust survival after burning. This thesis presents the first measurements of biocrusts and fire in the Kalahari. Future research can focus on investigating the relationship between mortality of biocrusts and their immediate protective effects at a global scale. A further timeline of biocrust regrowth should be established to quantify how quickly living biocrusts recolonise a surface after fire in the Kalahari.

The biocrust survival post-fire was not consistent at each site, with difficulties in detecting biocrusts (discussed below) limiting the ability to fully conclude biocrust coverage. Evidence of both biocrust survival and destruction post-fire was evident at site K09 (Figure 8.5). This grazed farm site was visited in 2023 during a drought and biocrust coverage was discontinuous in the unburned area, with some evidence of type 1 crusts. The burned plots had lots of evidence aeolian activity with scoured vegetation with exposed roots and ripples visible in the interdune (Figure 8.5). The burned interdune plot K09 showed signs of biological soil crust and survival and

erosion: in Figure 8.5 a crescent shaped section of biocrust contrasts starkly from the bare sediment around it. The crescent shape of the biocrust, in line with the ripples, indicates that the crust has been eroded, most likely through abrading sand grains. But the patch of biocrust that is still covering the surface provides some form of protection and indicates that the fire did not lead to complete crust mortality, but the subsequent wind erosion has abraded away surrounding crust, similar to findings by Aanderud et al. (2019). This example highlights the complexity of processes occurring post-fire in the Kalahari, the biocrust survived the initial burn event, but was unable to survive the subsequent aeolian abrasion.

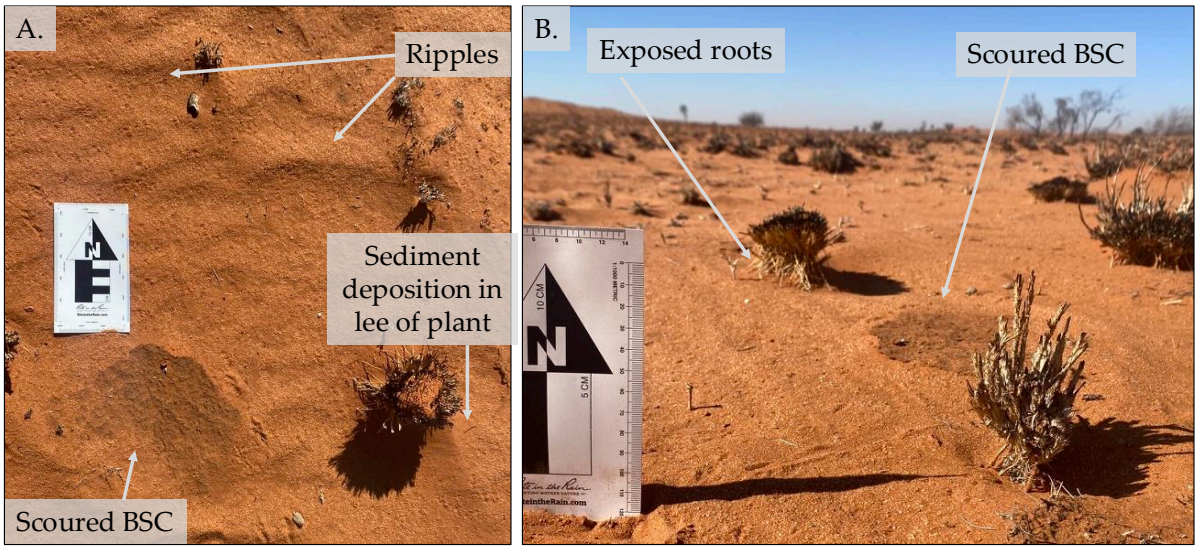

Figure 8.5. An example of eroded biological soil crust identified at site K09. (A) is from the birds-eye view whereas (B) from a low-angle. Evidence of aeolian erosion is highlighted.

The delineation of biocrust presence in this study was binary and did not calculate the percent biocrust cover. The determination of biocrusts is difficult using either ground

or space-based methods. The sediment profile trenches revealed biocrusts at 88% of the sites, but most crusts at the sites were type 1 (70%) with no discolouration and there was difficulty identifying the crusts without disturbing the surface (i.e., digging the sediment trench) to confirm their presence.

Space-based spectral indices also struggle to determine biocrust from the surface of drylands. The popular index the Biological Soil Crust Index (BSCI) - from which Levin et al. (2012) concluded mass biocrust mortality after fire in the Great Victoria Desert dune fields of Australia - struggles to differentiate at the ecosystem scale between bare ground and biocrust. The BSCI is also formed for detecting lichen-dominated biocrusts and struggles with cyanobacteria dominated biocrusts found in the Kalahari. Due to this lack of ability to accurately detect biocrust cover, the BSCI method was not used in this study. Rodríguez-Caballero et al. (2017) concluded that biocrusts are more correctly mapped using hyperspectral data as opposed to the multispectral BSCI. Several attempts to establish biocrust coverage using multispectral data were employed over the course of this thesis but did not yield substantive results. The failure of these experiments resulted from most the biocrusts being measured not photosynthesising after wetting and therefore not producing the spectral 'fingerprint' which identifies them and equipment error. Future work should investigate biocrust spectra in the Kalahari and response to wetting.

8.2.3 THEME 3 – The impact of dune morphological units on fire spread and dust emissions

This thesis provides a novel insight into burn dynamics (spatial extent, duration, and timing) on dunes in the southwest Kalahari. Presently, there has been little research into fires in the southwest Kalahari dune field both from an ecological or geomorphological perspective. Studies on fire in the Kalahari tend to encompass more northern or eastern regions without linear dune landscapes (Gillespie et al., 2024; Heinl et al., 2007; Holdo, 2005; Masunga et al., 2013; Nghalipo et al., 2019; Nghalipo and Throop, 2021; Verlinden and Laamanen, 2006) or generalise for the whole Kalahari savanna (Saha et al., 2019). The dunes are a unique environment in which fire occurs due to discontinuous fuel loads, particularly the large bare interspaces on the dune crests which impact fire spread. For fire to breach these gaps in fuel, conditions must be such that flames can breach the bare interspace between vegetation patches and ignite adjacent patches (Burrows et al., 2009). Many of the digitised fire scars showed some evidence of the fire being bounded by the dune crest, with the unvegetated crests acting as a natural fire break (Figure 8.6). Future research can involve investigating the degree to which dune morphology impacts fire spread.

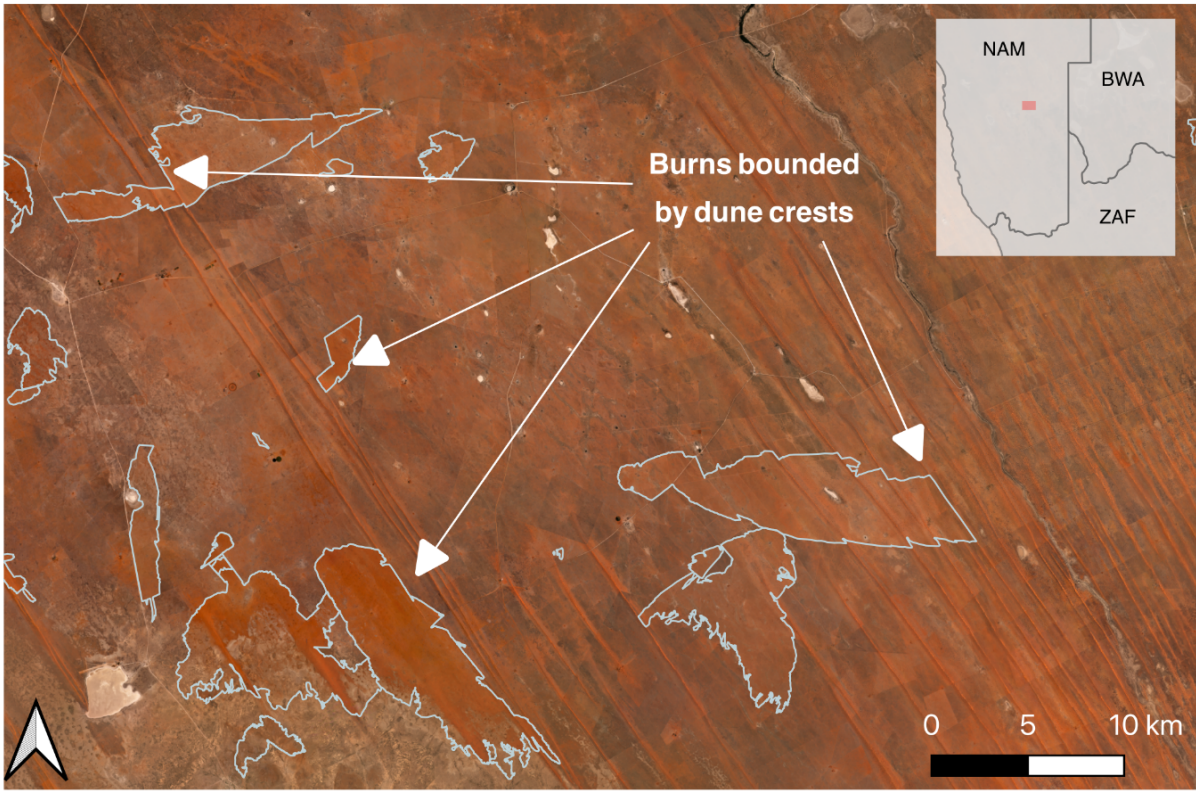

Figure 8.6. Fire scar perimeters where fire spread was limited by dune crests. Fire scar boundaries, outlined in white, were created through manual digitisation. Background image © 2022 Planet Labs PBC.

Examining the different morphological units of the dune is an integral part of establishing dust emissions from vegetated dune fields. This is due to complex factors that govern dust production on different parts of a dune. For example, the interdunes contain the finest sediment, but are not currently active because of high vegetation cover (Wiggs et al., 1995). Whereas the crests frequently have lower vegetation cover (Wiggs et al., 1995) and are more mobile, they also have the lowest proportion of fine material, making them less likely to emit dust. Therefore, when investigating the potential emissions from de-vegetated dune fields, emissions are often considered to be spatially discontinuous, and the crests of dunes are often discounted as being sources of dust due to these coarse grain sizes. For example, Bhattachan et al. (2012)

estimated the iron-in-dust potential for the Kalahari dune system if it was to become de-vegetated. This calculation excludes dune crests as being source areas (Bhattachan et al., 2012). Yet, for fire to breach the crest, the crest must be vegetated and when there is vegetation there is a build-up of fine material. Results from Chapter 6 of this thesis show that the vegetation state of the crest affects the grain size distribution, with more fine grains found on vegetated crests that burned. Crestal vegetation state also affects the emission flux potential and erosion threshold with burned crests recording higher potential flux and a higher threshold for erosion than unburned (and unvegetated) crests. Therefore, when estimating the potential emission from an entire vegetated dune system, dune morphological unit must be taken into consideration. The interdunes and flanks can emit the highest fluxes of dust, but the crest emits higher fluxes of dust (vegetated 0.467 mg m^{-2} s^{-1} and unvegetated 0.253 mg m^{-2} s^{-1}) when they are vegetated (and hence can burn). Consequently, results from this thesis suggest that rather than classifying the system by crest and interdune areas when predicting future dust emission flux from the Kalahari, a more nuanced approach of calculating first the proportion of vegetated crests may be more accurate.

8.2.4 THEME 4 – The impact of drought and human action on surface erodibility

A common theme throughout this thesis is the impact of other disturbance effects on the ability of the Kalahari dune field to emit dust after burning. Primarily, the other disturbance effects are humans and drought.

Land use impacts both fire occurrence (Chapter 5) and surface properties (Chapters 6 and 7). Fire has been shaped by humans in the Kalahari for the last 40,000 years, creating mosaics of burned and unburned areas (Velempini and Perkins, 2008). But practices of fire suppression are still enforced in many areas today where fire presents a risk to livelihoods and life (Humphrey et al., 2021). Subsequently, the current fire regime in the southwest Kalahari is impacted by land use and fire policies. Findings from Chapter 5 show that the primarily private land in the study area (where fires are actively suppressed; Humphrey et al., 2021) experience small and quick fires, whereas the National Park (where fires in the dry season are allowed to burn; Spies et al., 2016) experience infrequent fires, which burn for a long duration and over a large amount of land. These different fire management strategies impact the amount of area burned and therefore, the amount of land available to be eroded by the wind and the subsequent dust flux potential. The size of the burned area has particular importance in relation to the detection of dust emissions from space, with plumes from larger fires being easier to detect.

Land use also impacts surface properties, through altering biocrust coverage. Hoof action constantly disturbs the surface and biocrust cover is inversely related to grazing in the Kalahari (Elliott et al., 2024; Thomas and Dougill, 2007). The more developed biocrusts in the Park may be more resistant to wind erosion, but the use of the portable wind tunnel in the Park was not conducted in this study.

Drought is another common feature in the Kalahari system and is a large disturbance effect in particular relation to potential dust emissions. Drought was experienced from 2014 - 2020 and from 2023 – early 2025 in the study region (Smit et al., 2024; Southern African Development Community, 2024). During droughts there is extensive loss in standing biomass and herbaceous cover in the Kalahari (Figure 8.7; Smit et al., 2024), leaving large amounts of the surface bare and susceptible to wind erosion. Annual grasses (particularly *Schmidtia kalahariensis*) decrease in frequency during these below average rainfall periods (Smit et al., 2024). The effect of drought on vegetation cover was observed using space-based SATVI measurements and in the ground cover surveys at the site, both showing a large reduction in cover during dry periods. Significantly, the period of reduced vegetation cover calculated using SATVI was a similar duration (114 ± 16 days) as the fire disturbance. But drought acts upon the entire region unlike burned area and frequently impacts much larger portions of land. Therefore, drought has a similar effect as fire on vegetation cover, but a larger spatial extent. Subsequently, both fire and drought need to be considered when discussing dust emission potential from the southwest Kalahari.

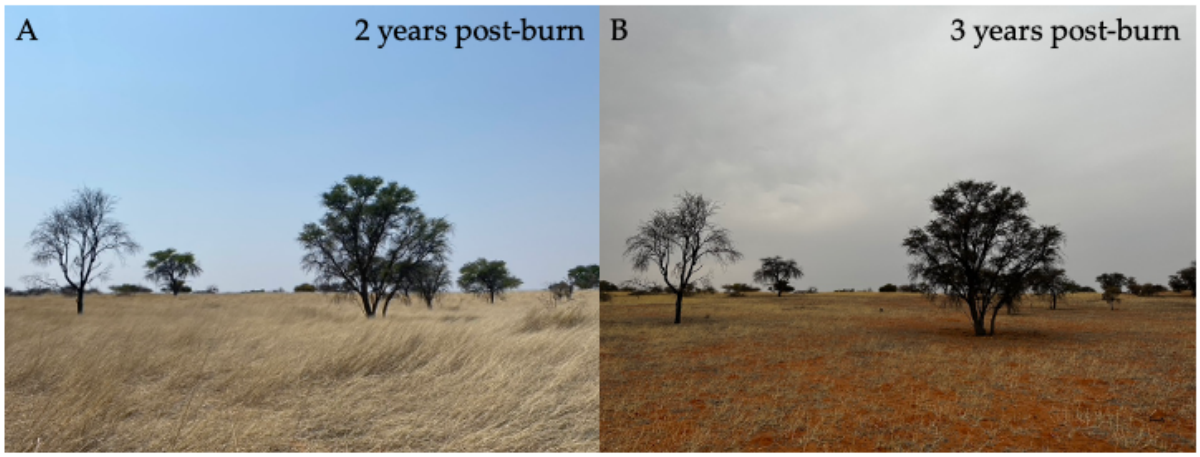

Figure 8.7. The impact of drought on above surface biomass. The images show the burned interdune plot at site K06 taken from the same spot (A) 2 years after fire in an above average rainfall season, and (B) 3 years after fire under drought conditions.

A four-year inventory of dust from the study region (09/2020 – 09/2024) using the Meteosat Second Generation - Spinning Enhanced Visible and Infrared Imager (MSG – SEVIRI) was conducted during the process of this thesis. Results found no plumes of dust originating from within fire scars. Yet, one dust event was observed with origins tracing back to within the dunes on the 07/07/2024 (Figure 8.6). The El Niño event of 2023/24 has brought severe drought to southern Africa, and there has been a reduction in vegetation cover (Southern African Development Community, 2024). Drought can induce mortality in biological soil crusts (Kidron et al., 2017; Thomas et al., 2022) and with only two wet years to recover after the previous droughts, coverage may not have fully reestablished. Dieback of biocrusts in the area may have contributed to the dust event observed in Figure 8.8. Although there is growing scientific interest in biocrusts, there is little information on the role that biocrusts have on supressing dust emissions in the southwest Kalahari and how southern African

assemblages of biocrusts respond to drought. This thesis provides the first evidence for dust emissions suppressed by biocrusts in southern Africa, showing that mechanically disturbed, un-crusted surface can emit dust fluxes up to 77 (CV 82.4%) times greater than bio-crusted surfaces. Understanding the role biocrusts (or lack of biocrusts) had in the 2024 large emission event in the southwest Kalahari, may provide crucial information over the future of Kalahari dust emissions under a warmer environment.

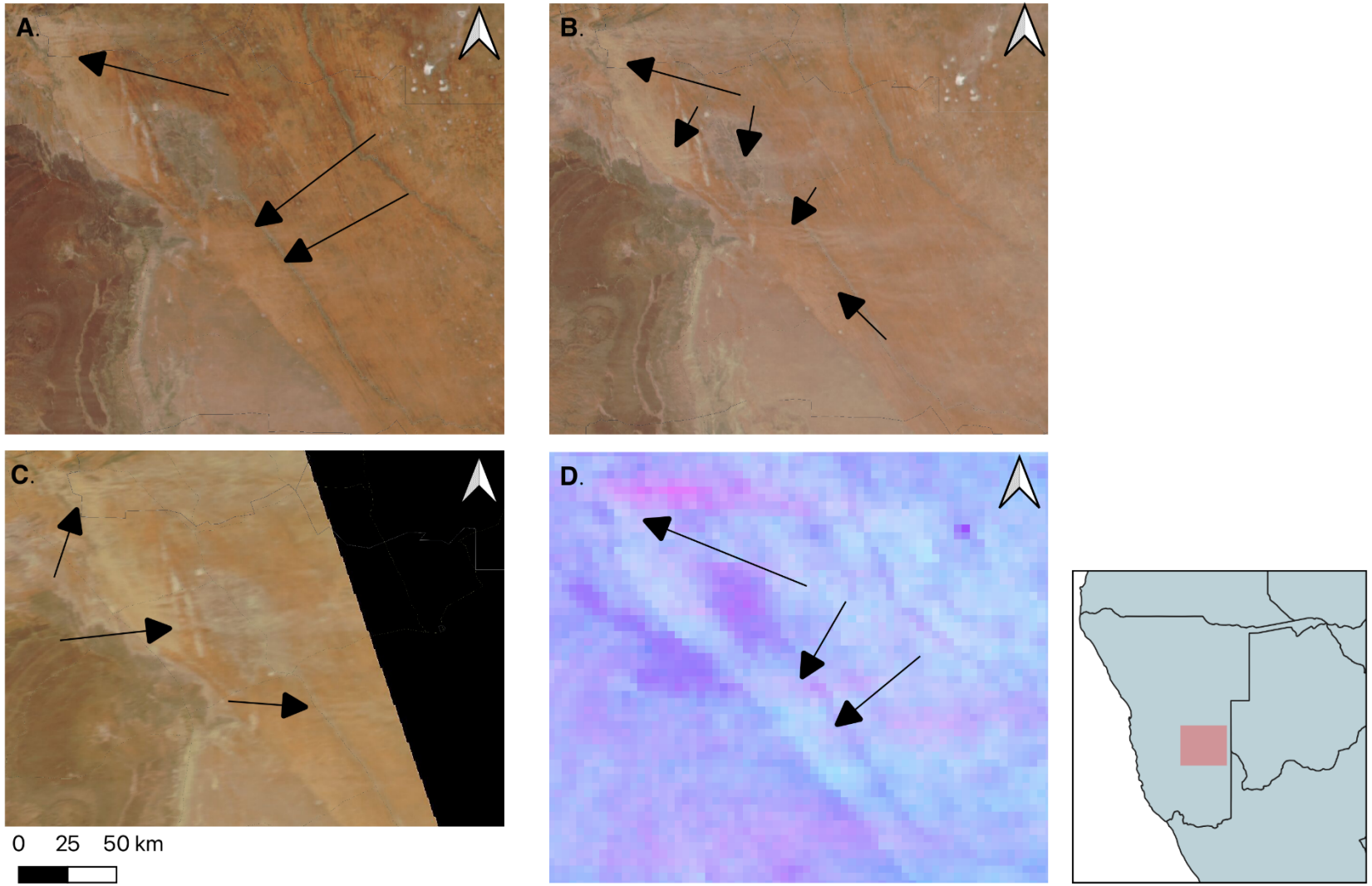

Figure 8.8. A dust event from the southwest Kalahari dunes on 07/07/2024 captured on multiple sensors. Arrows identify sources of dust. (A) was VIIRS/NOAA-20, (B) VIIRS Suomi NPP, (C) MODIS Aqua, (D) MSG-SEVRI in Pink RGB

Biological soil crusts are resilient organisms, their ability to withstand some droughts and recover after disturbance has been well documented (Belnap and Gillette, 1998, 1997; Bullard et al., 2022). In many desert ecosystems, biocrusts are the only living organism able to afford protection on the surface when droughts remove vegetation cover (Belnap and Gillette, 1998; Mager and Thomas, 2011). In the Kalahari, this is also true post-fire, with findings from this thesis indicating that biocrusts remain to stabilise the surface once vegetation has been burned. But biocrusts are vulnerable to both climate change and land use changes (Kidron et al., 2017; Pointing and Belnap, 2012; Rodríguez-Caballero et al., 2018). Subsequently 25 – 40% of the biocrust cover is expected to decrease in the next 65 years (Rodríguez-Caballero et al., 2018). One such explanation for the recently observed dust plumes originating from the Kalahari dunes (Figure 8.8) may be due to the death of biological crusts because of drought. With land-use, constant hoof action by grazing animals break-ups biocrusts, creating a discontinuous layer which can easily be scoured by the wind (Thomas and Dougill, 2007). Similar to climate change, increasing grazing pressure decrease biocrust cover making the surface more vulnerable to wind erosion and dust emission (Thomas and Dougill, 2007).

8.3 The future of dust emissions in the southwest Kalahari

The southwest Kalahari was selected as the site for this research because it has been hypothesised to become a future source of dust should the dunes lose the protective

vegetation cover (Bhattachan et al., 2012). Potential emissions from the region could have global implications, making it crucial to quantify factors that control dust emission to better understand future dust fluxes. The results presented in this thesis show little evidence for dust emission following de-vegetation by burning. However, with a changing climate in the region (Attwood et al., 2024; Dunning et al., 2018; Engelbrecht et al., 2015), the currently immobile fine-grained sediments may become mobilised and emitted as dust. This section explores and contextualises the findings of this thesis within the currently changing Kalahari climate.

The Kalahari is currently warming at over twice the global rate, and predicted to become drier in the future (Dunning et al., 2018; Engelbrecht et al., 2015). Patterns of rainfall are also changing, with marked increase in low pressure events (heat lows) which exert a strong influence on regional rainfall and have been attributed to the delayed onset of the wet season (Attwood et al., 2024). The heating and drying of the Kalahari, in turn, has implications for above ground biomass with vegetation productivity predicted to decline at both 1.5 °C and 2 °C of possible warming (Lawal et al., 2019). Globally, it has been found that biological soil crusts are projected to decrease by about 25 - 40% due to anthropogenically induced climate change (Rodríguez-Caballero et al., 2018).

To understand what the future of dust emissions from the southwest Kalahari may look like, both fire and drought need to be considered. Burning is dependent upon

precipitation with drought preventing fire through the lack of biomass build-up reducing the amount of fuel available to burn (Andela et al., 2019). Currently, the finding from this thesis establishes that there is little evidence for post-fire dust emission in the Kalahari because of high surface cover of burned debris in the initial post-fire period and the ability of biocrusts to survive burning. The lack of post-fire dust is evidenced in this thesis through; low emission fluxes recorded from the PI-SWERL (Chapter 6) and no large increases in in-situ aerosol concentrations (Chapter 7). Yet, dust emissions were observed from the dune field and can occur independently without fire under drought conditions (Figure 8.8). These emissions occurred during a large drought in southern Africa and may be an indicator of future conditions. Further, the predicted drying of the landscape may reduce biocrust cover (Rodríguez-Caballero et al., 2018), leaving the formerly fine-sediment availability limited systems able to emit dust. The findings of Chapter 6 show that if biocrusts are removed there is plenty of fine sediment available to be eroded by the wind. The recent dust event provides an evidence base for the work of Bhattachan et al. (2012) which predicts the Kalahari as a potential future dust source. Yet, it is unlikely that future dust emissions can remain sustained as there is no sediment recharge in the Kalahari system and there is no predicted large change in wind speed in the region (Fant et al., 2016; IPCC, 2023). Given this underlying capacity to emit dust, emissions may occur from burned areas if fire occurs and a drought commences afterwards, delaying the reestablishment of biocrusts and vegetation. These hypothetical scenarios are visualised in Figure 8.9, updating the work of Sweeney et al. (2023)

(Figure 2.3) using data from this thesis. For dust plumes from the fire scars to be detected using remote sensing technologies they would have to cover a significant area.

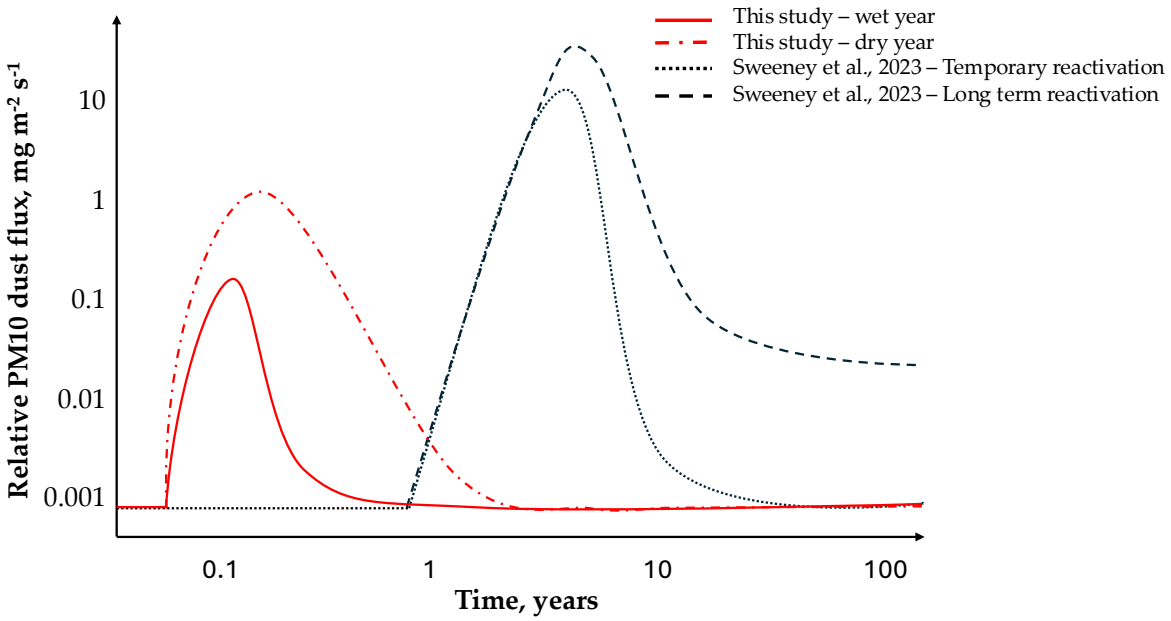

Figure 8.9. The updated hypothetical transition of a vegetated dune field from a dust sink to a dust source. Figure updated from Sweeney et al. (2023).

To find out if fire could lead to dust in the Kalahari in the future first the potential fire trends need to be ascertained. Currently, there is no consensus in model predictions on how fire patterning (frequency and extent) will change with the warming climate in the southwest Kalahari (Jones et al., 2022; Sullivan et al., 2022; Zhang et al., 2024). The United Nations Environment Programme special report on wildfire, indicates that southwest Kalahari occurrence of wildfire will largely not change under several climate scenarios (Sullivan et al., 2022). This conclusion is also supported by Burton et al. (2024), using an ensemble of global fire models to find that both climate change and

direct human forcing would not contribute to any change in fire patterns in southern Africa. However, Zhang et al. (2024) used neural networks to predict a very slight increase in fire occurrence in southwest Africa under a variety of climate scenarios. Further, Jones et al. (2022) model an marked increase in fire weather (note that biomass availability is not included in this calculation) for southern Africa into the future. With this lack of consensus in fire trends, it is difficult to conclude if dust from fire scars will occur in the future.

At present, fire is limited by precipitation in the region, as there must be enough precipitation to first ensure that vegetation cover is continuous for fire to propagate (Andela et al., 2019). Subsequently for fire to spread there must be a wet season, to allow vegetation to build-up, followed by a period of dryness to allow the vegetation to become flammable. The regions precipitation-limited fire regime is highlighted in Chapter 5 with the finding that fires occur most frequently during or just after wetter La Niña cycles and less commonly in El Niño cycles which are associated with drought in southern Africa. These alternations between very wet and very dry conditions (termed hydroclimate volatility or climate whiplash) have been linked to increased wildfire risk and have been attributed to large fires in semi-arid areas such as California, southeast Australia, southern Chile and Argentina (Homann et al., 2022; Swain et al., 2025). A recent review by Swain et al. (2025) on global trends in hydroclimate volatility displayed the whiplash between conditions are predicted to increase in frequency at a global scale. However, in southern Africa these events are

not predicted to change under future climates but instead are predicted to decrease (Swain et al., 2025). This may indicate lower fire risk for the Kalahari in the future, most likely due to the predicted drying limiting vegetation growth and fire fuel loads. The results from Chapters 4 and 5 demonstrate that fire is limited by precipitation in the southwest Kalahari highlighting not only the importance of hydroclimate volatility for fire propagation but also the current limitations in the detection of fire in the region.

Yet, increased atmospheric CO_2 may also increase plant biomass despite a drying trend. Recent research has found that drylands are greening despite reduced rainfall (Donohue et al., 2013; Gonsamo et al., 2021; Lu et al., 2016). Gonsamo et al. (2021) used satellite observations and found an increase in leaf area index (LAI) in the Kalahari despite lower soil moisture over the last 30 years. This increased LAI provides more biomass to burn, resulting in an increased fire risk as larger highly flammable material will cover the area and be able to burn. However, Jian et al. (2023) modelled decreasing LAI trends for the Kalahari for the last 20 years. The lack of agreement between different studies highlights how the impact of increased atmospheric CO_2 in drylands is not fully understood but could be a critical component of trying to predict the future of the Kalahari.

Part of the lack of reliability in the future of fire in the region may stem from the lack of quantitative understanding of the current fire regime. The work in this thesis aims

to help reduce this misunderstanding. The large occurrence of fire in the Northern Cape of South Africa over 2021 to 2022 austral summer was widely missed by automated products (Figure 4.5b). These fires occurred two years after a mega drought in the Kalahari and immediately before another drought. The fire scars are still visible using RGB satellite imagery in February 2025, indicating that the vegetation within the scars is still different from the surrounding fires. Ground-based studying of these fire scars and identifying potential emissions from them could be an indicator for future fires in the region with climate whiplash between dry to short wet period back to dry period in the future.

Chapter 9 - Overall conclusions and future work

The border of a recent fire scar in South Africa.

The overall aim of this thesis was to establish if the Kalahari dunes emit dust after burning, by destroying the protective vegetation cover and creating a more erodible surface. The findings from this thesis show **there is little evidence that the disturbance event triggered by fire leads to the emission of dust in the Kalahari**. This conclusion was reached through the following findings:

1. Although fire burns regularly in the Kalahari, it often occurs during wetter La Niña conditions which bring higher levels of precipitation allowing for vegetation to quickly regrow, creating a short temporal window for dust emission opportunity.

2. Land use alters fire duration, count, and size, with only the Kgalagadi Transfrontier Park, which makes up 11% of the study area, allowing fires to burn to their fullest extent. In the remaining parts of the study area, fire is actively suppressed by local landowners reducing the area of burned land available to be eroded by the wind.

3. The temporal window of opportunity for dust to be emitted post-fire is short and discontinuous. This is due to rapid vegetation regrowth during wet conditions after fire and higher vulnerability to droughts on burned sites even after recovery.

4. There is a statistically higher threshold for erosion on burned surfaces compared to control surfaces. But once the thresholds for erosion are exceeded similar levels of flux are recorded from the burned and control plots.

5. Fine grains are found within the sediment composition of the dunes. Yet, there is no evidence for the loss of fines from in the sediment samples between the burned and

unburned plots. This finding indicates that fine material is not being removed as dust after burning.

6. There were no high-magnitude in-situ dust emissions observed from two sites, even when high wind velocities were recorded.

7. The protective effects of biological soil crusts seem to withstand fire. The biocrusts increase the cohesivity of the surface which provides continued protection whilst vegetation cover is reduced post-burn.

Consequently, there are several key factors that operate in the southwest Kalahari in relation to dust, vegetation, and fire (Figure 9.1). The fine grains found within the sediment are there because of the plant canopies catching allochthonous grains in the atmosphere and pedogenesis occurring. Vegetation further protects the surface, preventing the fine grains from being eroded by the wind. Fire acts as a vegetation disturbance, removing overlying biomass and, after the burned debris is blown away, leaves a high proportion of the surface bare and vulnerable to wind erosion. Yet, dust emissions are not frequently observed due to biocrust withstanding fire and continuing to protect the surface during the period of low vegetation cover (Figure 9.1). Once sufficient rainfall has occurred to allow vegetation to regrow, plants again provide protective cover to the surface from the wind. Yet, biocrusts are vulnerable to drought and anthropogenic factors such as grazing. Should fire coincide with a drought period or occur on heavily grazed land where the biocrust cover is removed, then dust emission can occur.

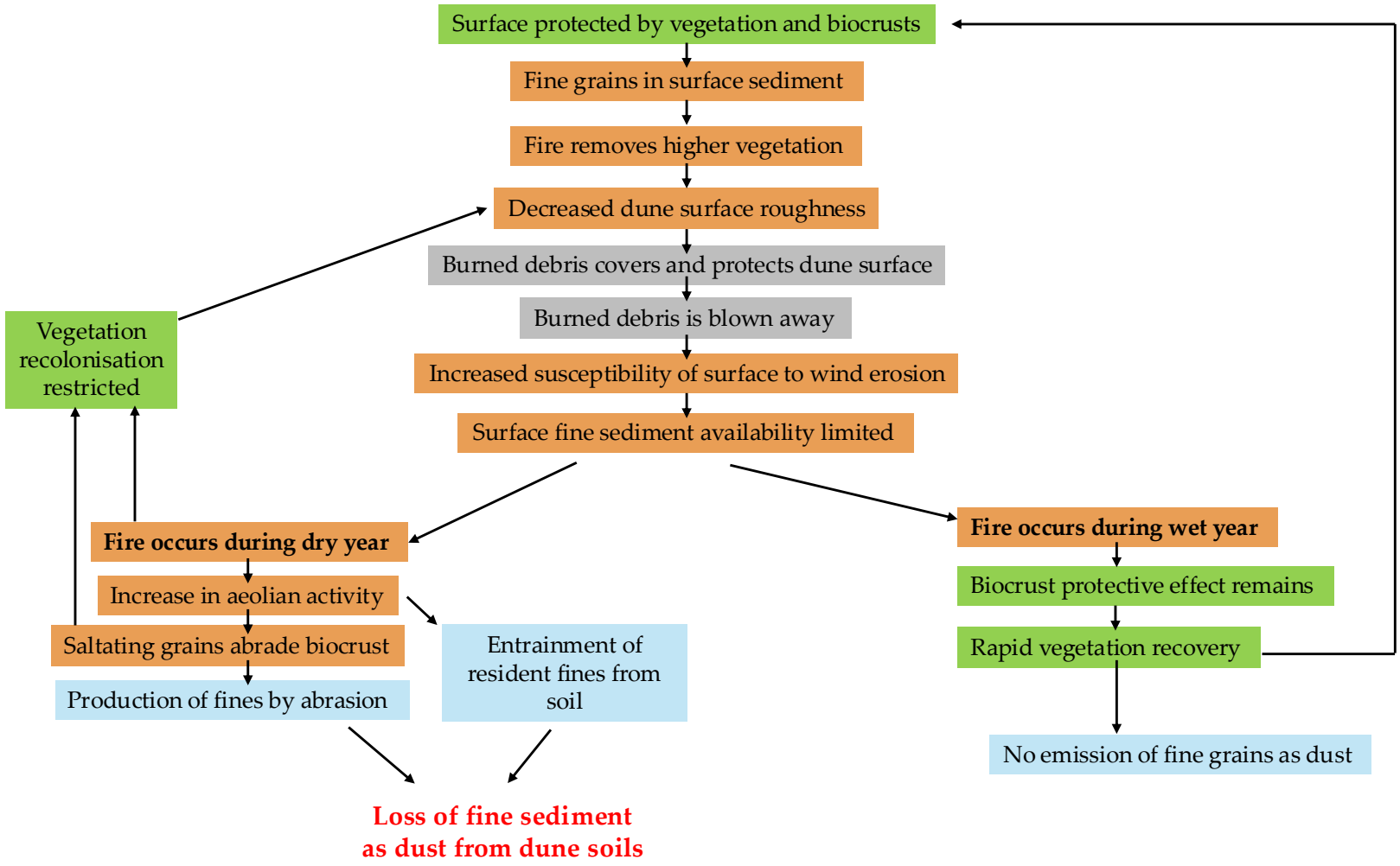

Figure 9.1. An updated version of Figure 2.14 from Strong et al. (2010) highlighting the key findings from this research.

Existing research suggests that vegetated dune systems contain fine grain material and subsequently should emit dust after vegetation is removed through disturbances such as fire (Bhattachan et al., 2012; Bullard et al., 2008; Pye, 1989; Sankey et al., 2012; Sweeney et al., 2023). But the evidence presented in this thesis demonstrates that this is not the case in the southwest Kalahari. The findings underpin the importance of erodibility and regional scale processes in governing post-fire dust emissions from the Kalahari. The erodibility of the surface is decreased by both vegetation and biological soil crusts. Vegetation acts as a roughness element, which is not completely incinerated when burned and burned vegetation in the form of litter protects the surface from wind erosion in the immediate aftermath of fire. Biological soil crusts create a three-dimensional matrix that bind individual grains together and can withstand burning. As both fire on sand dunes and dust from sand dunes are understudied phenomena, research to support the findings in this thesis are rare. Regional scale processes, such as precipitation, land use, and de-vegetated dune crests limit one or more of fire size, frequency and duration and are important factors to consider when seeking to understand the complex relationships between fire and dust emission. Therefore, it is suggested that attempts to better quantify the role of biological soil crusts in limiting wind erosion and the biocrusts ability to survive fire and drought conditions are needed to predict future post-fire dust emissions in the Kalahari.

This thesis provides an evidence base for the refinement of global scale dust and fire models. Remote sensing systems struggle to detect burning in the southwest Kalahari and connections drawn in this thesis highlight what causes these errors. Without adjustments to the current fire mapping in the region, it is not possible to predict future fire. Recent research has encouraged the representation of burned land as a transient and small-scale source of dust (Wagenbrenner et al., 2017; Yu and Ginoux, 2022). The innovative work by Yu and Ginoux (2022) and Wagenbrenner (2017) highlighted the need to incorporate post-fire dust emission in global dust emission models. But this thesis reveals the complexity of factors that prevent emissions, even on surfaces which are predicted to be emitters of dust if de-vegetated. Therefore, it is suggested that further research should be conducted into identifying further controls on post-fire dust emissions in the Kalahari, particularly the importance of biocrusts. This interdisciplinary work should integrate resilience frameworks, ecology, and geomorphology. Further, the approach used in this thesis should be applied to other vegetated dune systems which burn to identify if the controls on emission in the Kalahari are similar to those in other regions.

References

Aanderud, Z.T., Bahr, J., Robinson, D.M., Belnap, J., Campbell, T.P., Gill, R.A., McMillian, B., St. Clair, S., 2019. The Burning of Biocrusts Facilitates the Emergence of a Bare Soil Community of Poorly-Connected Chemoheterotrophic Bacteria With Depressed Ecosystem Services. Front. Ecol. Evol. 7, 1–14. https://doi.org/10.3389/fevo.2019.00467

Adebiyi, A.A., Kok, J.F., 2020. Climate models miss most of the coarse dust in the atmosphere. Sci. Adv. 6, 1–9. https://doi.org/10.1126/sciadv.aaz9507

Adebiyi, A.A., Kok, J.F., Murray, B.J., Ryder, C.L., Stuut, J.B.W., Kahn, R.A., Knippertz, P., Formenti, P., Mahowald, N.M., Pérez García-Pando, C., Klose, M., Ansmann, A., Samset, B.H., Ito, A., Balkanski, Y., Di Biagio, C., Romanias, M.N., Huang, Y., Meng, J., 2023. A review of coarse mineral dust in the Earth system. Aeolian Res. https://doi.org/10.1016/j.aeolia.2022.100849

Algarra, I., Eiras-Barca, J., Nieto, R., Gimeno, L., 2019. Global climatology of nocturnal low-level jets and associated moisture sources and sinks. Atmos. Res. 229, 39–59. https://doi.org/10.1016/j.atmosres.2019.06.016

Allen, C.J.T., Washington, R., 2014. The low-level jet dust emission mechanism in the central Sahara: Observations from Bordj-Badji Mokhtar during the June 2011 Fennec Intensive Observation. Nature 2990–3015. https://doi.org/10.1038/175238c0

Allen, C.J.T., Washington, R., Engelstaedter, S., 2013. Dust emission and transport mechanisms in the central Sahara: Fennec ground-based observations from Bordj Badji Mokhtar, June 2011. J. Geophys. Res. Atmos. 118, 6212–6232. https://doi.org/10.1002/jgrd.50534

Amit, R., Enzel, Y., Mushkin, A., Gillespie, A., Batbaatar, J., Crouvi, O., Vandenberghe, J., An, Z., 2014. Linking coarse silt production in asian sand deserts and quaternary accretion of the Chinese Loess Plateau. Geology 42, 23–26. https://doi.org/10.1130/G34857.1

Andela, N., Morton, D.C., Giglio, L., Chen, Y., Van Der Werf, G.R., Kasibhatla, P.S., DeFries, R.S., Collatz, G.J., Hantson, S., Kloster, S., Bachelet, D., Forrest, M., Lasslop, G., Li, F., Mangeon, S., Melton, J.R., Yue, C., Randerson, J.T., 2017. A human-driven decline in global burned area. Science (80-.). 356, 1356–1362. https://doi.org/10.1126/science.aal4108

Andela, N., Morton, D.C., Giglio, L., Paugam, R., Chen, Y., Hantson, S., Van Der Werf, G.R., Anderson, J.T., 2019. The Global Fire Atlas of individual fire size, duration, speed and direction. Earth Syst. Sci. Data 11, 529–552. https://doi.org/10.5194/essd-11-529-2019

Andela, N., Van Der Werf, G.R., 2014. Recent trends in African fires driven by cropland expansion and El Niño to la Niña transition. Nat. Clim. Chang. 4, 791–795. https://doi.org/10.1038/nclimate2313

Aranibar, J.N., Otter, L., Macko, S.A., Feral, C.J.W., Epstein, H.E., Dowty, P.R.,

Eckardt, F.D., Shugart, H.H., Swap, R.J., 2004. Nitrogen cycling in the soil-plant system along a precipitation gradient in the Kalahari sands. Glob. Chang. Biol. 10, 359–373. https://doi.org/10.1111/j.1365-2486.2003.00698.x

Archer, S.R., Andersen, E.M., Predick, K.I., Schwinning, S., Steidl, R.J., Woods, S.R., 2017. Woody Plant Encroachment: Causes and Consequences. https://doi.org/10.1007/978-3-319-46709-2_2

Archibald, S., Bond, W.J., Stock, W.D., Fairbanks, D.H.K., 2005. Shaping the landscape: Fire-grazer interactions in an African savanna. Ecol. Appl. 15, 96–109. https://doi.org/10.1890/03-5210

Archibald, S., Roy, D.P., van Wilgen, B.W., Scholes, R.J., 2009. What limits fire? An examination of drivers of burnt area in Southern Africa. Glob. Chang. Biol. 15, 613–630. https://doi.org/10.1111/j.1365-2486.2008.01754.x

Archibald, S., Scholes, R.J., Roy, D.P., Roberts, G., Boschetti, L., 2010. Southern African fire regimes as revealed by remote sensing. Int. J. Wildl. Fire 19, 861–878. https://doi.org/10.1071/WF10008

Ardon-Dryer, K., Aziz, T., 2025. Times Matter, the Impact of Convective Dust Events on Air Quality in the Greater Phoenix Area, Arizona. GeoHealth 9, e2024GH001209. https://doi.org/10.1029/2024GH001209

Ash, J.E., Wasson, R.J., 1983. Vegetation and sand mobility in the Australian desert dunefield. Zeitschrift fur Geomorphol. 45, 7–25.

Ashkenazy, Y., Yizhaq, H., Tsoar, H., 2012. Sand dune mobility under climate change in the Kalahari and Australian deserts. Clim. Change 112, 901–923. https://doi.org/10.1007/s10584-011-0264-9

Attwood, K., Washington, R., Munday, C., 2024. The Southern African Heat Low: Structure, Seasonal and Diurnal Variability, and Climatological Trends. J. Clim. 37, 3037–3053. https://doi.org/10.1175/jcli-d-23-0522.1

Azami, M.H. Bin, Orger, N.C., Schulz, V.H., Oshiro, T., Cho, M., 2022. Earth Observation Mission of a 6U CubeSat with a 5-Meter Resolution for Wildfire Image Classification Using Convolution Neural Network Approach. Remote Sens. 14. https://doi.org/10.3390/rs14081874

Baas, A.C.W., Nield, J.M., 2007. Modelling vegetated dune landscapes. Geophys. Res. Lett. 34, 1–5. https://doi.org/10.1029/2006GL029152

Bacon, S.N., McDonald, E. V., Amit, R., Enzel, Y., Crouvi, O., 2011. Total suspended particulate matter emissions at high friction velocities from desert landforms. J. Geophys. Res. Earth Surf. 116, 1–17. https://doi.org/10.1029/2011JF001965

Baddock, M.C., Boskovic, L., Strong, C.L., McTainsh, G., Bullard, J.E., Agranovski, I., Cropp, R., 2013. Iron-rich nanoparticles formed by aeolian abrasion of desert dune sand. Geochemistry, Geophys. Geosystems 14, 3720–3729. https://doi.org/10.1002/ggge.20229

Baddock, M.C., Bullard, J.E., Bryant, R.G., 2009. Dust source identification using MODIS: A comparison of techniques applied to the Lake Eyre Basin, Australia. Remote Sens. Environ. 113, 1511–1528. https://doi.org/10.1016/j.rse.2009.03.002

Baddock, M.C., Gill, T.E., Bullard, J.E., Acosta, M.D., Rivera, N.I.R., 2011.

Geomorphology of the Chihuahuan Desert based on potential dust emissions. J. Maps 7, 249–259. https://doi.org/10.4113/jom.2011.1178
Baddock, M.C., Strong, C.L., Leys, J.F., Heidenreich, S.K., Tews, E.K., McTainsh, G.H., 2014. A visibility and total suspended dust relationship. Atmos. Environ. 89, 329–336. https://doi.org/10.1016/j.atmosenv.2014.02.038
Bailey, R.M., 2011. Spatial and temporal signatures of fragility and threshold proximity in modelled semi-arid vegetation. Proc. R. Soc. B Biol. Sci. 278, 1064–1071. https://doi.org/10.1098/rspb.2010.1750
Bakker, N.L., Drake, N.A., Bristow, C.S., 2019. Evaluating the relative importance of northern African mineral dust sources using remote sensing. Atmos. Chem. Phys. 19, 10525–10535. https://doi.org/10.5194/acp-19-10525-2019
Ballinger, T.J., Mote, T.L., Mattingly, K., Bliss, A.C., Hanna, E., Van As, D., Prieto, M., Gharehchahi, S., Fettweis, X., Noël, B., Smeets, P.C.J.P., Reijmer, C.H., Ribergaard, M.H., Cappelen, J., 2019. Greenland Ice Sheet late-season melt: Investigating multiscale drivers of K-transect events. Cryosphere 13, 2241–2257. https://doi.org/10.5194/tc-13-2241-2019
Banks, J.R., Hünerbein, A., Heinold, B., Brindley, H.E., Deneke, H., Schepanski, K., 2019. The sensitivity of the colour of dust in MSG-SEVIRI Desert Dust infrared composite imagery to surface and atmospheric conditions. Atmos. Chem. Phys. 19, 6893–6911. https://doi.org/10.5194/acp-19-6893-2019
Bannari, A., Morin, D., Bonn, F., Huete, A.R., 1995. A review of vegetation indices. Remote Sens. Rev. 13, 95–120. https://doi.org/10.1080/02757259509532298
Barbosa, P.M., Stroppiana, D., Grégoire, J.M., Pereira, J.M.C., 1999. An assessment of vegetation fire in Africa (1981-1991): Burned areas, burned biomass, and atmospheric emissions. Global Biogeochem. Cycles 13, 933–950. https://doi.org/10.1029/1999GB900042
Belnap, J., Gillette, D.A., 1998. Vulnerability of desert biological soil crusts to wind erosion: The influences of crust development, soil texture, and disturbance. J. Arid Environ. 39, 133–142. https://doi.org/10.1006/jare.1998.0388
Belnap, J., Gillette, D.A., 1997. Disturbance of biological soil crusts: Impacts on potential wind erodibility of sandy desert soils in Southeastern Utah. L. Degrad. Dev. 8, 355–362. https://doi.org/10.1002/(SICI)1099-145X(199712)8:4<355::AID-LDR266>3.0.CO;2-H
Belnap, J., Phillips, S.L., Herrick, J.E., Johansen, J.R., 2007. Wind erodibility of soils at Fort Irwin, California (Mojave Desert), USA, before and after trampling disturbance: implications for land management. Earth Surf. Process. Landforms 32, 75–84. https://doi.org/10.1002/esp.1372
Bergametti, G., Rajot, J.L., Marticorena, B., Féron, A., Gaimoz, C., Chatenet, B., Coulibaly, M., Koné, I., Maman, A., Zakou, A., 2022. Rain, Wind, and Dust Connections in the Sahel. J. Geophys. Res. Atmos. 127, 1–22. https://doi.org/10.1029/2021JD035802
Bhattachan, A., D'Odorico, P., Baddock, M.C., Zobeck, T.M., Okin, G.S., Cassar, N., 2012. The Southern Kalahari: A potential new dust source in the Southern

Hemisphere? Environ. Res. Lett. 7. https://doi.org/10.1088/1748-9326/7/2/024001
Bhattachan, A., D'odorico, P., Dintwe, K., Okin, G.S., Collins, S.L., 2014. Resilience and recovery potential of duneland vegetation in the southern Kalahari. Ecosphere 5, 1–14. https://doi.org/10.1890/ES13-00268.1
Bhattachan, A., D'Odorico, P., Okin, G.S., 2015. Biogeochemistry of dust sources in Southern Africa. J. Arid Environ. 117, 18–27. https://doi.org/10.1016/j.jaridenv.2015.02.013
Bhattachan, A., D'Odorico, P., Okin, G.S., Dintwe, K., 2013. Potential dust emissions from the southern Kalahari's dunelands. J. Geophys. Res. Earth Surf. 118, 307–314. https://doi.org/10.1002/jgrf.20043
Bhattachan, A., Tatlhego, M., Dintwe, K., D'Odorico, P., Okin, G.S., 2022. Evaluation of dust production efficiencies in sandy sediments. Earth Surf. Process. Landforms 1–9. https://doi.org/10.1002/esp.5312
Blackwood, E.M.J., Rangers, K., Bayley, S., Bijlani, H., Fensham, R.J., Lindsay, M., Noakes, E., Wemyss, J., Legge, S., 2022. Pirra Jungku: Comparison of traditional and contemporary fire practices on Karajarri Country, Western Australia. Ecol. Manag. Restor. 23, 83–92. https://doi.org/10.1111/emr.12527
Bojdo, N., Filippone, A., Parkes, B., Clarkson, R., 2020. Aircraft engine dust ingestion following sand storms. Aerosp. Sci. Technol. 106, 106072. https://doi.org/10.1016/j.ast.2020.106072
Börker, J., Hartmann, J., Amann, T., Romero-Mujalli, G., 2018. Terrestrial sediments of the earth: Development of a global unconsolidated sediments map database (gum). Geochemistry, Geophys. Geosystems 19, 997–1024. https://doi.org/10.1002/2017GC007273
Boschetti, L., Roy, D.P., Giglio, L., Huang, H., Zubkova, M., Humber, M.L., 2019. Global validation of the collection 6 MODIS burned area product. Remote Sens. Environ. 235, 111490. https://doi.org/10.1016/j.rse.2019.111490
Bowker, M.A., 2007. Biological soil crust rehabilitation in theory and practice: An underexploited opportunity. Restor. Ecol. 15, 13–23. https://doi.org/10.1111/j.1526-100X.2006.00185.x
Bowker, M.A., Belnap, J., Rosentreter, R., Graham, B., 2004. Wildfire-resistant biological soil crusts and fire-induced loss of soil stability in Palouse prairies, USA. Appl. Soil Ecol. 26, 41–52. https://doi.org/10.1016/j.apsoil.2003.10.005
Bowman, D.M.J.S., Kolden, C.A., Abatzoglou, J.T., Johnston, F.H., van der Werf, G.R., Flannigan, M., 2020. Vegetation fires in the Anthropocene. Nat. Rev. Earth Environ. https://doi.org/10.1038/s43017-020-0085-3
Bowring, S.P.K., Li, W., Mouillot, F., Rosan, T.M., Ciais, P., 2024. Road fragment edges enhance wildfire incidence and intensity, while suppressing global burned area. Nat. Commun. 15, 9176. https://doi.org/10.1038/s41467-024-53460-6
Brun, J.M., Box, T.W., 1963. A Comparison of Line Intercepts and Random Point Frames for Sampling Desert Shrub Vegetation. J. Range Manag. 16, 21. https://doi.org/10.2307/3895032
Bryant, R.G., 2013. Recent advances in our understanding of dust source emission

processes. Prog. Phys. Geogr. 37, 397–421. https://doi.org/10.1177/0309133313479391
Bryant, R.G., 2003. Monitoring hydrological controls on dust emissions: Preliminary observations from Etosha Pan, Namibia. Geogr. J. 169, 131–141. https://doi.org/10.1111/1475-4959.04977
Buckland, C.E., Thomas, D.S.G., Bailey, R.M., 2019. Complex disturbance-driven reactivation of near-surface sediments in the largest dunefield in North America during the last 200 years. Earth Surf. Process. Landforms 44, 2794–2809. https://doi.org/10.1002/esp.4708
Buckley, R.C., 1981. Parallel dunefield ecosystems: southern Kalahari and central Australia. J. Arid Environ. 4, 287–298. https://doi.org/10.1016/s0140-1963(18)31475-7
Büdel, B., Darienko, T., Deutschewitz, K., Dojani, S., Friedl, T., Mohr, K.I., Salisch, M., Reisser, W., Weber, B., 2009. Southern african biological soil crusts are ubiquitous and highly diverse in drylands, being restricted by rainfall frequency. Microb. Ecol. 57, 229–247. https://doi.org/10.1007/s00248-008-9449-9
Bullard, J.E., Baddock, M.C., McTainsh, G., Leys, J., 2008. Sub-basin scale dust source geomorphology detected using MODIS. Geophys. Res. Lett. 35, 1–6. https://doi.org/10.1029/2008GL033928
Bullard, J.E., Harrison, S.P., Baddock, M.C., Drake, N., Gill, T.E., McTainsh, G., Sun, Y., 2011. Preferential dust sources: A geomorphological classification designed for use in global dust-cycle models. J. Geophys. Res. Earth Surf. 116. https://doi.org/10.1029/2011JF002061
Bullard, J.E., Mctainsh, G.H., Pudmenzky, C., 2007. Factors affecting the nature and rate of dust production from natural dune sands. Sedimentology 54, 169–182. https://doi.org/10.1111/j.1365-3091.2006.00827.x
Bullard, J.E., McTainsh, G.H., Pudmenzky, C., 2004. Aeolian abrasion and modes of fine particle production from natural red dune sands: An experimental study. Sedimentology 51, 1103–1125. https://doi.org/10.1111/j.1365-3091.2004.00662.x
Bullard, J.E., Nash, D.J., 1998. Linear dune pattern variability in the vicinity of dry valleys in the southwest Kalahari. Geomorphology 23, 35–54. https://doi.org/10.1016/S0169-555X(97)00090-1
Bullard, J.E., Ockelford, A., Strong, C., Aubault, H., 2018. Effects of Cyanobacterial Soil Crusts on Surface Roughness and Splash Erosion. J. Geophys. Res. Biogeosciences 123, 3697–3712. https://doi.org/10.1029/2018JG004726
Bullard, J.E., Strong, C.L., Aubault, H.A.P., 2022. Cyanobacterial Soil Crust Responses to Rainfall and Effects on Wind Erosion in a Semiarid Environment, Australia: Implications for Landscape Stability. J. Geophys. Res. Biogeosciences 127. https://doi.org/10.1029/2021JG006652
Bullard, J.E., Thomas, D.S.G., Livingstone, I., Wiggs, G.F.S., 1997. Dunefield activity and interactions with climatic variability in the southwest Kalahari desert. Earth Surf. Process. Landforms 22, 165–174. https://doi.org/10.1002/(SICI)1096-9837(199702)22:2<165::AID-ESP687>3.0.CO;2-9

Bullard, J.E., Thomas, D.S.G., Livingstone, I., Wiggs, G.F.S., 1996. Wind energy variations in the Southwestern Kalahari desert and implications for linear dunefield activity. Earth Surf. Process. Landforms 21, 263–278. https://doi.org/10.1002/(SICI)1096-9837(199603)21:3<263::AID-ESP627>3.0.CO;2-I

Bullard, J.E., Thomas, D.S.G., Livingstone, I., Wiggs, G.F.S., 1995. Analysis of linear sand dune morphological variability, southwestern Kalahari desert. Geomorphology 11, 189–203. https://doi.org/10.1016/0169-555X(94)00061-U

Bullard, J.E., White, K., 2005. Dust production and the release of iron oxides resulting from the aeolian abrasion of natural dune sands. Earth Surf. Process. Landforms 30, 95–106. https://doi.org/10.1002/esp.1148

Bullard, J.E., White, K., 2002. Quantifying iron oxide coatings on dune sands using spectrometric measurements: An example from the Simpson-Strzelecki Desert, Australia. J. Geophys. Res. Solid Earth 107. https://doi.org/10.1029/2001jb000454

Burrows, N.D., Burbidge, A.A., Fuller, P.J., Behn, G., 2006. Evidence of altered fire regimes in the Western Desert region of Australia. Conserv. Sci. West. Aust. 5, 14–26.

Burrows, N.D., Christensen, P., 1990. A survey of aboriginal fire patterns in the western desert of Australia,. Fire Environ. Ecol. Cult. Perspect. 42, 297–305.

Burrows, N.D., Ward, B., Robinson, A., 2009. Fuel Dynamics and Fire Spread in Spinifex Grasslands of the Western Desert. Proc. R. Soc. Queensl.

Burton, C., Betts, R.A., Jones, C.D., Feldpausch, T.R., Cardoso, M., Anderson, L.O., 2020. El Niño Driven Changes in Global Fire 2015/16. Front. Earth Sci. 8, 1–12. https://doi.org/10.3389/feart.2020.00199

Burton, C., Lampe, S., Kelley, D.I., Thiery, W., Hantson, S., Christidis, N., Gudmundsson, L., Forrest, M., Burke, E., Chang, J., Huang, H., Ito, A., Kou-Giesbrecht, S., Lasslop, G., Li, W., Nieradzik, L., Li, F., Chen, Y., Randerson, J., Reyer, C.P.O., Mengel, M., 2024. Global burned area increasingly explained by climate change. Nat. Clim. Chang. 14, 1186–1192. https://doi.org/10.1038/s41558-024-02140-w

Busch, B., 2020. Pilot study on provenance and depositional controls on clay mineral coatings in active fluvio-eolian systems, western USA. Sediment. Geol. 406, 105721. https://doi.org/10.1016/j.sedgeo.2020.105721

Campagnolo, M.L., Libonati, R., Rodrigues, J.A., Pereira, J.M.C., 2021. A comprehensive characterization of MODIS daily burned area mapping accuracy across fire sizes in tropical savannas. Remote Sens. Environ. 252, 112115. https://doi.org/10.1016/j.rse.2020.112115

Canfield, R.H., 1941. Application of the Line Interception Method in Sampling Range Vegetation. J. For. 39, 388–394. https://doi.org/doi.org/10.1093/jof/39.4.388

Castellanos, P., Colarco, P., Espinosa, W.R., Guzewich, S.D., Levy, R.C., Miller, R.L., Chin, M., Kahn, R.A., Kemppinen, O., Moosmüller, H., Nowottnick, E.P., Rocha-Lima, A., Smith, M.D., Yorks, J.E., Yu, H., 2024. Mineral dust optical properties for remote sensing and global modeling: A review. Remote Sens. Environ. 303, 113982. https://doi.org/10.1016/j.rse.2023.113982

Chappell, A., Webb, N.P., Hennen, M., Schepanski, K., Ciais, P., Balkanski, Y., Zender, C.S., Tegen, I., Zeng, Z., Tong, D., Baker, B., Ekström, M., Baddock, M.C., Eckardt, F.D., Kandakji, T., Lee, J.A., Nobakht, M., von Holdt, J.R.C., Leys, J.F., 2023. Satellites reveal Earth's seasonally shifting dust emission sources. Sci. Total Environ. 883. https://doi.org/10.1016/j.scitotenv.2023.163452

Chen, Y., Hall, J., Van Wees, D., Andela, N., Hantson, S., Giglio, L., Van Der Werf, G.R., Morton, D.C., Randerson, J.T., 2023. Multi-decadal trends and variability in burned area from the fifth version of the Global Fire Emissions Database (GFED5). Earth Syst. Sci. Data 15, 5227–5259. https://doi.org/10.5194/essd-15-5227-2023

Chen, Y., Morton, D.C., Andela, N., Van Der Werf, G.R., Giglio, L., Randerson, J.T., 2017. A pan-tropical cascade of fire driven by El Niño/Southern Oscillation. Nat. Clim. Chang. 7, 906–911. https://doi.org/10.1038/s41558-017-0014-8

Chikoore, H., Mbokodo, I.L., Singo, M. V., Mohomi, T., Munyai, R.B., Havenga, H., Mahlobo, D.D., Engelbrecht, F.A., Bopape, M.J.M., Ndarana, T., 2024. Dynamics of an extreme low temperature event over South Africa amid a warming climate. Weather Clim. Extrem. 44, 100668. https://doi.org/10.1016/j.wace.2024.100668

Chin, M., Diehl, T., Ginoux, P., Malm, W., 2007. Intercontinental transport of pollution and dust aerosols: Implications for regional air quality. Atmos. Chem. Phys. 7, 5501–5517. https://doi.org/10.5194/acp-7-5501-2007

Chuvieco, E., Aguado, I., Salas, J., García, M., Yebra, M., Oliva, P., 2020. Satellite Remote Sensing Contributions to Wildland Fire Science and Management Introduction : Why Using RS Methods in Fire. Curr. For. Reports 6, 81–96.

Chuvieco, E., Englefield, P., Trishchenko, A.P., Luo, Y., 2008. Generation of long time series of burn area maps of the boreal forest from NOAA-AVHRR composite data. Remote Sens. Environ. 112, 2381–2396. https://doi.org/10.1016/j.rse.2007.11.007

Chuvieco, E., Lizundia-Loiola, J., Lucrecia Pettinari, M., Ramo, R., Padilla, M., Tansey, K., Mouillot, F., Laurent, P., Storm, T., Heil, A., Plummer, S., 2018. Generation and analysis of a new global burned area product based on MODIS 250 m reflectance bands and thermal anomalies. Earth Syst. Sci. Data 10, 2015–2031. https://doi.org/10.5194/essd-10-2015-2018

Chuvieco, E., Martin, M.P., 1994. Global fire mapping and fire danger estimation using AVHRR images. Photogramm. Eng. Remote Sensing 60, 563–570.

Chuvieco, E., Mouillot, F., van der Werf, G.R., San Miguel, J., Tanasse, M., Koutsias, N., García, M., Yebra, M., Padilla, M., Gitas, I., Heil, A., Hawbaker, T.J., Giglio, L., 2019. Historical background and current developments for mapping burned area from satellite Earth observation. Remote Sens. Environ. 225, 45–64. https://doi.org/10.1016/j.rse.2019.02.013

Chuvieco, E., Roteta, E., Sali, M., Stroppiana, D., Boettcher, M., Kirches, G., Storm, T., Khairoun, A., Pettinari, M.L., Franquesa, M., Albergel, C., 2022. Building a small fire database for Sub-Saharan Africa from Sentinel-2 high-resolution images. Sci.

Total Environ. 845. https://doi.org/10.1016/j.scitotenv.2022.157139
Chuvieco, E., Yebra, M., Martino, S., Thonicke, K., Gómez-Giménez, M., San-Miguel, J., Oom, D., Velea, R., Mouillot, F., Molina, J.R., Miranda, A.I., Lopes, D., Salis, M., Bugaric, M., Sofiev, M., Kadantsev, E., Gitas, I.Z., Stavrakoudis, D., Eftychidis, G., Bar-Massada, A., Neidermeier, A., Pampanoni, V., Pettinari, M.L., Arrogante-Funes, F., Ochoa, C., Moreira, B., Viegas, D., 2023. Towards an Integrated Approach to Wildfire Risk Assessment: When, Where, What and How May the Landscapes Burn. Fire 6, 1–60. https://doi.org/10.3390/fire6050215
Clements, C.B., Zhong, S., Goodrick, S., Li, J., Aumann, X.B., Heilman, W.E., Charney, J.J., Perna, R., Jang, M., Lee, D., Patel, M., Street, S., Aumann, G., 2007. Observing the Dynamics of Wildland Grass Fires. Bull. Am. Meteorol. Soc. 99, 1369–1382.
Clements, M., Washington, R., 2021. Atmospheric Controls on Mineral Dust Emission From the Etosha Pan, Namibia: Observations From the CLARIFY-2016 Field Campaign. J. Geophys. Res. Atmos. 126. https://doi.org/10.1029/2021JD034746
Cochrane, M.A., Barber, C.P., 2009. Climate change, human land use and future fires in the Amazon. Glob. Chang. Biol. 15, 601–612. https://doi.org/10.1111/j.1365-2486.2008.01786.x
Cordero, R.R., Feron, S., Damiani, A., Carrasco, J., Karas, C., Wang, C., Kraamwinkel, C.T., Beaulieu, A., 2024. Extreme fire weather in Chile driven by climate change and El Niño–Southern Oscillation (ENSO). Sci. Rep. 14, 1–12. https://doi.org/10.1038/s41598-024-52481-x
Couradeau, E., Karaoz, U., Lim, H.C., Nunes Da Rocha, U., Northen, T., Brodie, E., Garcia-Pichel, F., 2016. Bacteria increase arid-land soil surface temperature through the production of sunscreens. Nat. Commun. 7, 1–7. https://doi.org/10.1038/ncomms10373
Courrech du Pont, S., Rubin, D.M., Narteau, C., Lapôtre, M.G.A., Day, M., Claudin, P., Livingstone, I., Telfer, M.W., Radebaugh, J., Gadal, C., Gunn, A., Hesp, P.A., Carpy, S., Bristow, C.S., Baas, A.C.W., Ewing, R.C., Wiggs, G.F.S., 2024. Complementary classifications of aeolian dunes based on morphology, dynamics, and fluid mechanics. Earth-Science Rev. 255, 104772. https://doi.org/10.1016/j.earscirev.2024.104772
Crouvi, O., Amit, R., Enzel, Y., Gillespie, A.R., 2010. Active sand seas and the formation of desert loess. Quat. Sci. Rev. 29, 2087–2098. https://doi.org/10.1016/j.quascirev.2010.04.026
Crouvi, O., Amit, R., Enzel, Y., Porat, N., Sandler, A., 2008. Sand dunes as a major proximal dust source for late Pleistocene loess in the Negev Desert, Israel. Quat. Res. 70, 275–282. https://doi.org/10.1016/j.yqres.2008.04.011
Crouvi, O., Schepanski, K., Amit, R., Gillespie, A.R., Enzel, Y., 2012. Multiple dust sources in the Sahara Desert: The importance of sand dunes. Geophys. Res. Lett. 39, 1–8. https://doi.org/10.1029/2012GL052145
Crusius, J., Schroth, A.W., Gassó, S., Moy, C.M., Levy, R.C., Gatica, M., 2011. Glacial

flour dust storms in the Gulf of Alaska: Hydrologic and meteorological controls and their importance as a source of bioavailable iron. Geophys. Res. Lett. 38, 1–5. https://doi.org/10.1029/2010GL046573

Crusius, J., Schroth, A.W., Resing, J.A., Cullen, J., Campbell, R.W., 2017. Seasonal and spatial variabilities in northern Gulf of Alaska surface water iron concentrations driven by shelf sediment resuspension, glacial meltwater, a Yakutat eddy, and dust. Global Biogeochem. Cycles 31, 942–960. https://doi.org/10.1002/2016GB005493

Cui, M., Lu, H., Wiggs, G.F.S., Etyemezian, V., Sweeney, M.R., Xu, Z., 2019. Quantifying the effect of geomorphology on aeolian dust emission potential in northern China. Earth Surf. Process. Landforms.

D'Odorico, P., Bhattachan, A., Davis, K.F., Ravi, S., Runyan, C.W., 2013. Global desertification: Drivers and feedbacks. Adv. Water Resour. 51, 326–344. https://doi.org/10.1016/j.advwatres.2012.01.013

D'Odorico, P., Okin, G.S., Bestelmeyer, B.T., 2012. A synthetic review of feedbacks and drivers of shrub encroachment in arid grasslands. Ecohydrology 5, 520–530. https://doi.org/10.1002/eco.259

Dansie, A.P., Thomas, D.S.G., Wiggs, G.F.S., Baddock, M.C., Ashpole, I., 2022. Plumes and blooms – Locally-sourced Fe-rich aeolian mineral dust drives phytoplankton growth off southwest Africa. Sci. Total Environ. 829, 154562. https://doi.org/https://doi.org/10.1016/j.scitotenv.2022.154562

Dansie, A.P., Wiggs, G.F.S., Thomas, D.S.G., 2017a. Iron and nutrient content of wind-erodible sediment in the ephemeral river valleys of Namibia. Geomorphology 290, 335–346. https://doi.org/10.1016/j.geomorph.2017.03.016

Dansie, A.P., Wiggs, G.F.S., Thomas, D.S.G., Washington, R., 2017b. Measurements of windblown dust characteristics and ocean fertilization potential: The ephemeral river valleys of Namibia. Aeolian Res. 29, 30–41. https://doi.org/10.1016/j.aeolia.2017.08.002

DaSilva, M.D., Bruce, D., Hesp, P.A., Miot da Silva, G., 2021. A new application of the disturbance index for fire severity in coastal dunes. Remote Sens. 13. https://doi.org/10.3390/rs13234739

Daudon, C., Beyers, M., Jackson, D., Avouac, J.P., 2024. Prediction of barchan dunes migration using climatic models and speed-up effect of dune topography on air flow. Earth Planet. Sci. Lett. 648, 119049. https://doi.org/10.1016/j.epsl.2024.119049

DeBano, L.F., 2000. The role of fire and soil heating on water repellency in wildland environments: A review. J. Hydrol. 231–232, 195–206. https://doi.org/10.1016/S0022-1694(00)00194-3

Delgado-Baquerizo, M., Maestre, F.T., Escolar, C., Gallardo, A., Ochoa, V., Gozalo, B., Prado-Comesaña, A., 2014. Direct and indirect impacts of climate change on microbial and biocrust communities alter the resistance of the N cycle in a semiarid grassland. J. Ecol. 102, 1592–1605. https://doi.org/10.1111/1365-2745.12303

Dettweiler-Robinson, E., Bakker, J.D., Grace, J.B., 2013. Controls of biological soil crust cover and composition shift with succession in sagebrush shrub-steppe. J. Arid Environ. 94, 96–104. https://doi.org/10.1016/j.jaridenv.2013.01.013

Di Biagio, C., Formenti, P., Balkanski, Y., Caponi, L., Cazaunau, M., Pangui, E., Journet, E., Nowak, S., Andreae, M.O., Kandler, K., Saeed, T., Piketh, S., Seibert, D., Williams, E., Doussin, J.F., 2019. Complex refractive indices and single-scattering albedo of global dust aerosols in the shortwave spectrum and relationship to size and iron content. Atmos. Chem. Phys. 19, 15503–15531. https://doi.org/10.5194/acp-19-15503-2019

Dickey, H., Schreuder, M., Schmid, B., Yimam, Y.T., 2023. Quantifying dust emission potential of playa and desert surfaces in the Salton Sea Air Basin, California, United States. Aeolian Res. 60, 100850. https://doi.org/10.1016/j.aeolia.2022.100850

Dintwe, K., Okin, G.S., Xue, Y., 2017. Fire-induced albedo change and surface radiative forcing in sub-Saharan Africa savanna ecosystems: Implications for the energy balance. J. Geophys. Res. 122, 6186–6201. https://doi.org/10.1002/2016JD026318

Doerr, S.H., 1998. On standardizing the "water drop penetration time" and the "molarity of an ethanol droplet" techniques to classify soil hydrophobicity: a case study using medium textured soils. Earth Surf. Process. Landforms 23, 663–668. https://doi.org/10.1002/(SICI)1096-9837(199807)23:7<663::AID-ESP909>3.0.CO;2-6

Dong, Z., Brahney, J., Kang, S., Elser, J., Wei, T., Jiao, X., Shao, Y., 2020. Aeolian dust transport, cycle and influences in high-elevation cryosphere of the Tibetan Plateau region: New evidences from alpine snow and ice. Earth-Science Rev. https://doi.org/10.1016/j.earscirev.2020.103408

Donohue, R.J., Roderick, M.L., McVicar, T.R., Farquhar, G.D., 2013. Impact of CO2 fertilization on maximum foliage cover across the globe's warm, arid environments. Geophys. Res. Lett. 40, 3031–3035. https://doi.org/10.1002/grl.50563

Dougill, A.J., Thomas, A.D., 2004. Kalahari sand soils: Spatial heterogeneity, biological soil crusts and land degradation. L. Degrad. Dev. 15, 233–242. https://doi.org/10.1002/ldr.611

Dufresne, J.L., Gautier, C., Ricchiazzi, P., 2002. Longwave scattering effects of mineral aerosols. J. Atmos. Sci. 59, 1959–1966. https://doi.org/10.1175/1520-0469(2002)059<1959:LSEOMA>2.0.CO;2

Dukes, D., Gonzales, H.B., Ravi, S., Grandstaff, D.E., Van Pelt, R.S., Li, J., Wang, G., Sankey, J.B., 2018. Quantifying Postfire Aeolian Sediment Transport Using Rare Earth Element Tracers. J. Geophys. Res. Biogeosciences 123, 288–299. https://doi.org/10.1002/2017JG004284

Dunning, C.M., Black, E., Allan, R.P., 2018. Later wet seasons with more intense rainfall over Africa under future climate change. J. Clim. 31, 9719–9738. https://doi.org/10.1175/JCLI-D-18-0102.1

Eckardt, F.D., Bekiswa, S., Von Holdt, J.R.C., Jack, C., Kuhn, N.J., Mogane, F., Murray, J.E., Ndara, N., Palmer, A.R., 2020. South Africa's agricultural dust sources and events from MSG SEVIRI. Aeolian Res. 47, 100637. https://doi.org/10.1016/j.aeolia.2020.100637

Eldridge, D.J., Bowker, M.A., Maestre, F.T., Roger, E., Reynolds, J.F., Whitford, W.G., 2011. Impacts of shrub encroachment on ecosystem structure and functioning: Towards a global synthesis. Ecol. Lett. 14, 709–722. https://doi.org/10.1111/j.1461-0248.2011.01630.x

Eldridge, D.J., Bradstock, R.A., 1994. The effect of time since fire on the cover and composition of cryptogamic soil crusts on a eucalypt shrubland soil. Cunninghamia.

Elliott, D.R., Thomas, A.D., Hoon, S.R., Sen, R., 2024. Spatial organisation of fungi in soil biocrusts of the Kalahari is related to bacterial community structure and may indicate ecological functions of fungi in drylands. Front. Microbiol. 15, 1–11. https://doi.org/10.3389/fmicb.2024.1173637

Elliott, D.R., Thomas, A.D., Hoon, S.R., Sen, R., 2014. Niche partitioning of bacterial communities in biological crusts and soils under grasses, shrubs and trees in the Kalahari. Biodivers. Conserv. 23, 1709–1733. https://doi.org/10.1007/s10531-014-0684-8

Elliott, D.R., Thomas, A.D., Strong, C.L., Bullard, J.E., 2019. Surface Stability in Drylands Is Influenced by Dispersal Strategy of Soil Bacteria. J. Geophys. Res. Biogeosciences 124, 3403–3418. https://doi.org/10.1029/2018JG004932

Engelbrecht, F., Adegoke, J., Bopape, M.J., Naidoo, M., Garland, R., Thatcher, M., McGregor, J., Katzfey, J., Werner, M., Ichoku, C., Gatebe, C., 2015. Projections of rapidly rising surface temperatures over Africa under low mitigation. Environ. Res. Lett. 10. https://doi.org/10.1088/1748-9326/10/8/085004

Engelstaedter, S., Kohfeld, K.E., Tegen, I., Harrison, S.P., 2003. Controls of dust emissions by vegetation and topographic depressions: An evaluation using dust storm frequency data. Geophys. Res. Lett. 30, 30–33. https://doi.org/10.1029/2002GL016471

Engelstaedter, S., Tegen, I., Washington, R., 2006. North African dust emissions and transport. Earth-Science Rev. 79, 73–100. https://doi.org/10.1016/j.earscirev.2006.06.004

Engelstaedter, S., Washington, R., 2007. Temporal controls on global dust emissions: The role of surface gustiness. Geophys. Res. Lett. 34, 1–5. https://doi.org/10.1029/2007GL029971

Etchberger, R.C., Krausman, P.R., 1997. Evaluation of Five Methods for Measuring Desert Vegetation. Wildl. Soc. Bull. 25, 604–609. https://doi.org/10.4135/9781446247501.n1030

Etyemezian, V., Gillies, J.A., Shinoda, M., Nikolich, G., King, J., Bardis, A.R., 2014. Accounting for surface roughness on measurements conducted with PI-SWERL: Evaluation of a subjective visual approach and a photogrammetric technique. Aeolian Res. 13, 35–50. https://doi.org/10.1016/j.aeolia.2014.03.002

Etyemezian, V., Nikolich, G., Ahonen, S., Pitchford, M., Sweeney, M.R., Purcell, R., Gillies, J., Kuhns, H., 2007. The Portable In Situ Wind Erosion Laboratory (PI-SWERL): A new method to measure PM10 windblown dust properties and potential for emissions. Atmos. Environ. 41, 3789–3796. https://doi.org/10.1016/j.atmosenv.2007.01.018

Evangelista, P., Stohlgren, T.J., Guenther, D., Stewart, S., 2004. Vegetation response to fire and postburn seeding treatments in juniper woodlands of the Grand Staircase-Escalante National Monument, Utah. West. North Am. Nat. 64, 293–305.

Fant, C., Adam Schlosser, C., Strzepek, K., 2016. The impact of climate change on wind and solar resources in southern Africa. Appl. Energy 161, 556–564. https://doi.org/10.1016/j.apenergy.2015.03.042

Feng, G., Sharratt, B., Vaddella, V., 2013. Windblown soil crust formation under light rainfall in a semiarid region. Soil Tillage Res. 128, 91–96. https://doi.org/10.1016/j.still.2012.11.004

Fick, S.E., Barger, N., Tatarko, J., Duniway, M.C., 2020. Induced biological soil crust controls on wind erodibility and dust (PM10) emissions. Earth Surf. Process. Landforms 45, 224–236. https://doi.org/10.1002/esp.4731

Fiedler, S., Schepanski, K., Heinold, B., Knippertz, P., Tegen, I., 2013. Climatology of nocturnal low-level jets over North Africa and implications for modeling mineral dust emission. J. Geophys. Res. Atmos. 118, 6100–6121. https://doi.org/10.1002/jgrd.50394

Field, J.P., Belnap, J., Breshears, D.D., Neff, J.C., Okin, G.S., Whicker, J.J., Painter, T.H., Ravi, S., Reheis, M.C., Reynolds, R.L., 2010. The ecology of dust. Front. Ecol. Environ. 8, 423–430. https://doi.org/10.1890/090050

Fisher, A., Hesse, P., 2019. The response of vegetation cover and dune activity to rainfall, drought and fire observed by multitemporal satellite imagery. Earth Surf. Process. Landforms 44, 2957–2967. https://doi.org/10.1002/esp.4721

Fuller, D.O., Murphy, K., 2006. The ENSO-fire dynamic in insular Southeast Asia. Clim. Change 74, 435–455. https://doi.org/10.1007/s10584-006-0432-5

Gadal, C., Delorme, P., Narteau, C., Wiggs, G.F.S., Baddock, M.C., Nield, J.M., Claudin, P., 2022. Local Wind Regime Induced by Giant Linear Dunes: Comparison of ERA5-Land Reanalysis with Surface Measurements. Boundary-Layer Meteorol. 185, 309–332. https://doi.org/10.1007/s10546-022-00733-6

Garcia-Pichel, F., Felde, V.J.M.N.L., Drahorad, S.L., Weber, B., 2016. Microstructure and Weathering Processes Within Biological Soil Crusts 237–255. https://doi.org/10.1007/978-3-319-30214-0_13

Garzanti, E., Pastore, G., Stone, A., Vainer, S., Vermeesch, P., Resentini, A., 2022. Provenance of Kalahari Sand: Paleoweathering and recycling in a linked fluvial-aeolian system. Earth-Science Rev. https://doi.org/10.1016/j.earscirev.2021.103867

Gaston, C.J., 2020. Re-examining Dust Chemical Aging and Its Impacts on Earth's Climate. Acc. Chem. Res. 53, 1005–1013.

https://doi.org/10.1021/acs.accounts.0c00102
Ge, J.M., Liu, H., Huang, J., Fu, Q., 2016. Taklimakan Desert nocturnal low-level jet: Climatology and dust activity. Atmos. Chem. Phys. 16, 7773–7783. https://doi.org/10.5194/acp-16-7773-2016
Giannadaki, D., Pozzer, A., Lelieveld, J., 2014. Modeled global effects of airborne desert dust on air quality and premature mortality. Atmos. Chem. Phys. 14, 957–968. https://doi.org/10.5194/acp-14-957-2014
Giglio, L., Boschetti, L., Roy, D.P., Humber, M.L., Justice, C.O., 2018. The Collection 6 MODIS burned area mapping algorithm and product. Remote Sens. Environ. 217, 72–85. https://doi.org/10.1016/j.rse.2018.08.005
Giglio, L., Loboda, T., Roy, D.P., Quayle, B., Justice, C.O., 2009. An active-fire based burned area mapping algorithm for the MODIS sensor. Remote Sens. Environ. 113, 408–420. https://doi.org/10.1016/j.rse.2008.10.006
Giglio, L., Randerson, J.T., Van Der Werf, G.R., 2013. Analysis of daily, monthly, and annual burned area using the fourth-generation global fire emissions database (GFED4). J. Geophys. Res. Biogeosciences 118, 317–328. https://doi.org/10.1002/jgrg.20042
Gill, T., 2018. Airborne dust: A primer for clinicians. Southwest Respir. Crit. Care Chronicles 6, 4–7. https://doi.org/10.12746/swrccc.v6i22.437
Gillespie, M., Okin, G.S., Meyer, T., Ochoa, F., 2024. Evaluating Burn Severity and Post-Fire Woody Vegetation Regrowth in the Kalahari Using UAV Imagery and Random Forest Algorithms.
Gillies, J.A., Furtak-Cole, E., Nikolich, G., Etyemezian, V., 2022. The role of off-highway vehicle activity in augmenting dust emissions at the Oceano Dunes State Vehicular Recreation Area, Oceano, CA. Atmos. Environ. X 13, 100146. https://doi.org/10.1016/j.aeaoa.2021.100146
Ginoux, P., Prospero, J.M., Gill, T.E., Hsu, N.C., Zhao, M., 2012. Global-scale attribution of anthropogenic and natural dust sources and their emission rates based on MODIS Deep Blue aerosol products. Rev. Geophys. https://doi.org/10.1029/2012RG000388
Gittings, J.A., Dall'olmo, G., Tang, W., Llort, J., Jebri, F., Livanou, E., Nencioli, F., Darmaraki, S., Theodorou, I., Brewin, R.J.W., Srokosz, M., Cassar, N., Raitsos, D.E., By, E., Palumbi, S., 2024. An exceptional phytoplankton bloom in the southeast Madagascar Sea driven by African dust deposition. PNAS Nexus 3, 1–13. https://doi.org/10.1093/PNASNEXUS/PGAE386
Goirán, S.B., Aranibar, J.N., Gomez, M.L., 2012. Heterogeneous spatial distribution of traditional livestock settlements and their effects on vegetation cover in arid groundwater coupled ecosystems in the Monte Desert (Argentina). J. Arid Environ. 87, 188–197. https://doi.org/10.1016/j.jaridenv.2012.07.011
Gonsamo, A., Ciais, P., Miralles, D.G., Sitch, S., Dorigo, W., Lombardozzi, D., Friedlingstein, P., Nabel, J.E.M.S., Goll, D.S., O'Sullivan, M., Arneth, A., Anthoni, P., Jain, A.K., Wiltshire, A., Peylin, P., Cescatti, A., 2021. Greening drylands despite warming consistent with carbon dioxide fertilization effect.

Glob. Chang. Biol. 27, 3336–3349. https://doi.org/10.1111/gcb.15658
Gonzales, H.B., Ravi, S., Li, J., Sankey, J.B., 2018. Ecohydrological implications of aeolian sediment trapping by sparse vegetation in drylands. Ecohydrology 11, 1–11. https://doi.org/10.1002/eco.1986
Goossens, D., 2004. Effect of soil crusting on the emission and transport of wind-eroded sediment: Field measurements on loamy sandy soil. Geomorphology 58, 145–160. https://doi.org/10.1016/S0169-555X(03)00229-0
Goudie, A.S., 2014. Desert dust and human health disorders. Environ. Int. 63, 101–113. https://doi.org/10.1016/j.envint.2013.10.011
Goudie, A.S., 1991. Pans. Prog. Phys. Geogr. 15, 221–237.
Greenville, A.C., Dickman, C.R., Wardle, G.M., Letnic, M., 2009. The fire history of an arid grassland: The influence of antecedent rainfall and ENSO. Int. J. Wildl. Fire 18, 631–639. https://doi.org/10.1071/WF08093
Greenwood, L., Bliege Bird, R., Nimmo, D., 2022. Indigenous burning shapes the structure of visible and invisible fire mosaics. Landsc. Ecol. 37, 811–827. https://doi.org/10.1007/s10980-021-01373-w
Hall, J. V., Loboda, T. V., Giglio, L., McCarty, G.W., 2016. A MODIS-based burned area assessment for Russian croplands: Mapping requirements and challenges. Remote Sens. Environ. 184, 506–521. https://doi.org/10.1016/j.rse.2016.07.022
Hamilton, D.S., Perron, M.M.G., Bond, T.C., Bowie, A.R., Buchholz, R.R., Guieu, C., Ito, A., Maenhaut, W., Myriokefalitakis, S., Olgun, N., Rathod, S.D., Schepanski, K., Tagliabue, A., Wagner, R., Mahowald, N.M., 2022. Earth, Wind, Fire, and Pollution: Aerosol Nutrient Sources and Impacts on Ocean Biogeochemistry. Ann. Rev. Mar. Sci. 14, 303–330. https://doi.org/10.1146/annurev-marine-031921-013612
Hao, Y., Hao, Z., Feng, S., Zhang, X., Hao, F., 2020. Response of vegetation to El Niño-Southern Oscillation (ENSO) via compound dry and hot events in southern Africa. Glob. Planet. Change 195, 103358. https://doi.org/10.1016/j.gloplacha.2020.103358
Hardtke, L.A., Blanco, P.D., Héctor, F., Metternicht, G.I., Sione, W.F., 2015. Semi-automated mapping of burned areas in semi-arid ecosystems using MODIS time-series imagery. Int. J. Appl. Earth Obs. Geoinf. 38, 25–35.
Harley, G.L., King, J., Maxwell, J.T., 2017. Trans-Atlantic connections between North African dust flux and tree growth in the Florida Keys, United States. Earth Interact. 21, 1–22. https://doi.org/10.1175/EI-D-16-0035.1
Harris, N.L., Gibbs, D.A., Baccini, A., Birdsey, R.A., de Bruin, S., Farina, M., Fatoyinbo, L., Hansen, M.C., Herold, M., Houghton, R.A., Potapov, P. V, Suarez, D.R., Roman-Cuesta, R.M., Saatchi, S.S., Slay, C.M., Turubanova, S.A., Tyukavina, A., 2021. Global maps of twenty-first century forest carbon fluxes. Nat. Clim. Chang. 11, 234–240. https://doi.org/10.1038/s41558-020-00976-6
Harrison, M., Meindl, C.F., 2001. A statistical relationship between El-Niño-Southern Oscillation and Florida wildfire occurrence. Phys. Geogr. 22, 187–203. https://doi.org/10.1080/02723646.2001.10642737

Hartshorn, E., Sion, B., Sweeney, M.R., McDonald, E., 2023. Visual Surface Roughness Look-up Table for PI-SWERL Measurements,.

Haustein, K., Washington, R., King, J., Wiggs, G.F.S., Thomas, D.S.G., Eckardt, F.D., Bryant, R.G., Menut, L., 2015. Testing the performance of state-of-the-art dust emission schemes using DO4Models field data. Geosci. Model Dev. 8, 341–362. https://doi.org/10.5194/gmd-8-341-2015

Hawbaker, T.J., Radeloff, V.C., Syphard, A.D., Zhu, Z., Stewart, S.I., 2008. Detection rates of the MODIS active fire product in the United States. Remote Sens. Environ. 112, 2656–2664. https://doi.org/10.1016/j.rse.2007.12.008

Heinl, M., Frost, P., Vanderpost, C., Sliva, J., 2007. Fire activity on drylands and floodplains in the southern Okavango Delta, Botswana. J. Arid Environ. 68, 77–87. https://doi.org/10.1016/j.jaridenv.2005.10.023

Heiri, O., Lotter, A.F., Lemcke, G., 2001. Loss on ignition as a method for estimating organic and carbonate content in sediments: reproducibility and comparability of results. J. Paleolimnol. 25, 101–110. https://doi.org/https://doi.org/10.1023/A:1008119611481

Hesse, P., 2016. How do longitudinal dunes respond to climate forcing? Insights from 25 years of luminescence dating of the Australian desert dunefields. Quat. Int. 410, 11–29. https://doi.org/10.1016/j.quaint.2014.02.020

Hesse, P., Simpson, R.L., 2006. Variable vegetation cover and episodic sand movement on longitudinal desert sand dunes. Geomorphology 81, 276–291. https://doi.org/10.1016/j.geomorph.2006.04.012

Hilly, J.J., Sinha, J., Mani, F.S., Turagabeci, A., Jagals, P., Thomas, D.S.G., Wiggs, G.F.S., Morawska, L., Singh, K., Gucake, J., Ashworth, M., Mataki, M., Hiba, D., Bainivalu, D., Knibbs, L.D., Stuetz, R.M., Dansie, A.P., 2025. PM2.5 and PM10 concentrations in urban and peri-urban environments of two Pacific Island Countries. Atmos. Pollut. Res. 16, 102454. https://doi.org/10.1016/j.apr.2025.102454

Hitchcock, H.C., Hoffer, R.M., 1974. Mapping a Recent Forest Fire With Erts-1 Mss Data. Conf Earth Resour Obs Inf Anal Syst, Remote Sens. Earth Resour.

Hladil, J., Cejchan, P., Babek, O., Koptikova, L., Navratil, T., Kubinova, P., 2010. Dust - A geology-orientated attempt to reappraise the natural components, amounts, inputs to sediment, and importance for correlation purposes. Geol. Belgica 13, 367–384.

Hoffmann, C., Funk, R., Wieland, R., Li, Y., Sommer, M., 2008. Effects of grazing and topography on dust flux and deposition in the Xilingele grassland, Inner Mongolia. J. Arid Environ. 72, 792–807. https://doi.org/10.1016/j.jaridenv.2007.09.004

Holdo, R.M., 2005. Stem mortality following fire in Kalahari sand vegetation: Effects of frost, prior damage, and tree neighbourhoods. Plant Ecol. 180, 77–86. https://doi.org/10.1007/s11258-005-2796-4

Homann, J., Oster, J.L., de Wet, C.B., Breitenbach, S.F.M., Hoffmann, T., 2022. Linked fire activity and climate whiplash in California during the early Holocene. Nat.

Commun. 13, 1–9. https://doi.org/10.1038/s41467-022-34950-x
Huang, B., Thorne, P.W., Banzon, V.F., Boyer, T., Chepurin, G., Lawrimore, J.H., Menne, M.J., Smith, T.M., Vose, R.S., Zhang, H.M., 2017. Extended reconstructed Sea surface temperature, Version 5 (ERSSTv5): Upgrades, validations, and intercomparisons. J. Clim. 30, 8179–8205. https://doi.org/10.1175/JCLI-D-16-0836.1
Huete, A.R., 1988. A Soil-Adjusted Vegetation Index. Remote Sens. Environ. 25, 295–309.
Huete, A.R., Justice, C., Liu, H., 1994. Develpment of Vegetation and Soil Indices for MODIS-EOS. Remote Sens. Environ. 49, 224–234.
Hugenholtz, C.H., Wolfe, S.A., 2005. Biogeomorphic model of dunefield activation and stabilization on the northern Great Plains. Geomorphology 70, 53–70. https://doi.org/10.1016/j.geomorph.2005.03.011
Humphrey, G.J., Gillson, L., Ziervogel, G., 2021. How changing fire management policies affect fire seasonality and livelihoods. Ambio 50, 475–491. https://doi.org/10.1007/s13280-020-01351-7
Huneeus, N., Schulz, M., Balkanski, Y., Griesfeller, J., Prospero, J., Kinne, S., Bauer, S., Boucher, O., Chin, M., Dentener, F., Diehl, T., Easter, R., Fillmore, D., Ghan, S., Ginoux, P., Grini, A., Horowitz, L., Koch, D., Krol, M.C., Landing, W., Liu, X., Mahowald, N.M., Miller, R., Morcrette, J.J., Myhre, G., Penner, J., Perlwitz, J., Stier, P., Takemura, T., Zender, C.S., 2011. Global dust model intercomparison in AeroCom phase i. Atmos. Chem. Phys. 11, 7781–7816. https://doi.org/10.5194/acp-11-7781-2011
Hyslop, N.P., 2009. Impaired visibility: the air pollution people see. Atmos. Environ. 43, 182–195. https://doi.org/10.1016/j.atmosenv.2008.09.067
Intergovernmental Panel on Climate Change (IPCC), 2023. Climate Change 2022 – Impacts, Adaptation and Vulnerability, O., Roberts, DC, Tignor, M., Poloczanska, ES, Mintenbeck, K., Ale, A., Eds. Cambridge University Press. https://doi.org/10.1017/9781009325844
Jackson, P.S., 1981. On the displacement height in the logarithmic velocity profile. J. Fluid Mech. 111, 15. https://doi.org/10.1017/S0022112081002279
Jian, D., Niu, G.Y., Ma, Z., Liu, H., Guan, D., Zhou, X., Zhou, J., 2023. Limited driving of elevated CO2 on vegetation greening over global drylands. Environ. Res. Lett. 18. https://doi.org/10.1088/1748-9326/acf6d3
Jickells, T.D., An, Z.S., Andersen, K.K., Baker, A.R., Bergametti, C., Brooks, N., Cao, J.J., Boyd, P.W., Duce, R.A., Hunter, K.A., Kawahata, H., Kubilay, N., LaRoche, J., Liss, P.S., Mahowald, N.M., Prospero, J.M., Ridgwell, A.J., Tegen, I., Torres, R., 2005. Global iron connections between desert dust, ocean biogeochemistry, and climate. Science (80-.). 308, 67–71. https://doi.org/10.1126/science.1105959
Johnston, F.H., Williamson, G., Borchers-Arriagada, N., Henderson, S.B., Bowman, D.M.J.S., 2024. Climate Change, Landscape Fires, and Human Health: A Global Perspective. Annu. Rev. Public Health 45, 295–314. https://doi.org/10.1146/annurev-publhealth-060222-034131

Jones, M.W., Abatzoglou, J.T., Veraverbeke, S., Andela, N., Lasslop, G., Forkel, M., Smith, A.J.P., Burton, C., Betts, R.A., van der Werf, G.R., Sitch, S., Canadell, J.G., Santín, C., Kolden, C., Doerr, S.H., Le Quéré, C., 2022. Global and Regional Trends and Drivers of Fire Under Climate Change. Rev. Geophys. https://doi.org/10.1029/2020RG000726

Journet, E., Desboeufs, K. V., Caquineau, S., Colin, J.L., 2008. Mineralogy as a critical factor of dust iron solubility. Geophys. Res. Lett. 35, 3–7. https://doi.org/10.1029/2007GL031589

Justice, C.O., Giglio, L., Korontzi, S., Owens, J., Morisette, J.T., Roy, D., Descloitres, J., Alleaume, S., Petitcolin, F., Kaufman, Y., 2002. The MODIS fire products. Remote Sens. Environ. 83, 244–262. https://doi.org/10.1016/S0034-4257(02)00076-7

Kadmon, R., Leschner, H., 1995. Ecology of linear dunes: efect of surface stability on the distribution and abundance of annual plants, in: Arid Ecosystems. pp. 125–143.

Kandakji, T., Gill, T.E., Lee, J.A., 2020. Identifying and characterizing dust point sources in the southwestern United States using remote sensing and GIS. Geomorphology 353, 107019. https://doi.org/10.1016/j.geomorph.2019.107019

Karydis, V.A., Tsimpidi, A.P., Bacer, S., Pozzer, A., Nenes, A., Lelieveld, J., 2017. Global impact of mineral dust on cloud droplet number concentration. Atmos. Chem. Phys. 17, 5601–5621. https://doi.org/10.5194/acp-17-5601-2017

Kaseke, K.F., Wang, L., Wanke, H., Turewicz, V., Koeniger, P., 2016. An analysis of precipitation isotope distributions across Namibia using historical data. PLoS One 11, 1–19. https://doi.org/10.1371/journal.pone.0154598

Kavouras, I.G., Etyemezian, V., Nikolich, G., Gillies, J., Sweeney, M.R., Young, M., Shafer, D., 2009. A new technique for characterizing the efficacy of fugitive dust suppressants. J. Air Waste Manag. Assoc. 59, 603–612. https://doi.org/10.3155/1047-3289.59.5.603

Kelley, D.I., Bistinas, I., Whitley, R., Burton, C., Marthews, T.R., Dong, N., 2019. How contemporary bioclimatic and human controls change global fire regimes. Nat. Clim. Chang. 9, 690–696. https://doi.org/10.1038/s41558-019-0540-7

Key, C.H., Benson, N.C., 2006. Landscape Assessment (LA) sampling and analysis methods. USDA For. Serv. - Gen. Tech. Rep. RMRS-GTR.

Khairoun, A., Mouillot, F., Chen, W., Ciais, P., Chuvieco, E., 2024. Coarse-resolution burned area datasets severely underestimate fire-related forest loss. Sci. Total Environ. 920, 170599. https://doi.org/10.1016/j.scitotenv.2024.170599

Kharuk, V.I., Kasischke, E.S., Yakubailik, O.E., 2007. The spatial and temporal distribution of fires on Sakhalin Island, Russia. Int. J. Wildl. Fire 16, 556–562. https://doi.org/10.1071/WF05009

Kidron, G.J., Ying, W., Starinsky, A., Herzberg, M., 2017. Drought effect on biocrust resilience: High-speed winds result in crust burial and crust rupture and flaking. Sci. Total Environ. 579, 848–859. https://doi.org/10.1016/j.scitotenv.2016.11.016

Kim, B., Lee, K., Park, S., 2024. Burned-Area Mapping Using Post-Fire PlanetScope Images and a Convolutional Neural Network. Remote Sens. 16, 1–16. https://doi.org/10.3390/rs16142629

Kim, D., Chin, M., Bian, H., Tan, Q., Brown, M.E., Zheng, T., You, R., Diehl, T., Ginoux, P., Kucsera, T., 2013. The effect of the dynamic surface bareness on dust source function, emission, and distribution. J. Geophys. Res. Atmos. 118, 871–886. https://doi.org/10.1029/2012JD017907

Kim, D., Chin, M., Schuster, G., Yu, H., Takemura, T., Tuccella, P., Ginoux, P., Liu, X., Shi, Y., Matsui, H., Tsigaridis, K., Bauer, S.E., Kok, J.F., Schulz, M., 2024. Where Dust Comes From: Global Assessment of Dust Source Attributions With AeroCom Models. J. Geophys. Res. Atmos. 129. https://doi.org/10.1029/2024JD041377

Kim, D.S., Cho, G.H., White, B.R., 2000. A wind-tunnel study of atmospheric boundary-layer flow over vegetated surfaces to suppress PM10 emission on owens (dry) lake. Boundary-Layer Meteorol. 97, 309–329. https://doi.org/10.1023/A:1002786323224

King, J., Etyemezian, V., Sweeney, M.R., Buck, B.J., Nikolich, G., 2011. Dust emission variability at the Salton Sea, California, USA. Aeolian Res. 3, 67–79. https://doi.org/10.1016/j.aeolia.2011.03.005

Klingmüller, K., Lelieveld, J., Karydis, V.A., Stenchikov, G.L., 2019. Direct radiative effect of dust-pollution interactions. Atmos. Chem. Phys. 19, 7397–7408. https://doi.org/10.5194/acp-19-7397-2019

Klose, M., Gill, T.E., Etyemezian, V., Nikolich, G., Ghodsi Zadeh, Z., Webb, N.P., Van Pelt, R.S., 2019. Dust emission from crusted surfaces: Insights from field measurements and modelling. Aeolian Res. 40, 1–14. https://doi.org/10.1016/j.aeolia.2019.05.001

Kok, J.F., Adebiyi, A.A., Albani, S., Balkanski, Y., Checa-Garcia, R., Chin, M., Colarco, P.R., Hamilton, D.S., Huang, Y., Ito, A., Klose, M., Leung, D.M., Li, L., Mahowald, N.M., Miller, R.L., Obiso, V., Pérez García-Pando, C., Rocha-Lima, A., Wan, J.S., Whicker, C.A., 2021a. Improved representation of the global dust cycle using observational constraints on dust properties and abundance. Atmos. Chem. Phys. 21, 8127–8167. https://doi.org/10.5194/acp-21-8127-2021

Kok, J.F., Adebiyi, A.A., Albani, S., Balkanski, Y., Checa-Garcia, R., Chin, M., Colarco, P.R., Hamilton, D.S., Huang, Y., Ito, A., Klose, M., Li, L., Mahowald, N.M., Miller, R.L., Obiso, V., Pérez García-Pando, C., Rocha-Lima, A., Wan, J.S., 2021b. Contribution of the world's main dust source regions to the global cycle of desert dust. Atmos. Chem. Phys. 21, 8169–8193. https://doi.org/10.5194/acp-21-8169-2021

Kok, J.F., Mahowald, N.M., Fratini, G., Gillies, J.A., Ishizuka, M., Leys, J.F., Mikami, M., Park, M.S., Park, S.U., Van Pelt, R.S., Zobeck, T.M., 2014. An improved dust emission model - Part 1: Model description and comparison against measurements. Atmos. Chem. Phys. 14, 13023–13041. https://doi.org/10.5194/acp-14-13023-2014

Kok, J.F., Parteli, E.J.R., Michaels, T.I., Karam, D.B., 2012. The physics of wind-blown sand and dust. Reports Prog. Phys. 75, 106901. https://doi.org/10.1088/0034-4885/75/10/106901

Kok, J.F., Ridley, D.A., Zhou, Q., Miller, R.L., Zhao, C., Heald, C.L., Ward, D.S., Albani, S., Haustein, K., 2017. Smaller desert dust cooling effect estimated from analysis of dust size and abundance. Nat. Geosci. 10, 274–278. https://doi.org/10.1038/ngeo2912

Kok, J.F., Storelvmo, T., Karydis, V.A., Adebiyi, A.A., Mahowald, N.M., Evan, A.T., He, C., Leung, D.M., 2023. Mineral dust aerosol impacts on global climate and climate change. Nat. Rev. Earth Environ. 4, 71–86. https://doi.org/10.1038/s43017-022-00379-5

Kolesar, K.R., Schaaf, M.D., Bannister, J.W., Schreuder, M.D., Heilmann, M.H., 2022. Characterization of potential fugitive dust emissions within the Keeler Dunes, an inland dune field in the Owens Valley, California, United States. Aeolian Res. 54, 100765. https://doi.org/10.1016/j.aeolia.2021.100765

Kolusu, S.R., Shamsudduha, M., Todd, M.C., Taylor, R.G., Seddon, D., Kashaigili, J.J., Ebrahim, G.Y., Cuthbert, M.O., Sorensen, J.P.R., Villholth, K.G., MacDonald, A.M., MacLeod, D.A., 2019. The El Niño event of 2015–2016: climate anomalies and their impact on groundwater resources in East and Southern Africa. Hydrol. Earth Syst. Sci. 23, 1751–1762. https://doi.org/10.5194/hess-23-1751-2019

Kono, A., Kimura, K., Yamada, S., Koyanagi, T.F., Yamanaka, N., Yoshikawa, K., Tsuchiya, K., Okuro, T., 2025. Effectiveness of sand-fixing measures for restoration of vegetation and mitigation of wind erosion and deposition in a degraded sandy rangeland, northern China. Ecol. Eng. 211, 107456. https://doi.org/10.1016/j.ecoleng.2024.107456

Kono, A., Okuro, T., 2021. Spatial distribution of shrubs impacts relationships among saltation, roughness, and vegetation structure in an east asian rangeland. Land 10. https://doi.org/10.3390/land10111224

Lambert, F., Kug, J.S., Park, R.J., Mahowald, N.M., Winckler, G., Abe-Ouchi, A., O'Ishi, R., Takemura, T., Lee, J.H., 2013. The role of mineral-dust aerosols in polar temperature amplification. Nat. Clim. Chang. 3, 487–491. https://doi.org/10.1038/nclimate1785

Lancaster, N., 1988. Development of linear dunes in the southwestern Kalahari, Southern Africa. J. Arid Environ. 14, 233–244. https://doi.org/10.1016/s0140-1963(18)31070-x

Lancaster, N., 1986. Grain-size characteristics of Linear Dunes in the Southwestern Kalahari. J. Sediment. Petrol. 56, 395–400.

Lancaster, N., Baas, A., 1998. Influence of vegetation cover on sand transport by wind: Field studies at Owens Lake, California. Earth Surf. Process. Landforms 23, 69–82. https://doi.org/10.1002/(SICI)1096-9837(199801)23:1<69::AID-ESP823>3.0.CO;2-G

Langston, G., McKenna Neuman, C., 2005. An experimental study on the susceptibility of crusted surfaces to wind erosion: A comparison of the strength

properties of biotic and salt crusts. Geomorphology 72, 40–53. https://doi.org/10.1016/j.geomorph.2005.05.003
Laris, P.S., 2005. Spatiotemporal problems with detecting and mapping mosaic fire regimes with coarse-resolution satellite data in savanna environments. Remote Sens. Environ. 99, 412–424. https://doi.org/10.1016/j.rse.2005.09.012
Lawal, S., Lennard, C., Hewitson, B., 2019. Response of southern African vegetation to climate change at 1.5 and 2.0° global warming above the pre-industrial level. Clim. Serv. 16, 100134. https://doi.org/10.1016/j.cliser.2019.100134
Le, T., Kim, S.H., Bae, D.H., 2022. Decreasing causal impacts of El Niño–Southern Oscillation on future fire activities. Sci. Total Environ. 826, 154031. https://doi.org/10.1016/j.scitotenv.2022.154031
Leenders, J.K., van Boxel, J.H., Sterk, G., 2007. The Effect of Single Vegetation Elements on Wind Speed and Sediment Transport in the Sahelian Zone of Burkina Faso J. Earth Surf. Process. Landforms 32, 1454–1474. https://doi.org/10.1002/esp
Lehmann, C.E.R., Anderson, T.M., Sankaran, M., Higgins, S.I., Archibald, S., Hoffmann, W.A., Hanan, N.P., Williams, R.J., Fensham, R.J., Felfili, J., Hutley, L.B., Ratnam, J., San Jose, J., Montes, R., Franklin, D., Russell-Smith, J., Ryan, C.M., Durigan, G., Hiernaux, P., Haidar, R., Bowman, D.M.J.S., Bond, W.J., 2014. Savanna vegetation-fire-climate relationships differ among continents. Science (80-.). 343, 548–552. https://doi.org/10.1126/science.1247355
Lehner, B., Grill, G., 2013. Global river hydrography and network routing: Baseline data and new approaches to study the world's large river systems. Hydrol. Process. 27, 2171–2186. https://doi.org/10.1002/hyp.9740
Leistner, O.A., 1959. Notes on the vegetation of the Kalahari Gemsbok National Park with special reference to its influence on the distribution of Antelopes. Koedoe. https://doi.org/10.4102/koedoe.v2i1.860
Lentile, L.B., Holden, Z.A., Smith, A.M.S., Falkowski, M.J., Hudak, A.T., Morgan, P., Lewis, S.A., Gessler, P.E., Benson, N.C., 2006. Remote sensing techniques to assess active fire characteristics and post-fire effects. Int. J. Wildl. Fire 15, 319–345. https://doi.org/10.1071/WF05097
Levin, N., Levental, S., Morag, H., 2012. The effect of wildfires on vegetation cover and dune activity in Australia's desert dunes: A multisensor analysis. Int. J. Wildl. Fire 21, 459–475. https://doi.org/10.1071/WF10150
Lewis, A.D., 1936. Sand Dunes of the Kalahari Within the Borders of the Union. South African Geogr. J. 19, 22–32. https://doi.org/10.1080/03736245.1936.10559174
Leys, J.F., Heidenreich, S.K., Strong, C.L., McTainsh, G.H., Quigley, S., 2011. PM10 concentrations and mass transport during " Red Dawn" - Sydney 23 September 2009. Aeolian Res. 3, 327–342. https://doi.org/10.1016/j.aeolia.2011.06.003
Li, J., Kandakji, T., Lee, J.A., Tatarko, J., Blackwell, J., Gill, T.E., Collins, J.D., 2018. Blowing dust and highway safety in the southwestern United States: Characteristics of dust emission "hotspots" and management implications. Sci.

Total Environ. 621, 1023–1032. https://doi.org/10.1016/j.scitotenv.2017.10.124
Li, J., Okin, G.S., Epstein, H.E., 2009. Effects of enhanced wind erosion on surface soil texture and characteristics of windblown sediments. J. Geophys. Res. Biogeosciences 114, 1–8. https://doi.org/10.1029/2008JG000903
Li, J., Ravi, S., Wang, G., Van Pelt, R.S., Gill, T.E., Sankey, J.B., 2022. Woody plant encroachment of grassland and the reversibility of shrub dominance: Erosion, fire, and feedback processes. Ecosphere 13, 1–13. https://doi.org/10.1002/ecs2.3949
Li, M., Shen, F., Sun, X., 2021. 2019–2020 Australian bushfire air particulate pollution and impact on the South Pacific Ocean. Sci. Rep. 11, 1–13. https://doi.org/10.1038/s41598-021-91547-y
Livingstone, I., Bullard, J.E., Wiggs, G.F.S., Thomas, D.S.G., 1999. Grain-size variation on dunes in the southwest Kalahari, southern Africa.
Livingstone, I., Thomas, D.S.G., 1993. Modes of linear dune activity and their palaeoenvironmental significance: An evaluation with reference to southern African examples. Geol. Soc. Spec. Publ. 72, 91–101. https://doi.org/10.1144/GSL.SP.1993.072.01.10
Lizundia-Loiola, J., Franquesa, M., Khairoun, A., Chuvieco, E., 2022. Global burned area mapping from Sentinel-3 Synergy and VIIRS active fires. Remote Sens. Environ. 282, 113298. https://doi.org/10.1016/j.rse.2022.113298
Lizundia-Loiola, J., Otón, G., Ramo, R., Chuvieco, E., 2020. A spatio-temporal active-fire clustering approach for global burned area mapping at 250 m from MODIS data. Remote Sens. Environ. 236, 111493. https://doi.org/10.1016/j.rse.2019.111493
Lobell, D.B., Asner, G.P., 2002. Moisture Effects on Soil Reflectance. Soil Sci. Soc. Am. J. 66, 722–727. https://doi.org/10.2136/sssaj2002.7220
Lu, X., Wang, L., McCabe, M.F., 2016. Elevated CO2 as a driver of global dryland greening. Sci. Rep. 6, 1–7. https://doi.org/10.1038/srep20716
Luiz, E.W., Fiedler, S., 2024. Global Climatology of Low-Level-Jets: Occurrence, Characteristics, and Meteorological Drivers. J. Geophys. Res. Atmos. 129. https://doi.org/10.1029/2023JD040262
Mabbutt, J.A., 1957. Physiographic evidence for the age of the Kalahari sands of the Kalahari., in: Clark, J.D. (Ed.), The 3rd Pan-African Congress on Prehistory, Livingstone 1955. Livingstone Museum, Livingstone.
Maestre, F.T., Delgado-Baquerizo, M., Jeffries, T.C., Eldridge, D.J., Ochoa, V., Gozalo, B., Quero, J.L., García-Gómez, M., Gallardo, A., Ulrich, W., Bowker, M.A., Arredondo, T., Barraza-Zepeda, C., Bran, D., Florentino, A., Gaitán, J., Gutiérrez, J.R., Huber-Sannwald, E., Jankju, M., Mau, R.L., Miriti, M., Naseri, K., Ospina, A., Stavi, I., Wang, D., Woods, N.N., Yuan, X., Zaady, E., Singh, B.K., 2015. Increasing aridity reduces soil microbial diversity and abundance in global drylands. Proc. Natl. Acad. Sci. U. S. A. 112, 15684–15689. https://doi.org/10.1073/pnas.1516684112
Mager, D.M., 2010. Carbohydrates in cyanobacterial soil crusts as a source of carbon

in the southwest Kalahari, Botswana. Soil Biol. Biochem. 42, 313–318. https://doi.org/10.1016/j.soilbio.2009.11.009
Mager, D.M., Thomas, A.D., 2011. Extracellular polysaccharides from cyanobacterial soil crusts: A review of their role in dryland soil processes. J. Arid Environ. 75, 91–97. https://doi.org/10.1016/j.jaridenv.2010.10.001
Mahowald, N.M., Albani, S., Kok, J.F., Engelstaedter, S., Scanza, R., Ward, D.S., Flanner, M.G., 2014. The size distribution of desert dust aerosols and its impact on the Earth system. Aeolian Res. 15, 53–71. https://doi.org/10.1016/j.aeolia.2013.09.002
Mahowald, N.M., Ballantine, J.A., Feddema, J., Ramankutty, N., 2007. Global trends in visibility: Implications for dust sources. Atmos. Chem. Phys. 7, 3309–3339. https://doi.org/10.5194/acp-7-3309-2007
Mahowald, N.M., Engelstaedter, S., Luo, C., Sealy, A., Artaxo, P., Benitez-Nelson, C., Bonnet, S., Chen, Y., Chuang, P.Y., Cohen, D.D., Dulac, F., Herut, B., Johansen, A.M., Kubilay, N., Losno, R., Maenhaut, W., Paytan, A., Prospero, J.M., Shank, L.M., Siefert, R.L., 2009. Atmospheric iron deposition: Global distribution, variability, and human perturbations. Ann. Rev. Mar. Sci. https://doi.org/10.1146/annurev.marine.010908.163727
Mahowald, N.M., Ginoux, P., Okin, G.S., Kok, J.F., Albani, S., Balkanski, Y., Chin, M., Bergametti, G., Eck, T.F., Pérez García-Pando, C., Gkikas, A., Gonçalves Ageitos, M., Kim, D., Klose, M., LeGrand, S., Li, L., Marticorena, B., Miller, R., Ryder, C., Zender, C., Yu, Y., 2024. Letter to the Editor regarding Chappell et al., 2023, "Satellites reveal Earth's seasonally shifting dust emission sources." Sci. Total Environ. 949, 174792. https://doi.org/10.1016/j.scitotenv.2024.174792
Mahowald, N.M., Hamilton, D.S., Mackey, K.R.M., Moore, J.K., Baker, A.R., Scanza, R.A., Zhang, Y., 2018. Aerosol trace metal leaching and impacts on marine microorganisms. Nat. Commun. 9. https://doi.org/10.1038/s41467-018-04970-7
Mahowald, N.M., Kloster, S., Engelstaedter, S., Moore, J.K., Mukhopadhyay, S., McConnell, J.R., Albani, S., Doney, S.C., Bhattacharya, A., Curran, M.A.J., Flanner, M.G., Hoffman, F.M., Lawrence, D.M., Lindsay, K., Mayewski, P.A., Neff, J., Rothenberg, D., Thomas, E., Thornton, P.E., Zender, C.S., 2010. Observed 20th century desert dust variability: Impact on climateand biogeochemistry. Atmos. Chem. Phys. 10, 10875–10893. https://doi.org/10.5194/acp-10-10875-2010
Manatsa, D., Reason, C., 2017. ENSO–Kalahari Desert linkages on southern Africa summer surface air temperature variability. Int. J. Climatol. 37, 1728–1745. https://doi.org/10.1002/joc.4806
Mangan, J., Overpeck, J., Webb, R., Wessman, C., Goetz, A., 2004. Shifts As Simulated By the Century Model. Clim. Change 63, 49–90.
Mariani, M., Fletcher, M.S., Holz, A., Nyman, P., 2016. ENSO controls interannual fire activity in southeast Australia. Geophys. Res. Lett. 43, 10,891-10,900. https://doi.org/10.1002/2016GL070572
Marsett, R.C., Qi, J., Heilman, P., Biedenbender, S.H., Watson, M.C., Amer, S., Weltz,

M., Goodrich, D., Marsett, R., 2006. Remote sensing for grassland management in the arid Southwest. Rangel. Ecol. Manag. 59, 530–540. https://doi.org/10.2111/05-201R.1
Masunga, G.S., Moe, S.R., Pelekekae, B., 2013. Fire and Grazing Change Herbaceous Species Composition and Reduce Beta Diversity in the Kalahari Sand System. Ecosystems 16, 252–268. https://doi.org/10.1007/s10021-012-9611-6
Mayaud, J.R., Bailey, R.M., Wiggs, G.F.S., 2017a. A coupled vegetation/sediment transport model for dryland environments. J. Geophys. Res. Earth Surf. 122, 875–900. https://doi.org/10.1002/2016JF004096
Mayaud, J.R., Bailey, R.M., Wiggs, G.F.S., 2017b. Modelled responses of the Kalahari Desert to 21st century climate and land use change. Sci. Rep. 7, 1–12. https://doi.org/10.1038/s41598-017-04341-0
Mayaud, J.R., Webb, N.P., 2017. Vegetation in drylands: Effects on wind flow and aeolian sediment transport. Land 6, 31–33. https://doi.org/10.3390/land6030064
Mayaud, J.R., Wiggs, G.F.S., Bailey, R.M., 2016a. Dynamics of skimming flow in the wake of a vegetation patch. Aeolian Res. 22, 141–151. https://doi.org/10.1016/j.aeolia.2016.08.001
Mayaud, J.R., Wiggs, G.F.S., Bailey, R.M., 2016b. Characterizing turbulent wind flow around dryland vegetation. Earth Surf. Process. Landforms 41, 1421–1436. https://doi.org/10.1002/esp.3934
Mayr, M.J., Vanselow, K.A., Samimi, C., 2018. Fire regimes at the arid fringe: A 16-year remote sensing perspective (2000–2016) on the controls of fire activity in Namibia from spatial predictive models. Ecol. Indic. 91, 324–337. https://doi.org/10.1016/j.ecolind.2018.04.022
McDonald, F., W., 1938. Atlas of climatic charts of the oceans.
McGowan, H.A., Clark, A., 2008. A vertical profile of PM10 dust concentrations measured during a regional dust event identified by MODIS Terra, western Queensland, Australia. J. Geophys. Res. Earth Surf. 113, 1–10. https://doi.org/10.1029/2007JF000765
McLauchlan, K.K., Higuera, P.E., Miesel, J., Rogers, B.M., Schweitzer, J., Shuman, J.K., Tepley, A.J., Varner, J.M., Veblen, T.T., Adalsteinsson, S.A., Balch, J.K., Baker, P., Batllori, E., Bigio, E., Brando, P., Cattau, M., Chipman, M.L., Coen, J., Crandall, R., Daniels, L., Enright, N., Gross, W.S., Harvey, B.J., Hatten, J.A., Hermann, S., Hewitt, R.E., Kobziar, L.N., Landesmann, J.B., Loranty, M.M., Maezumi, S.Y., Mearns, L., Moritz, M., Myers, J.A., Pausas, J.G., Pellegrini, A.F.A., Platt, W.J., Roozeboom, J., Safford, H., Santos, F., Scheller, R.M., Sherriff, R.L., Smith, K.G., Smith, M.D., Watts, A.C., 2020. Fire as a fundamental ecological process: Research advances and frontiers. J. Ecol. https://doi.org/10.1111/1365-2745.13403
Meinander, O., Dagsson-Waldhauserova, P., Amosov, P., Aseyeva, E., Atkins, C., Baklanov, A., Baldo, C., Barr, S.L., Barzycka, B., Benning, L.G., Cvetkovic, B., Enchilik, P., Frolov, D., Gassó, S., Kandler, K., Kasimov, N., Kavan, J., King, J., Koroleva, T., Krupskaya, V., Kulmala, M., Kusiak, M., Lappalainen, H.K., Laska,

M., Lasne, J., Lewandowski, M., Luks, B., Mcquaid, J.B., Moroni, B., Murray, B., Möhler, O., Nawrot, A., Nickovic, S., O'neill, N.T., Pejanovic, G., Popovicheva, O., Ranjbar, K., Romanias, M., Samonova, O., Sanchez-Marroquin, A., Schepanski, K., Semenkov, I., Sharapova, A., Shevnina, E., Shi, Z., Sofiev, M., Thevenet, F., Thorsteinsson, T., Timofeev, M., Umo, N.S., Uppstu, A., Urupina, D., Varga, G., Werner, T., Arnalds, O., Vukovic Vimic, A., 2022. Newly identified climatically and environmentally significant high-latitude dust sources. Atmos. Chem. Phys. 22, 11889–11930. https://doi.org/10.5194/acp-22-11889-2022

Meng, X., Yu, Y., Ginoux, P., 2025. Rise in dust emissions from burned landscapes primarily driven by small fires. Nat. Geosci. 18. https://doi.org/10.1038/s41561-025-01730-3

MET (Ministry of Environment and Tourism), 2016. Fire Management Strategy for Namibia's Protected Areas, Directorate of Wildlife and National Parks. Windhoek, Namibia.

Middleton, N.J., 2020. Health in dust belt cities and beyond - An essay by Nick Middleton. BMJ 371. https://doi.org/10.1136/bmj.m3089

Middleton, N.J., 2017. Desert dust hazards: A global review. Aeolian Res. 24, 53–63. https://doi.org/10.1016/j.aeolia.2016.12.001

Milczarek, M., Aleksandrowicz, S., Kita, A., Chadoulis, R.T., Manakos, I., Woźniak, E., 2023. Object- Versus Pixel-Based Unsupervised Fire Burn Scar Mapping under Different Biogeographical Conditions in Europe. Land 12. https://doi.org/10.3390/land12051087

Miller, J.D., Thode, A.E., 2007. Quantifying burn severity in a heterogeneous landscape with a relative version of the delta Normalized Burn Ratio (dNBR). Remote Sens. Environ. 109, 66–80. https://doi.org/10.1016/j.rse.2006.12.006

Miller, M.E., Bowker, M.A., Reynolds, R.L., Goldstein, H.L., 2012. Post-fire land treatments and wind erosion - Lessons from the Milford Flat Fire, UT, USA. Aeolian Res. 7, 29–44. https://doi.org/10.1016/j.aeolia.2012.04.001

Mills, M.G.., Retief, P.F., 1984. The response of ungulates to rainfall along the riverbeds of the southern Kalahari 1972-1982. Koedoe 129–141.

Milton, S.J., Dean, W.R.J., 2000. Disturbance, drought and dynamics of desert dune grassland, South Africa. Plant Ecol. 150, 37–51. https://doi.org/10.1023/A:1026585211708

Mockford, T., Bullard, J.E., Thorsteinsson, T., 2018. The dynamic effects of sediment availability on the relationship between wind speed and dust concentration. Earth Surf. Process. Landforms 43, 2484–2492. https://doi.org/10.1002/esp.4407

Moritz, M.A., Batllori, E., Bradstock, R.A., Gill, A.M., Handmer, J., Hessburg, P.F., Leonard, J., McCaffrey, S., Odion, D.C., Schoennagel, T., Syphard, A.D., 2014. Learning to coexist with wildfire. Nature 515, 58–66. https://doi.org/10.1038/nature13946

Moritz, M.A., Morais, M.E., Summerell, L.A., Carlson, J.M., Doyle, J., 2005. Wildfires, complexity, and highly optimized tolerance. Proc. Natl. Acad. Sci. U. S. A. 102,

17912–17917. https://doi.org/10.1073/pnas.0508985102
Moritz, M.A., Parisien, M.-A., Batllori, E., Krawchuk, M.A., Van Dorn, J., Ganz, D.J., Hayhoe, K., 2012. Climate change and disruptions to global fire activity. Ecosphere 3, art49. https://doi.org/10.1890/es11-00345.1
Mphale, K.M., Dash, S.K., Adedoyin, A., Panda, S.K., 2014. Rainfall regime changes and trends in Botswana Kalahari Transect's late summer precipitation. Theor. Appl. Climatol. 116, 75–91. https://doi.org/10.1007/s00704-013-0907-z
Muñoz-Sabater, J., Dutra, E., Agustí-Panareda, A., Albergel, C., Arduini, G., Balsamo, G., Boussetta, S., Choulga, M., Harrigan, S., Hersbach, H., Martens, B., Miralles, D.G., Piles, M., Rodríguez-Fernández, N.J., Zsoter, E., Buontempo, C., Thépaut, J.N., 2021. ERA5-Land: A state-of-the-art global reanalysis dataset for land applications. Earth Syst. Sci. Data 13, 4349–4383. https://doi.org/10.5194/essd-13-4349-2021
Munson, S.M., Belnap, J., Okin, G.S., 2011. Responses of wind erosion to climate-induced vegetation changes on the Colorado Plateau. Proc. Natl. Acad. Sci. U. S. A. 108, 3854–3859. https://doi.org/10.1073/pnas.1014947108
Murray, J.E., Brindley, H.E., Bryant, R.G., Russell, J.E., Jenkins, K.F., Washington, R., 2016. Enhancing weak transient signals in SEVIRI false color imagery: Application to dust source detection in southern Africa. J. Geophys. Res. Atmos. 121, 10199–10219. https://doi.org/10.1002/2016JD025221.Received
Mwangala, B.B., Banda, K., Chimuka, L., Uchida, Y., Nyambe, I., 2024. Analysis of streamflow and rainfall trends and variability over the Lake Kariba catchment, Upper Zambezi Basin. Hydrol. Res. 55, 683–710. https://doi.org/10.2166/nh.2024.122
Naple, P., Skiles, S.M., Lang, O.I., Rittger, K., Lenard, S.J.P., Burgess, A., Painter, T.H., 2025. Dust on Snow Radiative Forcing and Contribution to Melt in the Colorado River Basin. Geophys. Res. Lett. 52. https://doi.org/10.1029/2024GL112757
Nash, D.J., 2022. Calcretes, Silcretes and Intergrade Duricrusts, in: Gender, Development and Social Change. Springer International Publishing, pp. 223–246. https://doi.org/10.1007/978-3-030-86102-5_13
Neuman, C.M.K., Maxwell, C., 2002. Temporal aspects of the abrasion of microphytic crusts under grain impact. Earth Surf. Process. Landforms 27, 891–908. https://doi.org/10.1002/esp.360
Neves, A.K., Pereira, J.M.C., Silva, J.M.N., Catarino, S., Oliva, P., Chuvieco, E., Campagnolo, M.L., 2024. Active fire-based dating accuracy for Landsat burned area maps is high in boreal and Mediterranean biomes and low in grasslands and savannas. ISPRS J. Photogramm. Remote Sens. 209, 461–471. https://doi.org/10.1016/j.isprsjprs.2024.02.014
Nghalipo, E.N., Joubert, D., Throop, H., Groengroeft, A., 2019. The effect of fire history on soil nutrients and soil organic carbon in a semi-arid savanna woodland, central Namibia. African J. Range Forage Sci. 36, 9–16. https://doi.org/10.2989/10220119.2018.1526825

Nghalipo, E.N., Throop, H.L., 2021. Vegetation patch type has a greater influence on soil respiration than does fire history on soil respiration in an arid broadleaf savanna woodland, central Namibia. J. Arid Environ. 193, 104577. https://doi.org/10.1016/j.jaridenv.2021.104577

Nicholas, A.M.M., Franklin, D.C., Bowman, D.M.J.S., 2009. Coexistence of shrubs and grass in a semi-arid landscape: a case study of mulga (Acacia. Aust. J. ofBotany, 57, 396–405.

Nicholson, S.E., Leposo, D., Grist, J., 2001. The relationship between El Niño and drought over Botswana. J. Clim. 14, 323–335. https://doi.org/10.1175/1520-0442(2001)014<0323:TRBENO>2.0.CO;2

Nield, J.M., Baas, A.C.W., 2008. The influence of different environmental and climatic conditions on vegetated aeolian dune landscape development and response. Glob. Planet. Change 64, 76–92. https://doi.org/10.1016/j.gloplacha.2008.10.002

Nield, J.M., Wiggs, G.F.S., Squirrell, R.S., 2011. Aeolian sand strip mobility and protodune development on a drying beach: Examining surface moisture and surface roughness patterns measured by terrestrial laser scanning. Earth Surf. Process. Landforms 36, 513–522. https://doi.org/10.1002/esp.2071

Noojipady, P., Morton, C.D., Macedo, N.M., Victoria, C.D., Huang, C., Gibbs, K.H., Bolfe, L.E., 2017. Forest carbon emissions from cropland expansion in the Brazilian Cerrado biome. Environ. Res. Lett. 12. https://doi.org/10.1088/1748-9326/aa5986

Oehler, S., Stevens, T., Kolb, T., Possnert, G., Fuchs, M., 2024. Combined optically stimulated luminescence and radiocarbon dating of aeolian dunes in Arctic Sweden. Permafr. Periglac. Process. 35, 172–187. https://doi.org/10.1002/ppp.2216

Okin, G.S., 2008. A new model of wind erosion in the presence of vegetation. J. Geophys. Res. Earth Surf. 113, 1–11. https://doi.org/10.1029/2007JF000758

Okin, G.S., Bullard, J.E., Reynolds, R.L., Ballantine, J.A.C., Schepanski, K., Todd, M.C., Belnap, J., Baddock, M.C., Gill, T.E., Miller, M.E., 2011. Dust: Small-scale processes with global consequences. Eos (Washington. DC). 92, 241–242. https://doi.org/10.1029/2011EO290001

Okin, G.S., Gillette, D.A., Herrick, J.E., 2006. Multi-scale controls on and consequences of aeolian processes in landscape change in arid and semi-arid environments. J. Arid Environ. 65, 253–275. https://doi.org/10.1016/j.jaridenv.2005.06.029

Okin, G.S., Parsons, A.J., Wainwright, J., Herrick, J.E., Bestelmeyer, B.T., Peters, D.C., Fredrickson, E.L., 2009. Do Changes in Connectivity Explain Desertification? Bioscience 59, 237–244. https://doi.org/10.1525/bio.2009.59.3.8

Otón, G., Lizundia-Loiola, J., Pettinari, M.L., Chuvieco, E., 2021. Development of a consistent global long-term burned area product (1982–2018) based on AVHRR-LTDR data. Int. J. Appl. Earth Obs. Geoinf. 103. https://doi.org/10.1016/j.jag.2021.102473

Palmer, B., Hernandez, R., Lipson, D., 2020. The fate of biological soil crusts after fire: A meta-analysis. Glob. Ecol. Conserv. 24, e01380. https://doi.org/10.1016/j.gecco.2020.e01380
Palmer, B., Lawson, D., Lipson, D.A., 2023a. Prescribed fire and changes in annual precipitation alter biocrust cover in a coastal grassland. West. North Am. Nat. 83, 325–334. https://doi.org/10.3398/064.083.0303
Palmer, B., Lawson, D., Lipson, D.A., 2023b. Years After a Fire, Biocrust Microbial Communities are Similar to Unburned Communities in a Coastal Grassland. Microb. Ecol. 85, 1028–1044. https://doi.org/10.1007/s00248-022-02137-y
Parajuli, S.P., Zender, C.S., 2017. Connecting geomorphology to dust emission through high-resolution mapping of global land cover and sediment supply. Aeolian Res. 27, 47–65. https://doi.org/10.1016/j.aeolia.2017.06.002
Park, C.E., Jeong, S.J., Joshi, M., Osborn, T.J., Ho, C.H., Piao, S., Chen, D., Liu, J., Yang, H., Park, H., Kim, B.M., Feng, S., 2018. Keeping global warming within 1.5 °c constrains emergence of aridification. Nat. Clim. Chang. 8, 70–74. https://doi.org/10.1038/s41558-017-0034-4
Parks, S.A., Holsinger, L.M., Voss, M.A., Loehman, R.A., Robinson, N.P., 2018. Mean composite fire severity metrics computed with google earth engine offer improved accuracy and expanded mapping potential. Remote Sens. 10, 1–15. https://doi.org/10.3390/rs10060879
Parsons, D., Stern, D., Ndanguza, D., Sylla, M.B., 2022. Evaluation of Satellite-Based Air Temperature Estimates at Eight Diverse Sites in Africa. Climate 10. https://doi.org/10.3390/cli10070098
Patton, N.R., Shulmeister, J., Hua, Q., Almond, P., Rittenour, T.M., Hanson, J.M., Grealy, A., Gilroy, J., Ellerton, D., 2023. Reconstructing Holocene fire records using dune footslope deposits at the Cooloola Sand Mass, Australia. Quat. Res. (United States) 115, 67–89. https://doi.org/10.1017/qua.2023.14
Pereira, C.A., Martins, J.P., Fink, A.H., Pinto, J.G., Ramos, A.M., 2024. Drivers of seasonal rainfall variability over the Angolan and Namibian plateaus. Int. J. Climatol. 3706–3725. https://doi.org/10.1002/joc.8545
Perkins, J.S., 2018. Southern Kalahari piospheres: Looking beyond the sacrifice zone. L. Degrad. Dev. 29, 2778–2784. https://doi.org/10.1002/ldr.2968
Planet, T., 2017. Planet Application Program Interface: In Space for Life on Earth.
Pointing, S.B., Belnap, J., 2014. Disturbance to desert soil ecosystems contributes to dust-mediated impacts at regional scales. Biodivers. Conserv. 23, 1659–1667. https://doi.org/10.1007/s10531-014-0690-x
Pointing, S.B., Belnap, J., 2012. Microbial colonization and controls in dryland systems. Nat. Rev. Microbiol. 10, 551–562. https://doi.org/10.1038/nrmicro2831
Poitras, T.B., Villarreal, M.L., Waller, E.K., Nauman, T.W., Miller, M.E., Duniway, M.C., 2018. Identifying optimal remotely-sensed variables for ecosystem monitoring in Colorado Plateau drylands. J. Arid Environ. 153, 76–87. https://doi.org/10.1016/j.jaridenv.2017.12.008
Pressler, Y., Moore, J.C., Cotrufo, M.F., 2019. Belowground community responses to

fire: meta-analysis reveals contrasting responses of soil microorganisms and mesofauna. Oikos 128, 309–327. https://doi.org/10.1111/oik.05738
Preston, C.A., McKenna Neuman, C., Boulton, J.W., 2020. A wind tunnel and field evaluation of various dust suppressants. J. Air Waste Manag. Assoc. 70, 915–931. https://doi.org/10.1080/10962247.2020.1779148
Pricope, N.G., Binford, M.W., 2012. A spatio-temporal analysis of fire recurrence and extent for semi-arid savanna ecosystems in southern Africa using moderate-resolution satellite imagery. J. Environ. Manage. 100, 72–85. https://doi.org/10.1016/j.jenvman.2012.01.024
Prospero, J.M., Ginoux, P., Torres, O., Nicholson, S.E., Gill, T.E., 2002. Environmental characterization of global sources of atmospheric soil dust identified with the Nimbus 7 Total Ozone Mapping Spectrometer (TOMS) absorbing aerosol product. Rev. Geophys. 40, 2-1-2–31. https://doi.org/10.1029/2000RG000095
Pye, K., 1989. Processes of Fine Particle Formation, Dust Source Regions, and Climatic Changes, in: Paleoclimatology and Paleometeorology: Modern and Past Patterns of Global Atmospheric Transport. pp. 3–30. https://doi.org/10.1007/978-94-009-0995-3_1
Raanan, H., Oren, N., Treves, H., Keren, N., Ohad, I., Berkowicz, S.M., Hagemann, M., Koch, M., Shotland, Y., Kaplan, A., 2016. Towards clarifying what distinguishes cyanobacteria able to resurrect after desiccation from those that cannot: The photosynthetic aspect. Biochim. Biophys. Acta - Bioenerg. 1857, 715–722. https://doi.org/10.1016/j.bbabio.2016.02.007
Ramo, R., Roteta, E., Bistinas, I., van Wees, D., Bastarrika, A., Chuvieco, E., van der Werf, G.R., 2021. African burned area and fire carbon emissions are strongly impacted by small fires undetected by coarse resolution satellite data. Proc. Natl. Acad. Sci. U. S. A. 118, 1–7. https://doi.org/10.1073/pnas.2011160118
Ranasinghe, R., Ruane, A.C., Vautard, R., Arnell, N., Coppola, E., Cruz, F.A., Dessai, S., Islam, A.S., Rahimi, M., Carrascal, D.R., Sillmann, J., Sylla, M.B., Tebaldi, C., Wang, W., Zaaboul, R., 2023. Climate Change Information for Regional Impact and for Risk Assessment, in: Climate Change 2021 – The Physical Science Basis. Cambridge University Press, pp. 1767–1926. https://doi.org/10.1017/9781009157896.014
Ratcliffe, N.G., Ryder, C.L., Bellouin, N., Woodward, S., Jones, A., Johnson, B., Weinzierl, B., Wieland, L., Gasteiger, J., 2024. Long range transport of coarse mineral dust : an evaluation of the Met Office Unified Model against aircraft observations 1–32.
Ravi, S., Baddock, M.C., Zobeck, T.M., Hartman, J., 2012. Field evidence for differences in post-fire aeolian transport related to vegetation type in semi-arid grasslands. Aeolian Res. 7, 3–10. https://doi.org/10.1016/j.aeolia.2011.12.002
Ravi, S., D'Odorico, P., 2009. Post-fire resource redistribution and fertility island dynamics in shrub encroached desert grasslands: A modeling approach. Landsc. Ecol. 24, 325–335. https://doi.org/10.1007/s10980-008-9307-7
Ravi, S., D'Odorico, P., Breshears, D.D., Field, J.P., Goudie, A.S., Huxman, T.E., Li, J.,

Okin, G.S., Swap, R.J., Thomas, A.D., Van Pelt, S., Whicker, J.J., Zobeck, T.M., 2011. Aeolian processes and the biosphere. Rev. Geophys. 49, 1–46. https://doi.org/10.1029/2010RG000328

Ravi, S., D'Odorico, P., Herbert, B., Zobeck, T., Over, T.M., 2006. Enhancement of wind erosion by fire-induced water repellency. Water Resour. Res. 42, 1–9. https://doi.org/10.1029/2006WR004895

Ravi, S., D'Odorico, P., Wang, L., White, C.S., Okin, G.S., Macko, S.A., Collins, S.L., 2009a. Post-fire resource redistribution in desert grasslands: A possible negative feedback on land degradation. Ecosystems 12, 434–444. https://doi.org/10.1007/s10021-009-9233-9

Ravi, S., D'Odorico, P., Zobeck, T.M., Over, T.M., 2009b. The effect of fire-induced soil hydrophobicity on wind erosion in a semiarid grassland: Experimental observations and theoretical framework. Geomorphology 105, 80–86. https://doi.org/10.1016/j.geomorph.2007.12.010

Ravi, S., D'Odorico, P., Zobeck, T.M., Over, T.M., Collins, S.L., 2007. Feedbacks between fires and wind erosion in heterogeneous arid lands. J. Geophys. Res. 112, G04007.

Reynolds, R.L., Yount, J.C., Reheis, M., Goldstein, H., Chavez, P., Fulton, R., Whitney, J., Fuller, C., Forester, R.M., 2007. Dust emission from wet and dry playas in the Mojave Desert, USA. Earth Surf. Process. Landforms 32, 1811–1827. https://doi.org/10.1002/esp.1515

Richards, J., 2020. Environmental drivers of earthen heritage deterioration in dryland regions.

Rife, D.L., Pinto, J.O., Monaghan, A.J., Davis, C.A., Hannan, J.R., 2010. Global distribution and characteristics of diurnally varying low-level jets. J. Clim. 23, 5041–5064. https://doi.org/10.1175/2010JCLI3514.1

Rodríguez-Caballero, E., Belnap, J., Büdel, B., Crutzen, P.J., Andreae, M.O., Pöschl, U., Weber, B., 2018. Dryland photoautotrophic soil surface communities endangered by global change. Nat. Geosci. 11, 185–189. https://doi.org/10.1038/s41561-018-0072-1

Rodríguez-Caballero, E., Escribano, P., Olehowski, C., Chamizo, S., Hill, J., Cantón, Y., Weber, B., 2017. Transferability of multi- and hyperspectral optical biocrust indices. ISPRS J. Photogramm. Remote Sens. 126, 94–107. https://doi.org/10.1016/j.isprsjprs.2017.02.007

Rodríguez-Caballero, E., Reyes, A., Kratz, A., Caesar, J., Guirado, E., Schmiedel, U., Escribano, P., Fiedler, S., Weber, B., 2022a. Effects of climate change and land use intensification on regional biological soil crust cover and composition in southern Africa. Geoderma 406. https://doi.org/10.1016/j.geoderma.2021.115508

Rodríguez-Caballero, E., Stanelle, T., Egerer, S., Cheng, Y., Su, H., Canton, Y., Belnap, J., Andreae, M.O., Tegen, I., Reick, C.H., Pöschl, U., Weber, B., 2022b. Global cycling and climate effects of aeolian dust controlled by biological soil crusts. Nat. Geosci. 15, 458–463. https://doi.org/10.1038/s41561-022-00942-1

Roehner, C., Pierce, J.L., Yager, E.M., 2020. Spatial and temporal changes in aeolian

redistribution of sediments and nutrients following fire. Earth Surf. Process. Landforms 45, 2556–2571. https://doi.org/10.1002/esp.4913
Roffe, S.J., van der Walt, A.J., 2023. Representation and evaluation of southern Africa's seasonal mean and extreme temperatures in the ERA5-based reanalysis products. Atmos. Res. 284, 106591. https://doi.org/10.1016/j.atmosres.2022.106591
Roteta, E., Bastarrika, A., Padilla, M., Storm, T., Chuvieco, E., 2019. Development of a Sentinel-2 burned area algorithm: Generation of a small fire database for sub-Saharan Africa. Remote Sens. Environ. 222, 1–17. https://doi.org/10.1016/j.rse.2018.12.011
Roy, D.P., Boschetti, L., 2009. Southern Africa validation of the MODIS, L3JRC, and GlobCarbon burned-area products. IEEE Trans. Geosci. Remote Sens. 47, 1032–1044. https://doi.org/10.1109/TGRS.2008.2009000
Roy, D.P., Boschetti, L., Justice, C.O., Ju, J., 2008. The collection 5 MODIS burned area product - Global evaluation by comparison with the MODIS active fire product. Remote Sens. Environ. 112, 3690–3707. https://doi.org/10.1016/j.rse.2008.05.013
Ryder, C.L., Highwood, E.J., Walser, A., Seibert, P., Philipp, A., Weinzierl, B., 2019. Coarse and giant particles are ubiquitous in Saharan dust export regions and are radiatively significant over the Sahara. Atmos. Chem. Phys. 19, 15353–15376. https://doi.org/10.5194/acp-19-15353-2019
Ryder, C.L., Marenco, F., Brooke, J.K., Estelles, V., Cotton, R., Formenti, P., McQuaid, J.B., Price, H.C., Liu, D., Ausset, P., Rosenberg, P.D., Taylor, J.W., Choularton, T., Bower, K., Coe, H., Gallagher, M., Crosier, J., Lloyd, G., Highwood, E.J., Murray, B.J., 2018. Coarse-mode mineral dust size distributions, composition and optical properties from AER-D aircraft measurements over the tropical eastern Atlantic. Atmos. Chem. Phys. 18, 17225–17257. https://doi.org/10.5194/acp-18-17225-2018
Rykiel, E.J., 1985. Towards a definition of ecological disturbance. Aust. J. Ecol. 10, 361–365. https://doi.org/10.1111/j.1442-9993.1985.tb00897.x
Saha, M. V., D'Odorico, P., Scanlon, T.M., 2019. Kalahari wildfires drive continental post-fire brightening in sub-Saharan Africa. Remote Sens. 11, 1–9. https://doi.org/10.3390/rs11091090
Sankey, J.B., Eitel, J.U.H., Glenn, N.F., Germino, M.J., Vierling, L.A., 2011. Quantifying relationships of burning, roughness, and potential dust emission with laser altimetry of soil surfaces at submeter scales. Geomorphology 135, 181–190. https://doi.org/10.1016/j.geomorph.2011.08.016
Sankey, J.B., Germino, M.J., Glenn, N.F., 2012. Dust supply varies with sagebrush microsites and time since burning in experimental erosion events. J. Geophys. Res. Biogeosciences 117. https://doi.org/10.1029/2011JG001724
Sankey, J.B., Germino, M.J., Glenn, N.F., 2009. Relationships of post-fire aeolian transport to soil and atmospheric conditions. Aeolian Res. 1, 75–85. https://doi.org/10.1016/j.aeolia.2009.07.002
Schepanski, K., 2018. Transport of mineral dust and its impact on climate. Geosciences 8, 151. https://doi.org/10.3390/geosciences8050151

Schepanski, K., Tegen, I., Laurent, B., Heinold, B., Macke, A., 2007. A new Saharan dust source activation frequency map derived from MSG-SEVIRI IR-channels. Geophys. Res. Lett. 34, 1–5. https://doi.org/10.1029/2007GL030168
Schepanski, K., Tegen, I., Todd, M.C., Heinold, B., Bönisch, G., Laurent, B., Macke, A., 2009. Meteorological processes forcing Saharan dust emission inferred from MSG-SEVIRI observations of subdaily dust source activation and numerical models. J. Geophys. Res. Atmos. 114, 1–18. https://doi.org/10.1029/2008JD010325
Scholes, R.J., Dowty, P.R., Caylor, K., Parsons, D.A.B., Frost, P.G.H., Shugart, H.H., 2002. Trends in savanna structure and composition along an aridity gradient in the Kalahari. J. Veg. Sci. 13, 419–428. https://doi.org/10.1111/j.1654-1103.2002.tb02066.x
Schroeder, W., Oliva, P., Giglio, L., Csiszar, I.A., 2014. The New VIIRS 375m active fire detection data product: Algorithm description and initial assessment. Remote Sens. Environ. 143, 85–96. https://doi.org/10.1016/j.rse.2013.12.008
Shi, K., Touge, Y., 2022. Characterization of global wildfire burned area spatiotemporal patterns and underlying climatic causes. Sci. Rep. 12, 1–17. https://doi.org/10.1038/s41598-021-04726-2
Shikwambana, L., Kganyago, M., Xulu, S., 2022. Analysis of wildfires and associated emissions during the recent strong ENSO phases in Southern Africa using multi-source remotely-derived products. Geocarto Int. 37, 16654–16670. https://doi.org/10.1080/10106049.2022.2113449
Shumack, S., Farebrother, W., Hesse, P., 2022. Quantifying vegetation and its effect on aeolian sediment transport: A UAS investigation on longitudinal dunes. Aeolian Res. 54, 100768. https://doi.org/10.1016/j.aeolia.2021.100768
Shumack, S., Hesse, P., Turner, L., 2017. The impact of fire on sand dune stability: Surface coverage and biomass recovery after fires on Western Australian coastal dune systems from 1988 to 2016. Geomorphology 299, 39–53. https://doi.org/10.1016/j.geomorph.2017.10.001
Siegal, Z., Tsoar, H., Karnieli, A., 2013. Effects of prolonged drought on the vegetation cover of sand dunes in the nw negev desert: Field survey, remote sensing and conceptual modeling. Aeolian Res. 9, 161–173. https://doi.org/10.1016/j.aeolia.2013.02.002
Silva, J.M.N., Sá, A.C.L., Pereira, J.M.C., 2005. Comparison of burned area estimates derived from SPOT-VEGETATION and Landsat ETM+ data in Africa: Influence of spatial pattern and vegetation type. Remote Sens. Environ. 96, 188–201. https://doi.org/10.1016/j.rse.2005.02.004
Skiles, S.M.K., Flanner, M., Cook, J.M., Dumont, M., Painter, T.H., 2018. Radiative forcing by light-absorbing particles in snow. Nat. Clim. Chang. https://doi.org/10.1038/s41558-018-0296-5
Smalley, I., Marshall, J., Fitzsimmons, K., Whalley, W.B., Ngambi, S., 2019. Desert loess: A selection of relevant topics. Geologos 25, 91–102. https://doi.org/10.2478/logos-2019-0007
Smit, M., Malan, P., Smit, N., Deacon, F., 2024. Response of herbaceous vegetation in

the southern kalahari following a prolonged drought. J. Arid Environ. 222, 105157. https://doi.org/10.1016/j.jaridenv.2024.105157
Smits, N., Goossens, D., Riksen, M., 2024. Effect of pedestrian trampling on aeolian sand dynamics on beach surfaces: An experimental study. Geomorphology 455, 109181. https://doi.org/10.1016/j.geomorph.2024.109181
Southern African Development Community, 2024. SADC Regional Humanitarian Appeal 1–33.
Sowden, M., Mueller, U., Blake, D., 2018. Review of surface particulate monitoring of dust events using geostationary satellite remote sensing. Atmos. Environ. 183, 154–164. https://doi.org/10.1016/j.atmosenv.2018.04.020
Spavins-Hicks, Z.D., Washington, R., Munday, C., 2021. The Limpopo Low-Level Jet: Mean Climatology and Role in Water Vapor Transport. J. Geophys. Res. Atmos. 126, 1–17. https://doi.org/10.1029/2020JD034364
Spies, A., Knight, M., Bradshaw, P., Ferreira, S., Bezuidenhout, H., Bissett, C., Wigley-Coetsee, C., Govender, D., Zimmerman, D., Hofmeyr, M., Smit, I., Govender, N., Smith, S., Conradie, L., van Eeden, B., Kruger, J., Viljoen, A., Ferreira, M., Titus, M., Makondo, K., Riley, A., Daemane, E., Peterson, R., Cole, N., Dreyer, B.-J., Waterston, K., Isaks, A., Mhlongo, E., Moolman, L., 2016. Management Plan Kalahari Gemsbok National Park 132.
Stapelberg, F.H., Van Rooyen, M.W., Bothma, J.D.P., 2008. Seasonal nutrient fluctuation in selected plant species in the Kalahari. African J. Range Forage Sci. 25, 111–119. https://doi.org/10.2989/AJRF.2008.25.3.3.600
Stavi, I., 2019. Wildfires in grasslands and shrublands: A review of impacts on vegetation, soil, hydrology, and geomorphology. Water (Switzerland) 11. https://doi.org/10.3390/w11051042
Stavi, I., Barkai, D., Knoll, Y.M., Glion, H.A., Katra, I., Brook, A., Zaady, E., 2017. Fire impact on soil-water repellency and functioning of semi-arid croplands and rangelands: Implications for prescribed burnings and wildfires. Geomorphology 280, 67–75. https://doi.org/10.1016/j.geomorph.2016.12.015
Stone, A.E.C., Thomas, D.S.G., 2008. Linear dune accumulation chronologies from the southwest Kalahari, Namibia: challenges of reconstructing late Quaternary palaeoenvironments from aeolian landforms. Quat. Sci. Rev. 27, 1667–1681. https://doi.org/10.1016/j.quascirev.2008.06.008
Storelvmo, T., 2017. Aerosol Effects on Climate via Mixed-Phase and Ice Clouds. Annu. Rev. Earth Planet. Sci. 45, 199–222. https://doi.org/10.1146/annurev-earth-060115-012240
Strong, C.L., Bullard, J.E., Dubois, C., McTainsh, G.H., Baddock, M.C., 2010. Impact of wildfire on interdune ecology and sediments: An example from the Simpson Desert, Australia. J. Arid Environ. 74, 1577–1581. https://doi.org/10.1016/j.jaridenv.2010.05.032
Strydom, S., Savage, M.J., 2018. A spatio-temporal analysis of fires in the Southern African Development Community region. Nat. Hazards 92, 1617–1632. https://doi.org/10.1007/s11069-018-3268-1

Sullivan, A., Baker, E., Kurvits, T., Popescu, A., Paulson, A.K., Cardinal Christianson, A., Tulloch, A., Bilbao, B., Mathison, C., Robinson, C., Burton, C., 2022. Spreading like wildfire: The rising threat of extraordinary landscape fires, United Nations Environment Programme.

Suter-Burri, K., Gromke, C., Leonard, K.C., Graf, F., 2013. Spatial patterns of aeolian sediment deposition in vegetation canopies: Observations from wind tunnel experiments using colored sand. Aeolian Res. 8, 65–73. https://doi.org/10.1016/j.aeolia.2012.11.002

Swain, D.L., Prein, A.F., Abatzoglou, J.T., Albano, C.M., Brunner, M., Diffenbaugh, N.S., Singh, D., Skinner, C.B., Touma, D., 2025. Hydroclimate volatility on a warming Earth. Nat. Rev. Earth Environ. 6, 35–50. https://doi.org/10.1038/s43017-024-00624-z

Sweeney, M.R., Forman, S.L., McDonald, E. V., 2022. Contemporary and future dust sources and emission fluxes from gypsum and quartz-dominated eolian systems, New Mexico and Texas, USA. Geology 50, 356–360. https://doi.org/10.1130/G49488.1

Sweeney, M.R., Lacey, T., Forman, S.L., 2023. The role of abrasion and resident fines in dust production from aeolian sands as measured by the Portable in situ Wind Erosion Laboratory (PI-SWERL). Aeolian Res. 63–65, 100889. https://doi.org/10.1016/j.aeolia.2023.100889

Sweeney, M.R., Lu, H.Y., Cui, M.C., Mason, J.A., Feng, H., Xu, Z.W., 2016. Sand dunes as potential sources of dust in northern China. Sci. China Earth Sci. 59, 760–769. https://doi.org/10.1007/s11430-015-5246-8

Sweeney, M.R., Mason, J.A., 2013. Mechanisms of dust emission from Pleistocene loess deposits, Nebraska, USA. J. Geophys. Res. Earth Surf. 118, 1460–1471. https://doi.org/10.1002/jgrf.20101

Sweeney, M.R., McDonald, E. V., Etyemezian, V., 2011. Quantifying dust emissions from desert landforms, eastern Mojave Desert, USA. Geomorphology 135, 21–34. https://doi.org/10.1016/j.geomorph.2011.07.022

Swet, N., Kok, J.F., Huang, Y., Yizhaq, H., Katra, I., 2020. Low Dust Generation Potential From Active Sand Grains by Wind Abrasion. J. Geophys. Res. Earth Surf. 125, 1–15. https://doi.org/10.1029/2020JF005545

Swetnam, T.W., Betancourt, J.L., 2010. Mesoscale Disturbance and Ecological Response to Decadal Climatic Variability in the American Southwest. Adv. Glob. Chang. Res. 41, 329–359. https://doi.org/10.1007/978-90-481-8736-2_32

Swetnam, T.W., Betancourt, J.L., 1990. Fire-Southern Oscillation Relations in the Southwestern United States. Science (80-.). 249, 1017–1020.

Szopa, S., Naik, V., Adhikary, B., Artaxo, P., Berntsen, T., Collins, W.D., Fuzzi, S., Gallardo, L., Kiendler-Scharr, A., Klimont, Z., Liao, H., Unger, N., Zanis, P., 2021. Short-lived Climate Forcers, in: Climate Change 2021 – The Physical Science Basis. pp. 817–922. https://doi.org/10.1017/9781009157896.008

Tansey, K., Grégoire, J.M., Defourny, P., Leigh, R., Pekel, J.F., van Bogaert, E., Bartholomé, E., 2008. A new, global, multi-annual (2000-2007) burnt area

product at 1 km resolution. Geophys. Res. Lett. 35, 1–6. https://doi.org/10.1029/2007GL031567
Tansey, K., Grégoire, J.M., Stroppiana, D., Sousa, A., Silva, J., Pereira, J.M.C., Boschetti, L., Maggi, M., Brivio, P.A., Fraser, R., Flasse, S., Ershov, D., Binaghi, E., Graetz, D., Peduzzi, P., 2004. Vegetation burning in the year 2000: Global burned area estimates from SPOT VEGETATION data. J. Geophys. Res. D Atmos. 109, 1–22. https://doi.org/10.1029/2003JD003598
Tegen, I., Harrison, S.P., Kohfeld, K., Prentice, I.C., Coe, M., Heimann, M., 2002. Impact of vegetation and preferential source areas on global dust aerosol: Results from a model study. J. Geophys. Res. Atmos. 107. https://doi.org/10.1029/2001JD000963
Telfer, M.W., 2011. Growth by extension, and reworking, of a south-western Kalahari linear dune. Earth Surf. Process. Landforms 36, 1125–1135. https://doi.org/10.1002/esp.2140
Thomas, A.D., Dougill, A.J., 2007. Spatial and temporal distribution of cyanobacterial soil crusts in the Kalahari: Implications for soil surface properties. Geomorphology 85, 17–29. https://doi.org/10.1016/j.geomorph.2006.03.029
Thomas, A.D., Dougill, A.J., 2006. Distribution and characteristics of cyanobacterial soil crusts in the Molopo Basin, South Africa. J. Arid Environ. 64, 270–283. https://doi.org/10.1016/j.jaridenv.2005.04.011
Thomas, A.D., Elliott, D.R., Dougill, A.J., Stringer, L.C., Hoon, S.R., Sen, R., 2018. The influence of trees, shrubs, and grasses on microclimate, soil carbon, nitrogen, and CO2 efflux: Potential implications of shrub encroachment for Kalahari rangelands. L. Degrad. Dev. 29, 1306–1316. https://doi.org/10.1002/ldr.2918
Thomas, A.D., Elliott, D.R., Hardcastle, D., Strong, C.L., Bullard, J.E., Webster, R., Lan, S., 2022. Soil biocrusts affect metabolic response to hydration on dunes in west Queensland, Australia. Geoderma 405, 115464. https://doi.org/10.1016/j.geoderma.2021.115464
Thomas, A.D., Hoon, S.R., Mairs, H., Dougill, A.J., 2012. Soil Organic Carbon and Soil Respiration in Deserts: Examples from the Kalahari. Chang. Deserts Integr. People their Environ. 40–60. https://doi.org/10.3197/9781912186310.ch03
Thomas, D.S.G., 2011. Aeolian Landscapes and Bedforms. Arid Zo. Geomorphol. Process. Form Chang. Drylands 425–453. https://doi.org/10.1002/9780470710777.ch17
Thomas, D.S.G., Knight, M., Wiggs, G.F.S., 2005. Remobilization of southern African desert dune systems by twenty-first century global warming. Nature 435, 1218–1221. https://doi.org/10.1038/nature03717
Thomas, D.S.G., Leason, H.C., 2005. Dunefield activity response to climate variability in the southwest Kalahari. Geomorphology 64, 117–132. https://doi.org/10.1016/j.geomorph.2004.06.004
Thomas, D.S.G., Twyman, C., 2004. Good or bad rangeland? Hybrid knowledge, science and local understandings of vegetation dynamics in the Kalahari. L. Degrad. Dev. 15, 215–231. https://doi.org/10.1002/ldr.610

Thomas, D.S.G., Wiggs, G.F.S., 2022. Dunes of the Southern Kalahari, in: World Geomorphological Landscapes. pp. 131–154. https://doi.org/10.1007/978-3-030-86102-5_8
Tinebra, I., Alagna, V., Iovino, M., Bagarello, V., 2019. Comparing different application procedures of the water drop penetration time test to assess soil water repellency in a fire affected Sicilian area. Catena 177, 41–48. https://doi.org/10.1016/j.catena.2019.02.005
Treminio, R.S., Webb, N.P., Edwards, B.L., Faist, A., Newingham, B., Kachergis, E., 2024. Spatial Patterns and Controls on Wind Erosion in the Great Basin. J. Geophys. Res. Biogeosciences 129. https://doi.org/10.1029/2023JG007792
Tucker, C.J., 1979. Red and photographic infrared linear combinations for monitoring vegetation. Remote Sens. Environ. 8, 127–150. https://doi.org/10.1016/0034-4257(79)90013-0
Tueller, P.T., 1987. Remote sensing science applications in arid environments. Remote Sens. Environ. 23, 143–154. https://doi.org/10.1016/0034-4257(87)90034-4
Urban, F.E., Goldstein, H.L., Fulton, R., Reynolds, R.L., 2018. Unseen Dust Emission and Global Dust Abundance: Documenting Dust Emission from the Mojave Desert (USA) by Daily Remote Camera Imagery and Wind-Erosion Measurements. J. Geophys. Res. Atmos. 123, 8735–8753. https://doi.org/10.1029/2018JD028466
Usher, C.R., Michel, A.E., Grassian, V.H., 2003. Reactions on Mineral Dust. Chem. Rev. 103, 4883–4939. https://doi.org/10.1021/cr020657y
van der Velde, I.R., van der Werf, G.R., van Wees, D., Schutgens, N.A.J., Vernooij, R., Houweling, S., Tonucci, E., Chuvieco, E., Randerson, J.T., Frey, M.M., Borsdorff, T., Aben, I., 2024. Small Fires, Big Impact: Evaluating Fire Emission Estimates in Southern Africa Using New Satellite Imagery of Burned Area and Carbon Monoxide. Geophys. Res. Lett. 51. https://doi.org/10.1029/2023GL106122
Van Der Walt, P.T., Le Riche, E.A.N., 1984. The influence of veld fire on an Acacia erioloba community in the Kalahari Gemsbok National Park. Koedoe. https://doi.org/10.4102/koedoe.v27i2.571
Van Der Werf, G.R., Randerson, J.T., Giglio, L., Collatz, G.J., Mu, M., Kasibhatla, P.S., Morton, D.C., Defries, R.S., Jin, Y., Van Leeuwen, T.T., 2010. Global fire emissions and the contribution of deforestation, savanna, forest, agricultural, and peat fires (1997-2009). Atmos. Chem. Phys. 10, 11707–11735. https://doi.org/10.5194/acp-10-11707-2010
Van Der Werf, G.R., Randerson, J.T., Giglio, L., Van Leeuwen, T.T., Chen, Y., Rogers, B.M., Mu, M., Van Marle, M.J.E., Morton, D.C., Collatz, G.J., Yokelson, R.J., Kasibhatla, P.S., 2017. Global fire emissions estimates during 1997-2016. Earth Syst. Sci. Data 9, 697–720. https://doi.org/10.5194/essd-9-697-2017
van Etten, E.J.B., Davis, R.A., Doherty, T.S., 2021. Fire in Semi-Arid Shrublands and Woodlands: Spatial and Temporal Patterns in an Australian Landscape. Front. Ecol. Evol. 9, 1–12. https://doi.org/10.3389/fevo.2021.653870
van Leeuwen, C.C.E., Fister, W., Vos, H.C., Cammeraat, L.H., Kuhn, N.J., 2021. A

cross-comparison of threshold friction velocities for PM10 emissions between a traditional portable straight-line wind tunnel and PI-SWERL. Aeolian Res. 49, 100661. https://doi.org/10.1016/j.aeolia.2020.100661
van Rooyen, N., van Rooyen, M.W., 1998. Vegetation of the south-western arid kalahari: An overview. Trans. R. Soc. South Africa 53, 113–140. https://doi.org/10.1080/00359199809520381
Velempini, K., Perkins, J.S., 2008. Integrating Indigenous Technical Knowledge and Modern Scientific Knowledge for Biodiversity Conservation and Human Livelihoods in the Southern Kalahari , Botswana. Botsw. Notes Rec. 39, 75–88.
Verlinden, A., Laamanen, R., 2006. Long term fire scar monitoring with remote sensing in Northern Namibia: Relations between fire frequency, rainfall, land cover, fire management and trees. Environ. Monit. Assess. 112, 231–253. https://doi.org/10.1007/s10661-006-1705-1
Vermeire, L.T., Wester, D.B., Mitchell, R.B., Fuhlendorf, S.D., 2005. Fire and Grazing Effects on Wind Erosion, Soil Water Content, and Soil Temperature. J. Environ. Qual. 34, 1559–1565. https://doi.org/10.2134/jeq2005.0006
Verrecchia, E., Yair, A., Kidron, G.J., Verrecchia, K., 1995. Physical properties of the psammophile cryptogamic crust and their consequences to the water regime of sandy soils, north-western Negev Desert, Israel. J. Arid Environ. 29, 427–437. https://doi.org/10.1016/S0140-1963(95)80015-8
Vickery, K.J., Eckardt, F.D., Bryant, R.G., 2013. A sub-basin scale dust plume source frequency inventory for southern Africa, 2005-2008. Geophys. Res. Lett. 40, 5274–5279. https://doi.org/10.1002/grl.50968
Villarreal, M.L., Norman, L.M., Buckley, S., Wallace, C.S.A., Coe, M.A., 2016. Multi-index time series monitoring of drought and fire effects on desert grasslands. Remote Sens. Environ. 183, 186–197. https://doi.org/10.1016/j.rse.2016.05.026
von Holdt, J.R.C., Eckardt, F.D., Baddock, M.C., Hipondoka, M.H.T., Wiggs, G.F.S., 2021. Influence of sampling approaches on physical and geochemical analysis of aeolian dust in source regions. Aeolian Res. 50, 100684. https://doi.org/10.1016/j.aeolia.2021.100684
von Holdt, J.R.C., Eckardt, F.D., Baddock, M.C., Wiggs, G.F.S., 2019. Assessing Landscape Dust Emission Potential Using Combined Ground-Based Measurements and Remote Sensing Data. J. Geophys. Res. Earth Surf. 124, 1080–1098. https://doi.org/10.1029/2018JF004713
von Suchodoletz, H., Glaser, B., Thrippleton, T., Broder, T., Zang, U., Eigenmann, R., Kopp, B., Reichert, M., Ludwig, Z., 2013. The influence of Saharan dust deposits on La Palma soil properties (Canary Islands, Spain). Catena 103, 44–52. https://doi.org/10.1016/j.catena.2011.07.005
Vos, H.C., Fister, W., Eckardt, F.D., Palmer, A.R., Kuhn, N.J., 2020. Physical crust formation on sandy soils and their potential to reduce dust emissions from croplands. Land 9, 1–20. https://doi.org/10.3390/land9120503
Vos, H.C., Fister, W., von Holdt, J.R.C., Eckardt, F.D., Palmer, A.R., Kuhn, N.J., 2021. Assessing the PM10 emission potential of sandy, dryland soils in South Africa

using the PI-SWERL. Aeolian Res. 53, 100747. https://doi.org/10.1016/j.aeolia.2021.100747
Wagenbrenner, N.S., Chung, S.H., Lamb, B.K., 2017. A large source of dust missing in particulate matter emission inventories? Wind erosion of post-fire landscapes. Elementa 5. https://doi.org/10.1525/elementa.185
Wagenbrenner, N.S., Germino, M.J., Lamb, B.K., Robichaud, P.R., Foltz, R.B., 2013. Wind erosion from a sagebrush steppe burned by wildfire: Measurements of PM10 and total horizontal sediment flux. Aeolian Res. 10, 25–36. https://doi.org/10.1016/j.aeolia.2012.10.003
Wagner, R., Jähn, M., Schepanski, K., 2018. Wildfires as a source of airborne mineral dust - Revisiting a conceptual model using large-eddy simulation (LES). Atmos. Chem. Phys. 18, 11863–11884. https://doi.org/10.5194/acp-18-11863-2018
Wagner, R., Schepanski, K., 2025. Quantifying Fire-Driven Dust Emissions Using a Global Aerosol Model. J. Adv. Model. Earth Syst. 17. https://doi.org/10.1029/2024MS004466
Walker, I.J., Hilgendorf, Z., Gillies, J.A., Turner, C.M., Furtak-Cole, E., Nikolich, G., 2023. Assessing performance of a "nature-based" foredune restoration project, Oceano Dunes, California, USA. Earth Surf. Process. Landforms 48, 143–162. https://doi.org/10.1002/esp.5478
Wallum, N.S., 2024. Determining controls on aeolian dust emissions : analysis of dynamic processes. University of Oxford.
Wang, G., Li, J., Ravi, S., Theiling, B.P., Sankey, J.B., 2019. Fire changes the spatial distribution and sources of soil organic carbon in a grassland-shrubland transition zone. Plant Soil 435, 309–321. https://doi.org/10.1007/s11104-018-3895-z
Wang, X., Chancellor, G., Evenstad, J., Farnsworth, J.E., Hase, A., Olson, G.M., Sreenath, A., Agarwal, J.K., 2009. A novel optical instrument for estimating size segregated aerosol mass concentration in real time. Aerosol Sci. Technol. 43, 939–950. https://doi.org/10.1080/02786820903045141
Wang, Y.Q., Zhang, X.Y., Gong, S.L., Zhou, C.H., Hu, X.Q., Liu, H.L., Niu, T., Yang, Y.Q., 2008. Surface observation of sand and dust storm in East Asia and its application in CUACE/Dust. Atmos. Chem. Phys. 8, 545–553. https://doi.org/10.5194/acp-8-545-2008
Wang, Yong, Yan, P., Wang, Yijiao, Wang, X., Wu, W., Dong, M., 2025. Dust emission from different land use types based on the PI-SWERL test. Catena 248, 108577. https://doi.org/10.1016/j.catena.2024.108577
Warren, A., Chappell, A., Todd, M.C., Bristow, C., Drake, N., Engelstaedter, S., Martins, V., M'bainayel, S., Washington, R., 2007. Dust-raising in the dustiest place on earth. Geomorphology 92, 25–37. https://doi.org/10.1016/j.geomorph.2007.02.007
Washington, R., Todd, M., Middleton, N.J., Goudie, A.S., 2003. Dust-storm source areas determined by the total ozone monitoring spectrometer and surface observations. Ann. Assoc. Am. Geogr. 93, 297–313. https://doi.org/10.1111/1467-

8306.9302003
Washington, R., Todd, M.C., 2005. Atmospheric controls on mineral dust emission from the Bodélé Depression, Chad: The role of the low level jet. Geophys. Res. Lett. 32, 1–5. https://doi.org/10.1029/2005GL023597
Washington, R., Todd, M.C., Engelstaedter, S., Mbainayel, S., Mitchell, F., 2006. Dust and the low-level circulation over the Bodélé Depression, Chad: Observations from BoDEx 2005. J. Geophys. Res. Atmos. 111, 1–15. https://doi.org/10.1029/2005JD006502
Wasson, R.J., Nanninga, P.M., 1986. Estimating wind transport of sand on vegetated surfaces. Earth Surf. Process. Landforms 11, 505–514. https://doi.org/10.1002/esp.3290110505
Webb, N.P., McCord, S.E., Edwards, B.L., Herrick, J.E., Kachergis, E., Okin, G.S., Van Zee, J.W., 2021. Vegetation Canopy Gap Size and Height: Critical Indicators for Wind Erosion Monitoring and Management. Rangel. Ecol. Manag. 76, 78–83. https://doi.org/10.1016/j.rama.2021.02.003
Webb, N.P., Okin, G.S., Bhattachan, A., D'Odorico, P., Dintwe, K., Tatlhego, M., 2020. Ecosystem dynamics and aeolian sediment transport in the southern Kalahari. Afr. J. Ecol. 58, 337–344. https://doi.org/10.1111/aje.12700
Webb, N.P., Strong, C.L., 2011. Soil erodibility dynamics and its representation for wind erosion and dust emission models. Aeolian Res. 3, 165–179. https://doi.org/10.1016/j.aeolia.2011.03.002
Weber, B., Belnap, J., Büdel, B., Antoninka, A.J., Barger, N.N., Chaudhary, V.B., Darrouzet-Nardi, A., Eldridge, D.J., Faist, A.M., Ferrenberg, S., Havrilla, C.A., Huber-Sannwald, E., Malam Issa, O., Maestre, F.T., Reed, S.C., Rodríguez-Caballero, E., Tucker, C., Young, K.E., Zhang, Y., Zhao, Y., Zhou, X., Bowker, M.A., 2022. What is a biocrust? A refined, contemporary definition for a broadening research community. Biol. Rev. 97, 1768–1785. https://doi.org/10.1111/brv.12862
Weinzierl, B., Ansmann, A., Prospero, J.M., Althausen, D., Benker, N., Chouza, F., Dollner, M., Farrell, D., Fomba, W.K., Freudenthaler, V., Gasteiger, J., Groß, S., Haarig, M., Heinold, B., Kandler, K., Kristensen, T.B., Mayol-Bracero, O.L., Müller, T., Reitebuch, O., Sauer, D., Schäfler, A., Schepanski, K., Spanu, A., Tegen, I., Toledano, C., Walser, A., 2017. The Saharan aerosol long-range transport and aerosol-cloud-interaction experiment: Overview and selected highlights. Bull. Am. Meteorol. Soc. 98, 1427–1451. https://doi.org/10.1175/BAMS-D-15-00142.1
Whicker, J.J., Breshears, D.D., Wasiolek, P.T., Kirchner, T.B., Tavani, R.A., Schoep, D.A., Rodgers, J.C., 2002. Temporal and Spatial Variation of Episodic Wind Erosion in Unburned and Burned Semiarid Shrubland. J. Environ. Qual. 31, 599–612. https://doi.org/10.2134/jeq2002.5990
Wiggs, G.F.S., 2022. Dune Morphology and Dynamics, 2nd ed, Treatise on Geomorphology. Elsevier Inc. https://doi.org/10.1016/b978-0-12-818234-5.00073-0

Wiggs, G.F.S., 2011. Sediment Mobilisation by the Wind. Arid Zo. Geomorphol. Process. Form Chang. Drylands 455–486. https://doi.org/10.1002/9780470710777.ch18
Wiggs, G.F.S., Baddock, M.C., Thomas, D.S.G., Washington, R., Nield, J.M., Engelstaedter, S., Bryant, R.G., Eckardt, F.D., von Holdt, J.R.C., Kötting, S., 2022. Quantifying Mechanisms of Aeolian Dust Emission: Field Measurements at Etosha Pan, Namibia. J. Geophys. Res. Earth Surf. 127, 1–21. https://doi.org/10.1029/2022JF006675
Wiggs, G.F.S., Livingstone, I., Thomas, D.S.G., Bullard, J.E., 1994. Effect of vegetation removal on airflow patterns and dune dynamics in the southwest Kalahari desert. L. Degrad. Dev. 5, 13–24. https://doi.org/10.1002/ldr.3400050103
Wiggs, G.F.S., Thomas, D.S.G., Bullard, J.E., 1995. Dune Mobility and vegetation cover in the southwest Kalahari Desert. Earth Surf. Process. Landforms 20, 515–529.
Wiggs, G.F.S., Weaver, C.M., 2012. Turbulent flow structures and aeolian sediment transport over a barchan sand dune. Geophys. Res. Lett. 39, 1–7. https://doi.org/10.1029/2012GL050847
Winton, V.H.L., Charlier, B.L.A., Jolly, B.H., Purdie, H., Anderson, B., Hunt, J.E., Dadic, R., Taylor, S., Petherick, L., Novis, P.M., 2024. New Zealand Southern Alps Blanketed by Red Australian Dust During 2019/2020 Severe Bushfire and Dust Event. Geophys. Res. Lett. 51. https://doi.org/10.1029/2024GL112782
Wiston, M., 2017. Status of Air Pollution in Botswana and Significance to Air Quality and Human Health. J. Heal. Pollut. 7.
Wolfe, S.A., 1997. Impact of increased aridity on sand dune activity in the Canadian prairies. J. Arid Environ. 36, 421–432. https://doi.org/10.1006/jare.1996.0236
Wolfe, S.A., Nickling, W.G., 1993. The protective role of sparse vegetation in wind erosion. Prog. Phys. Geogr. 17, 50–68. https://doi.org/10.1177/030913339301700104
Wright, B.R., Laffineur, B., Royé, D., Armstrong, G., Fensham, R.J., 2021. Rainfall-Linked Megafires as Innate Fire Regime Elements in Arid Australian Spinifex (Triodia spp.) Grasslands. Front. Ecol. Evol. 9, 1–13. https://doi.org/10.3389/fevo.2021.666241
Wu, C., Lin, Z., Liu, X., 2020. Global dust cycle and uncertainty in CMIP5 models. Atmos. Chem. Phys. Discuss. 5, 1–52.
Wu, G.L., Wang, D., Liu, Y., Hao, H.M., Fang, N.F., Shi, Z.H., 2016. Mosaic-pattern vegetation formation and dynamics driven by the water-wind crisscross erosion. J. Hydrol. 538, 355–362. https://doi.org/10.1016/j.jhydrol.2016.04.030
Xiang, M., Xiao, C., Feng, Z., Ma, Q., 2023. Global distribution, trends and types of active fire occurrences. Sci. Total Environ. 902, 166456. https://doi.org/10.1016/j.scitotenv.2023.166456
Yan, Y., Xu, X., Xin, X., Yang, G., Wang, X., Yan, R., Chen, B., 2011. Effect of vegetation coverage on aeolian dust accumulation in a semiarid steppe of northern China. Catena 87, 351–356. https://doi.org/10.1016/j.catena.2011.07.002

Yang, X., He, Q., Ali, M., Huo, W., Liu, X., Strake, M., 2012. A field experiment on dust emission by wind erosion in the Taklimakan desert. Acta Meteorol. Sin. 26, 241–249. https://doi.org/10.1007/s13351-012-0209-x

Yizhaq, H., Ashkenazy, Y., Levin, N., Tsoar, H., 2013. Spatiotemporal model for the progression of transgressive dunes. Phys. A Stat. Mech. its Appl. 392, 4502–4515. https://doi.org/10.1016/j.physa.2013.03.066

Yizhaq, H., Ashkenazy, Y., Tsoar, H., 2009. Sand dune dynamics and climate change: A modeling approach. J. Geophys. Res. Earth Surf. 114, 1–11. https://doi.org/10.1029/2008JF001138

Yizhaq, H., Ashkenazy, Y., Tsoar, H., 2007. Why do active and stabilized dunes coexist under the same climatic conditions? Phys. Rev. Lett. 98, 98–101. https://doi.org/10.1103/PhysRevLett.98.188001

Yoshioka, M., Mahowald, N.M., Conley, A.J., Collins, W.D., Fillmore, D.W., Zender, C.S., Coleman, D.B., 2007. Impact of desert dust radiative forcing on sahel precipitation: Relative importance of dust compared to sea surface temperature variations, vegetation changes, and greenhouse gas warming. J. Clim. 20, 1445–1467. https://doi.org/10.1175/JCLI4056.1

Yu, Y., Ginoux, P., 2022. Enhanced dust emission following large wildfires due to vegetation disturbance. Nat. Geosci. 15, 878–884. https://doi.org/10.1038/s41561-022-01046-6

Zhang, G., Wang, M., Yang, B., Liu, K., 2024. Current and Future Patterns of Global Wildfire Based on Deep Neural Networks. Earth's Futur. 12. https://doi.org/10.1029/2023EF004088

Zhang, Y.M., Wang, H.L., Wang, X.Q., Yang, W.K., Zhang, D.Y., 2006. The microstructure of microbiotic crust and its influence on wind erosion for a sandy soil surface in the Gurbantunggut Desert of Northwestern China. Geoderma 132, 441–449. https://doi.org/10.1016/j.geoderma.2005.06.008

Zhang, Z., Dong, Z., Zhao, A., Yuan, W., Han, L., 2008. The effect of restored microbiotic crusts on erosion of soil from a desert area in China. J. Arid Environ. 72, 710–721. https://doi.org/10.1016/j.jaridenv.2007.09.001

Zhao, Y., Lei, S., 2025. Research on the Inversion Method of Dust Retention in Grassland Plant Canopies Based on UAV-Borne Hyperspectral Data. Land 14, 458. https://doi.org/10.3390/land14030458

Zheng, B., Ciais, P., Chevallier, F., Chuvieco, E., Chen, Y., Yang, H., 2021. Increasing forest fire emissions despite the decline in global burned area. Sci. Adv. 7. https://doi.org/10.1126/sciadv.abh2646

Zomer, R.J., Xu, J., Trabucco, A., 2022. Version 3 of the Global Aridity Index and Potential Evapotranspiration Database. Sci. Data 9, 1–15. https://doi.org/10.1038/s41597-022-01493-1

Appendix A: Statement of authorship

The vast majority of the work presented in this thesis is my own (Rosemary Huck). There were also small contributions from the co-authors on each of the papers comprising chapters 4, 5, 6, and 7. The contributions of the co-authors is outlined below:

Chapter 4: Rosemary Huck: Writing – original draft, Writing – review and editing, Conceptualization, Formal Analysis, Investigation, Methodology, Visualization. **Giles Wiggs:** Conceptualization, Methodology, Writing – review and editing, Supervision. **David Thomas:** Conceptualization, Methodology, Writing – review and editing, Supervision.

Chapter 5: Rosemary Huck: Writing – original draft, Writing – review and editing, Conceptualization, Formal Analysis, Investigation, Methodology, Visualization. **Giles Wiggs:** Conceptualization, Methodology, Writing – review and editing, Supervision. **David Thomas:** Conceptualization, Methodology, Writing – review and editing, Supervision.

Chapter 6: Rosemary Huck: Writing – original draft, Writing – review and editing, Conceptualization, Formal Analysis, Investigation, Methodology, Visualization. **David Thomas:** Conceptualization, Methodology, Writing – review and editing, Supervision. **Giles Wiggs:** Conceptualization, Methodology, Writing – review and editing, Supervision.

Chapter 7: Rosemary Huck: Writing – original draft, Writing – review and editing, Conceptualization, Formal Analysis, Investigation, Methodology, Visualization. **David Thomas:** Writing – review and editing, Conceptualization, Methodology, Supervision. **Giles Wiggs:** Writing – review and editing, Conceptualization, Methodology, Supervision.

By signing the Statement of Authorship, you are certifying that the candidate made a substantial contribution to the publications, and that the description above is accurate:

Signed (Rosemary Huck): 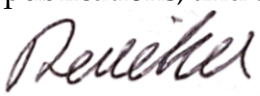 Date: 19/05/2025

Signed (Giles Wiggs):  Date: 19/05/2025

Signed (David Thomas): 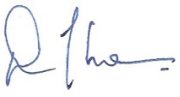 Date: 20/05/2023

Appendix B: Supplementary information for Chapter 7

S1. Poor relationship between wind speed and aerosol concentrations.

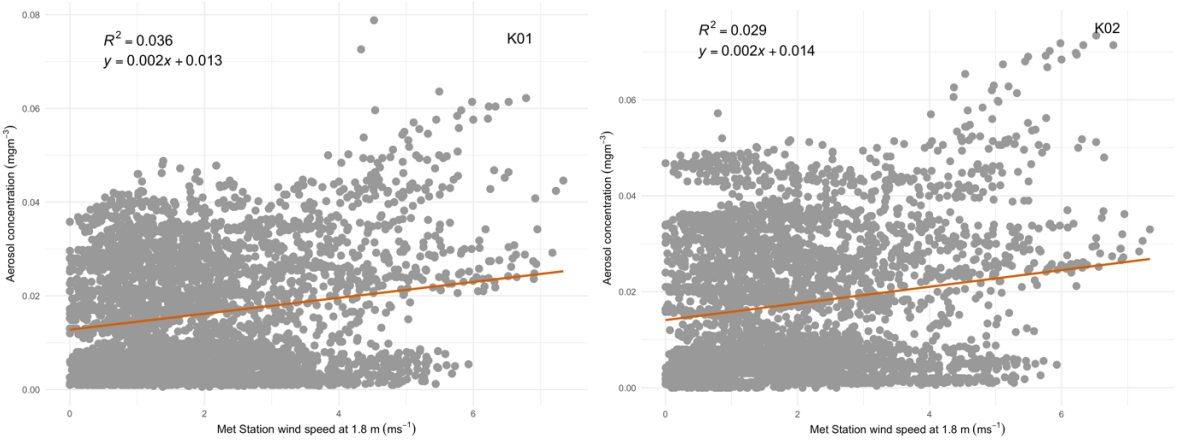

Figure S1. Scatter plots of the meteorological station 2-minute wind speed against the 2-minute DustTrak aerosol concentration. On the left is the measurements from site K01 and on the right from site K02. Both plots display poor correlation between the aerosol concentration and wind speed with R^2 values of 0.036 and 0.029 at site K01 and K02 respectively.

S2. The importance of timing for post-fire dust emissions using remote sensing for remote sensing

Many remote sensing studies which investigate post-fire emissions commence immediately after fire the fire (Yu and Ginoux, 2022). The data from the current study suggest that in the southwest Kalahari the surface is unlikely to emit dust due to high burned debris cover in the immediate post-fire period (0-2 months). K01 and K02, the two sites with the shortest interval between burning and investigation, follow a similar trend in surface cover change. Initially, post-fire, surface cover was high, comprising mainly of burned debris creating a sediment availability limited system. This finding corroborates remote sensing studies, which at a regional scale detected

darkening of the surface immediately after fire (Dintwe et al., 2017; Saha et al., 2019). Saha et al. (2019) found that fire scar sites initially darken for three months before brightening, although frequently the brightening can be more rapid. Brightening occurs when the burned debris is washed or blown away, which was observed at the recently burned sites (K01 and K02). This reduction in cover, combined with little precipitation recorded at the sites indicates that some of the burned debris may have been remobilised by the wind and the early increases in aerosol concentrations may have been recording ash blowing events instead of dust events.

As a result of the high burned debris cover immediately after fire, the temporal window for potential dust emission to occur does not start until burned debris has been removed from the surface. Measurements from this study show that burned debris removal occurred one to two months post-fire. K01 was measured three and 32 days after fire: surface cover dropped from 72.6% to 59.2% respectively. K02 was first measured 35 days after fire when surface cover was 28.9%. When remeasured 61 days post-fire, surface cover had substantially reduced to 5.7% of the area. Therefore, the temporal window for dust emission starts around two months post-fire. Yu and Ginoux (2022) also investigated post-fire dust emissions but, significantly, data collection occurred for two months, missing the potential to identify dust emission events several months after burning.

This removal of burned debris is significant. The aerosol concentrations measured by the DustTrak could represent the remobilisation of burned material. Ash-blowing events may have been detected at the sites as increases in aerosol concentration and are hard to differentiate from dust events without ground-based data (such as remote cameras) from the site, as it is difficult to distinguish burned debris and mineral dust aerosols using aerosol optical depth based remote sensing techniques. Indeed some studies on post-fire dust group both burned debris (ash) and mineral dust together as dust emissions (Wagenbrenner et al., 2017).

S3. Possibility of low-level jets in the region

The mean diurnal cycle of windspeed displayed in Figure S1 may be indicative of the down-mixing and break down of a nocturnal low-level jet (LLJ) in the morning (Fiedler et al., 2013). Such LLJs have been identified as a formative part of dust emission in many of the largest dust producing regions in the world (Allen and Washington, 2014; Fiedler et al., 2013; Ge et al., 2016; Schepanski et al., 2009; Washington et al., 2006; Washington and Todd, 2005; Wiggs et al., 2022). Currently, there are few studies which discuss LLJs within southern Africa, and observations are scarce (Algarra et al., 2019; Clements and Washington, 2021; Luiz and Fiedler, 2024; Pereira et al., 2024; Rife et al., 2010; Spavins-Hicks et al., 2021). With the increased temperature and drying predicted into the future in the Kalahari, where emission of dust may be possible due to drought-induced vegetation loss rather than burning, the morning downmixing of the LLJ may be an event that triggers dust emission. The

possible dust or ash emission event that occurred on 29/09/22 occurred during this morning downmixing of the LLJ.

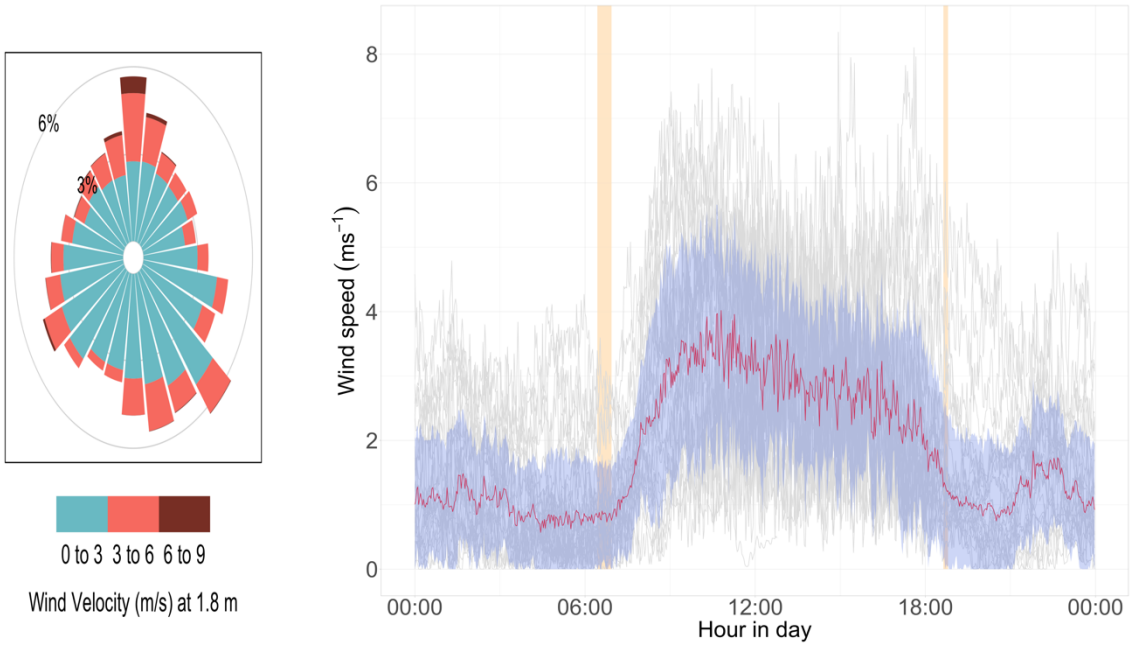

Figure S2. Wind measurements from site K02 from 04/09/2022 - 03/10/2022 measured at 1.8 m height. (A) Wind velocity (m s^{-1}) and direction. (B) Daily variation in wind speed. Daily wind speeds are displayed in grey with the average wind speed overlayed in red with +/- one standard deviation displayed in blue. The period of sunrise and sunsetting time over the month are shown in orange. There is a distinct daily patterning of wind speed.

S4. Study site context

Table S3 Images of the burned and control plots for each site.

Site	Burned	Control
K01		

K02	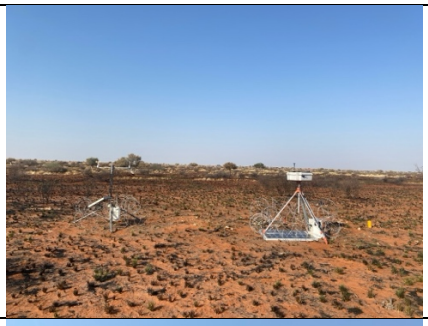	
K03		
K04		
K05		
K06		

K08	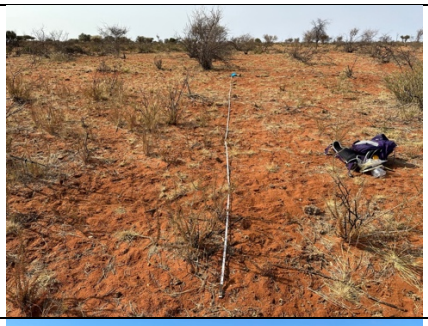	
K09		
K10		
K11		
K12		

Appendix B: Bibliography

Algarra I, Eiras-Barca J, Nieto R, Gimeno L. 2019. Global climatology of nocturnal low-level jets and associated moisture sources and sinks. Atmospheric Research **229** : 39–59. DOI: 10.1016/j.atmosres.2019.06.016 [online] Available from: https://doi.org/10.1016/j.atmosres.2019.06.016

Allen CJT, Washington R. 2014. The low-level jet dust emission mechanism in the central Sahara: Observations from Bordj-Badji Mokhtar during the June 2011 Fennec Intensive Observation. Nature : 2990–3015. DOI: 10.1038/175238c0

Clements M, Washington R. 2021. Atmospheric Controls on Mineral Dust Emission From the Etosha Pan, Namibia: Observations From the CLARIFY-2016 Field Campaign. Journal of Geophysical Research: Atmospheres **126** DOI: 10.1029/2021JD034746

Dintwe K, Okin GS, Xue Y. 2017. Fire-induced albedo change and surface radiative forcing in sub-Saharan Africa savanna ecosystems: Implications for the energy balance. Journal of Geophysical Research **122** : 6186–6201. DOI: 10.1002/2016JD026318

Fiedler S, Schepanski K, Heinold B, Knippertz P, Tegen I. 2013. Climatology of nocturnal low-level jets over North Africa and implications for modeling mineral dust emission. Journal of Geophysical Research Atmospheres **118** : 6100–6121. DOI: 10.1002/jgrd.50394

Ge JM, Liu H, Huang J, Fu Q. 2016. Taklimakan Desert nocturnal low-level jet: Climatology and dust activity. Atmospheric Chemistry and Physics **16** : 7773–7783. DOI: 10.5194/acp-16-7773-2016

Luiz EW, Fiedler S. 2024. Global Climatology of Low-Level-Jets: Occurrence, Characteristics, and Meteorological Drivers. Journal of Geophysical Research: Atmospheres **129** DOI: 10.1029/2023JD040262

Pereira CA, Martins JP, Fink AH, Pinto JG, Ramos AM. 2024. Drivers of seasonal rainfall variability over the Angolan and Namibian plateaus. International Journal of Climatology : 3706–3725. DOI: 10.1002/joc.8545

Rife DL, Pinto JO, Monaghan AJ, Davis CA, Hannan JR. 2010. Global distribution and characteristics of diurnally varying low-level jets. Journal of Climate **23** : 5041–5064. DOI: 10.1175/2010JCLI3514.1

Saha M V., D'Odorico P, Scanlon TM. 2019. Kalahari wildfires drive continental post-fire brightening in sub-Saharan Africa. Remote Sensing **11** : 1–9. DOI: 10.3390/rs11091090

Schepanski K, Tegen I, Todd MC, Heinold B, Bönisch G, Laurent B, Macke A. 2009. Meteorological processes forcing Saharan dust emission inferred from MSG-SEVIRI observations of subdaily dust source activation and numerical models. Journal of Geophysical Research Atmospheres **114** : 1–18. DOI: 10.1029/2008JD010325

Spavins-Hicks ZD, Washington R, Munday C. 2021. The Limpopo Low-Level Jet: Mean Climatology and Role in Water Vapor Transport. Journal of

Geophysical Research: Atmospheres **126** : 1–17. DOI: 10.1029/2020JD034364
Wagenbrenner NS, Chung SH, Lamb BK. 2017. A large source of dust missing in particulate matter emission inventories? Wind erosion of post-fire landscapes. Elementa **5** DOI: 10.1525/elementa.185
Washington R, Todd MC. 2005. Atmospheric controls on mineral dust emission from the Bodélé Depression, Chad: The role of the low level jet. Geophysical Research Letters **32** : 1–5. DOI: 10.1029/2005GL023597
Washington R, Todd MC, Engelstaedter S, Mbainayel S, Mitchell F. 2006. Dust and the low-level circulation over the Bodélé Depression, Chad: Observations from BoDEx 2005. Journal of Geophysical Research Atmospheres **111** : 1–15. DOI: 10.1029/2005JD006502
Wiggs GFS, Baddock MC, Thomas DSG, Washington R, Nield JM, Engelstaedter S, Bryant RG, Eckardt FD, von Holdt JRC, Kötting S. 2022. Quantifying Mechanisms of Aeolian Dust Emission: Field Measurements at Etosha Pan, Namibia. Journal of Geophysical Research: Earth Surface **127** : 1–21. DOI: 10.1029/2022JF006675
Yu Y, Ginoux P. 2022. Enhanced dust emission following large wildfires due to vegetation disturbance. Nature Geoscience **15** : 878–884. DOI: 10.1038/s41561-022-01046-6

Appendix C: Additional results from the thesis

C1. Surface strength

Measurements of surface strength (Figure C1) showed statistical difference between the burned and control plots (Table C1) However, there is no consistent state (burned or control plots) which have a greater shear or compressive strength (Figure C1). Compressive strength was low with half plots measured having no resistance to compressive forces. Plots that recorded no compressive strength also had low torsional strength (Figure C1).

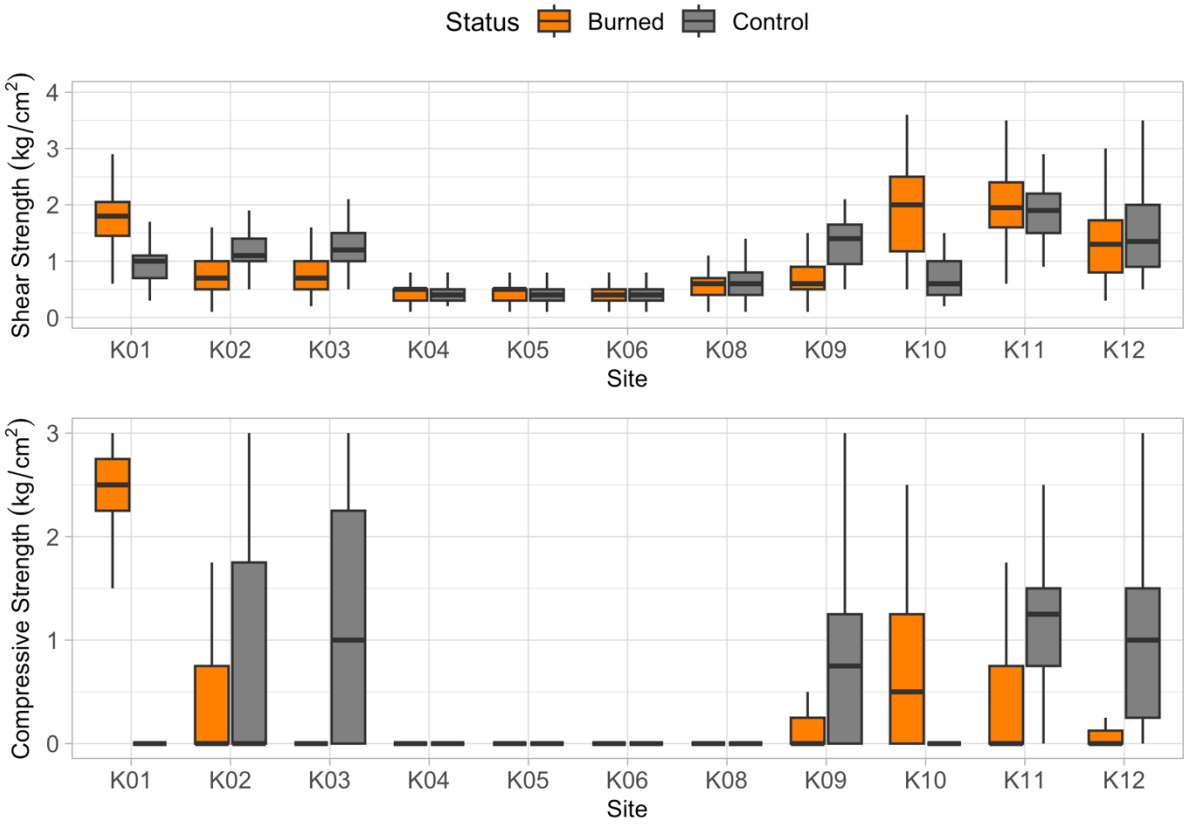

Figure C1. Surface shear strength (top) and compressive strength (bottom) measurements of each burned interdune plot. Burned plots are displayed in orange, with control plots displayed in grey.

Measurements of surface strength (Figure C1) show marked variability both between and within sites. Standard deviations for the measurements at each site varied from 0 – 1.41 kg cm^{-2} on the penetrometer readings and 0.13- 0.77 kg cm^{-2} on the shear vane measurements. This range in surface strength at each site indicate that the large sample size (100 measurements) is useful to fully characterise the surface at each site. Further, this range is suggestive of a non-uniform cover of biological soil crusts which aligns with previous findings of high variances in biocrust cover in the Kalahari. One main difficulty in constraining the impact of biocrusts, is trouble in identifying the spatial extent of biocrusts. Whilst surveying the Kalahari, the biocrusts were difficult to determine by surface observation leading to the decision to omit biocrusts in the ground cover surveys. But filamentous were visible when the trenches were dug leading to their presence being determined at the sites.

Kruskal-Wallis tests for statistical differences in the surface shear and compressive strength at each paired burned and control plot are reported in Table C1. Although seven out of the 11 pairs reported statistically different compressive strengths, whether this was the burned or control plot is variable, therefore there was no clear trend in the effect of burning on surface compressive strength. A similar observation is found with the shear strength, where six out of the 11 pairs reported statistically different shear strengths. This lack of consistent patterns suggests that biocrust strength is not impacted by burning. There are no studies investigating the relationship between wind erosion, biocrusts, and fire, but studies investigating the

final two factors have found no consistent relationship between biocrust mortality and fire (Palmer et al., 2020).

Table C1. Kruskal-Wallis p values assessing significant different between burned and co-located control interdune plots. NA is reported where all the values were 0. Statistically significant pairs are highlighted in grey. The state (burned or control) with the highest median strength is reported in the superscript. If there is no significant difference or if all the topography's medians are the same no superscript is reported.

	Compressive strength	Shear strength
K01	$p < 0.001^{B}$	$p < 0.001^{B}$
K02	$p < 0.001^{C}$	$p < 0.001^{C}$
K03	$p < 0.001^{C}$	$p < 0.001^{C}$
K04	$p < 0.01$	$p > 0.05$
K05	$p < 0.05$	$p < 0.01^{B}$
K06	NA	$p > 0.05$
K08	$p > 0.05$	$p > 0.05$
K09	$p < 0.001^{C}$	$p < 0.001^{C}$
K10	$p < 0.001^{B}$	$p < 0.001^{B}$
K11	$p < 0.001^{C}$	$p > 0.05$
K12	$p < 0.001^{C}$	$p > 0.05$

^{C} = *Control*, ^{B} = *Burned*

The biocrusts are another example of factors that impact the surface erodibility as biocrust increase the surface sediment cohesivity (Zhang et al., 2006). In this study, surfaces that have a low cover after burning always had some form of biocrust at the site. The presence of biocrust post-fire means that even though the surface cover is low, sediment is still not available to be eroded as it is bound together in biological soil crusts. Previous studies have found that even at low coverage biocrusts still

reduce erosion in sandy deserts (Belnap and Gillette, 1998, 1997; Zhang et al., 2006, 2008). For example, in the Gurbantunggut Desert in China, Zhang et al. (2006) found a reduction in wind erosion with as little as 20 % biocrust surface cover. As biocrust is present in the Kalahari, it is likely that the crust is reducing the emission of dust too.

C2. Burn severity

The index used to measure burn severity greatly impacted the results. In the study area, RdNBR was found to be much more effective than dNBR at displaying burned area (Figure C2); at all sites dNBR only detected at a maximum low-severity burns, even though there was high vegetation removal at the sites. RdNBR displays more sensitivity to burning, yet there is no distinctive pattern between burned sites. Six sites displayed high severity burns using RdNBR with 12 months of burning, whereas sites K06 and K11 show enhanced regrowth even within 1 month after fire.

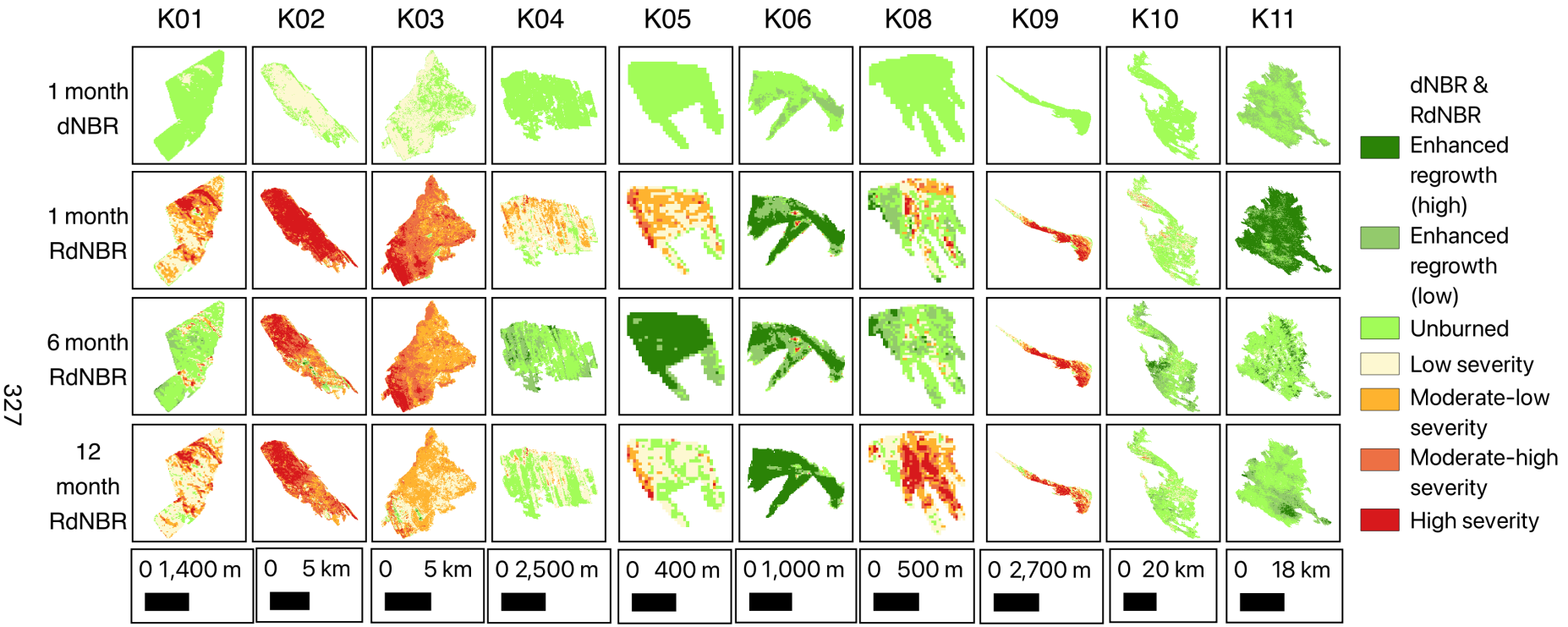

Figure C2. dNBR and RdNBR for sites K01 to K11 at 1 month, 6 months, and 12 months after being burned.

Appendix C Bibliography

Belnap, J., Gillette, D.A., 1998. Vulnerability of desert biological soil crusts to wind erosion: The influences of crust development, soil texture, and disturbance. J. Arid Environ. 39, 133–142. https://doi.org/10.1006/jare.1998.0388

Belnap, J., Gillette, D.A., 1997. Disturbance of biological soil crusts: Impacts on potential wind erodibility of sandy desert soils in Southeastern Utah. L. Degrad. Dev. 8, 355–362. https://doi.org/10.1002/(SICI)1099-145X(199712)8:4<355::AID-LDR266>3.0.CO;2-H

Palmer, B., Hernandez, R., Lipson, D., 2020. The fate of biological soil crusts after fire: A meta-analysis. Glob. Ecol. Conserv. 24, e01380. https://doi.org/10.1016/j.gecco.2020.e01380

Thomas, A.D., Dougill, A.J., 2007. Spatial and temporal distribution of cyanobacterial soil crusts in the Kalahari: Implications for soil surface properties. Geomorphology 85, 17–29. https://doi.org/10.1016/j.geomorph.2006.03.029

Zhang, Y.M., Wang, H.L., Wang, X.Q., Yang, W.K., Zhang, D.Y., 2006. The microstructure of microbiotic crust and its influence on wind erosion for a sandy soil surface in the Gurbantunggut Desert of Northwestern China. Geoderma 132, 441–449. https://doi.org/10.1016/j.geoderma.2005.06.008

Zhang, Z., Dong, Z., Zhao, A., Yuan, W., Han, L., 2008. The effect of restored microbiotic crusts on erosion of soil from a desert area in China. J. Arid Environ. 72, 710–721. https://doi.org/10.1016/j.jaridenv.2007.09.001